Transform and Denoising Frameworks for Deep Learning-Based CSI Compression in Massive MIMO

Thesis Submitted in Partial Fulfillment

for The Award of Degree of

DOCTOR OF PHILOSOPHY

by

AMIT KUMAR

RAJIV GANDHI INSTITUTE OF PETROLEUM TECHNOLOGY
JAIS, AMETHI, INDIA-229304

ROLL NUMBER	YEAR OF SUBMISSION
21EE0101	2025

CERTIFICATE

It is certified that the work contained in the thesis titled **Transform and Denoising Frameworks for Deep Learning-Based CSI Compression in Massive MIMO** by **Amit Kumar** has been carried out under my supervision and that this work has not been submitted elsewhere for a degree.

It is further certified that the student has fulfilled all the requirements of Comprehensive Examination, Candidacy, SOTA and Open Seminar.

Dr. Shivanshu Shrivastava

(Supervisor)

DECLARATION BY THE CANDIDATE

I, **Amit kumar**, certify that the work embodied in this thesis is my own bona fide work and carried out by me under the supervision of **Dr. Shivanshu Shrivastava** from **January 2022** to **December 2025**, at the **Department of Electrical and Electronics Engineering**, **Rajiv Gandhi Institute of Petroleum Technology, Jais, Amethi, India**. The matter embodied in this thesis has not been submitted for the award of any other degree/diploma. I declare that I have faithfully acknowledged and given credits to the research workers wherever their works have been cited in my work in this thesis. I further declare that I have not willfully copied any other's work, paragraphs, text, data, results, *etc.*, reported in journals, books, magazines, reports dissertations, theses, *etc.*, or available at websites and have not included them in this thesis and have not cited as my own work.

Date: **Amit Kumar**

Place: (21EE0101)

CERTIFICATE BY THE SUPERVISOR

It is certified that the above statement made by the student is correct to the best of our knowledge.

Dr. Shivanshu Shrivastava **Head of the Department**

(Supervisor) (Electrical and Electronics)

CERTIFICATE

CERTIFIED that the work contained in the thesis titled **"Transform and Denoising Frameworks for Deep Learning-Based CSI Compression in Massive MIMO"** by Mr. **Amit Kumar** has been carried out under my supervision. It is also certified that she ful-filled the mandatory requirement of TWO quality publications that arose out of her thesis work.

It is further certified that the two publications (copies enclosed) of the aforesaid Mr. **Amit Kumar** have been published in the Journals indexed by-

(a) SCI

(b) SCI Extended

(c) SCOPUS

Dr. Shivanshu Shrivastava	**Dr. Saurabh Pandey**
(Supervisor)	(Convener's, DPGC)

COPYRIGHT TRANSFER CERTIFICATE

Title of the Thesis: Transform and Denoising Frameworks for Deep Learning-Based CSI Compression in Massive MIMO

Name of the Student: Amit Kumar

COPYRIGHT TRANSFER

The undersigned hereby assigns to the Rajiv Gandhi Institute of Petroleum Technology, Jais, Amethi, India all rights under copyright that may exist in and for the above thesis submitted for the award of the DOCTOR OF PHILOSOPHY.

Date: **Amit Kumar**

Place: (21EE0101)

Note: However, the author may reproduce or authorize others to reproduce material extracted verbatim from the thesis or derivative of the thesis for the author's personal use provided that the source and the Institute's copyright notice are indicated.

ACKNOWLEDGMENT

First and foremost, I bow in gratitude to the Almighty for bestowing upon me the strength, wisdom, and perseverance needed to successfully complete my **Ph.D.** journey.

I would like to express my heartfelt and profound gratitude to my doctoral supervisor, **Dr. Shivanshu Shrivastava**, Department of Electrical and Electronics Engineering, Rajiv Gandhi Institute of Petroleum Technology (RGIPT), Amethi, India. His continuous support, insightful guidance, and invaluable mentorship at every stage of this research have shaped this thesis and my scientific outlook. Despite his demanding schedule, he was always available to provide direction, encouragement, and constructive suggestions. His open minded approach to research, unwavering trust, and patience allowed me the academic freedom to explore new ideas and develop independent thinking. Working under his supervision has been a deeply enriching experience, both professionally and personally. I have come to admire not only his excellence as a researcher but also his humility, integrity, and kindness as a human being. Our discussions have consistently motivated me and broadened my understanding of various aspects of research and professional development.

I am sincerely grateful to everyone who has contributed, directly or indirectly, to the successful completion of my doctoral studies and helped shape this journey towards the Doctor of Philosophy (Ph.D.) degree.

I would also like to express my sincere gratitude to the Head of the Department, **Dr. Umakant Dhar Dwivedi**, for his continual encouragement and support throughout my doctoral journey. My deep appreciation goes to Director, **Prof. Harish Hirani**, whose unwavering guidance and inspiration have been instrumental in shaping my academic and

research endeavors.

I am further grateful to my RPEC committee members, as well as the faculty and administrative staff of the Department of Electrical and Electronics Engineering, for their insightful suggestions, support, and assistance at various stages of my research work.

In addition, I am grateful to my collaborators and friends for their unwavering support, insightful discussions, and constant encouragement throughout this doctoral journey. Their willingness to collaborate and share knowledge has significantly shaped both my academic and personal growth. The warm and engaging environment we shared helped transform obstacles into learning experiences. Working alongside such enthusiastic and supportive colleagues made this journey intellectually rewarding and personally memorable. I truly appreciate the camaraderie, laughter, and discussion that we shared during our time together. These experiences and friendships will remain a cherished part of my Ph.D. journey.

Finally, and most importantly, I wish to express my deepest love, respect, and gratitude to my beloved parents, **Late Smt. Prabhawati Devi** and **Late Shri. Chhote Lal**, whose blessings, unconditional love, and sacrifices have been the foundation of my life and the driving force behind this achievement. Although they are not physically present with me today, their values, teachings, and blessings have guided me at every step of my academic and personal journey. They instilled in me the importance of hard work, perseverance, humility, and education, and encouraged me to dream beyond limitations. Their belief in my abilities often gave me the strength to move forward, especially in moments when I doubted myself. The virtues of patience and resilience that I learned from them have been instrumental in shaping not just this doctoral work, but also my character and outlook toward life. I am thankful to my family members and relatives for their encouragement and unwavering support, which kept me motivated and focused throughout this journey.

Amit Kumar

Dedicated to

Amma Ji - Babu Ji

and

My Family

List of Publications

Journal Publications

1. **Amit Kumar**, A. Raza, Shivanshu Shrivastava, P. Katragunta, M. Barbeau, D. Prahladadas Kothari, “A Novel DRT-Assisted Deep Learning-Based Channel Feedback Mechanism for Massive MIMO,” *IEEE Transactions on Consumer Electronics*, vol. 71, no. 2, pp. 6734–6743, 2025. DOI: 10.1109/TCE.2024.3520220 **(IF: 9.9)**

2. **Amit Kumar**, Shivanshu Shrivastava and Xiao-Zhi Gao, ”Enhanced CSI Feedback via Deep Learning Based Denoising in FDD Massive MIMO,” *AEU - International Journal of Electronics and Communications*, Volume 204, 2025, 156105, ISSN 1434-8411, https://doi.org/10.1016/j.aeue.2025.156105. **(IF: 3.1)**

3. T. Verma, A. Raza, S. Shrivastava, **Amit Kumar**, D. P. Kothari, and U. D. Dwivedi, “A Novel On-policy DRL-based Approach for Resource Allocation in Hybrid RF/VLC Systems,” *IEEE Transactions on Consumer Electronics*, vol. 71, no. 1, pp. 550–560, 2025. DOI: 10.1109/TCE.2025.3529846 **(IF: 9.9)**

4. **Amit Kumar**, A. Raza, Shivanshu Shrivastava, P. Katragunta and M. Barbeau, “A Hadamard Transform Enhanced DL-based Channel Feedback Mechanism for Massive MIMO,” *IEEE Transactions on Consumer Electronics*, 2026. (Revision Submitted) **(IF: 9.9)**

5. **Amit Kumar**, Shivanshu Shrivastava and Xiao-Zhi Gao, ”A Two-Tier Deep Learning Architecture for Efficient CSI Feedback in 5G and Beyond Massive MIMO,”

Computers and Electrical Engineering, 2026. (Revision Submitted) **(IF: 5.5)**

6. **Amit Kumar** and S. Shrivastava, “Efficient Deep Learning Frameworks for CSI Feedback Overhead Reduction in Massive MIMO,” *IEEE Transactions on Green Communications and Networking*, 2026. (Under Review) **(IF: 6.9)**

Conference Publications

1. **Amit Kumar** and S. Shrivastava, “Deep Learning-based CSI Feedback Enhancement for FDD Massive MIMO Systems,” in 2026 *IEEE Madhya Pradesh Section Conference (MPCON)*, IEEE, 2026, pp. 374–378. doi: 10.1109/MPCON69668.2026.11508579.

2. **Amit Kumar** and S. Shrivastava, “Deep Neural Network Denoising for Enhanced CSI Feedback in FDD Multi-User MIMO Systems,” in 2025 *IEEE 17th International Conference on Computational Intelligence and Communication Networks (CICN)*, IEEE, 2025, pp. 50–54. doi: 10.1109/CICN67655.2025.11368323.

Contents

List of Figures **xviii**

List of Tables **xix**

Abbreviations **xx**

Preface **xxiii**

1 Introduction **2**

1.1 Cellular System Evolution and Emergence of MIMO Systems 3

1.2 Massive MIMO for Fifth-Generation (5G) and Beyond 5

1.3 Motivation 6

1.4 Massive MIMO Systems 9

1.4.1 Massive MIMO CSI Feedback Limitations 12

1.4.2 Compressive Sensing for CSI Feedback Reduction 13

1.4.3 DL-Assisted CS for CSI Feedback Reduction 14

1.4.4 Transform-Assisted DL-Driven Frameworks 16

1.4.5 Impact of Sparse CSI Estimation Accuracy on Beamforming, Spatial Multiplexing, and Spectral Efficiency 20

1.5 Thesis Structure and Contributions 21

1.5.1 Contributions 24

2 A Review on DL-Based CSI Feedback Reduction in Massive MIMO **27**

2.1 Overview 28

2.1.1 Basic Introduction 28
2.1.2 Important Techniques for 5G and Next Generations 29
2.1.3 Massive MIMO Systems 31
2.1.4 Conventional CS and Sparsity Based Methods Using Massive MIMO 38
2.1.5 Deep Learning for Massive MIMO Systems 41
2.1.6 Generalization and Robustness Evaluation of CSI Compression Under Realistic Wireless Channel Conditions 44
2.2 Conclusion 45

3 DRT-Assisted DL for Massive MIMO CSI Feedback Reduction 47

3.1 Overview 48
3.1.1 MIMO Systems 48
3.1.2 Massive MIMO Systems 52
3.1.3 CSI-Feedback Reduction in Massive MIMO 54
3.1.4 Discrete Rajan Transform 57
3.1.5 Chapter Contributions 59
3.2 System Model 61
3.3 The proposed $\tilde{\boldsymbol{H}}$ Feedback Architecture 64
3.3.1 Discrete Rajan Transform 65
3.3.2 Inverse Discrete Rajan Transform 66
3.3.3 Problem Formulation 68
3.3.4 Why DRT Over Sparse FFT for CSI Compression? 70
3.3.5 Proposed Architecture 73
3.3.6 Inputs Parameterization 75
3.3.7 Normalization of Channel Parameters 76
3.3.8 Improvement in Noise Robustness 76
3.4 Algorithm Implementation 78
3.4.1 System-Level Impact of NMSE and Cosine Correlation 80
3.5 Simulations and Experimental Results 82

3.5.1 Generation of Training Data and Challenges 82
3.5.2 Data Preprocessing Phase 83
3.5.3 Performance Assessment 84
3.5.4 Real World Challenges for the Proposed Method and Solutions . . 86
3.6 Computation Complexity of the Proposed Scheme 88
3.6.1 Neural Network Complexity - Fully Connected Layer 88
3.6.2 Complexity of a Convolutional Layer 89
3.6.3 Total Computational Complexity for the NN 89
3.6.4 Processing Power and Time Complexity of NN 90
3.6.5 Comparison between Channel Coherence Time and Neural Network Inference Time 90
3.6.6 Throughput-Based Assessment of CSI Estimation Accuracy . . . 91
3.7 Conclusion 91

4 Hadamard Transform Enhanced DL-for Massive MIMO CSI Feedback Reduction 94

4.1 Overview 95
4.2 System Model 100
4.3 The Architecture of HaDLeMO 102
4.3.1 Problem Formulation 104
4.3.2 Discrete Hadamard Transform 105
4.3.3 Inputs Parameterization 107
4.4 Algorithm Implementation 108
4.5 Simulations and Experimental Results 109
4.6 Complexity Analysis of HaDLeMO 113
4.6.1 Discussion of Estimation Accuracy Between HaDLeMO and DRT 115
4.7 Conclusion 116

5 DL-Based Denoising in FDD Massive MIMO 118

5.1 Overview 118

5.2 System Model and Problem Formulation 120
5.2.1 DL-based Encoder and Decoder Method 122
5.3 DeNoNet Architecture 122
5.3.1 DeNoNet Optimization 126
5.4 Simulation Results 127
5.4.1 Performance Degradation of DeNoNet with Increasing Antennas . 130
5.4.2 Comparison with Diverse DNN Structures 132
5.5 Conclusion 134
5.6 Limitations and Future Work 134
5.7 Discussion on Compression Ratio 135
5.7.1 Adaptive CSI Feedback and Denoising Control Under Dynamic Channel Conditions 135

6 CDN and its Comparison with CNN for CSI Feedback Reduction in Massive MIMO 139
6.1 Overview 140
6.2 Related Works 143
6.3 System Model 144
6.3.1 DL-Driven Encoder and Decoder 146
6.4 Proposed Structure of Response $\tilde{\boldsymbol{H}}$ 147
6.4.1 Discrete Fourier Transform and Its Inverse 147
6.4.2 CNN-Based Architecture 148
6.4.3 CDN-Based Architecture 150
6.5 Implementation of Algorithms 152
6.6 Experiments and Simulations Results 155
6.6.1 Learning Data Acquisition and Constraints 157
6.6.2 Results Evaluation 157
6.7 Conclusion 162

7 Conclusion and Future Scope 164

7.1 Future Scope 166
7.1.1 Extension of the Proposed CSI Compression Framework to Cell-Free Massive MIMO and RIS-Assisted 6G Networks 167

References **169**

List of Figures

1.1 Peak Data Rate Comparison for 2G–5G (Log Scale) 6

1.2 Comparison of total population, internet users, and 5G users globally (in billions). 8

1.3 Simple Transmitter and Receiver MIMO Architecture 10

3.1 A Practical MIMO Systems 49

3.2 CSI Feedback Architecture Model of Downlink Pilot and Feedback Signals 54

3.3 System Model Structure of Transmitter (N_t) and Receiver (One User) Massive MIMO 62

3.4 (a) False color representation of the magnitude of the $\boldsymbol{H} \in \mathrm{C}^{32\times 32}$ (b) Encoder and Decoder architecture of proposed method. 73

3.5 Cosine correlation vs SNR (dB) with and without noise simulations results for DRT based DL (Indoor/Outdoor) and DFT based DL with different algorithms. 85

3.6 NMSE vs SNR with and without noise simulations results for DRT based DL (Indoor/Outdoor) and DFT based DL with different algorithms. 85

3.7 Cosine correlation vs SNR (dB) for different learning rates (LR). 86

3.8 NMSE vs SNR for different learning rates (LR). 86

3.9 Cosine correlation vs SNR (dB) comparison of 32 DFT and 32, 64, 128 and 256 DRT (Indoor/Outdoor) based antennas. 87

3.10 NMSE vs SNR comparison of 32 DFT and 32, 64, 128 and 256 DRT (Indoor/Outdoor) based antennas. 87

4.1 Structure Model of Downlink Pilot CSI Feedback Massive MIMO System 100
4.2 (a) $\boldsymbol{H} \in \mathrm{C}^{32\times 32}$ is the magnitude representation of false color. (b) Architecture of HaDLeMO Encoder and Decoder. 103
4.3 NMSE vs SNR (dB) for HaDLeMO and existing techniques. 111
4.4 Cosine correlation (ρ) vs SNR (dB) for HaDLeMO and existing techniques. 112
4.5 NMSE vs SNR (dB) comparison of existing 32 DFT and 32, 64 and 128 HaDLeMO based antennas. 113
4.6 Cosine correlation (ρ) vs SNR (dB) comparison of existing 32 DFT and 32, 64 and 128 HaDLeMO based antennas. 113
4.7 NMSE vs SNR (dB) for different learning rates (LR). 114
4.8 Cosine Correlation (ρ) vs SNR (dB) for different learning rates (LR). . . . 114

5.1 Encoder and Decoder Architecture of DeNoNet. 124
5.2 NMSE (dB) vs SNR (dB) for DeNoNet and existing methods. 129
5.3 Cosine correlation (ρ) vs SNR (dB) for DeNoNet and existing methods. . 129
5.4 NMSE (dB) vs SNR (dB) using 32, 64 antennas for our proposed DeNoNet technique and 32 antennas for existing techniques. 130
5.5 Cosine correlation (ρ) vs SNR (dB) using 32, 64 antennas for our proposed DeNoNet technique and 32 antennas for existing techniques. 130
5.6 NMSE (dB) vs SNR (dB) for DeNoNet and existing Bayesian-AE, sparse AE and vanilla AE methods. 133
5.7 Cosine correlation (ρ) vs SNR (dB) for proposed DeNoNet and existing Bayesian-AE, sparse AE and vanilla AE methods. 133

6.1 A color visualization of the magnitude of $\boldsymbol{H} \in \mathbb{C}^{32\times 32}$ illustrates the encoder–decoder architecture of the CNN approach. 149
6.2 CDN schematic architecture of encoder and decoder. 151
6.3 Overall structural representation of Deno-Net. 155
6.4 ρ vs SNR (dB) with and without noise simulations results for CDN, CNN based DFT DL and existing DeepAE based DL methods. 158

6.5 NMSE (dB) vs SNR (dB) with and without noise simulations results for CDN, CNN-based DFT DL and existing DeepAE based DL methods. . . 158

6.6 ρ vs SNR (dB) of existing DeepAE and CDN and CNN-based DFT DL for different LRs. 159

6.7 NMSE (dB) vs SNR (dB) of existing DeepAE and CDN and CNN-based DFT DL for different LRs. 159

6.8 ρ vs SNR (dB) comparison of existing DeepAE and CDN and CNN-based DFT DL for 32, 64 antennas. 160

6.9 NMSE (dB) vs SNR (dB) comparison of existing DeepAE and CDN and CNN-based DFT DL for 32, 64 antennas. 160

6.10 ρ vs SNR (dB) for proposed CDN, CNN based DFT DL and existing Bayesian-AE, Sparse-AE and Vanilla-AE techniques. 161

6.11 NMSE (dB) vs SNR (dB) for proposed CDN, CNN based DFT DL and existing Bayesian-AE, Sparse-AE and Vanilla-AE techniques. 161

List of Tables

1.1 Comparison of Wireless Communication Generations from 2G to 5G . . . 7

3.1 Simulation and Model Parameters 83

5.1 Layer-Wise Configuration of the Proposed DeNoNet Architecture 123

Abbreviations/Notations

Abbreviation	Definition
2G	Second Generation
3G	Third Generation
4G	Fourth Generation
5G	Fifth Generation
6G	Sixth Generation
MIMO	Multiple Input Multiple Output
LOS	Line-of-Sight
NLOS	Non Line-of-Sight
CS	Compressive Sensing
CSI	Channel State Information
LASSO	Least Absolute Shrinkage and Selection Operator
AMP	Approximate Message Passing
mmWave	Millimeter-Wave
BM3D-AMP	Block Matching 3D - Approximate Message Passing
ResNet	Deep Residual Network
CNN	Convolutional Neural Network
FDD	Frequency Division Duplex
DFT	Discrete Fourier Transform
DL	Deep Learning
DRT	Discrete Rajan Transform
IDRT	Inverse Discrete Rajan Transform

CDN	Channel Denoising Network
NEU	Noise Extraction Unit
RecUn	Rectified Linear Unit
Deno-Net	Denoising Deural Network
NMSE	Normalized Mean Square Error
TOA	Time of Arrival
FC	Fully Connected Layers
BN	Batch Normalization
DHT	Discrete Hadamard Transform
DIF	Decimation in Frequency
FFT	Fast Fourier Transform
MS	Mobile Station
DoD	Direction of Departure
DoA	Direction of Arrival
SNR	Signal-to-noise-ratio
SINR	Signal-to-interference-plus-noise-ratio
BS	Base Station
UE	User equipment
IM/DD	Intensity Modulation/Direct Detection
DNN	Deep neural network
CC	Channel capacity
AWGN	Additive white Gaussian noise
OFDM	Orthogonal Frequency Division Multiplexing
FLOPS	Floating Point Operations Per Second
WCN	Wireless Communication Network
EE	Energy Efficiency
SE	Spectral Efficiency
AI	Artificial Intelligence
IoT	Internet-of-Things

MSE	Mean Square Error
LR	Learning Rate
LTE	Long Term Evolution
HSPA	High-Speed Packet Access
FCC	Federal Communications Commission
UMTS	Universal Mobile Telecommunications System

Preface

The rapid evolution of wireless communication, particularly with the deployment of fifth-generation (5G) systems and the anticipated growth of sixth-generation (6G) technologies, has fundamentally transformed the demands placed on modern communication networks. Future wireless systems are expected to support unprecedented data rates, massive user connectivity, and significantly improved energy efficiency. Among the emerging technologies addressing these requirements, massive multiple input multiple output (MIMO) has become a cornerstone of next generation communication due to its ability to exploit spatial multiplexing and channel diversity for increased throughput and reduced multi-user interference.

However, realizing the full potential of massive MIMO systems is challenged by the need for accurate channel state information (CSI). As the number of antennas at the base station (BS) and user equipment (UE) scales into the hundreds or thousands, the volume of CSI data and the associated feedback overhead become prohibitively large, especially in frequency division duplex (FDD) systems where the BS relies on UE feedback for downlink CSI reconstruction. Traditional compressed sensing (CS) approaches aim to reduce this overhead by leveraging channel sparsity and projecting high dimensional CSI onto low dimensional subspaces. Although effective in theory, these techniques typically depend on discrete Fourier transform (DFT) representations, which introduce high computational complexity and experience performance degradation in real world scenarios where channel sparsity is not guaranteed.

To address these limitations, deep learning (DL) has emerged as a data-driven alternative capable of learning complex nonlinear mappings for CSI compression and reconstruction. State of the art frameworks such as Channel state information Network (CsiNet), enhanced Channel state information Network (CsiNet+), Compression–Reconstruction Network (CRNet), Probabilistic Representation Variational Network (PRVNet), Deep Autoencoder (DeepAE), and Transformer-based Network (TransNet) have demonstrated significant improvements in feedback efficiency and reconstruction accuracy. Nevertheless, such models continue to face challenges including increased computational burden, sensitivity to low signal-to-noise ratio (SNR) environments, and limited adaptability to practical deployments.

This thesis proposes computationally efficient, transform-assisted DL frameworks that strike a balance between practicality and performance for robust CSI feedback in massive MIMO systems. The developed models are designed to reduce complexity, enhance noise resilience, and remain adaptable to diverse channel conditions. First, a discrete Rajan transform (DRT) based DL architecture is introduced to achieve compact CSI representation with reduced parameters, demonstrating 126.19% improvement in cosine similarity and 81.81% improvement in normalized mean square error (NMSE) relative to conventional DFT-based systems. Building on this, a Hadamard transform assisted DL framework (HaDLeMO) is developed, leveraging the fast and multiplication free nature of the discrete Hadamard transform to achieve 109.52% improvement in cosine correlation and 257.14% enhancement in NMSE, in addition to improved convergence and scalability for large scale deployments.

To further strengthen robustness under noisy channel conditions, this thesis introduces DeNoNet, a DL-based denoising architecture that integrates noise suppression directly into the CSI encoding and decoding pipeline. DeNoNet delivers 113.18% NMSE improvement and 72.72% gain in cosine correlation over the DRT model, particularly excelling in low SNR environments where traditional methods experience significant degradation.

Finally, comparative evaluation across CNN-based and channel denoising neural (CDN) architectures demonstrates substantial gains over baseline deep autoencoder approaches, confirming the efficacy of spatial feature learning and integrated denoising for reliable CSI feedback. These advancements collectively contribute toward making massive MIMO deployment more feasible for future 5G and 6G systems, bridging the gap between theoretical innovation and practical wireless communication implementation.

This thesis develops computationally efficient deep learning frameworks for reliable and scalable CSI feedback in massive MIMO systems. The proposed transform-assisted architectures reduce model complexity while enhancing reconstruction accuracy, noise resilience, and minimizing feedback overhead for 5G and beyond wireless environments.

Chapter 1

Introduction

As of today, more than five billion people worldwide actively use the internet, and global mobile data traffic continues to grow exponentially with the proliferation of smartphones, cloud services, IoT devices and immersive applications [1]. Forecasts indicate that by 2030-2035, the number of connected devices will reach tens of billions, with data traffic increasing by an order of magnitude compared to current levels. Meeting these demands requires wireless technologies that can deliver much higher data rates, improved reliability, and efficient spectrum utilization. In this context, multiple input multiple output (MIMO) technology has emerged as one of the most effective solutions. Since its early theoretical foundations in the 1990s, MIMO has been shown to significantly enhance channel capacity and link robustness by exploiting spatial diversity and spatial multiplexing without requiring additional bandwidth or transmit power. Extensive historical evaluations and experimental studies have confirmed that MIMO enables substantial gains in spectral efficiency and reliability, making it a foundation of modern wireless standards and a key enabler for present and future high capacity communication networks.

1.1 Cellular System Evolution and Emergence of MIMO Systems

MIMO were developed for the first time in 1990s by Telatar & Foschini [2, 3]. The evolution of MIMO systems is directly related to the evolution of mobile communication networks. The developments in mobile communications are driven by the continuously growing demand for higher data rates, improved connectivity, and enhanced service reliability. Each generation of wireless technology has introduced new capabilities, expanded application domains, and transformed user experience. The journey from second-generation (2G) systems to fifth-generation (5G) and beyond networks [4] reflects major advances in digital modulation, spectrum utilization, radio access technologies, network architecture, and hardware capabilities, eventually paving the way for next-generation intelligent communication systems.

The introduction of 2G systems [5] in the early 1990s marked the transition from analog cellular communication to fully digital technology. 2G mobile networks are known for providing digital voice and early data services. The widely used 2G networks were global systems for mobile communications and code division for multiple access [6, 7]. They provided more efficient spectrum usage, better voice quality, and more robust security compared to 1G analog systems. Their primary purpose was reliable voice transmission, but they also enabled limited data services such as SMS and MMS. Typical data rates in GSM were around 9.6 kbps, which later increased with enhancements such as GPRS and EDGE [8]. GPRS, often termed 2.5G, allowed packet switching and increased data rates up to 56–114 kbps theoretically, while EDGE pushed rates up to approximately 384 kbps [9].

Although modest by modern standards, 2G laid the foundation for mobile digital communication and introduced mobility into data services. Users could browse simplified web pages, download small multimedia content, and send emails, marking the early rise of mobile Internet. The low data rate was acceptable since the applications of the time required minimal bandwidth. This era focused primarily on voice capacity and coverage rather than high speed data.

Growing demand for mobile Internet and multimedia applications led to the arrival of third-generation (3G) systems in the 2000s [10]. 3G mobile systems offered mobile internet and multimedia services. Technologies such as universal mobile telecommunications system (UMTS), wide-band code division multiple access (WCDMA) [11], and code division multiple access (CDMA2000) enabled significant increases in data rates and service flexibility [12]. Early 3G systems delivered peak speeds up to 384 kbps, sufficient for early Internet browsing and audio streaming. Subsequent improvements such as high-speed packet access (HSPA) [13] and HSPA+ dramatically improved theoretical data rates, with HSPA+ [14] offering downlink rates up to 42 Mbps.

3G networks introduced packet switched data as the core of network design and enabled consistent support for video streaming, email, social media, and mobile applications. This era brought smartphones and mobile applications to the mainstream, fundamentally transforming user interaction with wireless systems. Increasing smartphone penetration also led to exponential traffic growth and pushed networks toward more spectrally efficient radio access techniques. As real-time applications emerged, latency and throughput requirements increased, motivating further system enhancements and the eventual evolution toward broadband driven 4G systems.

Although the concept of MIMO dates back to the 1990s, MIMO techniques were standardized and commercially deployed for the first time in fourth-generation (4G) wireless systems. 4G systems, introduced around 2009, shifted the focus toward high speed mobile broadband capable of supporting multimedia rich applications [15, 16]. Long term evolution (LTE) and LTE-Advanced [17] standards adopted orthogonal frequency division multiple access (OFDMA) and advanced MIMO techniques to significantly improve spectral efficiency [18, 19]. LTE's initial theoretical downlink speed was around 100 Mbps, while LTE-Advanced [17] could reach up to 1 Gbps with carrier aggregation and higher order MIMO configurations. Latency improved dramatically, with radio link latency typically [20] in the range of 10-50 ms, enabling smoother interaction for real-time applications.

One of the most transformative aspects of 4G was the shift to a pure IP-based architecture [21]. Unlike earlier generations that still retained circuit switched control channels, LTE utilized packet switching for all data and voice traffic, laying the foundation for scalable, flexible, and converged mobile services. The availability of broadband speeds enabled widespread use of high definition video streaming, social media, cloud-based applications, real-time navigation, and online gaming. However, the increasing demand for data intensive applications began to strain network capacity, even with carrier aggregation and improved spectrum efficiency [22, 23]. As millions of users and devices started competing for radio resources, better spatial multiplexing and higher spectrum reuse became essential, setting the stage for massive MIMO deployment in 5G.

1.2 Massive MIMO for Fifth-Generation (5G) and Beyond

The introduction of fifth-generation (5G) networks represents one of the most significant leaps in wireless communication [24, 25, 26]. 5G is driven by three major application categories: enhanced mobile broadband (eMBB) [27, 28], ultra reliable low-latency communication (URLLC) [29, 30, 31], and massive machine type communication (mMTC) [32, 33]. While 4G mainly served human users and high data rate broadband, 5G supports not only faster mobile experiences but also industrial automation, autonomous vehicles, smart cities, and mission critical systems [34].

5G networks are engineered to achieve theoretical peak downlink rates of 10–20 Gbps and real world user rates in the range of hundreds (100s) of Mbps [35] as shown in Fig. 1.1. Latency targets reach as low as 1 ms for URLLC applications such as remote surgery, autonomous driving, and factory automation. To achieve these ambitious goals, 5G employs millimeter-wave (mmWave) frequency bands [36] with wide bandwidths, network slicing for service differentiation, and advanced massive MIMO beamforming to maximize spectral efficiency [37].

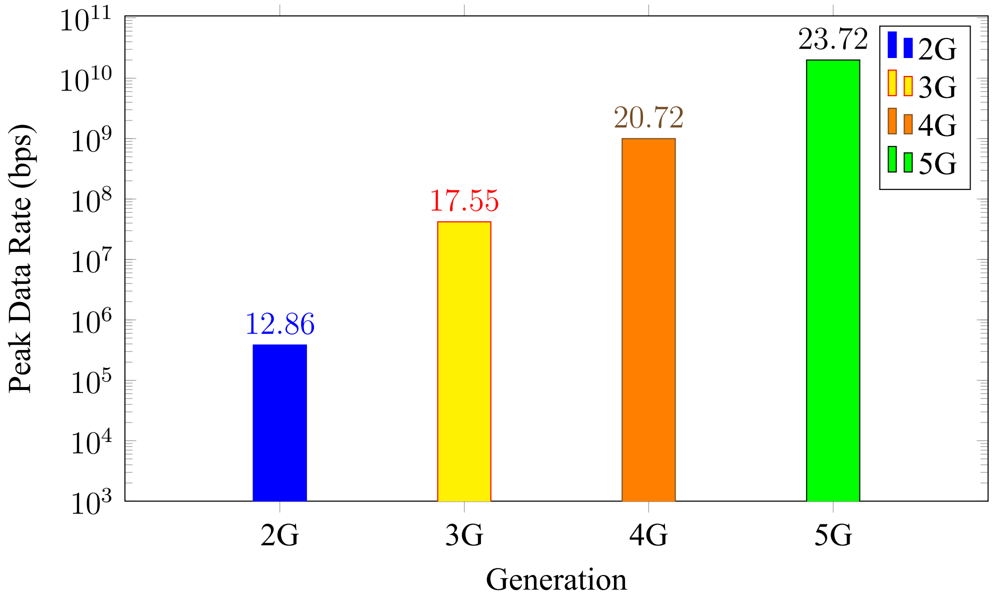

Figure 1.1: Peak Data Rate Comparison for 2G–5G (Log Scale)

Massive MIMO plays a central role in 5G [38, 39], with base stations (BS) deploying dozens to hundreds of antennas [40]. This allows simultaneous spatial multiplexing of many users on the same time frequency resource. Accurate beamforming significantly enhances SNR and reduces inter-user interference, improving reliability and signal quality. By tightly focusing radiation in specific directions, massive MIMO also improves energy efficiency and maximizes spectral utilization crucial for dense urban deployments [41].

Furthermore, 5G and upcoming generations introduces flexible frame structures, edge computing integration, and AI assisted network optimization. These features enable dynamic resource allocation, intelligent scheduling, and real-time adaptation to user mobility and radio conditions. The combination of new spectrum, massive MIMO, and advanced network design positions 5G as a transformative platform for next generation communication services and industrial digitalization.

1.3 Motivation

In the past two decades, wireless communication has undergone an unprecedented transformation driven by the massive increase in mobile subscribers, smart devices, and data hungry applications. The explosive growth of mobile internet traffic has pushed existing

Table 1.1: Comparison of Wireless Communication Generations from 2G to 5G

Generation	Example Standards	Peak Data Rate	Typical Data Rate	Key Services Enabled
2G	GSM, CDMA	9.6 kbps-384 kbps (EDGE)	5-150 kbps	Voice, SMS, basic data
3G	UMTS, WCDMA, CDMA2000	384 kbps-42 Mbps (HSPA+)	1-10 Mbps	Mobile Internet, email, early streaming
4G	LTE, LTE-A	100 Mbps-1 Gbps	10-100 Mbps	HD video, online gaming, mobile broadband
5G and Beyond	5G NR	10-20 Gbps	100 Mbps-several Gbps	VR/AR, autonomous systems, IoT, URLLC

radio frequency (RF) communication systems close to their operational limits. As highlighted by the Federal Communications Commission (FCC), the total amount of licensed RF spectrum allocated for commercial communication has already become insufficient to handle the rapid expansion in wireless users and services, making spectrum scarcity a critical concern [42]. Forecasts indicate that, if the current rate of demand continues, the RF spectrum may reach complete saturation by 2035 [43], posing significant challenges for the continued evolution of mobile broadband systems.

Industry reports further illustrate the scale of this ongoing transformation. According to the latest Cisco global networking study, nearly 66% of the world population is now connected to the internet, with an estimated 30 billion devices actively linked through wireless networks [44]. A substantial share of these devices belongs to smartphone users, IoT systems, industrial controllers, autonomous vehicles, and machine type communications, all of which continuously generate data traffic. As depicted in Fig. 1.2, nearly 2.4 billion users have already migrated to 5G communication networks. Moreover, the 2024 Ericsson mobility report estimates that by 2030, approximately 75 to 80% of all mobile data traffic worldwide will originate from 5G enabled devices [45]. This surge is driven by a wide range of modern services, including ultra high definition video streaming, augmented and virtual reality, real-time cloud gaming, industrial automation, autonomous systems, remote healthcare, and large scale Internet of Things (IoT) deployments.

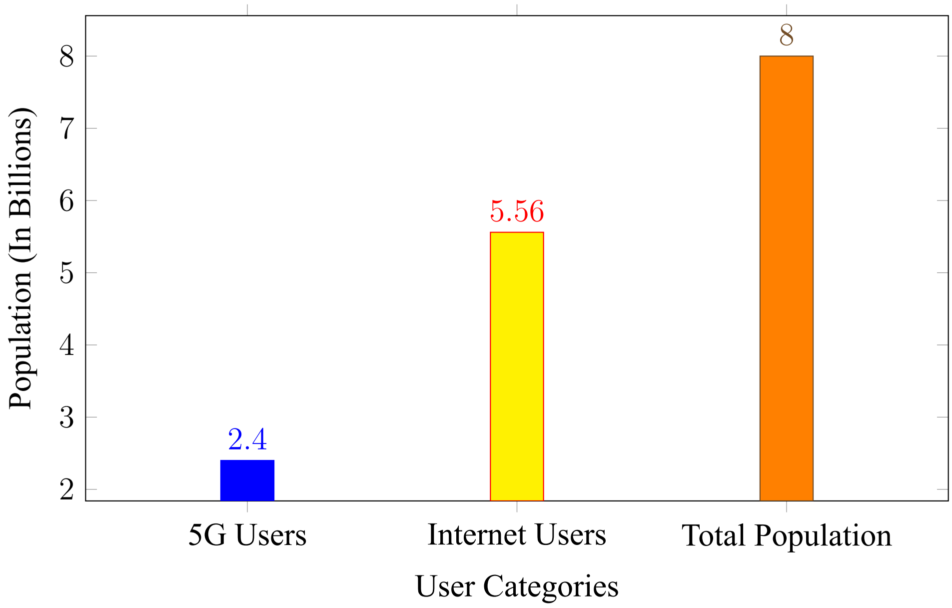

Figure 1.2: Comparison of total population, internet users, and 5G users globally (in billions).

However, such rapid expansion places tremendous pressure on the RF spectrum, which is inherently limited, heavily regulated, and shared among multiple services including mobile communication, radar, satellite systems, broadcast television, defense applications, and emergency services. Because the traditional RF bands are highly congested, simply allocating additional bandwidth is no longer sufficient. Instead, the wireless industry has shifted toward technologies that improve spectral efficiency, capacity, and communication reliability within the same or even smaller frequency resources.

This necessity has led to the development of several advanced wireless technologies, such as millimeter-wave (mmWave) transmission [46], coordinated multipoint communication [47], massive multiple-input multiple-output (MIMO) systems, intelligent reflecting surfaces (IRS) [48], dynamic spectrum sharing [49], advanced channel coding [50], and interference aware beamforming techniques [51]. Massive MIMO, in particular, represents a major technological milestone, as it leverages large antenna arrays to exploit spatial degrees of freedom, allowing multiple users and data streams to be served simultaneously within the same bandwidth. This significantly enhances system throughput, spectral efficiency, link reliability, and user experience while supporting high density deployments such as smart cities, stadiums, and transportation hubs.

Therefore, modern wireless communication research and deployment efforts focus not only on achieving higher data rates, but also on ensuring robustness, energy efficiency, scalability, and sustainable growth. With billions of devices expected to connect to future wireless ecosystems, the evolution of wireless communication is driven by continuous innovation in signal processing, antenna design, channel modeling, and intelligent resource management. Meeting the growing user demand while effectively managing the limited RF spectrum remains one of the most critical engineering challenges of the current and future communication era.

1.4 Massive MIMO Systems

To address the above challenges, the exploration of advanced communication and antenna technologies that can extract more capacity from the same limited bandwidth has become crucial. Among the various solutions proposed, massive MIMO systems [52] has emerged as one of the most promising and effective techniques. Unlike conventional RF systems that rely mainly on increasing transmission power or acquiring new spectrum, massive MIMO increases system capacity by exploiting spatial domain resources. It employs a large number of antennas at the BS, enabling spatial multiplexing, where multiple independent data streams can be transmitted simultaneously to different users using the same time frequency resources. This effectively increases throughput without requiring additional bandwidth [53].

Massive MIMO also enhances spectral efficiency, improves link reliability, and reduces interference by enabling highly directional beamforming. With narrow, steerable beams, power is focused toward intended users rather than radiating broadly, significantly improving signal-to-noise ratio (SNR) and reducing power wastage. Additionally, channel hardening in massive MIMO systems makes the channel response more deterministic as the number of antennas increases, improving system robustness.

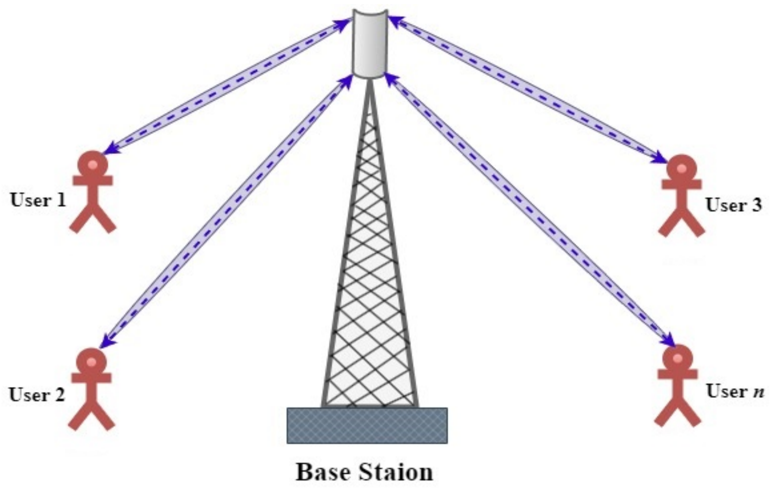

Figure 1.3: Simple Transmitter and Receiver MIMO Architecture

Because of these advantages, massive MIMO is considered a key enabler in 5G and beyond systems, where the need for high capacity and dense connectivity is paramount. It allows operators to support more users, higher data rates, and emerging applications such as autonomous vehicles, AR/VR services [54], industrial automation, smart grids, and tactile Internet without demanding large expansions of spectrum resources. Therefore, massive MIMO is not just a performance improvement but a strategic approach to overcoming the fundamental limitations of RF spectrum scarcity, making it one of the most important technologies shaping the evolution of future wireless communication networks.

Key features of massive MIMO systems are as follows:

- **Large scale antenna arrays:** Massive MIMO employs very large antenna arrays often hundreds of antennas at the BS to serve many users simultaneously over the same time-frequency resources. This large spatial dimension enables highly directional beamforming and fine grained spatial multiplexing, dramatically increasing system capacity and spectral efficiency. As a result, more users can be supported with higher data rates and improved link reliability.

- **High spectral efficiency:** By transmitting to many users over the same time-frequency resources through spatial multiplexing, massive MIMO significantly increases spectral efficiency. Each user is served through highly directional beams, minimizing mutual interference. This allows the same spectrum to be reused multiple times within the same cell. Consequently, system throughput improves by an order of magnitude compared to MIMO systems.

- **Improved energy efficiency:** Massive MIMO uses focused beamforming to direct signal energy only toward active users instead of broadcasting in all directions. This reduces unnecessary radiation and lowers overall transmit power requirements. Since many low-power amplifiers replace a few high-power ones, energy consumption is greatly reduced. This makes massive MIMO highly suitable for green and sustainable wireless networks.

- **Enhanced reliability:** The large number of antennas in massive MIMO provides strong spatial diversity, effectively mitigating fading and shadowing. This improves link stability and suppresses inter-user and inter-cell interference, ensuring reliable communication even in dynamic environments.

- **Spatial multiplexing:** Massive MIMO transmits multiple independent data streams to different users over the same time-frequency resources by separating them spatially. This enables near-linear capacity growth with the number of antennas, resulting in very high data rates.

- **Channel hardening:** As the antenna count increases, small-scale fading averages out across the array, a phenomenon known as channel hardening. This makes the channel more stable and predictable, improving reliability and simplifying system design.

- **Dependence on accurate CSI:** The performance of massive MIMO relies heavily on accurate channel state information (CSI). Precise CSI enables effective beamforming and interference mitigation, while estimation errors can significantly degrade system performance.

- **Feedback overhead challenges:** In frequency division duplex (FDD) systems, CSI must be fed back from the user to the BS, which becomes extremely costly as antenna numbers grow. The feedback overhead scales with the product of transmit and receive antennas. This creates bandwidth, latency, and energy challenges. As a result, CSI compression, sparsity exploitation, and deep learning (DL)-based feedback reduction schemes have become active research areas.

1.4.1 Massive MIMO CSI Feedback Limitations

In massive MIMO systems, overall performance relies heavily on obtaining accurate CSI, which represents the known properties of the wireless propagation channel. CSI explains how signals travel from the transmitter to the receiver under the combined influence of scattering, multipath fading, shadowing, and distance dependent power loss. In FDD systems, the downlink CSI is first estimated at the user equipment (UE) using pilot signals transmitted by the BS. Since channel reciprocity does not hold in FDD, this estimated CSI must then be fed back from the UE to the BS through a limited capacity uplink control channel. However, due to the large number of antennas at the BS, the CSI dimension becomes very high, leading to excessive feedback overhead. As the number of antennas increases in massive MIMO, the channel dimension grows proportionally, making CSI feedback substantially more complex. This creates significant CSI feedback overhead, consuming valuable uplink bandwidth and increasing system latency. The need to frequently update CSI due to channel variations makes the problem even more challenging for high mobility users.

Additionally, in realistic wireless environments, massive MIMO channels often exhibit sparse behavior, where only a few dominant propagation paths contribute significantly to the channel response. While sparsity can theoretically simplify estimation, it also introduces vulnerability, the channel becomes more sensitive to noise, estimation errors, and rapid time variations. If sparse CSI is inaccurately estimated or outdated, it leads to channel mismatch, reduced beamforming gain, degraded spatial multiplexing performance, and lower spectral efficiency. Therefore, although massive MIMO promises substantial capacity and reliability enhancements, its practical implementation remains limited by heavy CSI acquisition requirements, strict feedback constraints, and the inherently unreliable and time varying nature of sparse wireless channels.

CSI refers to the comprehensive knowledge of the properties of a wireless communication channel, usually represented by the channel gain matrix [55]. It characterizes how a transmitted signal propagates through the wireless medium from the transmitter to the receiver. This includes the combined effects of reflection, scattering, refraction, multipath fading, Doppler spread, and power attenuation with distance. By knowing channel matrix, the transmitter and receiver can understand how each antenna path modifies the amplitude and phase of the transmitted signal. CSI can be classified as either instantaneous (short term) or statistical (long term). Instantaneous CSI reflects the channel conditions at a specific moment in time, while statistical CSI models the long term behavior of the channel. In modern multi-antenna systems, such as MIMO and massive MIMO, CSI is crucial for enabling advanced techniques like beamforming, power optimization, adaptive modulation and coding, and spatial multiplexing [56].

The importance of CSI lies in its direct influence on wireless system reliability, efficiency, and data throughput. Accurate CSI allows transmitters to dynamically adapt transmission parameters based on real-time channel variations, ensuring higher data rates and better link quality. For example, when channel conditions are favorable, higher order modulation schemes such as 64-QAM or 256-QAM can be used; when the channel deteriorates, the system can switch to more robust modulation and coding. In MIMO systems, CSI enables spatial multiplexing, allowing multiple data streams to be transmitted simultaneously over the same frequency band, thereby significantly increasing spectral efficiency significantly. However, obtaining precise CSI becomes challenging in large scale systems due to increased dimensionality, mobility of users, and environmental changes. Systems like massive MIMO require frequent and large CSI feedback, which leads to huge computational burden and signaling overhead. Therefore, CSI remains a fundamental yet technically demanding aspect of modern wireless communication system design.

1.4.2 Compressive Sensing for CSI Feedback Reduction

Compressed Sensing (CS)-based methods [57] utilize the sparsity of wireless channels to reduce the feedback overhead in massive MIMO systems. By assuming that only a small number of dominant channel components are significant, CS reconstructs the full channel information from fewer measurements, helping to reduce the required feedback bandwidth. However, these methods also face several limitations in practice. Their performance is heavily dependent on the assumption of channel sparsity, which may not always hold true in realistic propagation environments where channels are less structured or rapidly varying [58].

Additionally, CS-based techniques often require computationally expensive operations, such as large scale discrete Fourier transform (DFT) calculations, making real-time implementation challenging in large systems [59]. When the channel is not sufficiently sparse, reconstruction accuracy degrades significantly, leading to poor CSI quality and reduced communication performance. Therefore, despite their theoretical advantages, CS-based methods demand new, adaptive, and more efficient CSI feedback mechanisms to ensure robust performance under practical wireless conditions.

1.4.3 DL-Assisted CS for CSI Feedback Reduction

DL, a specialized branch of machine learning, is primarily driven by artificial neural networks (ANNs) [60], which are computational models inspired by the structure and functioning of human brain neurons. An ANN consists of interconnected processing nodes (neurons), and unlike traditional algorithms that rely heavily on handcrafted mathematical modeling, DL learns complex patterns directly from data. This data-driven learning approach enables DL to model highly nonlinear relationships, making it suitable for complicated signal processing tasks such as CSI compression, prediction, and reconstruction in massive MIMO systems [61]. Unlike conventional frameworks where fixed mathematical formulas dictate the system behavior, DL-based systems store information across the network weights, offering improved reliability, adaptive learning capability, and fault tolerance in the presence of channel variability.

In the context of CSI acquisition and feedback, DL-based methods bring significant advantages over traditional approaches such as CS [62]. First, DL eliminates the requirement for strict sparsity assumptions and instead learns channel structure from real or simulated datasets, allowing it to adapt to practical channels that may not always be sparse. Second, DL can achieve very high compression efficiency, significantly reducing the CSI feedback load while still maintaining strong reconstruction performance. Through trained neural autoencoders or deep CNN/Transformer-based networks, the system can learn compact channel representations and reconstruct full CSI at the receiver with high accuracy. This helps mitigate the large feedback overhead challenge that affects massive MIMO systems, especially in FDD-based architectures.

Moreover, DL-based methods provide improved robustness under noisy transmission conditions, rapid channel fluctuations, and hardware impairments [63]. Since the learning process incorporates real world channel distortions and nonlinear propagation effects, DL models can exploit their internal learned representations to achieve better generalization and higher accuracy compared to classical statistical or CS-based estimators. These benefits compression efficiency, accurate reconstruction, and robust performance under interference and noise make deep learning a powerful and scalable solution for next-generation wireless communication systems, enabling more efficient and reliable CSI feedback in large scale massive MIMO deployments.

Here are some important features and limitations of DL:

DL, a powerful subset of machine learning based on artificial neural networks (ANNs), has emerged as a transformative tool for modern wireless communication systems. By mimicking the learning behavior of biological neurons through interconnected layers, ANNs are capable of capturing highly complex nonlinear relationships in data. This makes DL particularly well suited for data-driven modeling tasks such as CSI compression, reconstruction, channel estimation, and beamforming in massive MIMO systems. Unlike traditional model-based approaches, DL learns directly from data, allowing it to adapt to dynamic wireless environments and hardware imperfections with minimal prior assumptions.

One of the most significant advantages of DL in massive MIMO lies in its ability to achieve high compression efficiency and superior reconstruction accuracy. DL-based CSI feedback frameworks can extract compact yet highly informative representations of high-dimensional channel matrices, substantially reducing feedback overhead especially critical in FDD systems. At the receiver, DL enables highly accurate CSI reconstruction, which directly improves channel estimation, precoding, and overall system throughput. Moreover, DL models exhibit strong robustness to noise, interference, and real-world channel impairments, ensuring reliable performance even under challenging propagation conditions.

Despite these advantages, DL also introduces several important challenges in large-scale wireless systems. Training deep models requires massive CSI datasets to achieve high accuracy and generalization capability, which can be difficult and costly to obtain. The computational complexity of deep networks is high, leading to increased energy consumption and latency, particularly in real-time massive MIMO deployments. Furthermore, DL models may suffer from slow convergence when dealing with very high-dimensional channels, making their direct implementation in practical large-scale systems more challenging without further optimization and model compression techniques.

1.4.4 Transform-Assisted DL-Driven Frameworks

ANNs have demonstrated strong learning capability for complex wireless communication tasks, including CSI compression and reconstruction. However, their application in massive MIMO systems brings several challenges. As the dimensionality of CSI increases with the number of antennas, ANN-based models require large training datasets to learn meaningful relationships, making data collection and labeling expensive. Moreover, the computational effort required to train deep ANN architectures becomes significant, leading to slow convergence, high memory usage, and increased processing time. This complexity translates into higher power consumption, making standard ANN solutions less practical for real-time deployment in large scale massive MIMO systems.

To overcome these drawbacks, the thesis proposes Transform-assisted DL frameworks that combine the adaptability of neural networks with the mathematical efficiency of signal transforms. Instead of relying solely on deep layers to learn feature representations, the proposed models utilize transforms such as the discrete Rajan transform (DRT), discrete Hadamard transform (DHT), and a noise-aware DeNoNet structure to extract compact and discriminative CSI features. This hybrid approach reduces the dependency on excessively deep architectures and minimizes the overall number of trainable parameters. As a result, the models achieve faster convergence, lower computational cost, and reduced energy consumption, addressing key limitations of conventional ANN-based solutions.

Furthermore, by incorporating transform domain processing before neural decoding, the proposed frameworks deliver better performance in noisy, dynamic, and practical deployment environments. The transforms help in compactly representing CSI, allowing more efficient encoding and transmission with significantly lower feedback overhead. Meanwhile, the neural network components ensure robust reconstruction and improved nonlinear approximation capability. Together, this synergy results in substantial improvements in reconstruction accuracy, resilience to interference, and scalability for future 5G and beyond wireless systems, offering a practical and high performance solution for massive MIMO CSI feedback.

ANNs have shown strong potential for CSI processing in massive MIMO systems. However, they suffer from several critical limitations. Large-scale ANN models incur high computational complexity due to the massive number of parameters required to learn high-dimensional CSI. Their performance is also heavily dependent on the availability of large labeled training datasets, which are difficult and costly to obtain in practical wireless environments. Furthermore, ANN training often experiences slow convergence when dealing with high-dimensional channel data, and the extensive matrix computations lead to high energy consumption, making direct ANN deployment challenging for real-time, large-scale wireless systems.

The need for efficient CSI feedback mechanisms is therefore increasingly critical in massive MIMO, especially in FDD systems where downlink CSI must be explicitly fed back to the BS. As the number of antennas grows, the CSI dimension increases drastically, causing severe feedback overhead, latency, and signaling congestion. This feedback burden directly limits real-time deployment, system scalability, and overall spectral efficiency. Consequently, efficient CSI compression and accurate reconstruction have become fundamental requirements for practical massive MIMO operation.

To address these challenges, transform-assisted deep learning frameworks have emerged as a powerful solution. These approaches integrate mathematical transforms such as DRT, DHT, and DeNoNet with neural networks to first obtain a compact and sparse CSI representation before neural processing. This strategy significantly reduces the number of trainable parameters, lowers processing time, and improves convergence speed. Moreover, transform-domain sparsification enhances reconstruction accuracy and robustness to noise, while also enabling a substantial reduction in CSI feedback overhead. As a result, these hybrid frameworks offer faster learning, lower energy and computational requirements, and superior performance under practical wireless channel conditions, making them highly suitable for real-time deployment in 5G and upcoming 6G massive MIMO systems.

1.4.4.1 Transform Selection Criteria for CSI Compression

The selection of a transform for CSI compression should be based on a set of mathematical, statistical, and implementation oriented criteria rather than solely on reconstruction performance. A suitable transform should generate a sparse and compact representation of the channel while preserving the essential information required for accurate reconstruction. The primary criterion is energy compaction, which measures the ability of a transform to concentrate most of the channel energy into a small number of coefficients. This can be quantified as

$$E_K = \frac{\sum_{i=1}^{K} |x_i|^2}{\sum_{i=1}^{N} |x_i|^2}, \tag{1.1}$$

where $\boldsymbol{x} = T\boldsymbol{h}$ denotes the transformed CSI vector and $K \ll N$. A larger value of E_K indicates that the transform captures most of the channel information using fewer coefficients, thereby enabling higher compression efficiency. Closely related to energy compaction is sparsity generation, which reflects the ability of the transform to reduce the number of significant coefficients. Greater sparsity directly translates into lower CSI feedback overhead and more effective DL-based compression.

Beyond sparsity, a suitable transform should exhibit strong de-correlation capability, information preservation, and robustness to noise. Massive MIMO channels contain significant spatial and frequency-domain correlations, and an effective transform should reduce these correlations so that the transformed coefficients become nearly independent. Furthermore, the transform should preserve the essential characteristics of the original CSI, which can be evaluated using metrics such as NMSE and cosine similarity. Since practical wireless environments are affected by noise, interference, mobility, and channel estimation errors, the transformed representation should maintain its sparsity and energy-compaction properties even under perturbations. A transform whose coefficient distribution remains stable under varying channel conditions is generally more reliable for real-world deployment.

DFT is particularly effective for channels exhibiting strong stationary and frequency selective characteristics. In environments where the channel contains well defined angular-delay structures and dominant multipath components remain relatively stable, the sinusoidal basis functions of the DFT provide excellent energy compaction and sparse representations. The availability of efficient FFT implementations further makes the DFT computationally attractive with complexity $O(N \log N)$. However, because the DFT relies on a fixed sinusoidal basis, its performance may degrade when the channel becomes irregular, only approximately sparse, or subject to changes in antenna ordering and scattering patterns.

DRT is more suitable for irregular, non-stationary, and dynamically varying channels. Its recursive basis structure enables it to adapt more effectively to localized channel features, non-uniform energy distributions, and time-varying propagation conditions. Consequently, DRT often achieves superior sparsity and energy concentration in channels that do not conform well to conventional Fourier-domain representations.

DHT is particularly attractive when computational efficiency and hardware simplicity are primary design objectives. The DHT employs orthogonal binary basis functions consisting only of $+1$ and -1, allowing implementation through additions and subtractions without requiring multiplications. This property significantly reduces computational complexity, power consumption, and hardware cost, making it highly suitable for resource-constrained user equipment and real-time CSI feedback systems. In addition, the DHT preserves signal energy through its orthogonal structure and often provides strong energy compaction for highly correlated massive MIMO channels. Therefore, a general transform-selection framework should jointly consider energy compaction, sparsity, decorrelation capability, reconstruction fidelity, robustness, and computational complexity. Under this framework, DFT is preferred for spectrally structured and stationary channels, DRT is advantageous for irregular and dynamically varying channels, and DHT is particularly effective for highly correlated massive MIMO channels where both reconstruction performance and hardware efficiency are critical design requirements.

1.4.5 Impact of Sparse CSI Estimation Accuracy on Beamforming, Spatial Multiplexing, and Spectral Efficiency

The accuracy of sparse CSI estimation is fundamentally linked to beamforming gain, spatial multiplexing performance, and spectral efficiency because CSI serves as the basis for all transmission decisions at the BS. In massive MIMO systems, beamforming vectors are designed using the estimated CSI to direct energy toward the intended user. When the sparse CSI is estimated accurately, the beamforming vector closely aligns with the true channel direction, resulting in maximum array gain and received signal power. However, if the CSI is inaccurately estimated or becomes outdated due to feedback delay, a mismatch occurs between the actual channel and the estimated channel. This mismatch causes beam misalignment, reduces the received signal strength, and increases interference leakage to other users. Consequently, the effective SNR decreases, leading to lower data rates and reduced spectral efficiency.

The impact is even more significant in spatial multiplexing systems, where multiple data streams are transmitted simultaneously using the spatial dimensions of the channel. Accurate CSI is required to separate users and data streams effectively and to design precoders that minimize inter-stream interference. Errors in sparse CSI estimation distort the channel subspace and weaken the orthogonality between different transmission paths, resulting in increased interference and degraded multiplexing performance. Since spectral efficiency depends directly on the achievable SNR and the number of reliably supported spatial streams, any reduction in CSI accuracy ultimately translates into lower system capacity and throughput. Therefore, sparse CSI estimation accuracy is not merely a reconstruction quality metric, it directly determines the effectiveness of beamforming, the achievable spatial multiplexing gain, and the overall spectral efficiency of the wireless communication system. This relationship should indeed be clearly introduced in the introductory chapter to emphasize the practical importance of accurate CSI compression and reconstruction.

1.5 Thesis Structure and Contributions

The structure of the thesis are as follows:

Chapter 1: Introduction–This chapter provides an overview of the fundamental concepts and existing mechanisms related to CSI acquisition and feedback in massive MIMO systems. It discusses the limitations of traditional CS-based techniques and highlights the motivation for adopting DL-based approaches to enhance compression efficiency, reconstruction accuracy, and robustness under practical conditions. The chapter further outlines the key challenges addressed in this research work and briefly introduces the transform-assisted DL frameworks proposed in this thesis as potential solutions to overcome these limitations.

Chapter 2: A Review on DL applications in CSI Feedback Reduction–This chapter explores the existing literature on the researches on CSI feedback reduction in massive MIMO. Recent research on CSI feedback has focused on enhancing compression efficiency and reconstruction accuracy through both CS and DL methods. Adaptive CS-based techniques exploit spatial and block sparsity to reduce pilot overhead and complexity, while iterative models like LASSO and AMP-Net improve sparse signal recovery. DL-based frameworks such as CsiNet and CsiNet+ employ end-to-end encoder decoder architectures for compact CSI representation. Extensions including CRNet, PRVNet, TransNet, DeepAE and CSI-StripeFormer leverage multi resolution and Transformer based mechanisms for higher accuracy. Despite their success, high computational demands motivate hybrid transform integrated DL architectures for scalable and energy efficient CSI feedback.

Chapter 3: DRT-Assisted DL for Massive MIMO CSI Feedback Reduction–This chapter introduces the importance of minimizing CSI feedback overhead which is a critical requirement in 5G and upcoming 6G massive multiple input multiple output (MIMO) systems. Although CS-based techniques have been explored to tackle this issue, the use of the DFT introduces considerable computational complexity. To overcome this limitation, this study proposes a novel DRT-based DL framework for efficient CSI feedback enhancement in massive MIMO networks. Simulation results demonstrate that the proposed DRT-based model achieves performance gains of 126.19% and 81.81% in cosine correlation and normalized mean square error (NMSE), respectively, compared to the conventional DFT-based DL approach across various signal-to-noise ratio (SNR) conditions. Furthermore, the DRT-based algorithm exhibits robust performance under low SNR environments, underscoring its suitability for practical large scale wireless communication systems.

Chapter 4: Hadamard Transform Enhanced DL for Massive MIMO CSI Feedback Reduction–Building upon the concept of transform-based learning, we presents HaDLeMO, a deep learning framework leveraging the DHT. The DHT offers low computational complexity, permutation invariance, and high energy compaction, enabling efficient CSI representation within a CS-DL architecture. Through extensive simulations, HaDLeMO demonstrates significant performance gains achieving improvements of 109.52% in cosine correlation and 257.14% in NMSE compared to the DFT-based DL algorithm. The method exhibits rapid convergence, reduced training complexity, and resilience across diverse SNR scenarios, making it a practical candidate for large scale 5G/6G massive MIMO systems.

Chapter 5: Deep Learning Based Denoising in FDD Massive MIMO–In this Chapter, our research introduces DeNoNet, a DL-based denoising network designed to handle the effects of channel interference, noise, and nonlinearities in CSI feedback. DeNoNet encodes CSI into compact, noise resistant representations that facilitate accurate reconstruction under degraded conditions. Simulation analysis indicates that DeNoNet surpasses the DRT-based DL approach by 113.18% in NMSE and 72.72% in cosine correlation (ρ). The model performs exceptionally well under low SNR conditions, where traditional models typically fail, validating its robustness and adaptability for real time wireless communication environments.

Chapter 6: CDN and its Comparison with CNN for CSI Feedback Reduction in Massive MIMO–To further validate the effectiveness of the proposed frameworks, this chapter evaluates the performance of Convolutional Neural Network (CNN) and Channel Denoising Network (CDN) architectures against the baseline DeepAE model. The results show that the CNN-based DFT model achieves a cosine similarity of 0.770, while the CDN model improves this to 0.890, compared to 0.567 for DeepAE. Similarly, NMSE improves from -5.33 (DeepAE) to -11.42 (CNN-based DFT) and -16.30 (CDN). These consistent gains across SNR levels up to 10 dB demonstrate the superior noise handling capabilities and structural efficiency of the proposed DL- based methods. Furthermore, both the CNN-based DFT and CDN frameworks show strong performance in low SNR environments, underscoring their suitability for real world 5G/6G applications that demand reliability under varying channel conditions.

Chapter 7: Conclusion–This chapter summarizes the key outcomes of the research focused on efficient CSI feedback in massive MIMO systems using transform-assisted DL frameworks. It highlights how the proposed DRT, DHT (HaDLeMO), and DeNoNet architectures achieve improved accuracy, robustness, and computational efficiency compared to conventional DFT-based and autoencoder-based models. The chapter concludes that hybrid mathematical-neural approaches effectively capture channel sparsity and offer a promising direction for low complexity, high performance CSI feedback in future 6G networks.

1.5.1 Contributions

The major contributions of this thesis are summarized as follows:

1. A comprehensive investigation of conventional CS and state-of-the-art DL-based CSI feedback techniques for massive MIMO systems has been carried out, identifying their limitations in terms of computational complexity, reconstruction accuracy, and robustness under practical wireless channel conditions.

2. A novel DRT-assisted deep learning framework has been proposed for CSI compression and reconstruction. By exploiting the sparsity-enhancing capability of DRT, the proposed framework achieves performance improvements of 126.19% in cosine correlation and 81.81% in NMSE compared with the conventional DFT-based DL approach.

3. A HaDLeMO has been developed by integrating the DHT with a deep learning architecture. The proposed framework leverages the low-complexity, orthogonal, and permutation-invariant properties of DHT to achieve efficient CSI representation, resulting in improvements of 109.52% in cosine correlation and 257.14% in NMSE over the DFT-based baseline.

4. A DL-based DeNoNet has been designed to mitigate the effects of channel noise, interference, and nonlinear distortions during CSI feedback. The proposed denoising framework improves reconstruction robustness and achieves gains of 113.18% in NMSE and 72.72% in cosine correlation compared with the DRT-based DL framework.

5. A CDN has been developed and evaluated against CNN-based and DeepAE-based CSI feedback models. Experimental results demonstrate superior reconstruction

performance, achieving a cosine similarity of 0.890 and an NMSE of -16.30 dB, outperforming existing benchmark approaches.

6. Extensive simulation studies have been conducted under various compression ratios, SNR conditions, antenna dimensions, and noisy channel environments. The results validate the effectiveness, robustness, and scalability of the proposed transform-assisted DL frameworks for CSI feedback in massive MIMO systems.

7. The thesis demonstrates that the integration of mathematical transforms with deep learning provides a low-complexity, energy-efficient, and highly accurate CSI feedback solution, making the proposed frameworks promising candidates for practical deployment in future 5G and beyond-6G massive MIMO networks.

Chapter 2

A Review on DL-Based CSI Feedback Reduction in Massive MIMO

In this chapter, a comprehensive literature review on CSI feedback reduction for massive MIMO systems is presented. The discussion highlights key methodologies, their strengths, limitations, and the evolution of strategies aimed at improving CSI compression, reconstruction accuracy, and robustness in practical wireless environments. As mentioned in Chapter 1, DL has emerged as a powerful solution for addressing the critical challenge of CSI feedback reduction in massive MIMO systems for 5G and beyond. Traditional compressed sensing and codebook-based schemes struggle with high dimensionality, low-SNR operation, and non-sparse channel conditions. DL-based architectures including CsiNet [64], CsiNet+ [65], CRNet [66], TransNet [67], PRVNet [68], and attention or transformer-driven models have demonstrated remarkable capability in learning compact representations of CSI through end-to-end autoencoders. These methods significantly reduce feedback overhead, improve reconstruction accuracy, and enhance robustness against noise, mobility, and hardware imperfections. Recent advances incorporate domain transforms, multi-rate learning, denoising modules, and hybrid signal DL processing to further boost efficiency and adaptability in real world environments [69]. Our focus in this thesis is on domain transforms and denoising models for CSI-feedback reduction in massive MIMO systems.

2.1 Overview

Accurate downlink CSI at the transmitter is essential for beamforming, precoding, and spatial multiplexing in multi-antenna wireless systems. In FDD massive MIMO, the BS cannot rely on uplink-downlink reciprocity and therefore depends on explicit CSI feedback from the UE [70]. As antenna counts grow into the tens or hundreds, due to uplink bandwidth limits and computational complexity, direct feedback of the entire downlink CSI is no longer possible. Conventional CS frameworks [71] exploit sparse channel representations in a transform domain to reduce dimensionality. However, in practice CS frameworks suffer from performance loss when channels are not strictly sparse and from the high complexity of iterative solvers and DFT-based transforms. These limitations have motivated the application of DL to learn compact, nonlinear mappings between high dimensional CSI and low dimensional codewords, enabling dramatic reductions in feedback overhead while improving reconstruction fidelity [72, 73].

2.1.1 Basic Introduction

With rapid globalization and unprecedented advancements in technology, modern wireless networks are experiencing explosive growth in data traffic. To accommodate these escalating demands, cellular infrastructures are now deployed with much smaller inter site distances. Often these distances are around a few hundred meters. On the other hand, wireless local area networks (WLANs) have become ubiquitous across homes, commercial establishments, and public environments [4]. Beyond the surge in mobile broadband usage, emerging paradigms such as the Internet of Things (IoT) [74], machine-to-machine (M2M) communication [75], Industry 4.0 [76], and smart city ecosystems collectively generate massive [77], continuous volumes of wireless traffic. Consequently, users increasingly depend on high speed, low latency connectivity for video calling, ultra-HD streaming, online gaming, virtual collaboration, and engagement with social media platforms. These services have been made possible by the evolution of wireless technologies from 3G systems to 4G LTE, and more recently to 5G networks, which offer enhanced reliability, drastically reduced latency, and multi gigabit data rates.

Early generations of cellular communication followed the concept of dividing a geographic region into cells. Each cell was served by a fixed base station. These systems initially relied on single input single output (SISO) antenna configurations which used one transmit antenna and one receive antenna [78]. While SISO systems are simple and easy to implement, they offered limited capacity, poor spectral efficiency, and were highly susceptible to multipath fading. To address these limitations, MIMO systems were introduced [79]. MIMO employed multiple antennas at both the transmitter and receiver, enabling spatial diversity, spatial multiplexing, and improved robustness against fading. This innovation dramatically enhanced data throughput and spectral efficiency without requiring additional bandwidth or increased transmit power. MIMO marked a transformative milestone in wireless communication.

However, as global data consumption surged due to smartphones, real time applications, IoT connectivity, and the demands of 5G use cases, conventional MIMO systems sufficed limitations. These limitations led to the emergence of massive MIMO [80], where base stations are equipped with tens to hundreds of antennas. Massive MIMO delivers substantial gains in spectral efficiency, user capacity, and energy efficiency by forming highly directional beams and achieving large scale spatial multiplexing. Modern 5G and upcoming 6G networks extend this paradigm further by integrating massive MIMO with advanced technologies such as millimeter wave (mmWave) communications, hybrid analog digital beamforming [81, 82], reconfigurable intelligent surfaces (RIS) [83, 84], and AI-driven channel estimation [85, 86]. These advancements collectively enable ultra high data rates, extremely low latency, massive device connectivity, and robust performance under diverse propagation conditions forming the backbone of next generation wireless communication systems.

2.1.2 Important Techniques for 5G and Next Generations

To achieve the challenging performance objectives of 5G and future 6G wireless networks, a range of advanced enabling technologies has been proposed and extensively investigated. These next-generation systems are driven by innovations such as millimeter-wave (mmWave) communication for multi-gigabit data rates, ultra-dense small-cell deployments for improved coverage, and intelligent beamforming for highly directional and energy efficient transmission. In addition, emerging paradigms including device-centric architectures, full-duplex communication, terahertz (THz) bands, visible light communication (VLC), and massive MIMO systems significantly enhance network capacity and flexibility. With, these technologies form the foundation for supporting ultra-high throughput, low latency, massive connectivity, and superior spectral efficiency required in 5G and beyond networks.

Traditionally, cellular communication has operated below 6 GHz, while higher frequencies have been reserved for applications such as medical imaging, remote sensing, and radio astronomy [87]. However, the exponential growth in mobile data traffic has resulted in severe spectrum overload, limiting per user bandwidth and degrading service quality. To address this challenge, research has increasingly focused on extending wireless communication to frequencies above 6 GHz, particularly mmWave bands [88]. Operating in the 30–300 GHz range, mmWave communication offers bandwidths nearly ten times larger than the entire 4G spectrum [89]. Despite this potential, mmWave signals suffer from high path loss, limited penetration, and sensitivity to blockages and rain attenuation, which have historically restricted their use in mobile broadband [90, 91].

As data demand continues to accelerate and 6G development progresses, spectrum beyond mmWave is becoming essential. The THz band (300 GHz–3 THz) provides vast unused bandwidth and offers advantages such as low interference, enhanced security, compact antennas, and highly directional beams [92, 93]. These properties make THz communication attractive for applications including holographic telepresence, Industry 4.0, and ultra-high speed data transmission. However, THz systems face major challenges, including severe propagation loss, complex antenna and circuit design, and mobility management [94]. To address these issues, ultra-massive MIMO (UM-MIMO) has emerged, utilizing plasmonic materials such as graphene to enable nanoscale antenna arrays capable of operating efficiently in the THz band [95]. While promising, THz UM-MIMO requires further research in channel estimation, beamforming, precoding, and signal processing [96].

Another important enabler for future networks is full-duplex communication, which allows simultaneous transmission and reception on the same frequency band, potentially doubling spectral efficiency [97, 98]. While self interference remains a key challenge, advanced cancellation techniques have demonstrated the feasibility of full-duplex operation in practical systems [99, 100]. VLC represents a complementary short-range optical wireless technology that utilizes the visible spectrum (380–780 nm) for data transmission [101, 102]. By modulating light intensity using IM/DD at imperceptible frequencies above 200 Hz, VLC enables high speed, secure, and interference free communication while maintaining illumination quality [103, 104]. VLC channel characteristics have been studied extensively in indoor, underground, and outdoor environments, demonstrating its suitability for diverse deployment scenarios [105, 106, 107, 108].

Beamforming plays a critical role across massive MIMO and mmWave systems by enabling dynamic shaping and steering of antenna radiation patterns toward intended users while suppressing interference [109]. In massive MIMO, beamforming improves spectral efficiency and reliability through spatial focusing and coordinated transmission from large antenna arrays [110]. For mmWave links, highly directional beams compensate for severe attenuation and extend communication range [111].

2.1.3 Massive MIMO Systems

MIMO technology has become a cornerstone of modern wireless communication systems, enabling significant gains in spectral efficiency, reliability, and energy efficiency. Prior to its introduction, conventional single-input single-output (SISO) systems [112] suffered from low throughput and were incapable of supporting large numbers of users with high reliability. To address growing user demand, several MIMO advancements were developed, including single-user MIMO (SU-MIMO) [113, 3], multi-user MIMO (MU-MIMO) [114, 115, 116, 117], and network MIMO [118, 119].

Single-user MIMO [120] represents the earliest and most fundamental form of multi-antenna communication, where multiple transmit and receive antennas are used to serve a single user over a point-to-point link. The pioneering work by Paulraj et al. [113], demonstrated that employing multiple antennas can significantly increase channel capacity through spatial diversity and spatial multiplexing, without requiring additional bandwidth or transmit power. This concept was further formalized by Foschini et al. [3], who showed that, under rich scattering environments, the capacity of a MIMO channel grows linearly with the minimum number of transmit and receive antennas. In [121], SU-MIMO has been widely adopted in standards such as LTE and Wi-Fi to enhance peak data rates and link reliability. However, since it serves only one user at a time, its scalability is limited in dense networks with many active users.

Multi-user MIMO extends the MIMO concept by allowing a BS equipped with multiple antennas to simultaneously serve multiple users on the same time-frequency resources. Spencer et al. [114], provided an early introduction to MU-MIMO systems, highlighting their ability to significantly improve system throughput by exploiting spatial separation between users. Subsequent works investigated practical aspects such as precoding, scheduling, and performance evaluation under realistic channel conditions [115, 116]. Jiang et al. [117], analyzed multi-user precoding strategies and demonstrated that MU-MIMO can substantially outperform SU-MIMO in terms of spectral efficiency, especially in multi-cell environments. MU-MIMO forms the basis of modern cellular downlink transmission in LTE-Advanced and 5G. However, its performance is highly dependent on accurate CSI and efficient user scheduling.

Network MIMO, also known as coordinated multipoint (CoMP) transmission [122], further generalizes MU-MIMO by allowing multiple BS to cooperate and jointly serve users. Instead of treating inter-cell interference as noise, network MIMO exploits it as a useful signal through joint processing. Hui et al. [118], analyzed the performance benefits of network MIMO and showed that BS cooperation can significantly improve cell-edge user rates. Caire et al. [119], considering the cellular architecture and demonstrated that large-scale cooperation among BS can approach the performance of a single large distributed antenna system. While network MIMO offers notable gains in spectral efficiency and fairness, it introduces substantial challenges related to transportation capacity, synchronization, and CSI sharing, which have limited its large-scale practical deployment.

While these techniques improved performance, they remained insufficient for the exponential rise in wireless devices and data consumption. In addition to mobile users, billions of IoT devices spanning smart healthcare, smart homes, industrial automation, and smart energy have further intensified traffic demands, with projections estimating nearly 50 billion connected devices by 2025. The MIMO solutions deployed in 4G/LTE networks are therefore unable to cope with this unprecedented surge in data volume and reliability requirements.

To overcome these limitations, 5G and beyond networks have turned to massive MIMO, a transformative extension of conventional MIMO that employs large scale antenna arrays comprising hundreds or even thousands of antennas at the base station to simultaneously serve numerous users [123, 124, 125, 126]. By dramatically increasing the number of antennas, massive MIMO enables highly focused and directional beamforming, concentrating radiated energy into narrow spatial regions. This spatial focusing not only enhances the desired user's signal strength but also reduces interference to neighboring users, substantially improving both spectral efficiency and throughput [127]. Numerous studies have demonstrated the significant advantages of massive MIMO over traditional MIMO architectures, highlighting its potential as a key enabler for 5G and future wireless networks [128, 125, 129]. Here different configurations of massive MIMO systems are explained.

2.1.3.1 Co-located Massive MIMO

Co-located massive MIMO refers to the conventional architecture where a large number of antennas are deployed at a single BS site. This is the most studied and standardized form of massive MIMO and forms the backbone of current 5G deployments [130]. Early foundational work by Marzetta [131], established that co-located massive MIMO can achieve near-optimal performance using simple linear processing such as maximum ratio combining (MRC) and zero forcing (ZF) as the number of antennas grows large. Subsequent studies focused on channel hardening, favorable propagation, pilot contamination, and low-complexity precoding and detection schemes [132]. Extensive experimental validations and testbeds have demonstrated that co-located massive MIMO can achieve very high spectral and energy efficiency with relatively simple hardware, making it practical for real-world cellular networks. However, performance degradation at cell edges and pilot contamination remain key challenges.

2.1.3.2 Cell-Free Massive MIMO

Cell-free massive MIMO is an evolution of the co-located [133] architecture in which a large number of geographically distributed access points (APs), each with a few antennas, jointly serve all users without cell boundaries [134]. Introduced to overcome inter-cell interference and edge user performance limitations, cell-free massive MIMO provides uniformly good service quality across the coverage area. Research by Ngo et al. [135] showed that coherent joint transmission from distributed APs significantly improves fairness and spectral efficiency. Subsequent works investigated scalable fronthaul architectures, power control, pilot assignment, and distributed signal processing. While cell-free systems reduce pilot contamination and shadowing effects, they introduce new challenges such as fronthaul capacity constraints, synchronization, and distributed CSI acquisition, which remain active research topics for 5G and beyond-6G systems [136].

2.1.3.3 Terahertz (THz) Massive MIMO

THz [137] massive MIMO extends massive MIMO concepts to the terahertz frequency band (300 GHz-3 THz), which offers enormous unused bandwidth for 5G future 6G communications [138]. Due to extremely high path loss at THz frequencies, very large antenna arrays are required to achieve sufficient beamforming gain. Research in this area focuses on ultra-massive MIMO (UM-MIMO), where thousands of nano-scale antennas are enabled using plasmonic materials such as graphene [139]. Studies have explored THz channel modeling, hybrid beamforming, beam squint effects, and molecular absorption. Although THz massive MIMO promises ultra-high data rates, it faces significant challenges related to hardware realization, channel estimation, beam alignment, and mobility management, making it a long-term research direction rather than an immediate deployment solution [140].

2.1.3.4 Single-User Massive MIMO (SU-Massive MIMO)

Single-user massive MIMO focuses on serving one user with a very large number of BS antennas, primarily to maximize link reliability and peak data rates [141]. Early theoretical work demonstrated that SU-massive MIMO achieves enormous array and diversity gains, making the channel nearly deterministic. Research in this area has concentrated on beamforming design, channel estimation accuracy, and hardware impairments [142]. SU-massive MIMO is particularly attractive for fixed wireless access, backhaul links, and high-reliability communications. However, it does not fully exploit the spatial multiplexing potential of massive MIMO and is therefore often considered a special case or building block for multi-user systems [143, 144].

2.1.3.5 Multi-User Massive MIMO (MU-Massive MIMO)

Multi-user massive MIMO [145] is the most practically relevant form, where a BS simultaneously serves many users on the same time-frequency resources using spatial multiplexing. Research has shown that MU-massive MIMO can dramatically increase system capacity and spectral efficiency by separating users in the spatial domain [146]. Key studies have investigated linear and nonlinear precoding schemes, user scheduling, pilot contamination mitigation, and fairness optimization. MU-massive MIMO is central to 5G NR standards and commercial deployments. However, its performance strongly depends on accurate CSI, making CSI acquisition and feedback overhead critical challenges especially in FDD systems [147].

2.1.3.6 Massive MIMO with Non-Orthogonal Multiple Access (NOMA)

The integration of NOMA with massive MIMO aims to further enhance spectral efficiency by allowing multiple users to share the same spatial beam using power-domain multiplexing [148]. Research has demonstrated that massive MIMO-NOMA systems [149] can outperform conventional orthogonal multiple access schemes in terms of user connectivity and throughput, particularly in dense networks. Studies focus on power allocation, user pairing, beamforming design, and successive interference cancellation (SIC) [150]. While promising, massive MIMO-NOMA systems face increased receiver complexity, error propagation in SIC, and challenging resource allocation problems, which limit their practical deployment [151, 152].

2.1.3.7 Learning-Assisted Massive MIMO

More recently, DL and machine learning (ML) techniques have been incorporated into massive MIMO systems to address challenges such as CSI estimation, feedback reduction, beam selection, and interference management [153, 154]. Data-driven models such as CNNs, ANNs, autoencoders, and transformer-based networks have been shown to outperform conventional model-based methods in complex and dynamic environments [155]. Research has explored DL-assisted precoding, CSI compression, channel prediction, and hybrid beamforming [156]. Although massive MIMO based on learning offers strong performance gains, issues such as training data requirements, generalization, computational complexity, and real-time deployment remain open challenges [157].

2.1.3.8 Significance of Massive MIMO in 5G Networks & Beyond

Note that as for as 5G & beyond networks are convened, massive MIMO has become more essential for 5G and beyond networks due to its ability to handle massive wireless traffic, device density, and high-rate applications such as IoT, AR/VR, and real-time video services. On the other hand, MIMO systems cannot deliver the required spectral efficiency and reliability demanded by modern applications, while massive MIMO equipping BS with 64 to 128 (or more) antennas provides over 10 times higher spectral efficiency, improved energy efficiency, and substantial data-rate enhancements through spatial multiplexing and narrow beamforming [123]. Real world deployments further validate its practicality. The Lund-Bristol experiment demonstrated a record spectral efficiency of 145.6 bits/s/Hz using 128 antennas at 3.51 GHz [158, 159], and commercial operators like SoftBank [160], Vodafone [161], Nokia, Samsung, and Sprint have successfully implemented massive MIMO in live LTE and 5G networks, achieving multi-hundred-Mbps to gigabit level performance. Its advantages such as high reliability, reduced fading, lower latency, enhanced physical layer security, user tracking precision, and low-power operation using ultra-low-power amplifiers make it an important technology for supporting billions of devices in dense urban environments [162].

Massive MIMO offers a wide range of transformative benefits that make it a very important technology for 5G and upcoming networks. By employing large antenna arrays, massive MIMO can form highly directional narrow beams toward individual users, enabling spectral efficiency gains exceeding tenfold compared to conventional 4G/LTE MIMO systems [123]. This focused beamforming also enhances energy efficiency, as the system radiates power only where needed, significantly reducing overall transmission energy. The combination of array gain and spatial multiplexing dramatically boosts data rates. This enables simultaneous high-speed service to many users. Such high speed service capability is demonstrated in large-scale field trials achieving record spectral efficiencies using 128-antenna base stations [162]. Massive MIMO further improves link reliability through diversity gain and reduced fading. This ensures robust user tracking with narrow beams, and supports low latency transmission which is essential for real-time applications [163, 164]. Its inherent resistance to interference and jamming enhances robustness, while beam orthogonality improves physical-layer security [165]. Additionally, the large number of antennas allows the use of low-complexity linear processing [166] (e.g., MRC and ZF). This makes implementation more practical and cost-effective. Together, these advantages position massive MIMO as a critical enabler of high-capacity, reliable, and secure next-generation wireless networks.

2.1.3.9 The Challenges in Massive MIMO Systems

Massive MIMO, despite its remarkable potential, faces several fundamental challenges that must be addressed for reliable large-scale deployment in 5G and beyond wireless systems. One of the most critical issues is pilot contamination [167], which arises when neighboring cells reuse the same pilot sequences due to the limited coherence interval. This leads to strong inter-cell interference during channel estimation, preventing the base station from accurately separating users' channels even when the number of antennas grows very large. Additionally, channel estimation [168] itself becomes significantly more complex in massive MIMO, as estimating channels for tens or hundreds of antennas requires substantial pilot overhead, computational resources, and storage. Hardware limitations such as phase noise, finite resolution ADCs, and amplifier nonlinearities also become more pronounced with large antenna arrays, collectively degrading system performance [169].

Beyond estimation, massive MIMO requires efficient precoding [170] and detection [171, 172] algorithms that can scale with large antenna dimensions while keeping computational complexity manageable. User scheduling [173, 174] becomes more challenging as well, since large numbers of users must be coordinated while maintaining fairness, minimizing interference, and exploiting spatial correlation. Energy efficiency [175] is another major concern because powering, cooling, and processing across hundreds of RF chains demand substantial resources. Although massive MIMO is theoretically robust, real deployments face issues related to calibration errors in TDD systems, high interconnect bandwidth requirements, and practical constraints on antenna array size and placement. Addressing these challenges remains an active area of research, essential for unlocking the full benefits of massive MIMO in future ultra-dense, high-capacity wireless networks.

2.1.4 Conventional CS and Sparsity Based Methods Using Massive MIMO

CS-based feedback reduction approaches leveraged physical channel sparsity by projecting the high dimensional CSI onto a reduced basis (e.g., DFT/angular domain) and then applying sparse recovery methods. CS [176] has been widely explored as a promising solution to mitigate the prohibitive downlink CSI feedback overhead in FDD massive MIMO systems [177]. Since massive MIMO channels exhibit spatial correlation and approximate sparsity in specific transform domains, researchers have leveraged these properties to recover high dimensional CSI from a small number of linear measurements. Gao et al. [178] utilized the inherent spatial correlation across large antenna arrays and proposed adaptive CS-based feedback protocols that dynamically adjust compression levels depending on instantaneous channel conditions. Their approach allows users to feed back only a reduced set of measurements while still maintaining acceptable reconstruction accuracy. Similarly, Ge et al. [179] demonstrated that temporally and spatially correlated CSI can be transformed into an uncorrelated sparse vector, enabling the use of CS solvers for reliable signal recovery even in under determined measurement scenarios. These foundational studies established CS as a mathematically grounded strategy to reduce feedback load without significantly compromising system performance.

CS theory, originally introduced by Donoho [180], for sparse signal processing, has attracted significant attention in past years for sparse channel estimation in massive MIMO systems [181, 182, 183, 184]. In particular, Gao et al. [182] demonstrated that massive MIMO channels exhibit joint sparsity across different antenna links. Building on this property, a compression-based linear minimum mean square error (CLMMSE) [179] channel estimation algorithm was proposed to reduce the high computational complexity of conventional LMMSE while improving upon pure CS-based estimators. The key idea of CLMMSE is to exploit prior channel information obtained via CS to estimate the channel autocorrelation matrix using optimal rank reduction, rather than computing a full-dimensional matrix. Furthermore, singular value decomposition (SVD) is employed to replace direct channel matrix inversion, leading to a substantial reduction in computational complexity.

The performance of the CLMMSE algorithm strongly depends on accurate estimation of channel sparsity. When sparsity is correctly identified, the dimension of the autocorrelation matrix can be significantly reduced, resulting in further complexity savings. Consequently, sparsity-adaptive estimation methods are also investigated. Traditional CS-based estimators, such as orthogonal matching pursuit (OMP) [185] and subspace pursuit (SP) [186], require prior knowledge of channel sparsity, which limits their practical applicability. To overcome this, sparsity adaptive matching pursuit (SAMP) [187] was proposed, enabling channel recovery without explicit sparsity knowledge. However, its fixed step size may lead to excessive iterations when the step size is smaller than the true sparsity level. Exploiting the fact that sub-channels in massive MIMO share a common sparsity support [182], an adaptive structured SP (ASSP) algorithm was introduced in [183]. Nevertheless, the fixed step-size mechanism in ASSP restricts sparsity estimation to integer multiples of the step size, preventing precise sparsity identification. These limitations motivate further research into more accurate and flexible sparsity adaptive channel estimation techniques for massive MIMO systems.

In addition to algorithmic developments, researchers proposed specialized feedback architectures for spatially correlated and massive scale systems. Sim et al. [188] presented a compressed analog feedback strategy for spatially correlated massive MIMO systems, showing that analog CS measurement transmission can significantly reduce overhead while achieving a near optimal sum rate under noisy feedback channels. In [189], Wavelet-based compression schemes were explored to exploit the energy compaction properties of wavelet transforms, providing lower dimensional representations of correlated CSI. Meanwhile, compressed channel feedback designs such as those proposed by Shen et al. [190] and Min Soo Sim et al. [188] introduced differential and correlation aware CS-based feedback mechanisms, demonstrating notable improvement in compression efficiency for correlated propagation environments. Two dimensional CS approaches, such as the method proposed by Kai et al. [191], exploited joint spatial frequency sparsity to further enhance CSI recoverability. Collectively, these studies illustrate that CS techniques can effectively exploit structured sparsity in practical wireless scenarios, thereby reducing bandwidth and computational burden.

These CS pipelines can reduce feedback by transmitting a small set of coefficients or compressed measurements, but they require (i) that the channel be well represented in the chosen basis and (ii) iterative, often computationally expensive solvers at the receiver or BS. In practical, non ideal channels (dense multipath, mobility, hardware nonlinearity) the sparsity assumption weakens and CS performance degrades. Additionally, the commonly used discrete Fourier transform (DFT) or DFT like transforms introduce computational overhead and are not tailored to the statistical structure of the deployed environment. For these reasons, researchers have investigated hybrid schemes that combine transform preprocessing with adaptive sparsity estimation and lightweight estimation algorithms, yet fundamental fragilities remain in many practical scenarios.

2.1.5 Deep Learning for Massive MIMO Systems

DL has emerged as a powerful enabling technology for massive MIMO systems due to its strong capability to handle high-dimensional, nonlinear, and dynamic wireless environments. Traditional optimization tools such as stochastic geometry and game theory often demand excessive computational resources, whereas DL offers data-driven, low-complexity alternatives for tasks such as beamforming, channel estimation, signal detection, load balancing, and spectrum optimization [192, 193]. In massive MIMO, channel estimation can be viewed as a big-data problem, and DL models such as CNNs, ANNs, LSTMs, and RNNs have demonstrated superior performance over conventional methods, especially under complex channel conditions and channel aging effects. Treating CSI as images has also enabled effective denoising and super resolution using deep networks, leading to improved accuracy and throughput. Moreover, DL-based sparse channel estimation and CSI prediction significantly reduce estimation overhead and feedback burden, making DL a key technology for realizing reliable, high capacity massive MIMO in 5G and beyond networks.

DL has emerged as one of the most significant breakthroughs in CSI feedback reduction for massive MIMO communication systems [194]. Traditional CS approaches rely heavily on predefined sparsity assumptions and random projections to compress CSI, which limits their performance when the channel does not exhibit strict sparsity. To overcome these limitations, the seminal work CsiNet introduced by Wen et al. [64] marked a transformative shift toward data driven CSI compression. CsiNet employs an end-to-end encoder decoder architecture, where the encoder at the user equipment (UE) extracts meaningful feature maps from the channel and compresses them into a low dimensional codeword, while the decoder at the base station (BS) reconstructs the CSI using convolutional neural networks. Instead of using random projection matrices as in CS methods, CsiNet learns the nonlinear compression mapping directly from data, enabling significantly improved NMSE and correlation performance across a wide range of compression ratios. The authors also incorporated DFT preprocessing to convert the CSI into a more compact representation, but the primary compression relies on learned representations rather than hand designed transforms [195].

As CSI exhibits strong temporal correlation in mobile channels, researchers have extended CsiNet to exploit this property. CsiNet-LSTM integrates long short term memory (LSTM) [196] units into the decoder to track temporal variations and exploit channel coherence over time [197]. This hybrid CNN LSTM architecture significantly improves robustness under high mobility, providing smoother reconstruction and reduced error propagation across time slots. The success of CsiNet demonstrated that learned nonlinear mappings can outperform classical CS techniques by large margins, especially at aggressive compression ratios where CS typically fails.

To further enhance adaptability and support real time varied feedback budgets, CsiNet+ was introduced by Guo et al. [65]. This extended framework incorporates multi rate compression, quantization aware training, and variable length codeword generation, enabling the system to dynamically adjust feedback overhead depending on channel conditions or system constraints. Although CsiNet+ achieves higher reconstruction accuracy and practical quantization capability, it comes at the expense of increased network depth, higher memory consumption, and more complex training.

Following the initial success of CsiNet and its extensions, a rich body of research has focused on designing more advanced DL-based architectures for CSI compression and feedback in massive MIMO systems. These models aim to capture richer spatial frequency structures, enhance reconstruction fidelity, reduce computational burden, and improve robustness under practical impairments such as noise, quantization, and mobility. One notable advancement is CRNet [66], which introduces a multi resolution convolutional architecture capable of extracting both fine grained and global channel features.

By expanding the receptive field and learning hierarchical feature representations, CRNet effectively models the complex spatial correlations present in massive MIMO channels, resulting in improved reconstruction accuracy and reduced artifacts relative to single resolution CNNs.

Building on the need to capture long range dependencies within CSI matrices, TransNet [67] adopts a Transformer-based encoder decoder instead of conventional convolutional layers. The self attention mechanism within Transformers enables the model to learn relations between widely separated elements of the channel matrix, allowing it to capture global structural patterns that CNNs often miss. This makes TransNet particularly effective in scenarios involving high mobility or wideband channels, where temporal and frequency correlations span large dimensions.

To improve robustness under noise and uncertainty, PRVNet [68] integrates probabilistic modeling by drawing inspiration from variational autoencoders (VAEs). PRVNet learns a latent probability distribution of CSI rather than a deterministic mapping, enabling it to better handle channel perturbations, noisy observations, and imperfect feedback conditions. The probabilistic latent space also helps regularize the learned representation, reducing overfitting and improving generalization to unseen environments.

Another significant development is CSI-StripeFormer [198], which employs axial attention and stripe based feature extraction to overcome the computational complexity of full transformer blocks. By decomposing attention into horizontal and vertical stripes, the model balances computational efficiency with the ability to capture long range dependencies across two dimensional CSI structures. This design allows CSI-StripeFormer to achieve high reconstruction accuracy while maintaining scalability for very large antenna arrays and wideband frequency channels.

In parallel, other approaches have focused on improving robustness to real world impairments. DeepAE [199] introduces a denoising oriented autoencoder that is trained not only on ideal CSI but also on delayed, noisy, and quantized channel samples. This training strategy mimics practical deployment conditions, enabling the model to tolerate channel aging, feedback quantization errors, and receiver hardware distortions. By explicitly incorporating impaired CSI samples into the training dataset, DeepAE achieves strong resilience in challenging operational environments where many earlier DL models tend to degrade.

2.1.6 Generalization and Robustness Evaluation of CSI Compression Under Realistic Wireless Channel Conditions

To rigorously evaluate the generalization capability of the proposed CSI compression framework, I would design a comprehensive robustness study that extends beyond the current COST 2100 and Gaussian noise-based evaluation. The model would be trained exclusively on COST 2100 data and then tested, without retraining, on diverse channel sources including 3GPP TR 38.901 channel models such as Urban Macro (UMa), Urban Micro (UMi), Rural Macro (RMa), and Indoor Hotspot (InH), as well as real measured CSI collected through SDR-based indoor and outdoor measurement campaigns. This would reveal whether the learned representation captures fundamental channel characteristics or is overly dependent on the statistical properties of a specific dataset. In addition, I would evaluate channel ageing by introducing explicit feedback delays and investigate high-mobility scenarios through Doppler-based channel evolution, reporting NMSE, ρ, beamforming gain, and spectral efficiency as functions of user velocity and CSI staleness. Such experiments would provide a clear understanding of the framework's robustness under realistic time-varying wireless environments.

A second set of experiments would focus on practical deployment impairments that are often neglected in simulation studies. The compressed codewords would be subjected to finite-bit quantization and burst-error channels modeled using a Gilbert-Elliott process to emulate realistic digital feedback links. Furthermore, hardware impairments such as power-amplifier nonlinearities, phase noise, IQ imbalance, ADC quantization effects, and carrier-frequency offsets would be incorporated to assess robustness beyond idealized additive Gaussian noise assumptions. To evaluate out-of-distribution performance, the model would be trained on one propagation environment (e.g., indoor picocellular channels) and tested on entirely different environments such as urban, suburban, or rural scenarios. The resulting performance gap would directly quantify the framework's adaptability to previously unseen propagation conditions, while a few-shot fine-tuning study could assess how quickly performance can be recovered using limited new data. By reporting all results with confidence intervals and system-level metrics such as beamforming gain, spectral efficiency, BER, and energy efficiency, this study would provide strong evidence of the framework's practical robustness and deployment readiness for future 5G and 6G wireless networks.

2.2 Conclusion

This chapter provided a comprehensive review of CSI feedback reduction techniques for massive MIMO systems, with emphasis on DL–based solutions. Efficient CSI feedback has become a key challenge in FDD massive MIMO, where downlink CSI must be explicitly returned from the UE to the BS. Conventional CS-based methods exploit channel sparsity but suffer from high complexity, noise sensitivity, and limited adaptability. To overcome these issues, DL-based frameworks such as CsiNet, CsiNet+, CRNet, PRVNet, TransNet, DeepAE, and CSI-StripeFormer have been introduced, achieving superior compression efficiency and reconstruction accuracy through end-to-end learning and advanced architectures. Despite their effectiveness, DL models require large training datasets, incur high computational and energy costs, and face scalability concerns for real-time systems. These challenges highlight the need for more efficient solutions. Consequently, hybrid transform-assisted DL approaches have emerged as promising alternatives, combining structured signal representations with learning-based models. Motivated by these insights, the following chapters present the proposed CSI feedback reduction techniques for massive MIMO systems.

Chapter 3

DRT-Assisted DL for Massive MIMO CSI Feedback Reduction

As mentioned earlier, the reduction of CSI feedback overhead is significant in fifth generation and emerging sixth generation technologies involving massive MIMO systems. We begin our study by analyzing the impact of different transforms in achieving CSI reduction with CS. While CS is an efficient mechanism to address this challenge, the involvement of DFT in CS results into higher computational complexity. This chapter introduces a novel discrete Rajan transform (DRT)-based DL to enhance channel feedback in massive MIMO systems. We address the issues that arise due to the use of DFT in CS and show that they can be overcome by using DRT assisted DL based CSI reduction. Through simulations, it is shown that the proposed mechanism outperforms the DFT based DL algorithm by 126.19% and 81.81% for cosine correlation and normalized mean square error in channel estimation, respectively, across varying SNR scenarios. Notably, the proposed DRT-based DL algorithm showing, its potential for practical implementation in real world communication systems.

3.1 Overview

The advent of 5G and the upcoming 6G wireless communications involves the use of advanced technologies, aiming to improve data rate, channel capacity, and mitigate feedback overhead [200, 201]. One of these technologies is massive MIMO, which necessitates the deployment of multi-antenna base stations and access points. Massive MIMO can be regarded as a large-scale extension of conventional MIMO systems.

3.1.1 MIMO Systems

MIMO is a wireless communication technology that uses multiple antennas at both the transmitter and the receiver to increase data throughput and reliability. By exploiting spatial diversity and spatial multiplexing, MIMO sends multiple data streams simultaneously over the same frequency band. These systems make use of multipath propagation. In the spatial diversity mode, different copies of the same signal are transmitted. This improves communication reliability. Further, the transmission of independent data stream in parallel increases capacity. MIMO is generally combined with orthogonal frequency division multiplexing (OFDM) in modern wireless systems, making it a MIMO-OFDM system. MIMO-OFDM divides a channel into many parallel subcarriers, allowing robust high speed transmission [202, 203].

In MIMO communications, narrow-band systems [204] assume that the channel experiences flat fading, meaning the signal bandwidth is smaller than the coherence bandwidth of the channel. As a result, all frequency components of the signal experience approximately the same gain and phase shift, and the channel can be modeled using a single complex matrix $\boldsymbol{H}$. In contrast, wide-band MIMO systems [205, 206] operate over bandwidths larger than the coherence bandwidth, causing frequency selective fading. Here, different frequency components undergo different channel responses, requiring more complex models such as OFDM-based subcarrier channels, or multi-MIMO impulse responses. Wide-band systems therefore demand significantly more CSI and complex equalization.

The narrow-band model is commonly used because it offers a simple, tractable representation of MIMO behavior. It simplifies the analysis of essential spatial concepts such as beamforming, precoding, and multiplexing by removing the complication of frequency selective channels. This foundational model can be extended to wide-band systems by applying it to each OFDM subcarrier.

Mathematically, a narrow-band MIMO system is represented as

$$\boldsymbol{y} = \boldsymbol{H}\boldsymbol{x} + \boldsymbol{w} \tag{3.1}$$

where $\boldsymbol{y} = [y_1, y_2, ..., y_{N_r}]^T$ is received signal vector, $\boldsymbol{H} = [\boldsymbol{h}_{ij}]_{N_r \times N_t}$ is channel matrix, $\boldsymbol{x} = [x_1, x_2, ..., x_{N_t}]^T$ is transmitted signal vector and $\boldsymbol{w} = [w_1, w_2, ..., w_{N_r}]^T$ is additive noise.

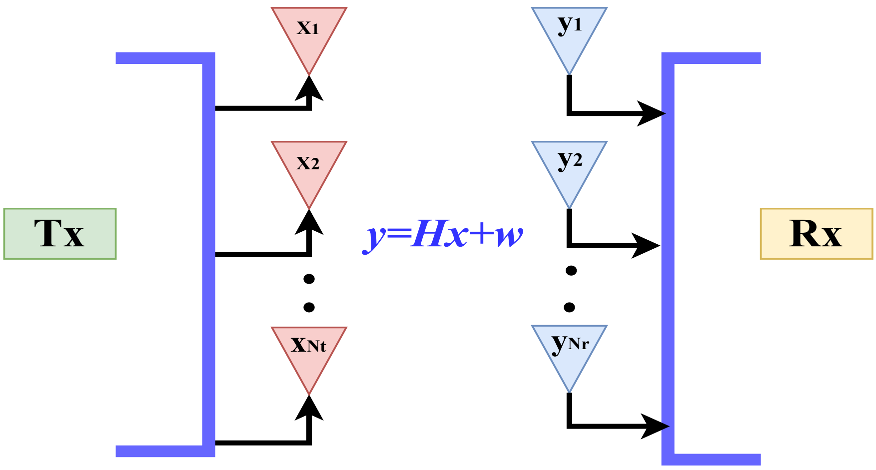

Figure 3.1: A Practical MIMO Systems

It is significant to note that MIMO acts as a core physical layer component of 4G LTE networks [207]. Typical LTE deployments include $2 \times 2, 4 \times 4$ and 8×8 antenna configurations, combined with OFDM to support high data rates over frequency selective channels [208].

MIMO exploits spatial multiplexing to transmit independent data streams simultaneously over the time frequency resources. General MIMO systems transmit upto four layers of data streams. This increases user data rates without requiring additional bandwidth or transmit power. MIMO has been extensively used in LTE. LTE improves link reliability through transmit diversity coding, which enhances error performance under low SNR and deep fading channel conditions by transmitting redundant versions of the signal over multiple antennas. LTE also supports multi-user MIMO (MU-MIMO) [209], where a single base station can schedule and serve multiple users on the same resource block. This significantly improves network spectral efficiency, as multiple users can be spatially separated using advanced precoding techniques.

LTE operates using feedback based precoding. In this mechanism, the UE estimates the downlink channel matrix $\boldsymbol{H}$ and reports quantized CSI back to the base station. The BS can then design an appropriate precoding matrix $\boldsymbol{p}$ based on the reported CSI. The resulting transmitted and received signals can be modeled as

$$\boldsymbol{x} = \boldsymbol{p}\boldsymbol{s}, \qquad \boldsymbol{y} = \boldsymbol{H}\boldsymbol{p}\boldsymbol{s} + \boldsymbol{w}, \tag{3.2}$$

where $\boldsymbol{s} \in \mathbb{C}^{N_s \times 1}$ is the transmitted symbol vector containing N_s data streams, $\boldsymbol{p} \in \mathbb{C}^{N_t \times N_s}$ is the precoding (beamforming) matrix applied at the transmitter with N_t antennas, $\boldsymbol{x} \in \mathbb{C}^{N_t \times 1}$ is the precoded transmit vector, $\boldsymbol{y} \in \mathbb{C}^{N_r \times 1}$ is the received signal, and $\boldsymbol{w} \in \mathbb{C}^{N_r \times 1}$ represents additive channel noise. The objective of designing $\boldsymbol{H} \in \mathbb{C}^{N_r \times N_t}$ is to maximize received signal power while minimizing inter user interference [210].

Traditional MIMO systems significantly improved spectral efficiency and reliability, but they face fundamental limitations in antenna scalability, spectrum reuse, and the overhead required for accurate CSI feedback [157]. As modern wireless networks move toward ultra-dense deployments and support millions of interconnected devices, the constraints of MIMO particularly in terms of feedback signaling and practical antenna integration become major problems. These challenges have driven the evolution toward massive MIMO, where BSs are equipped with tens to hundreds of antennas [123]. Massive MIMO provides several transformative advantages. It delivers substantial beamforming gains that enhance SNR and coverage, enables near-linear increases in spectral efficiency with the number of antennas, and supports the spatial multiplexing of many users simultaneously within the same time-frequency resources. Together, these capabilities make massive MIMO a foundational technology for scalable, high capacity 5G and future 6G wireless communication systems.

Recent research has expanded the scope of massive MIMO by exploring more advanced architectures and intelligent processing techniques to meet the demands of future 6G networks. One key research in this direction is cell-free massive MIMO [211], where the traditional notion of cell boundaries is removed. Instead of each user being served by a single BS, a large number of geographically distributed access points jointly and coherently serve all users in the network. This architecture significantly improves uniformity in service quality, mitigates cell edge issues, and offers high macro diversity gains [211]. By eliminating inter-cell interference and leveraging distributed beamforming, cell-free systems [212] provide consistent user experiences even in dense urban or indoor environments.

Another emerging paradigm is extremely large-scale MIMO (XL-MIMO) [213], which envisions antenna arrays with physically massive apertures integrated into building facades, walls, lamp posts, vehicles, or indoor infrastructures. The XL-MIMO introduces spatially non-stationary propagation, which means that different parts of the antenna array may experience different channel characteristics due to the large aperture size. This requires new channel models, beamforming strategies, near-field signal processing, and user specific sub-array coordination to fully harness the enormous spatial resolution and sensing capabilities of XL-MIMO systems [214]. XL-MIMO is expected to play a key role in 6G applications involving high precision localization, holographic communications, and highly directional short range links.

The third significant idea is the integration of DL for CSI processing driven by the substantial CSI feedback burden in FDD massive MIMO [215]. Traditional CS techniques struggle with nonlinear channel variations and high mobility. DL-based frameworks, such as CsiNet, CsiNet+, CRNet, and Transformer-based architectures like TransNet, learn compact representations of CSI through nonlinear feature extraction, enabling efficient compression, prediction, and reconstruction. These models significantly reduce feedback overhead, improve robustness against noise and interference, and generalize better under dynamic channel conditions. As a result, DL has become one of the most promising tools for next-generation CSI acquisition, supporting both high capacity and low latency communication in future 6G systems.

3.1.2 Massive MIMO Systems

In light of the above discussion, massive MIMO has become a significant technology for modern and future wireless communication systems, particularly 5G and 6G. Unlike conventional MIMO, which employs only a few antennas, massive MIMO uses hundreds of antennas at a base station to serve many users simultaneously on the same time frequency resources. This enables strong spatial multiplexing and highly focused beamforming, and allows tremendous performance gains up to 10 times higher spectral efficiency and more than 100 times improvement in energy efficiency. Massive MIMO systems benefit from channel hardening, where small-scale fading averages out, resulting in more stable and reliable communication links reduced sensitivity to fading, and the ability to operate efficiently even with low-cost RF hardware. Furthermore, time division duplexing (TDD) operation enables channel reciprocity. This reduces downlink CSI feedback upto a certain extent and makes implementation more efficient. [123].

Massive MIMO offers several exciting advantages that make it a important technology for 5G and beyond. By making use of spatial multiplexing, it achieves exceptionally high spectral efficiency, enabling many users to be served simultaneously on the same time-frequency resources. Its highly directional beamforming greatly improves energy efficiency by focusing power only toward intended users while also suppressing inter-user and inter-cell interference. With a large number of antennas, the system experiences channel hardening. Additionally, massive MIMO can support massive connectivity and is inherently more tolerant to hardware imperfections, and impairments such as phase noise or gain mismatch.

Inspite of these benefits, massive MIMO faces several notable challenges. The acquisition and feedback of CSI become increasingly difficult as the number of antennas grows, leading to substantial CSI overhead. Pilot contamination caused by pilot reuse across neighboring cells remains one of the most critical performance limitations. The system also requires extensive computational resources for large scale precoding and detection, making real time processing complex. On the hardware side, scaling up the number of antennas increases the demand for RF chains, ADCs, and precise calibration. Even in TDD systems, maintaining accurate uplink-downlink reciprocity is difficult due to calibration requirements. These challenges highlight the need for new architectures and intelligent processing techniques to fully harness the potential of massive MIMO.

Additional implementation constraints include synchronization across hundreds of RF chains, high computational and power requirements for large matrix operations, and the need for more accurate channel models that reflect the spatially non-stationary behavior of large antenna arrays. Research efforts continue to explore scalable pilot design, blind or semi-blind CSI estimation, low power distributed processing, and integration with emerging technologies such as heterogeneous networks and dense small cell deployments to improve system robustness and efficiency.

A particularly critical challenge that persists despite progress in other areas is the problem of CSI feedback overhead. Although TDD systems partially alleviate downlink CSI acquisition through uplink-downlink reciprocity, this benefit is limited in practical deployments due to hardware mismatches and calibration errors. As a result, accurate downlink CSI is still required at the BS, and the feedback overhead becomes prohibitively large as antenna arrays scale into the hundreds. In FDD systems, the problem is even more severe because CSI must be explicitly fed back from the user equipment. Therefore, achieving efficient and scalable CSI feedback reduction remains one of the central problems in realizing the full potential of massive MIMO, motivating extensive research into CS-based, codebook design, and DL-based CSI compression methods.

3.1.3 CSI-Feedback Reduction in Massive MIMO

As discussed above, massive MIMO involves numerous antennas on the BS [216]. The number of antennas can range from hundreds to thousands. They are employed in a centralized [217] or a decentralized [218] manner. Massive MIMO effectively reduces multi-user interference and enhances overall throughput [219]. However, this setup entails complex signal processing and energy-intensive devices, incurring substantial costs. Hence, it is imperative to explore simple and energy-efficient implementation techniques aligning with sustainable and green solutions.

In MIMO systems, downlink channel information is obtained from users during training [220]. It is sent back to the base station through a feedback link. The challenge in massive MIMO systems lies in efficient reduction of feedback-overhead of channel state information (CSI) [221][222]. In their study, Gao et al. [178] propose using CS to reduce the feedback overhead load for CSI in massive MIMO systems. Using the sparsity in spatially correlated antenna arrays, the authors present adaptive feedback protocols that dynamically adjust based on channel conditions.

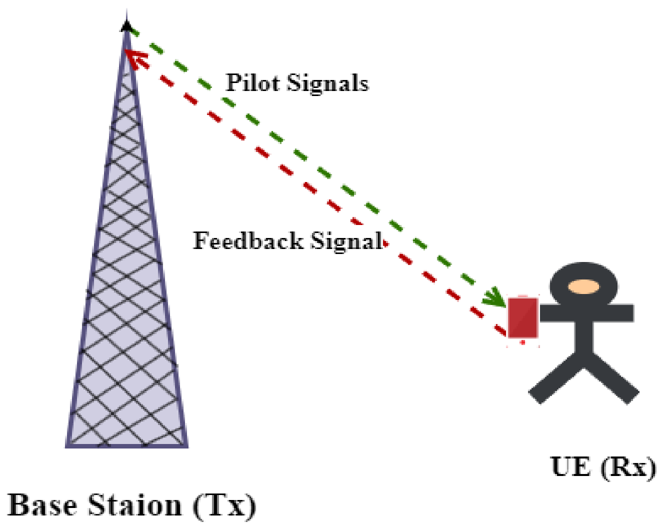

Figure 3.2: CSI Feedback Architecture Model of Downlink Pilot and Feedback Signals

Ge et al. [179] show that it is possible to convert correlated CSI into an uncorrelated sparse vector, allowing the use of CS to estimate a sparse vector from an under-determined linear system accurately. Dai et al. [223] propose least absolute shrinkage and selection operator

(LASSO) l_1-solver a regression analysis technique that performs both variable selection and regularization to improve the prediction accuracy and interpretability of the statistical model. The l_1-solver is the optimization algorithm to solve the LASSO problem. In [224], approximate message passing (AMP) has been proposed. It is a CS-based technique used for solving sparse recovery problems by iteratively updating estimates of the sparse signal using AMP. An extension to [224], block matching 3D - approximate message passing (BM3D-AMP) [225], combines the principles of BM3D with AMP. BM3D-AMP is a denoising algorithm based on block matching and collaborative filtering, with the approximate message passing framework. It is a method for efficiently solving sparse [226] signal recovery problems. However, it can face difficulties in CSI recovery due to a simple sparsity assumption. The channel matrix exhibits approximate sparsity, complicating prior modeling and significantly hindering reconstruction quality.

Applying CS in the above mechanisms uses random projections to compress data. Random projection is a simple dimensionality reduction technique that compresses high dimensional data by multiplying it with a randomly generated matrix, producing a compact representation while roughly preserving data structure [227, 228]. However, because the projection is completely random, it does not learn or utilize the underlying channel characteristics, leading to significant information loss in practical CSI scenarios. This limitation becomes more severe when channels are non-sparse, noisy, or highly dynamic, causing reduced reconstruction accuracy. Random projections also lack adaptability to real world variations, making them unreliable for complex massive MIMO environments. Therefore, while easy to implement, random projection is inadequate for high precision CSI feedback in modern wireless systems. Wen et al. [64] propose a DL-based mechanism that relies on the information in the feature maps to create a compressed codeword [195], rather than on random projections. The authors use DFT and inverse DFT for sparsifying the data at the encoder end and retrieving the data at the decoder end, respectively.

The DFT converts the CSI data from the antenna/spatial domain into the angular frequency domain. This transformation makes important channel patterns like dominant paths and angles clearer and easier to identify. DFT also compresses the channel energy into a few significant components, which helps the neural network learn more meaningful features. The IDFT then converts these learned frequency domain features back to the spatial domain to reconstruct the original CSI. Thus, DFT and IDFT reveal hidden structures in the channel, reduce redundancy, and help the model focus on essential propagation characteristics.

However the use of DFT has certain disadvantages. When sparse signals are involved, applying DFT can slow down the algorithm convergence [229]. Sparse signals contain many zero or near-zero coefficients. DFT decomposes signals into sums of sinusoidal functions. Hence, it is not inherently designed to handle sparsity efficiently. DFT based algorithms require more iterations for processing sparse signals and converging to a solution, resulting into increased computational load and inefficient data compression. As a result, such mechanisms can suffer limitations in meeting the data rate requirements of fifth generation (5G) and beyond communications. Also, DL-based applications demand transforms that can recognize patterns regardless of the order of input elements. The dependence of DFT on the order of input elements further limits their use in DL.

3.1.3.1 Impact of DL-Based CSI Compression on Throughput and Beamforming Gain

The implementation of DL-based CSI compression in massive MIMO systems primarily improves communication performance by enabling more accurate CSI reconstruction with significantly lower feedback overhead. When the reconstructed CSI closely matches the true channel, the BS can design more accurate beamforming and precoding vectors, resulting in improved alignment between the transmitted signal and the actual propagation channel. This leads to higher beamforming gain, increased received signal power, and reduced interference leakage among users and spatial streams. Consequently, the effective SNR at the receiver improves, enhancing the reliability and efficiency of wireless communication.

The improvement in beamforming accuracy directly translates into higher system throughput and spectral efficiency. According to Shannon's capacity principle, throughput increases with SNR. Therefore, more accurate CSI enables the system to support higher data rates and more efficient spatial multiplexing. In addition, CSI compression reduces the amount of feedback information that must be transmitted over the uplink, freeing valuable feedback resources and reducing latency. As a result, DL-based CSI compression provides a dual benefit: it maintains high CSI accuracy for effective beamforming while simultaneously reducing feedback overhead, thereby improving overall throughput, spectral efficiency, and resource utilization in massive MIMO systems. Although the exact throughput or beamforming gain depends on factors such as compression ratio, channel conditions, mobility, and system configuration, improvements in reconstruction metrics such as NMSE and cosine correlation are generally associated with corresponding gains in beamforming performance and achievable data rates.

3.1.4 Discrete Rajan Transform

In this chapter, we propose a discrete Rajan transform (DRT) [230, 231] enhanced DL based mechanism for acquiring the CSI in a massive MIMO system.

The DRT originated with foundational works by V. Rajan in the 1980s, where the transform's recursive structure and theoretical basis were first formalized. Unlike conventional transforms built on sinusoidal bases, the DRT relies on hierarchical ordering of signal components, making it inherently lightweight and well suited for pattern extraction and structured data representation. Rajan's early work established the core principles of the transform, showing how its deterministic reordering mechanism provides a strong foundation for efficient and scalable signal processing.

Later studies formalized the mathematical properties of the DRT, proving its invertibility, monotonicity, and favorable computational complexity of $O(N \log N)$ achieved through simple comparisons rather than multiplications. These characteristics make the DRT both energy efficient and hardware friendly. Its ability to produce ordered, noise resilient feature representations has led to growing interest in modern applications such as compression, image analysis, and DL pipelines. In particular, its lightweight structure and robustness make it a strong candidate for wireless systems like massive MIMO CSI feedback, where low complexity and high efficiency are essential.

DRT is a nonlinear integer transform introduced primarily for applications in digital signal processing (DSP), pattern recognition, and image analysis, particularly in contexts where noise robustness and efficient feature extraction are essential. Unlike classical linear transforms such as the Fourier, Walsh, or discrete cosine transform (DCT), the DRT belongs to a family of combinatorial and order statistical transforms, in which the operations are based on integer comparisons and magnitude selections rather than arithmetic additions and multiplications. This makes the transform attractive for low-complexity implementations, hardware realizations, and environments where signals are subject to quantization or impulsive noise [232].

DRT is a comparison based signal transform defined on sequences of length $N = 2^k$. It belongs to the class of order statistical transforms, where operations are based on comparisons rather than linear combinations. This distinguishes the DRT from classical linear transforms such as the DFT or the DCT, which rely on convolutional and inner product structures. Instead, the DRT employs lattice theoretic operations specifically the binary operators $\min$ and $\max$, which form a complete distributive lattice.

Consider an input vector $\mathbf{x} = (x_0, x_1, \ldots, x_{N-1})$. The DRT proceeds in $k = \log_2(N)$ stages. At each stage $s \in \{0, 1, \ldots, k-1\}$, the vector is partitioned into disjoint index pairs of the form $(i,\, i+2^s)$. For each such pair, the transform outputs

$$x_i^{(s+1)} = \min\left(x_i^{(s)},\, x_{i+2^s}^{(s)}\right), \qquad x_{i+2^s}^{(s+1)} = \max\left(x_i^{(s)},\, x_{i+2^s}^{(s)}\right). \tag{3.3}$$

This recursive procedure resembles a structured sorting network, with each layer preserving enough ordering information to allow perfect inversion. After the final stage, the output vector is

$$\mathbf{y} = \mathrm{DRT}(\mathbf{x}) = \mathbf{x}^{(k)}, \tag{3.4}$$

which contains a partially ordered representation of the input. Because the DRT uses only the lattice operations $\min$ and $\max$, it is a nonlinear, monotone, and scale invariant transform. In particular, for any constants $a > 0$ and $b \in \mathbb{R}$,

$$\mathrm{DRT}(a\mathbf{x} + b) = a\,\mathrm{DRT}(\mathbf{x}) + b, \tag{3.5}$$

indicating that affine transformations of the input simply scale and shift the output. This property establishes the DRT robustness against impulsive noise, outliers, and quantization distortions conditions under which linear transforms often degrade.

The inverse DRT reconstructs the original sequence by reversing the sequence of min-max pairings. Since each operation encodes a two element total order, the inverse transform systematically restores the original pairwise relationships, enabling recovery of the original vector as

$$\mathbf{x} = \mathrm{IDRT}(\mathbf{y}). \tag{3.6}$$

This shows that the DRT is bijective for vectors with distinct entries and conditionally invertible for those with equal values. The DRT has also notable applications in image processing, texture classification, robust feature extraction, and nonlinear pattern recognition. In images, the DRT preserves edges and structural discontinuities while suppressing amplitude perturbations. For two-dimensional data, the 2D DRT [233] is defined via separable row-column operations applied to $N \times N$ blocks.

The application of DRT can be further extended with the use of multilevel Rajan transform (MRT), multidimensional Rajan transforms [233], and hybrid schemes combining the DRT with wavelet and morphological operators. Modern applications link the DRT to nonlinear spectral decompositions, rank based feature hashing, and VLSI efficient DSP architectures.

3.1.5 Chapter Contributions

The contributions made in this work are as follows:

1. *Enhanced Data Sparsification for Efficient CSI Feedback*: The proposed DL-

assisted massive MIMO CSI feedback framework introduces a significantly improved sparsification strategy by integrating the DRT as a feature extraction module. DL models benefit greatly from structured and discriminative representations, and DRT being inherently nonlinear and order statistical captures the essential geometric and magnitude based relationships within the CSI tensor. This transforms the raw high-dimensional CSI into a more compact, informative, and DL friendly representation. As a result, the encoder learns more meaningful latent features, enabling substantial compression gains without compromising reconstruction fidelity at the receiver.

2. *Immunity to the Order of Input Elements*: Permutation invariance is a desirable property in CSI sparsification because the spatial ordering of channel coefficients may vary depending on antenna indexing, measurement sequences, or preprocessing arrangements. The DRT possesses an intrinsic immunity to the order of input elements due to its min-max lattice-based operations. Unlike linear transforms that are highly sensitive to positional shifts, DRT preserves the structural relationships among CSI coefficients irrespective of input permutations. Consequently, the learned model remains robust to reordering effects, allowing it to consistently recognize underlying channel patterns and improving generalization across diverse deployment scenarios.

3. *Improved Noise Robustness*: Wireless channels in practical systems are often contaminated by measurement noise, quantization distortions, and unpredictable distortions. The proposed system inherits the strong noise immunity properties of the DRT, which systematically emphasizes order relations while suppressing extreme outliers and non-Gaussian perturbations. This yields transformed CSI representations that retain critical structural information such as fading patterns and multipath signatures while being inherently less sensitive to additive noise or phase distortions. As a result, the reconstructed CSI at the base station is cleaner, more stable, and more reliable, leading to improved multi-user precoding and enhanced system throughput under challenging SNR conditions.

4. *Reduced Computational Complexity*: Massive MIMO systems involve extremely large CSI matrices. Thus, computational efficiency a key requirement for real time feedback. The DRT operates using simple comparison based operations (min and max), enabling an overall complexity on the order of $\mathrm{O}(N \log N)$, which is significantly lower than many conventional feature extraction or sparsification methods. The proposed framework exploits this efficiency to reduce both the computational and memory footprint of the CSI encoder. This accelerates feedback generation on resource constrained user devices and ensures that the method scales seamlessly to next-generation large array configurations, including XL-MIMO and cell free architectures.

5. *Adaptive and Flexible CSI Feedback Mechanism*: To accommodate the highly dynamic nature of wireless propagation environments, the system incorporates an adaptive thresholding mechanism. This mechanism adaptively tunes feedback sparsity based on network conditions, channel quality, and system level performance targets. It ensures that the amount of CSI sent to the BS is continuously optimized during channel variations and reducing redundancy during stable conditions. Such flexibility allows the system to balance feedback overhead with reconstruction accuracy, providing a robust and energy efficient solution suitable for diverse mobility scenarios, from stationary IoT devices to high speed vehicular users.

The rest of the chapter is arranged as follows: Section 3.2 introduces the system model and DRT. Section 3.3 shows the architecture for channel feedback. Section 3.4 presents the methodology of the proposed DRT based mechanism. Section 3.5 shows the simulation and experimental results. Section 3.6 present the computational complexity of this chapter and finally, Section 3.7 concludes the work.

3.2 System Model

In a FDD massive MIMO system, the down-link and up-link operate in different frequency bands, which prevents channel reciprocity and makes explicit CSI feedback essential. The process begins when the BS transmits downlink pilot signals across its large antenna array. The UE receives these pilots and performs channel estimation typically using least squares (LS) or linear NMSE estimation to obtain an initial CSI matrix that describes the propagation conditions between each BS antenna and each subcarrier. This raw CSI is high dimensional, often noisy, and may contain redundant information across antennas, frequency tones, and spatial directions, motivating the need for efficient compression and sparsification before feedback.

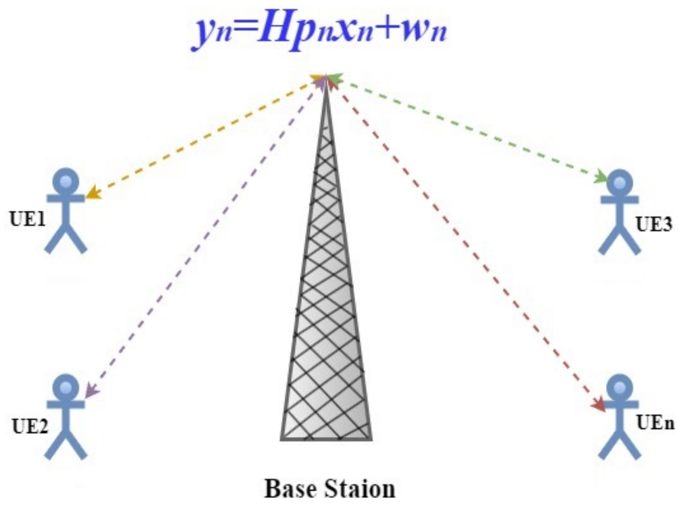

Figure 3.3: System Model Structure of Transmitter (N_t) and Receiver (One User) Massive MIMO

To reduce the feedback overhead, the UE applies sparsification and feature extraction, by using a transform mechanism, or other domain conversions that make the CSI more compressible. We use the DRT to achieve this objective. After transformation, the UE compresses the CSI using neural network encoders, quantization, or thresholding techniques, significantly lowering the dimension of the data to be fed back. This compressed representation is then transmitted from the UE to the BS through the up-link channel, using the up-link frequency band without interfering with the down-link data transmission.

At the BS, the received compressed CSI is decoded using a reconstruction network or inverse transform to recover an accurate approximation of the down-link channel. Once reconstructed, the CSI is used to compute precoding and beamforming weights such as zero forcing, NMSE, or hybrid precoding to enable efficient and interference aware down-link data transmission to multiple users simultaneously. Because wireless channels change over time due to mobility and environmental variations, the system continuously updates CSI through repeated pilot transmissions, adaptive sparsification thresholds, and dynamic feedback intervals. This ensures that the FDD massive MIMO framework remains accurate, scalable, and robust, supporting high throughput and low latency communication even in rapidly varying propagation environments.

We assume a downlink massive MIMO system in a single cell consisting of N_t transmit antennas at the BS and one receiver antenna at the UE. The system operates at orthogonal frequency division multiple access (OFDMA) over $\tilde{N}_c$ sub-carriers. The signal obtained at the n^{th} sub-carrier serves as below.

$$y_n = \tilde{\boldsymbol{h}}_n^H \boldsymbol{p}_n x_n + w_n, \tag{3.7}$$

where $\tilde{\boldsymbol{h}}_n \in \mathrm{C}^{N_t \times 1}, \boldsymbol{p}_n \in \mathrm{C}^{N_t \times 1}, x_n \in \mathrm{C}$ and $w_n \in \mathrm{C}$ represent the channel matrix-vector, precoding vector, data-bearing symbols and noise added to the n^{th} sub-carrier, accordingly.

Let $\tilde{\boldsymbol{H}} = [\tilde{\boldsymbol{h}}_1, \tilde{\boldsymbol{h}}_2 .....\tilde{\boldsymbol{h}}_{\tilde{N}c}]^H \in \mathrm{C}^{\tilde{N}_c \times N_t}$ be stacked in the spatial frequency domain as the CSI. The precoading vector $[\boldsymbol{p}_n, n = 1, 2.......\tilde{N}_c]$ can be designed by the BS after it has received $\tilde{\boldsymbol{H}}$ feedback. In the FDD system, there should be a way for the UE to send $\tilde{\boldsymbol{H}}$ back to the BS. The whole set of feedback values, $N_t \tilde{N}_c$, is large and is not permitted for the limited feedback links. Note that downlink channel estimation at the UE is outside the purview of our research. It is assumed that perfect CSI has been achieved through pilot-based training at the UE [234]. We focus on the feedback side of the scheme.

We propose using DRT to sparsify $\tilde{\boldsymbol{H}}$ in the angular-delay domain as a way to minimize feedback overhead.

$$\boldsymbol{H} = X_d \tilde{\boldsymbol{H}} X_a^H, \tag{3.8}$$

where X_d and X_a are $\tilde{N}_c \times \tilde{N}_c$ and $N_t \times N_t$ DRT matrices, respectively. Liu et al. in [235] perform a realization of the value of $\boldsymbol{H}$ with the Cooperation in Science and Technology

(COST 2100) model. It was found that $\boldsymbol{H}$ comprises a very small percentage of big components. The power delay profile of multi-path arrivals has a limited duration. As a result, only the first N_c rows have significant value. Thus, we retain only the first N_c rows in $\boldsymbol{H}$. Further, for simplicity, we write $\boldsymbol{H}$ to represent the truncated $N_c \times N_t$ matrix. In massive MIMO, the total number of feedback parameters can be decreased to $N = N_c N_t$, which still has a high value.

In this chapter, our attention lies in creating an encoder as

$$s = f_{en}(\boldsymbol{H}), \tag{3.9}$$

for transforming the $\boldsymbol{H}$ into an M-dimensional vector (codeword), where $M < N$. $\gamma = M/N$ represents the ratio of data compression. The original channel will be decoded from the codeword as

$$\boldsymbol{H} = f_{de}(s), \tag{3.10}$$

For CSI feedback, after acquiring the channel matrix $\tilde{\boldsymbol{H}}$ at the UE side, we implement DRT on equation (3.8) to produce the truncated matrix $\boldsymbol{H}$. We next utilize the encoder in equation (3.9) to generate a codeword s. Afterward, s is sent back to the BS, where the decoder equation (3.10) is utilized to produce the result $\boldsymbol{H}$. To get the final channel matrix in the spatial frequency domain, the inverse DRT can be applied.

3.3 The proposed $\tilde{\boldsymbol{H}}$ Feedback Architecture

We propose a DRT-based DL architecture for efficient and faster channel feedback. We discuss in detail about the computation of DRT and inverse DRT. Subsequently, the implementation of DRT in DL-based CSI feedback reduction will be explained.

3.3.1 Discrete Rajan Transform

Let $x(n)$ be a number series of length N. $x(n)$ is divided into two parts of length $N/2$ as follows,

$$\begin{aligned} l(i) &= x(i) + x\left(i + \frac{N}{2}\right), \quad 0 \leq i \leq \frac{N}{2} - 1, \\ m(i) &= \left| x\left(i + \frac{N}{2}\right) - x(i) \right|, \quad 0 \leq i \leq \frac{N}{2} - 1. \end{aligned} \tag{3.11}$$

Further, each of the $N/2$ points is divided into two halves of length $N/4$. Each gives the following equations:

$$\begin{aligned} l_1(i) &= l(i) + l\left(i + \frac{N}{4}\right), \quad 0 \leq i \leq \frac{N}{4} - 1, \\ l_2(i) &= \left| l\left(i + \frac{N}{4}\right) - l(i) \right|, \quad 0 \leq i \leq \frac{N}{4} - 1, \\ m_1(i) &= m(i) + m\left(i + \frac{N}{4}\right), \quad 0 \leq i \leq \frac{N}{4} - 1, \\ m_2(i) &= \left| m\left(i + \frac{N}{4}\right) - m(i) \right|, \quad 0 \leq i \leq \frac{N}{4} - 1. \end{aligned} \tag{3.12}$$

This procedure is repeated until further division is not possible. The final sequence having N elements will be labeled as

$$X_{N\times 1} = [X(0), X(1), \ldots, X(N-1)] \tag{3.13}$$

here $\log_2 N$ is the total number of possible states. DRT is obtained with the help of a matrix operator known as R matrix operated over the input sequence $X_{N\times 1}$ as

$$A_{N\times 1} = R_{N\times N} X_{N\times 1} \tag{3.14}$$

where

$$R_{N\times N} = \begin{bmatrix} I_{\frac{N}{2}\times\frac{N}{2}} & I_{\frac{N}{2}\times\frac{N}{2}} \\ -e_k I_{\frac{N}{2}\times\frac{N}{2}} & e_k I_{\frac{N}{2}\times\frac{N}{2}} \end{bmatrix}_{N\times N} \tag{3.15}$$

and matrix X represents the length N column input sequence and e_k is an transformation function. The identity matrix $I_{N/2}$ has a dimension of $N/2$, which is half of the size of the input sequence matrix $X_{N\times 1}$. The transformation function e_k is given as

$$e_k = (-1)^k \tag{3.16}$$

such that

$k = 1$; for $X(i + N/2) < X(i)$; $0 \leq i \leq N/2 - 1$ and

$k = 0$; otherwise.

Here, $X(i)$ is the i^{th} element of $X_{N\times 1}$. The matrix $A_{N\times 1}$ is split into two $N/2$-sized column matrices, A_{00} and A_{01}. These matrices use the operator $R_{N/2}$ for both sequences to generate the two new matrices, A_{10} and A_{11}, from the two input sequences. Note that the size of the $R_{N/2}$ matrices is half that of the R_N matrix. Iteratively carrying out the procedure continues until the submatrices' size is decreased to two. Thus, we have $N = 2^{n-p}$, for p^{th} iteration stage, with $p = 1, 2, 3....n$. Every binary value is encrypted and denoted by k. They are generated throughout the computational process at each iteration. To acquire the primary sequence value using the inverse transformation approach, they must be connected to the final spectrum. This closed-form statement exactly defines the algorithm described at the beginning of this section.

3.3.2 Inverse Discrete Rajan Transform

As previously discussed, the DRT establishes an isomorphism between a domain set consisting of inverse, cyclic, dyadic, and dual class permutations of a sequence, and a corresponding range set composed of sequences of the form $X(k)E(k)$. Here, $X(k)$ represents the permutation invariant output of the DRT, while $E(k)$ denotes an encryption code uniquely associated with each permutation in the domain. This mapping is bijective, meaning it is both one-to-one and onto, and therefore an inverse mapping necessarily exists. Owing to this bijective structure, DRT can properly be regarded as a transform.

In the following, we present a systematic method for constructing the inverse DRT and recovering the original sequence from its DRT representation.

The signal $x(n)$ is retrieved using the inverse DRT [230], [236], which is a recursive algorithm. It converts the reverse transform code $X(k)E(k)$ of length $N(1+m)$, where $N = 2^m$ and m is the number of stages of computation, into one of its original sequences belonging to its permutation class depending on the encryption code $E(k)$. Based on the transformation code $E(k)$, the code is converted into one of the original sequences. The input sequence is divided into two-point segments to compute the IDRT as

$$g(2k+1) = (X(2k) + X(2k+1))/2 \tag{3.17}$$

$$\text{if } E_1(2k) = 0 \text{ and } E_2(2k+1) = 0, \quad \text{for } 0 \leq k \leq N, \tag{3.18}$$

$$g(2k) = \max\Big(X(2k),\, X(2k+1)\Big) - g(2k+1). \tag{3.19}$$

$$g(2k) = (X(2k) + X(2k+1))/2, \tag{3.20}$$

$$\text{if} \quad E_1(2k) = 1 \text{ or } E_1(2k+1) = 1, \quad 0 \leq k \leq N, \tag{3.21}$$

$$g(2k+1) = \max\Big(X(2k),\, X(2k+1)\Big) - g(2k). \tag{3.22}$$

Each segment of the resultant sequence contains four data points. These segments are recursively divided into eight-point segments and further processed, continuing until no further division is possible.

As discussed, the reverse transform cancels the negative sign, adding $N(2^M - 1)$ to $X(0)$ to recover the initial order. The DRT coefficients are represented as the column matrix X_{NX1} of length N. The transformation values from each iteration are organized into column matrices: $E^1, E^2, \ldots, E^{n-1}$, each of length $N/2$, where $n = \log_2 N$. For $N = 8$, we get E^1 and E^2 as two 4×1 matrices with binary values. In this context, $X_{N\times1}$ is the DRT coefficient matrix, $R_{N\times1}$ is the intermediate matrix, and $A_{N\times1}$ is the matrix with elements arranged using the transformation matrix E_r. Additionally, $\bar{E}_r$ is obtained by element-wise complementation of E_r, where r ranges from $n-1$ to 1.

Starting with $N = 2^p$ where p ranges from 1 to n, we use the final forward RT matrix, then apply the remaining matrices in reverse for IRT. Each matrix is used according to the IRT algorithm's requirements. To illustrate this, let's take an example involving a sequence denoted as $x(n)$, which exhibits a maximum value with the following expression:

$$[R_{NX1}] = \begin{bmatrix} \max(X_1, X_{N/2}) \\ . \\ . \\ \max(X_{N/2}, X_N) \\ 0 \\ . \\ . \\ \text{up to } \frac{1}{2} \text{ (zeros)} \end{bmatrix} - \frac{1}{2} \times \begin{bmatrix} I_{N/2} & I_{N/2} \\ -I_{N/2} & -I_{N/2} \end{bmatrix} [X_{NX1}] \tag{3.23}$$

$$[A_{NX1}] = \begin{bmatrix} I_{N/2} & I_{N/2} \\ I_{N/2} & I_{N/2} \end{bmatrix} [R_{NX1}] - \begin{bmatrix} [E'_{N/2}] \cdot [I_{N/2}] & [\overline{E'_{N/2}}] \cdot [I_{N/2}] \\ \overline{E'_{N/2}} \cdot [I_{N/2}] & [E'_{N/2}] \cdot [I_{N/2}] \end{bmatrix} [R_{NX1}] \tag{3.24}$$

3.3.3 Problem Formulation

The proposed DNN architecture relies extensively on the efficient computation of the DFT. Although the DFT is a fundamental tool for spectral analysis, its performance becomes suboptimal in scenarios where the underlying signals exhibit sparsity or strong structural asymmetry. For a K-sparse input sequence $x[n]$, the DFT produces coefficients

$$X[k] = \sum_{n=0}^{N-1} x[n] e^{-j2\pi kn/N}, \tag{3.25}$$

but this linear transformation typically spreads the sparse energy across the entire spectrum. As a result, the transformed output is no longer sparse, increasing the feature dimension that the DNN must process and thereby reducing computational efficiency and learning performance.

In contrast, DRT [237] has been shown to be significantly more efficient under sparse signal conditions. The DRT employs a permutation invariant max-sum decomposition that preserves the structural sparsity of the input. For paired samples $X(2k)$ and $X(2k+1)$, the forward DRT is computed as

$$g(2k+1) = \frac{X(2k) + X(2k+1)}{2}, \quad g(2k) = \max\Big(X(2k), X(2k+1)\Big) - g(2k+1), \tag{3.26}$$

or its dual form depending on the associated encryption code. Unlike the DFT, which requires complex exponential evaluations, the DRT involves only additions, comparisons, and scalar multiplications. Consequently, the computational complexity of DRT is lower than the DFT. Thus, in sparse signal environments, the DRT provides a faster, structurally faithful, and more computationally efficient alternative to the DFT. Its ability to preserve sparsity while reducing computational load makes it particularly suitable as a preprocessing transform for DNN, leading to improved inference speed and enhanced feature extraction performance.

3.3.3.1 Sparse Signal Conditions and the Applicability of DRT for CSI Compression

The term "sparse signal condition" refers to a scenario in which only a small fraction of the transform-domain coefficients contain most of the channel energy, meaning that the channel can be represented accurately using relatively few significant coefficients. In practice, sparsity should be quantified explicitly, for example, by the percentage of coefficients required to capture a specified amount of energy (e.g., 90% or 95%) or by the sparsity ratio $\frac{K}{N}$, where K is the number of significant coefficients and N is the total number of coefficients.

The DRT does not require a fixed minimum sparsity level for implementation. It can be applied to both sparse and non-sparse signals. However, its relative advantage becomes more pronounced as the channel becomes increasingly sparse. In highly sparse channels, DRT typically provides better energy compaction and compression efficiency than conventional transforms, whereas in near-dense channels its performance tends to converge toward that of the DFT. Therefore, the term “sparse signal condition” should be accompanied by a quantitative sparsity measure when first introduced to avoid ambiguity and to clearly explain the conditions under which DRT offers the greatest benefit.

3.3.3.2 Performance Comparison of DRT and DFT in Non-Sparse Channels

DRT does not require sparsity for implementation; however, its performance advantage is primarily derived from its ability to provide stronger energy compaction and a more compact representation of sparse signals. When the channel is non-sparse or nearly dense, meaning that the signal energy is distributed across a large number of coefficients rather than concentrated in a few dominant ones, the benefits of DRT become significantly less pronounced. In such cases, the coefficient representations produced by DRT and DFT tend to be similarly dense, and their compression and reconstruction performances become comparable. Consequently, there is no inherent guarantee that DRT will outperform DFT in the absence of sparsity. In fact, for near-dense channels, DFT may be equally effective or even preferable due to its strong theoretical foundation, physical interpretation in the frequency domain, and highly optimized FFT implementation. Therefore, the superiority of DRT is most evident in moderately to highly sparse channel conditions, while for non-sparse channels the performance gap between DRT and DFT largely diminishes.

3.3.4 Why DRT Over Sparse FFT for CSI Compression?

Sparse FFT (SFFT) algorithms are designed to recover only the k largest Fourier coefficients of a signal with reduced computational complexity under the assumption that the signal is highly sparse in the Fourier domain. While this can provide computational advantages, SFFT still relies on the fixed sinusoidal basis of the DFT and therefore performs best only when the channel exhibits strong Fourier-domain sparsity. If the channel structure deviates from this assumption due to antenna reordering, mobility, or changes in the propagation environment, the sparsity representation and reconstruction accuracy may deteriorate. In addition, SFFT retains complex-valued operations and employs sampling and aliasing strategies to achieve sub-linear complexity, which increases implementation complexity compared to conventional transform-based approaches.

DRT was selected over SFFT because it does not depend on sparsity specifically in the frequency domain and can more effectively capture the inherent structure of transformed CSI data. Furthermore, DRT exhibits greater robustness to channel structural variations and antenna reordering through its permutation-invariant property, leading to more stable sparsity characteristics across different channel conditions. Its recursive, real-valued formulation also results in a simpler implementation based primarily on addition and subtraction operations, making it attractive for practical CSI compression systems. Nevertheless, an explicit experimental comparison between DRT and SFFT in terms of NMSE, cosine correlation, computational complexity, and runtime would further strengthen this justification and has been identified as a valuable direction for future evaluation.

3.3.4.1 Permutation Invariance

Unlike DFT, DRT is permutation invariant. The output of DRT does not change when the input sequence is permuted (reordered).

Let $x = [x_0, x_1, x_2, \ldots, x_n]$ be an input sequence. If $\pi(x)$ represents a permutation of x, a transform $T(x)$ is permutation invariant if:

$$T(x) = T(\pi(x)) \tag{3.27}$$

Here permutation π is a rearrangement of the elements of the vector x. For example, if $x = [x_1, x_2, x_3]$, a permutation π might rearrange this to $\pi(x) = [x_3, x_2, x_1]$. Consider a simple case where $x = [x_1, x_2, x_3]$ and $\pi(x) = [x_3, x_2, x_1]$. If we apply the DRT to both x and $\pi(x)$ the result will be the same:

$$T(x) = T([x_1, x_2, x_3]) = T([x_3, x_2, x_1]) \tag{3.28}$$

The DRT matrix A is constructed such that for any permutation matrix P (which rearranges the elements of a vector), A commutes with P. This means $A.P = P.A$, ensuring that $T(x) = T(\pi(x))$ for any x. For example we consider a input sequence $x = [1, 2, 3, 4]$ and the output DFT is $X = [10, -2 + 2j, -2, -2 - 2j]$ similarly the input sequence $x = [4, 3, 2, 1]$ and the output sequence of DFT is $X = [10, 2-2j, 2, 2+2j]$. In case DRT input $x = [1, 2, 3, 4]$ the output will be $X = [10, -2, 10, -2]$ and for input $x = [4, 3, 2, 1]$ the output of DRT is $X = [10, -2, 10, -2]$.

3.3.4.2 High Correlation in Transformed Sequence:

The DRT produces sequences with higher concentration and auto-correlation compared to the DFT. The higher correlation in DRT indicates that the transformed sequences retain more of the original structure, making them more robust noise reduction and accurate estimation.

Consider sequence $x_n = [1, -1, 1, -1]$. Obtaining DFT [238] of x_n with $X_k = \sum_{n=0}^{3} x_n.e^{-j\frac{2\pi}{N}kn}$ gives $X_k = [0, 0, 4, 0]$ for $k = 0, 1, 2, 3$. Similarly, we applying the same input sequence for DRT [232]

$$y = A.x \tag{3.29}$$

where A Rajan transform matrix. For input sequence $x = [1, 2, 3, 4]$ the auto-correlations output of DFT is $R_X = \text{IDFT}([100, 8, 4, 8])$ similarly in case DRT when the input $x = [1, 2, 3, 4]$, using $R_Y[k] = \text{Inverse DRT}(Y[k] \cdot Y^*[k])$, the output will come $R_Y = \text{Inverse DRT}([100, 4, 100, 4])$.

Computation Complexity and Energy Compaction: DRT and FFT have the same computational complexity $O(N \log N)$, but it compacts energy into fewer coefficients. For a sequence x of length 8, DFT distributed the energy evenly across its 8 complex coefficients. However DRT [233] distributes energy compactly on fewer coefficients, which results into a more efficient feedback, as fewer coefficients need to be transmitted.

Noise Resilience and Isomorphism: DRT's mapping of input sequences into a correlated form increases noise resilience in MIMO systems, where channel conditions can introduce

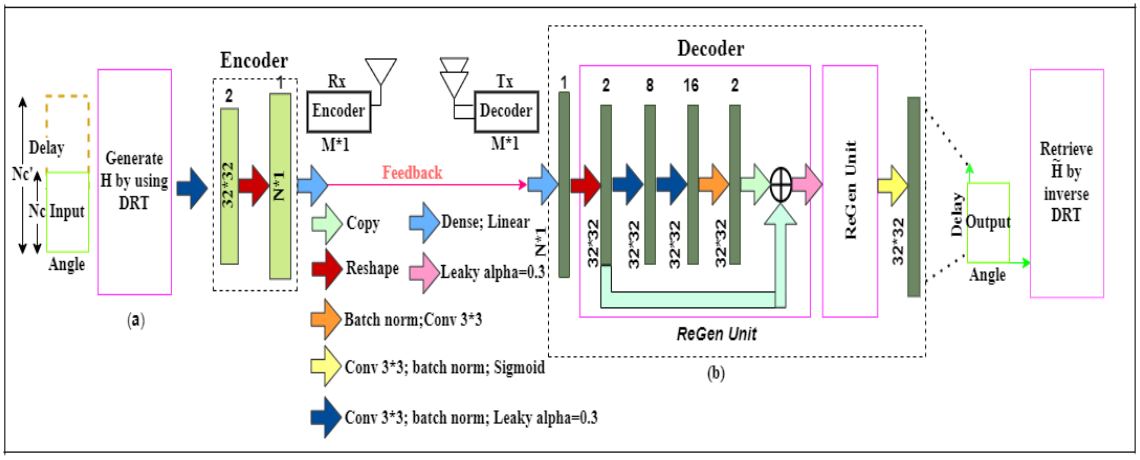

Figure 3.4: (a) False color representation of the magnitude of the $\boldsymbol{H} \in \mathbb{C}^{32\times 32}$ (b) Encoder and Decoder architecture of proposed method.

significant noise. While DFT may spread noise across coefficients, DRT maps a noisy sequence $x + n$ near the noiseless sequence x, reducing the impact of noise n on key signal components.

3.3.5 Proposed Architecture

We aim to obtain feedback $\boldsymbol{H}$ using a convolutional neural network (CNN), as it effectively captures spatial correlations through connected neurons in neighboring layers as shown in Fig. 3.4. The DL architecture has parameters length (L_1), width (W_2), and feature maps (N_3). Let $\boldsymbol{H}_r$ and $\boldsymbol{H}_i$ be the real and imaginary parts of the sparsified $\tilde{\boldsymbol{H}}$ generated by DRT. These are input into the encoder's first convolutional layer with 3×3 kernels, producing two feature maps. The feature maps are converted into a real vector s of size M, known as the codeword, via a fully connected layer. The initial layers, based on CS principles, compress data effectively while retaining key information.

After obtaining the codeword s, it is used to reconstruct $\boldsymbol{H}$. The first fully connected layer takes s as input and produces two preliminary estimates of $\boldsymbol{H}_r$ and $\boldsymbol{H}_i$ each sized $N_c \times N_t$. Each ReGen unit, as shown in Fig 3.4, has four layers. The first is the input layer, while the next three use 3×3 kernels. The second and third layers generate 8 and 16 feature maps, respectively. The output layer provides the final estimate of $\boldsymbol{H}$, with zero padding applied to match dimensions. The ReUn function, $\text{ReUn}(\gamma) = \max(\gamma, 0)$, is used for batch normalization and as the activation function.

The ReGen unit has two key features [239], [240]. First, unlike typical CNN that use pooling for downsampling, our approach focuses on refinement, maintaining the same size for both the channel matrix and the ReGen unit output. Second, we incorporate short connections, inspired by deep residual network (ResNet) [241] [242], which allow direct data flow between layers and help prevent the vanishing gradient issue caused by multiple non-linear transformations.

Incorporating two ReGen units gives optimal performance. After refinement, the channel matrix is passed to the final convolutional layer using a sigmoid function. The technique can be extended by adding more feature maps to handle multiple antennas.

In this method, we take end-to-end learning for all kernel and dominant values of the encoder and decoder. This procedure is different from the two-step technique used in [241]. The collection of parameters is represented as $\Delta = \{\Delta_{en}, \Delta_{de}\}$. The input in the proposed method is normalized $\boldsymbol{H}_i$, represented as $\boldsymbol{H}_i = f(\boldsymbol{H}_i; \Delta) = f_{de}(f_{en}(\boldsymbol{H}_i; \Delta_{en}); \Delta_{de})$ for the ith patch. Like the autoencoder, our proposed method operates as an unsupervised learning algorithm.

The ADAM (adaptive moment estimation) optimizer is implemented as an adaptive gradient descent method that simultaneously leverages momentum and per parameter learning rate scaling to achieve stable and efficient convergence in deep neural network training. At each iteration, given the gradient $g_t = \Delta_\theta \mathcal{L}(\theta_t)$, ADAM computes two exponential moving averages: the first moment estimate m_t, which captures the mean of past gradients, and the second moment estimate v_t, which accumulates the squared gradients. These are updated using

$$m_t = \beta_1 m_{t-1} + (1 - \beta_1) g_t, \quad v_t = \beta_2 v_{t-1} + (1 - \beta_2) g_t^2,$$

where β_1 and β_2 control how strongly previous information influences the estimates. Because these moments start at zero, ADAM applies bias correction to ensure unbiased estimates in early iterations:

$$\hat{m}_t = \frac{m_t}{1-\beta_1^t}, \quad \hat{v}_t = \frac{v_t}{1-\beta_2^t}.$$

The parameter update is then computed adaptively using

$$\theta_{t+1} = \theta_t - \alpha \frac{\hat{m}_t}{\sqrt{\hat{v}_t} + \varepsilon},$$

which scales the learning rate inversely with the gradient variance. This mechanism enables ADAM to take larger steps in dimensions with low gradient energy and smaller steps in directions with high curvature or noisy gradients. In the proposed system, implementing ADAM ensures faster convergence, greater robustness to noise, and stable optimization even when the training data exhibits sparsity or large dynamic range. Its ability to automatically tune effective learning rates makes it especially suitable for deep architectures and high dimensional parameter spaces.

The ADAM algorithm is used to update the set of parameters, and the loss function utilized is mean square error (MSE), which is determined as follows:

$$L(\Delta) = \frac{1}{T}\sum_{i=1}^{T} ||f(\boldsymbol{s}_i;\Delta) - \boldsymbol{H}_i||_2^2, \tag{3.30}$$

The Euclidean norm is denoted by $\| \ . \ \|_2$, while T represents the total number of samples in the training set.

3.3.6 Inputs Parameterization

We consider outdoor and indoor rural environments at 400 MHz, 3.6 GHz [243] and 5.6 GHz [244] bands, respectively. A double-directional channel with the broadcast and received antenna vectors s_t and s_r is given as [245]

$$\boldsymbol{H}(t,\tau) = \frac{1}{L}\sum_{n\in\alpha} V_n \sqrt{\frac{S_n}{L_n}} [\sum_{p=1}^{p} a_{n,p}\, s_t(\Omega_{n,p}) s_r(\Psi_{n,p}) \delta(\tau - \tau_n^l - \tau_{n,p}^M)] \tag{3.31}$$

where V_n denotes the cluster visibility gain that accounts for the change in the visibility region (VR), S_n the cluster shadow fading, L_n the cluster attenuation, and L denotes the overall pathloss which gives the reliance on the distance between the mobile station (MS) and BS. The collection of visible clusters defined by the MS position is α. The cluster-link latency is τ_n^l. The geometric delay, $\tau_n^M{}_{,p}$, corresponds to the path from the base station to the scatterer and MS. $a_{n,p}$ represents the complex Gaussian fading of cluster n's p^{th} multipath components (MPCs). $\Omega_{n,p}$ and $\psi_{n,p}$ represent the p^{th} MPC's direction of departure (DoD) and arrival (DoA) in cluster n. $\delta(.)$ is the Dirac function.

3.3.7 Normalization of Channel Parameters

Normalization of channel parameters to the range $[0, 1]$ typically involves scaling the values using a linear transformation. This can be done using the min-max normalization technique as

$$\boldsymbol{H}_{\text{norm}} = \frac{\boldsymbol{H} - \boldsymbol{H}_{\text{min}}}{\boldsymbol{H}_{\text{max}} - \boldsymbol{H}_{\text{min}}} \tag{3.32}$$

where $\boldsymbol{H}$ is the original channel parameter, $\boldsymbol{H}_{min}$ is the minimum value in the data set, and H_{max} is the maximum value in the data set. This scales the data to the range $[0, 1]$.

When dealing with complex channel coefficients, the phase changes can introduce negative values. The DRT approach described in the chapter involves handling negative values through a DC shift of $K = N(2^M - 1)$ to the sequence to shift all values, where N is the length of the sequence, and M is the bit length required to represent the maximum quantization level of the samples.

For the inverse transformation, the same constant K is subtracted from the cumulative point index (CPI) value to retrieve the original values.

3.3.8 Improvement in Noise Robustness

The primary reason for the noise robustness offered by the proposed mechanism is data segregation. Splitting data into smaller segments or patches before processing can lead to better noise handling [246, 247]. As it is known, the first step in DRT data segregation, where the input sequence is recursively divided into smaller segments. When data is divided, each segment can be analyzed and processed independently, which allows for more localized noise reduction techniques to be applied.

The noise robustness offered by DRT is precisely achieved due to the following reasons:

1. Localized Processing: When the data is split into smaller chunks (e.g., patches in an image), each segment is treated independently, which reduces the spread of noise across the entire dataset. In the context of DRT, splitting the data before applying the transform allows the DRT to handle each segment's noise separately. The transform can then smooth out noise within each segment while preserving the key features.

2. Error Localization: Splitting the data localizes any noise-induced errors to specific segments. This means that even if noise significantly affects one segment, it won't necessarily propagate to the entire dataset, thus maintaining the overall integrity of the data. The DRT, with its noise-compaction properties, further reduces the impact of noise within each segment.

DRT is designed with a recursive structure, similar to the decimation-in-frequency (DIF) fast Fourier transform (FFT). In this structure, the input sequence $x(n)$ of length N (where N is a power of 2) is recursively divided into smaller segments. At each stage, the sequence is split into two halves, and operations are performed to obtain new sequences $g(j)$ and $h(j)$ as follows: $g(j) = x(i) + x(i + \frac{N}{2})$ and $h(j) = |x(i) + x(i + \frac{N}{2})|$. This decomposition continues until no further division is possible, providing a hierarchical representation of the signal. Such decomposition allows the transform to manage and reduce noise effects by isolating noise components at different levels of the signal structure.

Consider a simple sequence x with some added noise: $x = [1, 2, 3, 4]+$noise. Let's assume the noise added is a small random variation at each point: noise $= [0.1, -0.2, 0.15, -0.1]$, so the noisy sequence becomes: $x_{\text{noisy}} = [1.1, 1.8, 3.15, 3.9]$. The original sequence is $x_{\text{orig}} = [1, 2, 3, 4]$ and the noisy sequence is $x_{\text{noisy}} = [1.1, 1.8, 3.15, 3.9]$. After applying the DRT we get the original DRT result: $[10, -2, 10, -2]$ and noisy DRT result: $[9.95, -1.45, 9.95, -1.45]$.

Despite the added noise, the DRT result for the noisy sequence is very close to that of the original sequence. This shows that the DRT has smoothed out the noise, preserving the main features of the data.

3.4 Algorithm Implementation

We now present a practical implementation of the scheme proposed above. We show the algorithmic implementation of a DL-based approach to enhance CSI feedback in FDD massive MIMO systems. This comprehensive process involves data preprocessing in the initial stage and training and evaluation of neural network models in latter stage.

In the initial phase of data preprocessing, the script employs DRT to convert complex channel data ($\boldsymbol{H}_r$ and $\boldsymbol{H}_i$) into polar coordinates (magnitude r and phase Φ) as

$$\begin{aligned} \phi &= \arctan 2(\boldsymbol{H}_r, \boldsymbol{H}_i), \\ r &= \sqrt{{\boldsymbol{H}_r}^2 + {\boldsymbol{H}_i}^2}. \end{aligned} \tag{3.33}$$

The DRT is subsequently used to revert the polar coordinates back to complex numbers, expressed by:

$$\begin{aligned} \boldsymbol{H}_r &= r \cdot \cos(\phi), \\ \boldsymbol{H}_i &= r \cdot \sin(\phi). \end{aligned} \tag{3.34}$$

Following preprocessing, the focus shifts to the neural network architecture. The script details the construction of an autoencoder model. This model comprises convolutional layers with rectified unit (ReUn) activation functions for encoding spatial hierarchies and dense layers for transforming these features into a lower-dimensional space. The decoding process then utilizes convolutional layers with linear activation functions to reconstruct the data.

Additionally, a ResNet is integrated into the model to refine its output. This network is composed of residual blocks containing Conv2D and Batch Normalization layers. The

Algorithm 1 DRT-based DL for Channel Estimation in Massive MIMO

1. Data Preprocessing Phase:
a. Convert complex channel data to polar coordinates ϕ and r using DRT.

$$\phi = \arctan\left(\frac{\mathrm{Im}(\mathbf{H})}{\mathrm{Re}(\mathbf{H})}\right),$$
$$r = \sqrt{(\mathrm{Re}(\mathbf{H}))^2 + (\mathrm{Im}(\mathbf{H}))^2}.$$

b. Revert polar coordinates back to complex numbers $\mathbf{H}_r$ and $\mathbf{H}_i$ using inverse DRT.

$$\mathbf{H}_r = r\cos(\phi),$$
$$\mathbf{H}_i = r\sin(\phi).$$

2. Neural Network Architecture:
a. Construct an Autoencoder Model with:
- ReLU activated convolutional layers for encoding.
- Dense layers for feature transformation.
- Linear activated convolutional layers for decoding.

b. Integrate ResNet for output refinement with:
- Residual blocks with Conv2D and Batch Normalization.
- Identity function learning to prevent degradation.

3. DNNet Model Development:
a. Denoise CSI feedback and fine tune for noise reduction.
b. Similar model with the autoencoder.
4. Training and Optimization:
a. Utilize Adam optimizer with a learning rate of 0.001.
b. Minimize MSE loss during training.
c. Monitor performance using custom callbacks.
5. Model Evaluation:
a. Utilize normalized NMSE and ρ metrics.
b. Assess reconstructed signal accuracy with NMSE.
c. Check data similarity with ρ.

purpose of these blocks is to facilitate learning of the identity function, which is crucial in preventing performance degradation in deeper models.

Parallel to the autoencoder, a DNNet model is also developed, specifically for the purpose of denoising CSI feedback. This model shares a similar structure to the autoencoder but is fine-tuned for effective noise reduction.

These models are trained and optimized using an Adam optimizer with a predefined learning rate of 0.001. They are trained to minimize the MSE loss over a series of epochs, and performance is monitored through custom callbacks (LossHistory).

Two key metrics are utilized to evaluate model performance: NMSE and cosine correlation (ρ). NMSE is calculated as

$$\text{NMSE} = E\left\{\frac{\|\boldsymbol{H}_o - \boldsymbol{H}_p\|_2^2}{\|\boldsymbol{H}_o\|_2^2}\right\} \tag{3.35}$$

where $\boldsymbol{H}_o$ and $\boldsymbol{H}_p$ denote original and predicted data respectively. This metric is essential for assessing the accuracy of the reconstructed signal. Cosine correlation, on the other hand, is used to evaluate the similarity between the original and predicted data, determined by,

$$\rho = E\left\{\frac{\sum(\boldsymbol{H}_o \times \boldsymbol{H}_p)}{\|\boldsymbol{H}_o\|_2 \times \|\boldsymbol{H}_p\|_2}\right\} \tag{3.36}$$

The final stage involves testing the models under varying SNR conditions by introducing Gaussian noise to the test data. The performances of the models are then evaluated across a spectrum of SNR values using the aforementioned metrics.

3.4.1 System-Level Impact of NMSE and Cosine Correlation

NMSE and cosine correlation (ρ) are widely used as surrogate measures of CSI reconstruction quality because they quantify how accurately the reconstructed channel $\hat{\boldsymbol{h}}$ matches the true channel $\boldsymbol{h}$. However, their true significance lies in their impact on end-to-end communication performance. Among the two metrics, cosine correlation has the most direct relationship with beamforming gain, which can be expressed as

$$G = \frac{|\boldsymbol{h}^H \hat{\boldsymbol{h}}|^2}{||\boldsymbol{h}||^2 ||\hat{\boldsymbol{h}}||^2} = \rho^2. \tag{3.37}$$

Thus, a higher ρ directly translates into better alignment between the beamforming vector derived from the reconstructed CSI and the optimal beamforming direction, resulting in higher array gain and received signal power. Similarly, lower NMSE indicates a more accurate reconstruction of the channel coefficients, which generally improves precoding and resource allocation decisions. Consequently, improvements in NMSE and ρ typically lead to higher effective SINR and, therefore, higher spectral efficiency according to

$$R = \log_2(1 + \mathrm{SNR}). \tag{3.38}$$

The impact of CSI reconstruction quality extends beyond throughput to link reliability and energy consumption. More accurate CSI enables better interference suppression and signal detection, leading to lower BER, particularly in high order modulation schemes where channel estimation errors have a pronounced effect. Furthermore, accurate CSI allows the transmitter to focus energy more effectively toward the intended user, reducing the transmit-power margin required to achieve a target SNR. This improves energy efficiency and reduces the need for retransmissions, thereby enhancing overall network performance. Therefore, improvements in NMSE and ρ indirectly contribute to gains in beamforming efficiency, spectral efficiency, BER performance, and energy consumption.

However, two models with similar NMSE values can still produce substantially different communication performance. NMSE is an average error metric and does not reveal where the reconstruction errors occur within the CSI matrix. Communication performance depends disproportionately on the accuracy of dominant propagation paths, spatial directions, and phase information. A model whose error is uniformly distributed across all coefficients may preserve the dominant channel structure and beamforming direction very well, resulting in high ρ and excellent system performance. In contrast, another model with the same NMSE may concentrate its errors on the strongest channel components, leading to poorer beamforming alignment, lower spectral efficiency, and higher BER. Therefore, NMSE alone is insufficient to fully characterize communication performance, which is why both NMSE and ρ should be evaluated alongside system-level metrics such as beamforming gain and spectral efficiency.

3.5 Simulations and Experimental Results

Simulations were conducted in an indoor pico-cellular setup at 5.3 GHz with 1024 subcarriers, using a 32-antenna BS in a 20 m × 20 m area and randomly placed UE. The ResNet model incorporated two residual blocks with a 512-dimensional encoded layer, optimized for a $32 \times 32 \times 2$ CSI matrix input. Training used $100,000$ samples, with $30,000$ for validation and $20,000$ for testing, learning rate 0.001, batch size 200, and 500 epochs for both the autoencoder and DRT models. Model performance was evaluated across SNR levels from -5 to 40 dB using NMSE and cosine correlation metrics on noisy test data. Results showed the DRT model's enhanced noise robustness and accuracy, with consistently lower NMSE and higher cosine correlation than baseline models.

3.5.1 Generation of Training Data and Challenges

The DL model's training data was generated using the COST 2100 model, simulating CSI with varying SNRs, antenna configurations, and environmental settings. Training data was calculated for N_t, N_c, SNR, and $\boldsymbol{H}_n = [h_{n,1}, h_{n,2}, \ldots, h_{n,N_t}] \in \mathbb{C}^{1\times N_t}$, for $n = 1, 2, \ldots, N_c$. The dataset includes 100,000 training, 30,000 validation, and 20,000 test samples, with each CSI matrix of size $32 \times 32 \times 2$ (for 32 subcarriers and antennas). Each sample thus contains 2048 values, separating real and imaginary parts.

Generating realistic training data is challenging due to the complexity of massive MIMO channels, sparsity, and feedback overhead, addressed here using DRT. Massive MIMO, with many antennas (N_t) and subcarriers (N_c), results in high-dimensional CSI matrices, demanding efficient data handling to manage storage and processing loads-a need met by

Table 3.1: Simulation and Model Parameters

Parameter	Value
Carrier frequency	5.3 GHz
Cell environment	Indoor pico-cell
Cell area	20 m $\times$ 20 m
Number of subcarriers (N_c)	1024
Number of BS antennas (N_t)	32
UE placement	Random within cell
CSI matrix dimension	$32 \times 32 \times 2$
Number of CSI values per sample	2048
Model architecture	ResNet with 2 residual blocks
Encoded feature dimension	512
Batch size	200
Learning rate	0.001
Epochs (Autoencoder & DRT models)	500
Training samples	100,000
Validation samples	30,000
Test samples	20,000
Channel model	COST 2100
SNR range	-5 to 40 dB
Noise type	Additive synthetic noise
Performance metrics	NMSE, Cosine Correlation

DRT. Noise significantly impacts CSI in practice, so the training data covers various SNRs, with synthetic noise added to enhance model robustness. The sparse CSI representation from DRT allows faster, computationally efficient processing, making the model suitable for real-time applications.

The training data was generated with parameters from (3.14) to capture the complexity of massive MIMO systems. The dataset size was designed to ensure good model generalization, with emphasis on managing the high dimensionality, sparsity, and noise robustness of the CSI matrices.

3.5.2 Data Preprocessing Phase

The data preprocessing phase in Algorithm 1 plays a critical role in obtaining the CSI with DL. This phase transforms the complex channel data into a more manageable form.

The DRT first converts the complex channel data into polar coordinates (magnitude and phase). This transformation essentially reduces the feedback overhead. The preprocessing step also helps to isolate the key features of the data that are most relevant for the DL model, thereby improving its focus and accuracy. The dimensionality reduction achieved during this phase also helps in decreasing the computational load and accelerating the training process without sacrificing model accuracy. Additionally, this transformation enhances noise robustness, which helps in maintaining a high performance in noisy environments.

3.5.3 Performance Assessment

Fig. 3.5 shows ρ performance across varying SNR (dB) levels, comparing our method with the DFT based DL mechanism [248] and other techniques. The noise free ideal threshold (ρ or NMSE without noise) is also shown. ρ values for all algorithms increase with SNR, with the proposed DRT consistently outperforming others at all SNR levels, with a 126.19% improvement in performance observed.

Fig. 3.6 shows the NMSE performance of the DFT based DL algorithm with noise [65], DeepAE [199], and the proposed DRT based DL, following pre-training. The horizontal line at -30 dB represents the benchmark NMSE for the DFT based DL algorithm under noise free conditions. In noisy environments, the NMSE of the DFT based DL algorithm degrades significantly. As SNR increases, both DFT based and DRT based mechanisms show a gradual NMSE reduction. The proposed DRT based DL method improves performance by 81.81% over the DFT based DL algorithm.

Figs. 3.7 and 3.8 assess the performance of DRT based DL at different learning rates (LRs). Fig. 3.7 presents cosine correlation vs SNR, showing that DRT based DL outperforms the DFT based DL across various LRs. Fig. 3.8 depicts NMSE vs SNR for both methods at different LRs, with the DRT based DL method exhibiting lower error compared to the DFT based DL.

The Fig. 3.9, represent the relation between cosine correlation vs SNR (dB) for 32 DFT based DL and 32, 64, 128 and 256 DRT (Indoor/Outdoor) based DL antennas. After simulating the DRT and DFT based DL algorithm for different size of antennas our DRT

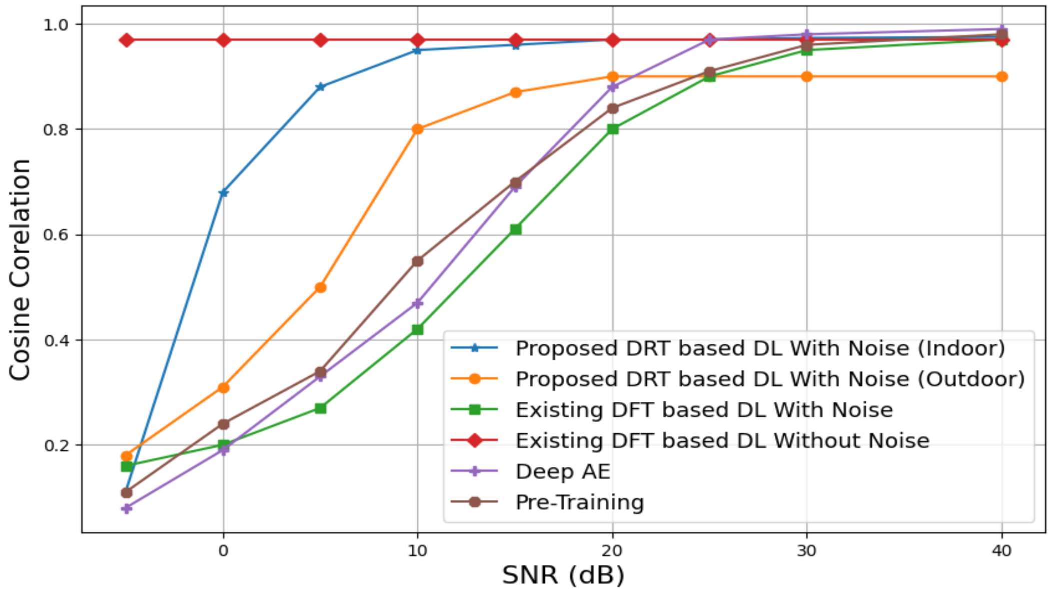

Figure 3.5: Cosine correlation vs SNR (dB) with and without noise simulations results for DRT based DL (Indoor/Outdoor) and DFT based DL with different algorithms.

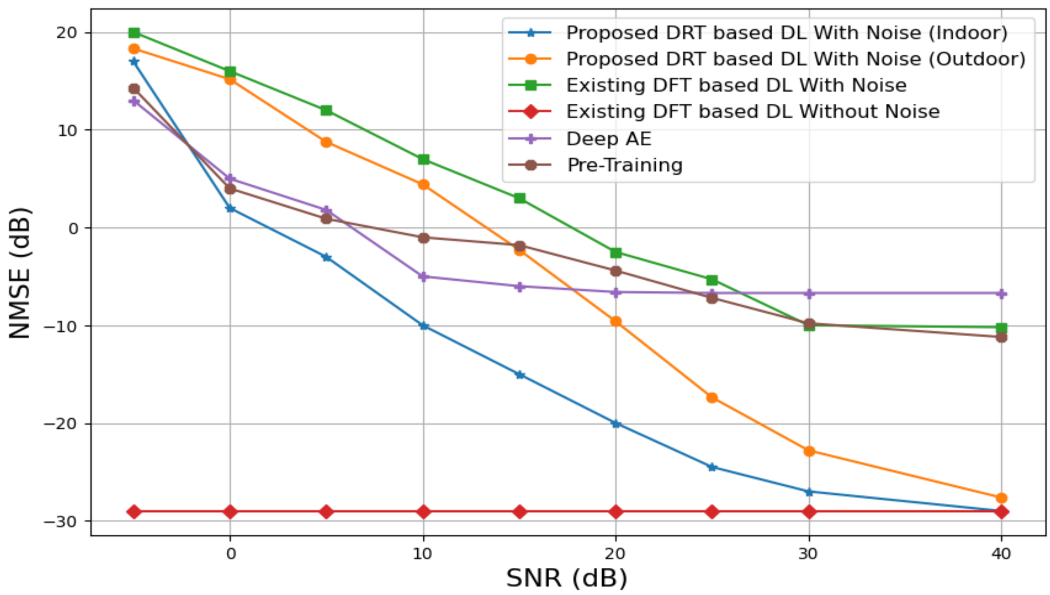

Figure 3.6: NMSE vs SNR with and without noise simulations results for DRT based DL (Indoor/Outdoor) and DFT based DL with different algorithms.

gives better result. Fig. 3.10, shows the relation between NMSE vs SNR of 32 DFT based DL and 32, 64, 128 and 256 DRT (Indoor/Outdoor) based DL antennas. After comparison the results the DRT based DL method give better as DFT.

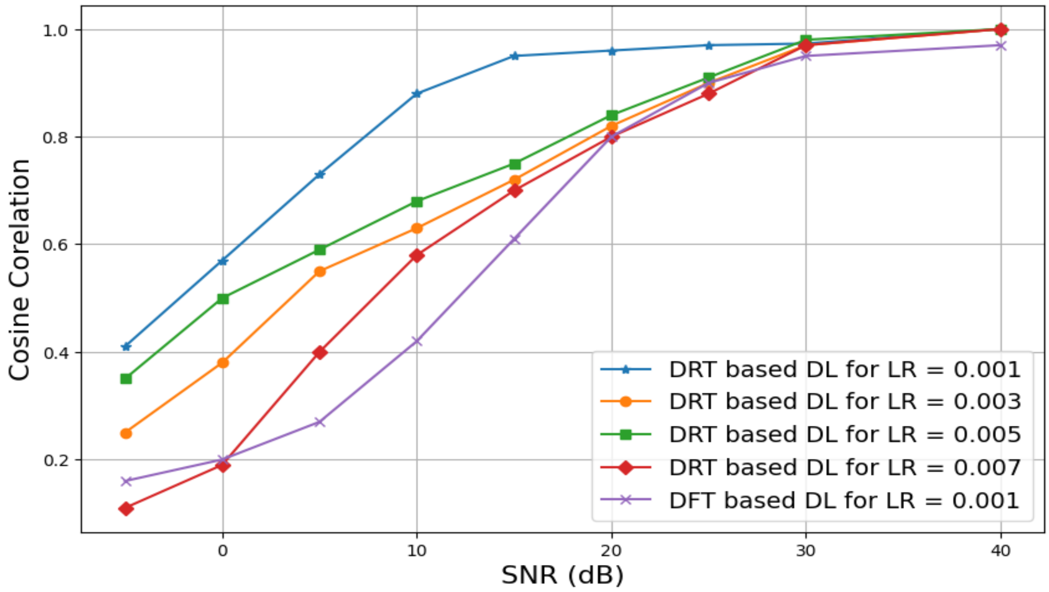

Figure 3.7: Cosine correlation vs SNR (dB) for different learning rates (LR).

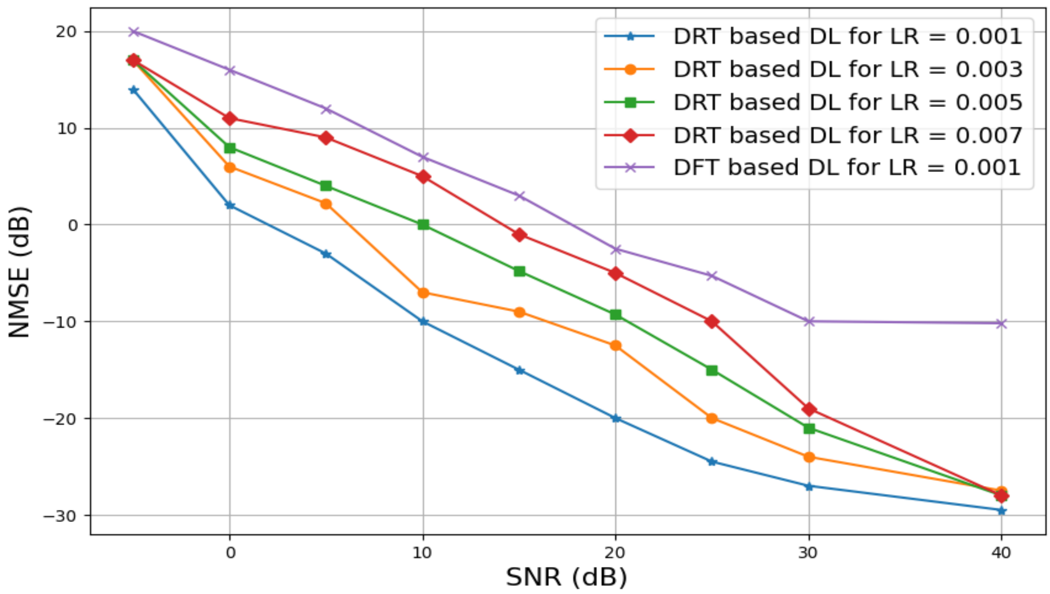

Figure 3.8: NMSE vs SNR for different learning rates (LR).

3.5.4 Real World Challenges for the Proposed Method and Solutions

Real-time implementation of the proposed scheme faces challenges due to massive MIMO and DL application complexities. Practical massive MIMO systems encounter hardware issues like high complexity, cost, and scalability. The proposed system antennas and RF chains require in the orders of 32×32, 64×64, up to 256×256, leading to challenges in power, calibration, and synchronization. These challenges can be addressed by using hybrid beamforming with dedicated RF chains, rather than full digital beamforming [249,

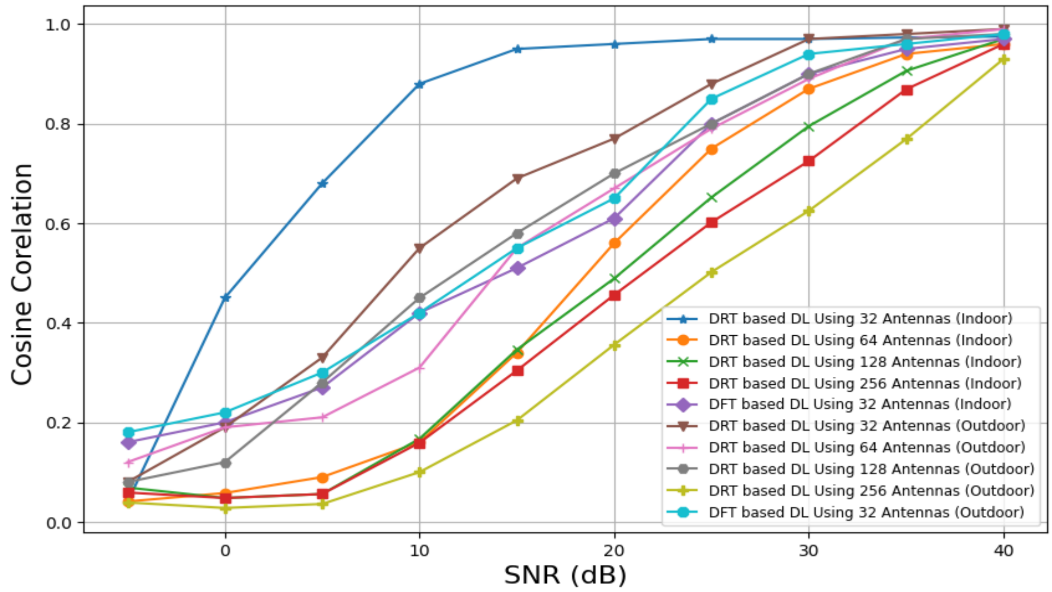

Figure 3.9: Cosine correlation vs SNR (dB) comparison of 32 DFT and 32, 64, 128 and 256 DRT (Indoor/Outdoor) based antennas.

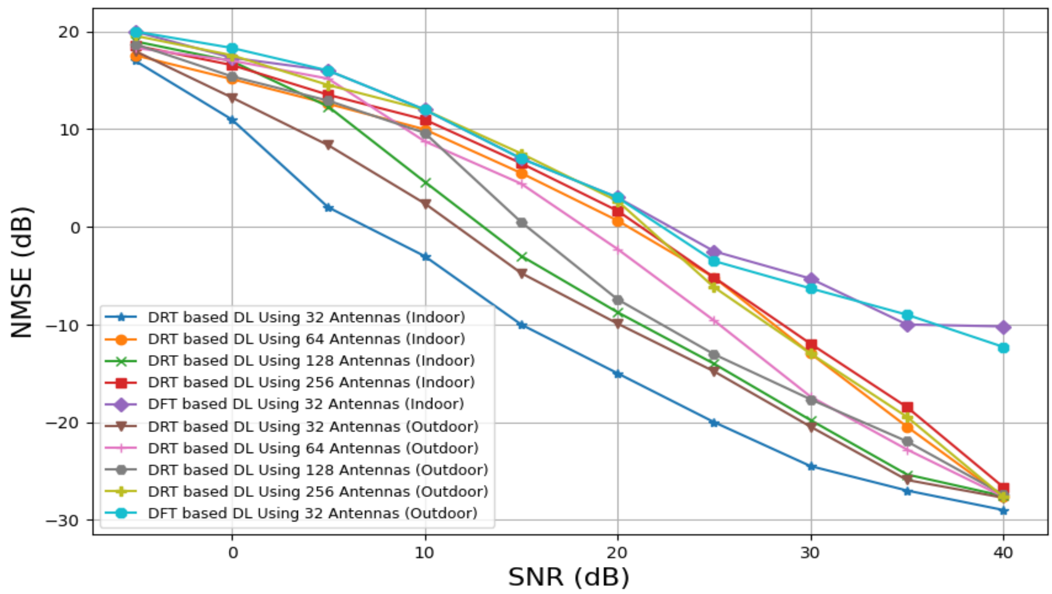

Figure 3.10: NMSE vs SNR comparison of 32 DFT and 32, 64, 128 and 256 DRT (Indoor/Outdoor) based antennas.

250], and low-resolution ADCs at each antenna can help reduce power and cost [251, 252]. Further, the challenges due to DL applications in MIMO arise due to the use of ADAM optimization for high dimension gradients. The DL model uses the ADAM optimization algorithm [253] for training. The ADAM algorithm updates the parameters based on the gradients $\mathbf{g}_t$ at time step t, with the following updates:

$$\begin{aligned}\mathbf{m}_t &= \beta_1 \mathbf{m}_{t-1} + (1-\beta_1)\mathbf{g}_t \\ \mathbf{v}_t &= \beta_2 \mathbf{v}_{t-1} + (1-\beta_2)\mathbf{g}_t^2 \\ \theta_{t+1} &= \theta_t - \alpha \cdot \frac{\mathbf{m}_t}{\sqrt{\mathbf{v}_t}+\epsilon}\end{aligned} \tag{3.39}$$

Here, $\mathbf{g}_t$ is the gradient of the loss with respect to the weights, $\mathbf{m}_t$ and $\mathbf{v}_t$ are the first and second moment estimates, and α, β_1, β_2, and ϵ are hyperparameters. In large-scale MIMO, the gradient dimension corresponds to the antenna count, so a 256×256 system has a $\mathbf{g}_t$ with 65,536 elements, making updates computationally demanding and challenging memory/speed. These challenges can be eased using gradient pruning [254], parallel computing, or 16-bit precision for updates.

3.6 Computation Complexity of the Proposed Scheme

The implementation of the proposed scheme first involves the application of DRT, where conventionally, DFT has been used. The direct computation of DFT requires $O(N^2)$ operations. However, the fast Fourier transform (FFT) - an optimized algorithm to compute the DFT - reduces this computational complexity to $O(N \log N)$. The complexity of DRT is similar to the FFT, that is $O(N \log N)$. The recursive structure of DRT, which involves operations like splitting and summing sequences, allows it to achieve this efficiency. However, the operations in DRT are tailored to enhance specific properties like high correlation and energy compaction, which are beneficial for certain applications. Computational complexity of a DRL model, we analyze the different components involved in the learning and inference processes. The complexity is expressed in terms of floating point operations per second (FLOPS).

3.6.1 Neural Network Complexity - Fully Connected Layer

For a fully connected (dense) layer, the computational complexity [255][256] can be calculated based on the input size n_{in} (number of input features) and the output size n_{out} (number of neurons in the layer). In a fully connected layer, as each input feature is multiplied by a weight for each output neuron $n_{\text{out}} \times n_{\text{in}}$ multiplications are needed. Then the products are summed up for each output neuron excluding the initial term, giving $n_{\text{out}} \times (n_{\text{in}} - 1)$ additions. Additionally, a bias term is added for each neuron. Therefore, the total FLOPS for one fully connected layer is $\text{FLOPS}_{\text{FC}} = n_{\text{out}} \times n_{\text{in}} + n_{\text{out}} \times (n_{\text{in}} - 1)$ which simplifies to $\text{FLOPS}_{\text{FC}} = 2 \times n_{\text{out}} \times n_{\text{in}} - n_{\text{out}}$. As for large networks $n_{\text{out}} << n_{\text{in}}$, Thus,

$$\text{FLOPS}_{\text{FC}} \approx 2 \times n_{\text{out}} \times n_{\text{in}} \tag{3.40}$$

3.6.2 Complexity of a Convolutional Layer

For a convolutional layer, the complexity [257] depends on: Input Feature Map Size: $H \times W$ (height and width) Number of Input Channels: C_{in} Kernel Size: $K \times K$ (assuming square filters) Number of Output Channels: C_{out} Output Feature Map Size: $H_{\text{out}} \times W_{\text{out}}$ (height and width of the output feature map) each output pixel requires $K \times K$ multiplications for each input channel and the sum of these products. Therefore, the FLOPS for a convolutional layer is:

$$\text{FLOPS}_{\text{Conv}} = H_{\text{out}} \times W_{\text{out}} \times C_{\text{out}} \times \left(C_{\text{in}} \times K^2\right) \times 2 \tag{3.41}$$

3.6.3 Total Computational Complexity for the NN

For a neural network with multiple layers, the total FLOPS can be obtained by summing the FLOPS for each layer:

$$\text{FLOPS}_{\text{NN}} = \sum_{l=1}^{L} \text{FLOPS}_l, \tag{3.42}$$

where L is the total number of layers in the network, and FLOPS_l represents the FLOPS for the l-th layer, which can be a fully connected layer, convolutional layer or another type of layer.

3.6.4 Processing Power and Time Complexity of NN

Let P be the processing power in FLOPS, which represents the number of floating-point operations the hardware can perform per second. The time taken to execute the neural network T_{NN} can be calculated as: $T_{\text{NN}} = \frac{\text{FLOPS}_{\text{NN}}}{P}$, where T_{NN} is the inference time of the neural network in seconds.

3.6.5 Comparison between Channel Coherence Time and Neural Network Inference Time

A fundamental requirement for the proposed scheme, the channel gain $\boldsymbol{H}$ must remain constant during one NN inference time, T_{NN}. The channel coherence time, T_c, defines the duration in which $\boldsymbol{H}$ is constant. Thus, $T_{NN} \ll T_c$. If T_{NN} exceeds T_c, channel conditions change during processing, leading to outdated CSI and lower performance. The coherence time, inversely related to the Doppler spread f_D, is $T_c \approx \frac{1}{f_D} = \frac{c}{vf_c}$ where v is the receiver speed (m/s), f_c the carrier frequency (Hz), and c the speed of light (3×10^8 m/s). For a car moving at $v = 27.78$ m/s with $f_c = 5.3$ GHz, we get $f_D = 490.47$ Hz and $T_c \approx 2.038$ ms.

Let T_{NN} depend on NN complexity C (FLOPS) and processing power P (FLOPS), then $T_{NN} \approx \frac{C}{P}$. as detailed in Section VI.

As mentioned above,

$$T_{NN} < T_c \tag{3.43}$$

We calculate T_{NN} for the parameters used in our work, that is $n_{\text{in}} = 1024$ and $n_{\text{out}} = 512$, $H = W = 32$, $C_{\text{in}} = 64$, kernel size $K = 3$, and $C_{\text{out}} = 128$. The FLOPS for the fully connected layer are obtained as, $\text{FLOPS}_{\text{FC}} = 2 \times 512 \times 1024 = 1,048,576$ FLOPS The FLOPS for the convolutional layer are obtained as $\text{FLOPS}_{\text{Conv}} = 32 \times 32 \times 128 \times (64 \times 3^2) \times 2 = 32 \times 32 \times 128 \times 576 \times 2 = 754,974,720$ FLOPS. The total FLOPS for the NN are obtained as $\text{FLOPS}_{\text{NN}} = 1,048,576 + 754,974,720 \approx 756,023,296$ FLOPS

Inference Time with Processing Power $P = 1$ TFLOPS ($P = 10^{12}$ FLOPS)

$T_{\text{NN}} = \frac{756{,}023{,}296}{10^{12}}$ seconds $= 0.756$ ms. Thus, $T_{NN} < T_c$, which shows that during one inference cycle of the NN, the channel gain will remain unchanged, thereby allowing efficient estimation.

3.6.6 Throughput-Based Assessment of CSI Estimation Accuracy

Yes. CSI estimation accuracy can be measured in terms of throughput by using the reconstructed channel matrix $\hat{\boldsymbol{H}}$ to design the precoder and then evaluating its performance on the true channel $\boldsymbol{H}$. The resulting SNR can be used to compute the achievable throughput through Shannon's capacity relation. This approach provides a direct system-level assessment of CSI quality, since more accurate CSI reconstruction generally leads to better beamforming, reduced interference, higher SNR, and consequently higher throughput. Therefore, throughput serves as a practical and communication-oriented measure of CSI estimation accuracy, complementing traditional reconstruction metrics such as NMSE and cosine correlation.

3.7 Conclusion

In summary, this chapter presents a novel DL-based channel feedback framework that integrates the DRT to significantly enhance CSI reduction and reconstruction performance in massive MIMO systems. Our analysis highlights the limitations of conventional DFT-based CS methods, particularly their higher computational complexity and degraded efficiency in sparse or noisy environments. By contrast, the proposed DRT enabled DL architecture preserves structural sparsity, reduces complexity, and enables more effective feature extraction for CSI compression.

Extensive simulations conducted using the COST 2100 channel model demonstrate the superiority of the proposed scheme across a wide SNR range. Quantitatively, the DRT-assisted algorithm achieves notable performance gains improving cosine correlation by 126.19% and NMSE by 81.81% compared to the DFT-based DL approach. These improvements are especially prominent in low SNR conditions, where accurate CSI estimation is typically challenging. The enhanced robustness, reduced feedback overhead, and scalability offered by the DRT-based framework position it as a strong prospect for next-generation wireless communication systems.

Overall, the findings of this work underscore the potential of DRT-assisted DL for efficient and reliable channel feedback in advanced massive MIMO deployments. By addressing key bottlenecks associated with DFT-based CSI reduction, our approach contributes a practical, high performance solution for 5G and future 6G networks requiring fast, accurate, and low complexity channel estimation.

Chapter 4

Hadamard Transform Enhanced DL-for Massive MIMO CSI Feedback Reduction

As discussed in the last chapter, reducing the CSI feedback overhead is essential in massive MIMO 5G and emerging 6G technologies. Although CS has been proposed to address this issue, the use of the DFT within CS results in high computational complexity. For efficient CSI feedback reduction via CS, DRT-based DL was introduced. However, DRT-based DL also has some limitations. DRT-based DL is not strictly orthogonal for all signal lengths. Thus, energy is not perfectly preserved and inverse reconstruction can introduce numerical errors. This non-orthogonality can amplify small perturbations during decoding, reducing numerical stability, especially under less SNR conditions. Additionally, this method requires external normalization or scaling to enable accurate reconstruction, increasing processing steps. Its transform structure is also sensitive to input ordering, making it less robust for DL models that require permutation invariant feature extraction. To overcome these limitations, this chapter proposes HaDLeMO: **Ha**damard **D**eep **Le**arning for massive MI**MO** which uses the discrete Hadamard transform (DHT). HaDLeMO offers superior energy compaction, permutation invariance, and pattern recognition capabilities with lower computational overhead compared to DFT. With the application of

DHT into a CS-DL framework, our approach enhances sparsity representation and convergence efficiency. At an SNR of 10 dB, the simulation results clearly demonstrate the superiority of the proposed HaDLeMO scheme. For NMSE, the existing DFT-based DL method achieves a baseline value of 7.0, while DeepAE improves it to -5.01. In contrast, HaDLeMO significantly outperforms both with an NMSE of -11.04. Similarly, in terms of cosine correlation, the baseline DFT-based DL scores 0.42, and DeepAE reaches 0.471, whereas HaDLeMO achieves a much higher value of 0.880. These results confirm that HaDLeMO delivers substantially better CSI reconstruction accuracy compared to the existing methods.

4.1 Overview

The arrival of 5G and impending 6G communications have led to the development of novel technologies, to increase data throughput, channel capacity, and reduction of feedback overhead [200, 258]. Massive MIMO, is one of these technologies that employs multi-antenna base stations and access points.

Massive MIMO uses a huge number of antennas [216] at the BS. The number of antennas can vary from hundreds to thousands, used in a centralized [259] or decentralized [260, 261] manner. This results in improved overall throughput and a significant reduction in interference [262]. However, this system requires energy-intensive devices and sophisticated signal processing, which is expensive. Therefore, it is essential to investigate simple and energy-efficient implementation strategies that support sustainable and environmentally friendly solutions.

As discussed in chapter 3, the downlink CSI, in modern MIMO systems [263, 264] is acquired from users during the training process. The information is transmitted through a feedback link back to the BS [265]. The amount of feedback in massive MIMO is significantly high, resulting in important overhead. Minimizing the feedback load [221] while maintaining communication efficiency is a fundamental problem addressed in several research works [266, 179, 267, 177, 224, 268, 184, 64].

Liang et al. [266] use CS in massive MIMO systems to reduce the feedback load for CSI. The authors introduce sparsity-based adaptive feedback algorithms that dynamically adapt in response to channel conditions in spatially correlated antenna arrays. Ge et al. [179] demonstrate the possible transformation of correlated CSI into an uncorrelated sparse vector, which enables CS to calculate a sparse vector accurately using an inadequately specified linear system. To increase the predictive accuracy and interpretability of the statistical model, Shalom and Han et al. [267, 177] suggest the LASSO-l1-solver, a regression analysis technique that carries out both variable selection and regularization. The authors in [224] introduced AMP, a method based on CS and updating estimates of sparse signals. In [268], block matching 3D-approximate message passing (BM3D-AMP) has been proposed. In [225], AMP-Net is a deep unfolding framework designed to enhance compressive image sensing by integrating denoising techniques into the AMP algorithm. It is an expansion that combines the ideas of BM3D with AMP. In [184], block matching and collaborative filtering form the foundation of the BM3D-AMP denoising algorithm, which uses an approximation message forwarding framework. However, due to a basic sparsity assumption, a high dimensional signal can be represented using only a small number of significant coefficients, with the remaining values being zero or negligibly small, it can have problems when recovering the CSI. The approximate sparsity of the channel matrix makes previous CS-based modeling difficult and severely degrades reconstruction quality.

Data are compressed using random projections when CS is applied in the aforementioned mechanisms. It involves reducing the dimensionality of the data by multiplying it by a random matrix. Wen et al. [64] present a DL-based mechanism that uses the information in the feature maps rather than random projections to construct a compressed codeword. The authors sparsify the data, at the encoder end, and retrieve the data, at the decoder end, using the DFT and inverse DFT.

Using DFT in sparse data can cause a delay in algorithm convergence [229]. Sparse signals contain many zero- or almost zero-coefficients. The DFT application involves breaking the signals into sums of sinusoidal functions. Sinusoids distribute energy across many frequency components. As a result, DFT fails to localize sharp features and introduces spectral leakage when a signal frequency does not perfectly match the discrete frequency bins of the transform. The energy spreads across multiple bins, distorting frequency analysis, which results in an inefficient handling of sparsity. In order to interpret sparse signals and converge to a solution, DFT-based algorithms need additional iterations, which increases computational burden and results in poor data compression. Consequently, these methods may face limitations in meeting the data rate demands of 5G and beyond communications. Furthermore, CS-based applications require transforms that can identify patterns regardless of the order of input pieces.

To overcome the limitations of DFT based CS, in the last chapter, a DRT-based DL mechanism was proposed for CSI feedback reduction in massive MIMO. However, DRT-based DL mechanisms further have certain limitations. It significantly reduces CSI feedback overhead and computational complexity compared to DFT-based CS, it still suffers from important limitations. The DRT-based DL method is not strictly orthogonal for all signal lengths, leading to imperfect energy preservation and reconstruction errors during inverse transformation. Its non-orthogonality can also amplify small numerical problems, reducing stability in noisy or low-SNR environments. Additionally, this method requires additional normalization or scaling steps to recover the original signal, adding implementation overhead. These factors limit the robustness and reconstruction accuracy of DRT-based DL frameworks, especially in practical massive MIMO scenarios with noise, mobility, and hardware imperfections.

Although, DHT based prior works also emphasize image coding [269], mathematical theory [270] and analog compression limits [271]. Pan and Park et al. [272, 273] employed DHT-based neural networks to reduce computational cost. Pan et al. [272], introduced a novel neural network layer that replaces conventional 1×1 convolutions with a fast DHT combined with a smooth thresholding denoiser. They further proposed multiplication free Hadamard-based operators to implement 3×3 depthwise separable convolutions. By integrating these lightweight DHT layers into MobileNet-V2, the model achieves a substantial reduction in parameters with only a minor accuracy loss. But, their design focuses on feature representation along the width and height dimensions through a scaling layer. More recently, Pan et al. [274] extended this framework by introducing channel wise processing in the Hadamard domain, enabling the extraction of channel specific features and proposing a quantum computing-based network realization.

In this chapter, we propose Hadamard DL for massive MIMO (HaDLeMO) optimization. HaDLeMO is an improved CS-based DL mechanism assisted by the DHT to obtain the CSI in a massive MIMO system. A similar approach has been proposed in [272] but the author donot incorporate channel wise feature extraction. Specifically, we exploit neural architectures to jointly learn feature extraction, denoising, and efficient feedback coding, addressing the challenges of scalability, robustness, and real-time adaptation in next-generation wireless communications. DHT has a permutation invariant property and produce a sequence with a higher correlation value compared to DFT.

The contributions made in this work are as follows.

1. *Effective feedback with improved data sparsification*: HaDLeMO enhances CSI feedback by combining DL with the DHT, which produces highly sparse and structured representations of the channel. Since DL models rely on meaningful feature extraction, the DHT reorganizes CSI into patterns that are easier for the network to learn. Its orthogonal and multiplication free nature preserves signal energy while highlighting dominant components. This allows the DL encoder to generate compact, informative feature maps. Consequently, HaDLeMO provides efficient sparsification and significantly reduces feedback overhead with improved reconstruction performance.

2. *Independence from the sequence of input variables*: Permutation invariance is crucial for DL-based sparsification of MIMO-CSI, as the network must recognize patterns regardless of how input elements are ordered. HaDLeMO achieves this because the DHT is inherently insensitive to permutations in the input sequence. This ensures that the extracted features remain stable even when CSI elements vary in arrangement. As a result, the model becomes more robust, learns more generaliz-

able representations, and avoids errors caused by order dependent transforms like the DFT.

3. *Enhanced resilience to noise*: HaDLeMO exhibits strong robustness to noise because the DHT is insensitive to phase distortions and focuses on capturing essential structural patterns in the CSI. This characteristic is crucial for DL models, which often degrade when trained or tested on noisy inputs. By providing noise resilient feature representations, HaDLeMO enables more accurate CSI reconstruction even under severe SNR degradation. Consequently, the framework maintains stable performance and reliability in practical massive MIMO deployments.

4. *Decreased computational intricacy*: HaDLeMO benefits from the DHT's multiplication free structure, which significantly reduces computational cost, especially when processing large CSI datasets typical of massive MIMO. This reduction in arithmetic operations enables faster feature extraction and lighter DL models. As a result, the overall system becomes more scalable, energy efficient, and suitable for real time CSI feedback. The reduced complexity also helps deploy the model on hardware constrained devices without sacrificing performance.

5. *Feedback mechanism for adaptive and flexible CSI*: The proposed framework incorporates an adjustable thresholding mechanism that adapts to varying channel conditions and system requirements. This flexibility enables dynamic tuning of the feedback rate, allowing the system to trade off reconstruction accuracy and feedback overhead intelligently. As network conditions fluctuate, the model automatically adjusts its sparsification level to maintain reliable CSI quality. Such adaptive behavior ensures consistently optimal performance across diverse scenarios.

The remainder of the chapter is structured as follows. Section 4.2 presents the system model. Section 4.3 presents the structural design for channel feedback and outlines the HaDLeMO mechanism. Implementation of the algorithm in Section 4.4. Section 4.5 presents the simulation and experimental findings, and Section 4.6 illustrates the complexity of HaDLeMO, while Section 4.7 provides the concluding remarks.

4.2 System Model

We assume a massive downlink MIMO system in a single cell consisting of N_t transmit antennas at the BS and one receiver antenna at the UE. The system functions at OFDMA over $\tilde{N}_c$ sub-carriers.

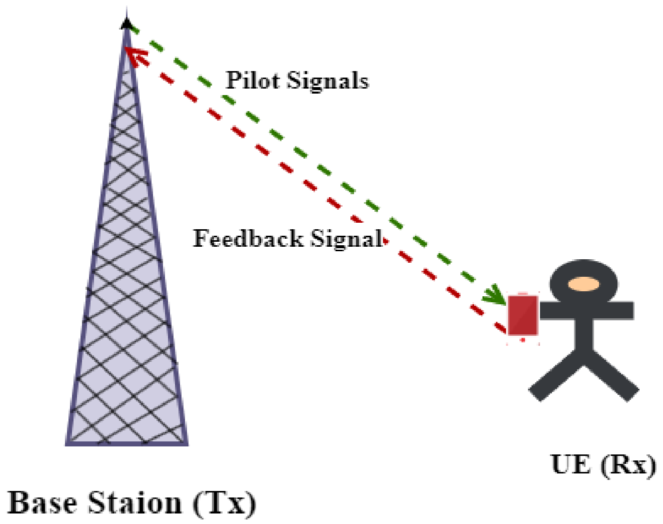

Figure 4.1: Structure Model of Downlink Pilot CSI Feedback Massive MIMO System

Let $\tilde{\boldsymbol{H}} = [\tilde{\boldsymbol{h}}_1, \tilde{\boldsymbol{h}}_2.....\tilde{\boldsymbol{h}}_{\tilde{N}c}]^H \in \mathrm{C}^{\tilde{N}_c \times N_t}$ be stacked in the spatial frequency domain as the CSI. The BS needs the CSI of the downlink channel gain $\tilde{\boldsymbol{H}}$ to design its precoding vector $\boldsymbol{p}_n$ to steer the signal to the designated UE. To gather the information of $\tilde{\boldsymbol{H}}$, the BS transmits pilot signals to the UE over the downlink [275]. The UE receives the pilot signals and estimates the downlink channel $\tilde{\boldsymbol{H}}$. Next, the UE sends the CSI feedback $\tilde{\boldsymbol{H}}$ to the BS on feedback channels. Finally, the BS uses this CSI feedback to perform precoding and optimize the next transmission.

Let $\tilde{\boldsymbol{h}}_n^H \in \mathrm{C}^{1 \times N_t}$ and $\boldsymbol{p}_n \in \mathrm{C}^{N_t \times 1}$ denote the channel matrix-vector and precoding vector. The signal y_n received the n^{th} subcarrier on UE is expressed as

$$y_n = \tilde{\boldsymbol{h}}_n^H \boldsymbol{p}_n x_n + w_n, \tag{4.1}$$

where $x_n \in \mathrm{C}$ and $w_n \in \mathrm{C}$ represent data-bearing symbols and noise added to the n^{th} sub-carrier.

The precoding vector $[\boldsymbol{p}_n, n = 1, 2.......\tilde{N}_c]$ can be designed by the BS after it has received the feedback $\tilde{\boldsymbol{H}}$. As mentioned above, in the FDD system, the UE sends $\tilde{\boldsymbol{H}}$ back to the BS. In the massive MIMO, the whole set of feedback values, $N_t\tilde{N}_c$, is large and cannot be transmitted efficiently through a limited number of input links. Note that the estimation of the downlink channel in UE is outside the scope of our research. It is assumed that the perfect CSI has been achieved by pilot training at UE [234]. We focus on the feedback side of the scheme.

Employing HaDLeMO, we propose using DHT to sparsify $\tilde{\boldsymbol{H}}$ within the area of angular delay to minimize the feedback overhead. The sparsified channel matrix $\boldsymbol{H}$ is given as

$$\boldsymbol{H} = X_d\tilde{\boldsymbol{H}}X_a^H, \tag{4.2}$$

where X_d and X_a are $\tilde{N}_c \times \tilde{N}_c$ and $N_t \times N_t$ DHT matrices, respectively. Liu et al. performed a realization of the value of $\boldsymbol{H}$ with the COST 2100 model [235]. It was found that $\boldsymbol{H}$ comprises a very small percentage of large-magnitude components. The power delay profile of multi-path arrivals has a limited duration. As a result, only the first $N_c < \tilde{N}_c$ rows have significant values. Thus, we retain only the first N_c rows of $\boldsymbol{H}$. Further, for simplicity, we write $\boldsymbol{H}$ to represent the truncated $N_c \times N_t$ matrix. However, in massive MIMO, even the reduced overall feedback parameters $N = N_cN_t$ has a high value.

The focus of HaDLeMO lies in creating an encoder as

$$s = f_{en}(\boldsymbol{H}), \tag{4.3}$$

for transforming $\boldsymbol{H}$ into an M-dimensional vector (codeword), where $M < N$. $\gamma = M/N$ represents the ratio of data compression. The original channel is decoded from the codeword as

$$\hat{\boldsymbol{H}} = f_{de}(s). \tag{4.4}$$

The function $f_{en}(\cdot)$ represents the encoder that extracts features and compresses the CSI into a compact codeword, while $f_{de}(\cdot)$ denotes the decoder that reconstructs the CSI from this compressed representation. Together, they form the end-to-end DL pipeline for CSI feedback. For the CSI feedback, after acquiring the channel matrix $\tilde{\boldsymbol{H}}$ at the UE side, we implement DHT, equation (4.2), to produce the truncated matrix $\boldsymbol{H}$. We next utilize the encoder, equation (4.3), to produce a codeword s. Afterward, s is transmitted back to the BS, where the decoder, equation (4.4), is utilized to produce the result $\hat{\boldsymbol{H}}$. To get the final channel matrix in the spatial frequency domain, the inverse DHT can be applied.

4.3 The Architecture of HaDLeMO

The objective of HaDLeMO is to develop an efficient feedback representation $\boldsymbol{H}$. We employ CNNs [276] because they effectively capture spatial correlations in the encoder and decoder by connecting neurons in adjacent layers. The length ($L1$), width ($W2$), and number of feature maps ($N3$) of the proposed DL architecture are illustrated in Fig. 4.2. Let $\boldsymbol{H}_r$ and $\boldsymbol{H}_i$ represent the real and imaginary components of $\boldsymbol{H}$, which is the form of $\tilde{\boldsymbol{H}}$ after sparsification by the use of DHT. $\boldsymbol{H}_i$ and $\boldsymbol{H}_r$ are supplied as input to the encoder's first layer. This layer uses 3×3 kernels, a convolutional layer, and two feature maps. After the feature maps are transformed into a vector, an actual vector s of size M is produced. Thus, a codeword is generated by a completely linked layer. The design of the first two layers is based on CS theory. These layers serve as encoders, reducing the data size without sacrificing any important information.

On the decoder side, we use multiple layers that function as decoders to transform the codeword s back into the channel matrix $\hat{\boldsymbol{H}}$. The completely linked first layer views the symbol s as an input. It generates two matrices, each of the order $N_c \times N_t$, representing an initial approximation of the real and imaginary components of $\boldsymbol{H}$. As shown in Fig. 4.2, each regeneration (ReGen) [277] unit consists of four layers, with the input layer being the first. The subsequent three levels employ 3×3 similar kernels. Eight feature maps are created using the next two layers, and the third creates sixteen layers. The final estimate

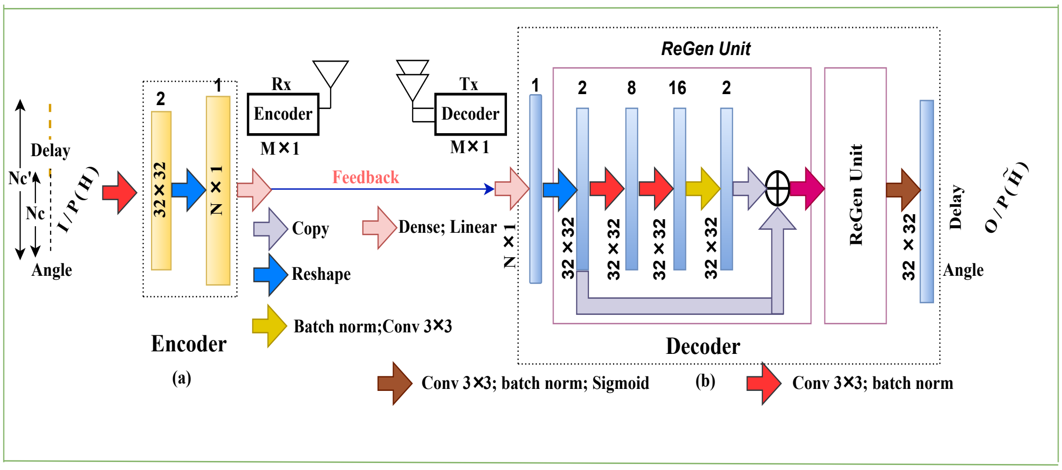

Figure 4.2: (a) $\boldsymbol{H} \in \mathbb{C}^{32\times 32}$ is the magnitude representation of false color. (b) Architecture of HaDLeMO Encoder and Decoder.

of $\boldsymbol{H}$ is the result of the last layer.

The feature maps generated by the three convolutional layers are scaled using zero padding to fit the dimensions of the input channel matrix, which has a size of $N_c \times N_t$. The rectified unit, denoted as ReUn$(\gamma) = \max(\gamma, 0)$, is used to apply batch normalization to each layer and function as the activation function.

In contrast to CNNs, which use a pooling layer to decrease the dimensions by down-sampling, HaDLeMO seeks refinement instead of dimensionality reduction. As a result, the outcome size of the ReGen unit and the channel matrix size are equal. Secondly, HaDLeMO uses the idea of deep residual networks (ResNet) [241, 278] and employs comparably shorter connections in the ReGeN unit to enable direct data transmissions to higher layers. This prevents the disappearing gradient issue that can occur when many layered nonlinear transformations are applied.

The real-world results demonstrate that the two ReGen units work best when combined [279, 240]. After being refined by a number of ReGen units, the channel matrix enters the final convolutional layer, where the sigmoid function scale value $[0, 1]$ is used. More feature maps can be added to our suggested method to cover scenarios where the UE has more than one antenna.

Using this method, we assume that all the kernels and the dominant values of the encoder and decoder are learned end-to-end. This process is fundamentally different from the two-stage approach used by Yao et al. [241]. In DR2-Net, image reconstruction from compressive measurements is performed through a linear mapping network that produces a coarse but high quality initial estimate, followed by a residual learning network that further refines the reconstruction. This joint design enables substantial performance gains over traditional CS-based techniques by effectively correcting errors left from the initial linear reconstruction. The collection of parameters is shown as $\Delta = \{\Delta_{en}, \Delta_{de}\}$. The suggested approach takes $\boldsymbol{H}_i$ as input. When an encoding operation followed by a decoding operation is performed on $\boldsymbol{H}_i$, it is expressed as $\boldsymbol{H}_i = f(\boldsymbol{H}_i; \Delta) = f_{de}(f_{en}(\boldsymbol{H}_i; \Delta_{en}); \Delta_{de})$ for the ith patch. Furthermore, the normalized channel matrices our suggested approach produces as input and output have elements scaled by the $[0, 1]$ range. HaDLeMO functions as an unsupervised learning algorithm, as the autoencoder. The MSE loss function is employed to update the set of parameters using the ADAM algorithm. The MSE is computed as follows:

$$L(\Delta) = \frac{1}{T}\sum_{i=1}^{T} ||f(\boldsymbol{s}_i; \Delta) - \boldsymbol{H}_i||_2^2, \tag{4.5}$$

where $\| \, . \, \|_2$ indicates the Euclidean standard, whereas the symbol T represents the total number of training set samples extracted.

4.3.1 Problem Formulation

The proposed HaDLeMO architecture heavily relies on efficient DFT computation. However, DFT is likely to face inefficiency in an environment with sparse signals. As a relatively faster algorithm, DHT [280] is optimal in these situations. It was developed similar to the decimation in frequency (DIF) and fast Fourier transform (FFT).

DFT has a long history of use in ML applications based on signal processing and spectral analysis. However, in the case of sparse [229] data, DFT might impede algorithm convergence. Consequently, it may be unable to handle the data rates needed for 5G and beyond. Its dependence on the order of elements causes difficulties in DL applications owing to permutation invariance [64]. Transforms that can identify patterns independently of the order of input items are required for DL applications. Additionally, DL is highly noise-sensitive. However, as DHT is less sensitive to phase information and can capture important patterns, it provides improved noise robustness to DL. DL necessitates the extraction of features for various data structures.

4.3.2 Discrete Hadamard Transform

DHT [281] is a mathematical transformation used to process signals. It transforms a vector of real numbers into another vector of real numbers, using an orthogonal matrix called the Hadamard matrix. The Hadamard transform $\boldsymbol{H_m}$ is a $2^m \times 2^m$ matrix, scaled by a normalization factor, that can transform 2^m real numbers of x_n into 2^m real numbers of X_k. The 1×1 Hadamard matrix $\boldsymbol{H_0}$ can be defined as the identity matrix $\boldsymbol{H_0} = 1$. The first order Hadamard matrix is represented as

$$\boldsymbol{H_1} = \begin{bmatrix} 1 & 1 \\ 1 & -1 \end{bmatrix}. \tag{4.6}$$

In general, for $m > 0$,

$$\boldsymbol{H_m} = \begin{bmatrix} \boldsymbol{H_{m-1}} & \boldsymbol{H_{m-1}} \\ \boldsymbol{H_{m-1}} & -\boldsymbol{H_{m-1}} \end{bmatrix}. \tag{4.7}$$

For higher orders, the Hadamard matrix $\boldsymbol{H_m}$ can be obtained by the tensor product

$$\boldsymbol{H_m} = \boldsymbol{H_1} \otimes \boldsymbol{H_{m-1}}, \tag{4.8}$$

where $\otimes$ is the Kronecker product operator [282]. Therefore, the Hadamard matrix elements are only +1 and -1. After performing the transform, the result is scaled by $\frac{1}{M}$ or $\frac{1}{\sqrt{M}}$, making the transformation orthonormal.

The forward Hadamard transform for the column vector x of length 2^m the Hadamard yields

$$Y = \boldsymbol{H_m} x \tag{4.9}$$

Since $\boldsymbol{H_m}$ is orthogonal, the inverse Hadamard transform is given as

$$x = \frac{1}{m} \boldsymbol{H_m} Y \tag{4.10}$$

The one-dimension Hadamard transform equation is represented as

$$\boldsymbol{H}(x, u) = \frac{1}{M} (-1)^{\sum_{i=0}^{M-1} (x_i u_i)} \tag{4.11}$$

where $M = 2^m$. The terms x_i and u_i are the binary representations of x and y. For example,

$$(u)_{decimal} = (u_{n-1} u_{n-2} .... u_1 u_0)_{binary} \tag{4.12}$$

where $u_i \in \{0, 1\}$

$$F = \boldsymbol{H} f \tag{4.13}$$

Similarly, the two-dimensional Hadamard transform is given as

$$\boldsymbol{H}(u, v) = \frac{1}{M} \sum_{x=0}^{M-1} \sum_{y=0}^{M-1} f(x, y)(-1)^{\phi(x,u,y,v)} \tag{4.14}$$

where $M = 2^m$, $\phi(x, u, y, v) = \sum_{i=0}^{n-1} (x_i u_i + y_i v_i)$ and $n = \log_2 M$ is the number of bits in the binary representations of (x, u, y, v). The exponent $\phi(x, u, y, v)$ computes a sum of binary products (modulo 2). The terms x_i, u_i, y_i, and v_i are the binary representations of x, u, y, and v. This transform is mathematically equivalent to applying the recursive

Hadamard matrix $\boldsymbol{H}_m$ from (4.7) via the matrix multiplication

$$F = \boldsymbol{H} f \boldsymbol{H^T}, \tag{4.15}$$

where, $\boldsymbol{H}$ is is the Hadamard matrix of size of size $2^m \times 2^m$ recursively constructed as shown in (4.7).

In Equation (4.14), the exponent $\phi(x, u, y, v)$ denotes a sum of binary products (modulo 2), equivalent to the XOR operation. Note that the Hadamard transform in Equation (4.14) is mathematically equivalent to applying the Hadamard matrix $\boldsymbol{H_m}$ in Equation (4.7) to the input data. Thus, the Hadamard transform in Equation (4.14) is implemented using the recursive Hadamard matrix $\boldsymbol{H_m}$ defined in Equation (4.7), where the transform operation corresponds to matrix multiplication with $\boldsymbol{H_m}$.

4.3.3 Inputs Parameterization

The existing research works study parameterized macro, micro and picocellular ecosystems. In the present work, we incorporate both outdoor and interior rural settings using the frequencies 400 MHz, 3.6 GHz [283], and 5.6 GHz [244]. The distributions and parameters considered can be found in [284]. To run the recommended model, it is necessary to provide a comprehensive description of the environment. The two-way channel through the transmission and reception arrays s_t and s_r is represented as [245]

$$\begin{aligned} \boldsymbol{H}(t,\tau) =& \frac{1}{L} \sum_{n \in \alpha} V_n \sqrt{\frac{S_n}{L_n}} \cdot \\ & \left[\sum_{p=1}^{P} a_{n,p}\, s_t(\Omega_{n,p}) . s_r(\Psi_{n,p}) \delta\left(\tau - \tau_n^l - \tau_{n,p}^M\right) \right] \end{aligned} \tag{4.16}$$

where V_n, S_n, and L_n represent the cluster sight gain, shadow fading, and cluster reduction in intensity. τ_n^l represents the cluster link latency, $\tau_{n,p}^M$ represents the geometric delay, $a_{n,p}$ indicates the complex Gaussian fading of the cluster n's p^{th} multipath component (MPC), $\Omega_{n,p}$ and $\psi_{n,p}$ indicate the direction of departure (DoD) and direction of arrival (DoA) of the p^{th} MPC in the cluster n. $\delta(.)$ represents the Dirac function. As the cluster excess delay increases, the latter increases exponentially. The total path loss L, depends on the separation between the mobile station (MS) and BS. The MS position defines a collection of visible clusters, known as α.

4.4 Algorithm Implementation

We propose a DL-based mechanism to improve the quality of CSI feedback in FDD massive MIMO systems. The proposed method is extensive. It includes data preparation, at the beginning, and training and evaluating neural network models, in the later stages.

If the real and imaginary components obtained with the help of DHT are expressed as $\boldsymbol{H_r}$ and $\boldsymbol{H_i}$, the channel gain $\boldsymbol{H}$ is expressed in terms of polar coordinates as

$$\phi = \arctan_2(\boldsymbol{H}_i, \boldsymbol{H}_r),\ r \quad = \sqrt{{\boldsymbol{H}_i}^2 + {\boldsymbol{H}_r}^2}. \tag{4.17}$$

Subsequently, the polar coordinates are converted back to complex numbers as

$$\boldsymbol{H}_i = r \cdot \sin(\phi),\ \boldsymbol{H}_r \quad = r \cdot \cos(\phi). \tag{4.18}$$

After preprocessing, the neural network comes in which involves the autoencoder model. To encode spatial hierarchies, this model consists of convolutional layers with rectified unit (ReUn) activation functions and dense layers that translate these features into a lower dimensional space. Then, convolutional layers with linear activation functions are used in the decoding procedure to reassemble the data.

Furthermore, a ResNet is included in the model, where residual blocks include Batch Normalization and Conv2D layers. These blocks help to enable learning of the identity function.

Together with the autoencoder, a DNNet model is also designed with the aim of removing noise from the CSI input. The model is similar to the autoencoder, but it has been fine-tuned to reduce noise more effectively.

An Adam optimizer is used to train and fine-tune these models, and a learning rate of 0.001 is set beforehand. Their performance is tracked by bespoke callbacks, and their training focuses on minimizing the mean squared error (MSE) loss over a number of epochs (History of Loss).

The model's performance is assessed using two important metrics: normalized mean squared error (NMSE) and cosine correlation (ρ) given as

$$\text{NMSE} = E\left\{\frac{\|\boldsymbol{H}_o - \boldsymbol{H}_p\|_2^2}{\|\boldsymbol{H}_o\|_2^2}\right\}, \tag{4.19}$$

and

$$\rho = E\left\{\frac{\sum(\boldsymbol{H}_o \times \boldsymbol{H}_p)}{\|\boldsymbol{H}_o\|_2 \times \|\boldsymbol{H}_p\|_2}\right\}, \tag{4.20}$$

where $\boldsymbol{H}_o$ and $\boldsymbol{H}_p$ signify the original and projected channel data. This metric is critical for determining the correctness of the reconstructed signal. In contrast, cosine correlation is used to measure the similarity between the original and predicted data, which is determined by Equation (4.20).

The last step is adding Gaussian noise to the test data to test the models under various signal to noise ratio (SNR) scenarios. The performance of the models is then evaluated using the metrics described above in a range of SNR values.

4.5 Simulations and Experimental Results

The simulations use an indoor picocellular scenario with a 5.3 GHz carrier frequency, 1024 subcarriers, and a BS of 32 uniform linear array antennas in a $20 \times 20\ m^2$ area, with UE units randomly distributed. The ResNet model contains two residual blocks and a 512-dimensional encoder, optimized for $32 \times 32 \times 2$ CSI input. Training employed 100,000 samples, with 30,000 for validation and 20,000 for testing, using a learning rate of 0.001, batch size 200, and 500 epochs; the DHT model used the same regimen.

Performance was evaluated under SNR levels from –5 dB to 40 dB using NMSE and co-

Algorithm 2 Implementation of HaDLeMO

1. Data Preprocessing:

a. Transform channel data to polar coordinates via DHT.

$$\phi = \arctan\left(\frac{\mathrm{Im}(\mathbf{H})}{\mathrm{Re}(\mathbf{H})}\right), \quad r = \sqrt{(\mathrm{Re}(\mathbf{H}))^2 + (\mathrm{Im}(\mathbf{H}))^2}.$$

b. Reconstruct complex values from polar coordinates using inverse DHT.

$$\boldsymbol{H}_i = r \cdot \sin(\phi),\ \boldsymbol{H}_r = r \cdot \cos(\phi).$$

2. Neural Network Architecture:

a. Construct Autoencoder.

- Encoding: Convolutional layers with ReLU.
- Feature Transformation: Dense layers.
- Decoding: Convolutional layers with linear activation.

b. Refine with ResNet blocks.

- Residual blocks including Conv2D and BatchNorm.
- Enhances learning stability via identity mapping.

3. HaDLeMO Denoising Development:

a. Design a model for denoising CSI feedback.

b. Structure based on autoencoder, optimized for noise resilience.

4. Training and Optimization:

a. Adam optimizer with update rule

$$\theta_{t+1} = \theta_t - \eta \frac{m_t}{\sqrt{v_t} + \epsilon}$$

where learning rate $(\eta) = 0.001$, m_t and v_t are first and second moment estimates.

b. Minimize MSE loss function.

c. Monitor with custom training callbacks.

5. Evaluation:

a. Metrics: normalized NMSE and correlation ρ.

b. Assess reconstruction accuracy via NMSE.

c. Evaluate data similarity using ρ.

6. Testing under Varying SNR:

a. Introduce Gaussian noise to test data.

$$\tilde{\boldsymbol{H}} = \boldsymbol{H} + n, \quad n \sim \mathcal{N}(0, \sigma^2)$$

b. Measure performance across SNR levels

$$\mathrm{SNR} = 10 \log_{10}\left(\frac{\mathbb{E}[\|\boldsymbol{H}\|_2^2]}{\mathbb{E}[\|n\|_2^2]}\right)$$

sine correlation on noise-affected test data. Results showed consistent gains over baseline models, with HaDLeMO achieving superior noise robustness and estimation accuracy, indicated by lower NMSE and higher cosine correlation across all SNR levels.

In Fig. 4.3, the NMSE of the DFT-based DL algorithm with noise [65], DeepAE [199], and the proposed HaDLeMO (post pre-training) is shown. The -30 dB line marks the benchmark NMSE for the DFT-based DL algorithm under noise-free conditions. With noise (w), the DFT-based DL suffers severe degradation, while higher SNR gradually reduces NMSE for both DFT-based DL and HaDLeMO, indicating less noise influence. At 10 dB, HaDLeMO achieves -11.01 NMSE, while DFT-based DL with noise can achieve 7, Deep AE can achieve -5.0, and pre-training can achieve -1.01 values.

Fig. 4.4 compares the performance of HaDLeMO with DeepAE, Pre-Training methods and DFT-based DL mechanism [248] for ρ variation under varying SNR (dB) conditions. The ideal threshold, which is the ρ or NMSE values without noise, has also been shown. The application of a DFT-based DL mechanism in a noise-free condition has been considered as a benchmark for the evaluation. At 10 dB, HaDLeMO achieves 0.88 cosine correlation, while DFT-based DL with noise can achieve 0.42, Deep AE can achieve 0.470, and pre-training can achieve 0.55 values. DFT-based DL without noise is the threshold considered here and achieves a cosine correlation of 1.

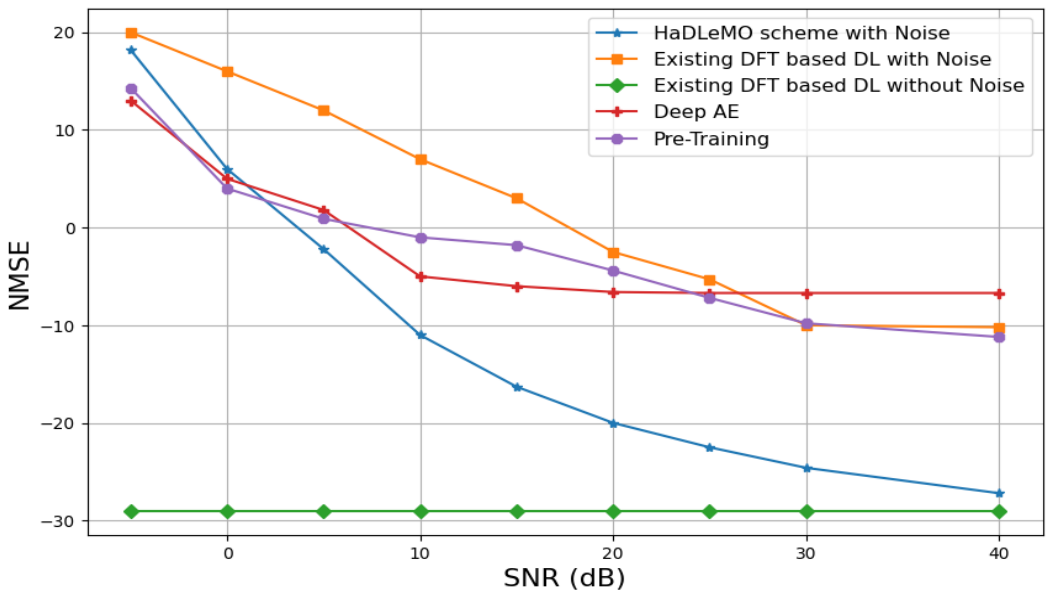

Figure 4.3: NMSE vs SNR (dB) for HaDLeMO and existing techniques.

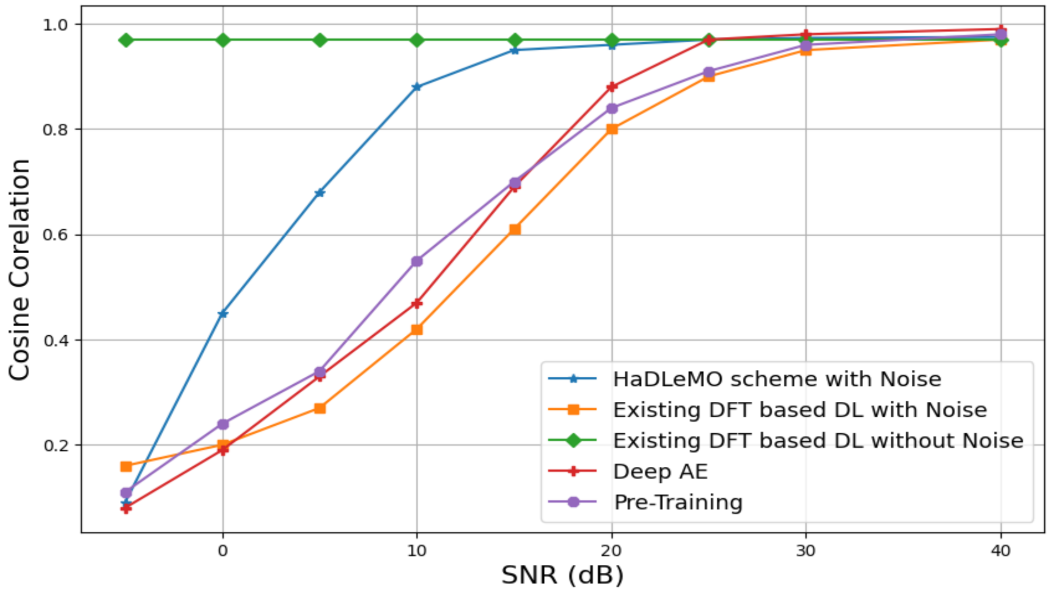

Figure 4.4: Cosine correlation (ρ) vs SNR (dB) for HaDLeMO and existing techniques.

Fig. 4.5, shows the relation between NMSE vs SNR (dB) for a DFT-based DL scheme with 32 antennas and a HaDLeMO scheme with 32, 64, and 128 antennas. After comparison, we can clearly see that HaDLeMO gives better result than the DFT-based DL method.

Fig. 4.6 represents the relation between Cosine correlation (ρ) vs SNR (dB) for 32 DFT-based DL antennas and 32, 64 and 128 HaDLeMO-based antennas. After simulating the HaDLeMO method and the DFT-based DL algorithm for different number of antennas HaDLeMO gives a better result.

In Figs. 4.7 and 4.8, an assessment of the performance of HaDLeMO at different learning rates (LRs) has been shown. Fig. 4.7 shows NMSE vs SNR for the application of HaDLeMO and DFT-based DL methods for different learning rates. For the same learning rates, we compare the NMSE, HaDLeMO shows less error compared to DFT based DL method.

Fig. 4.8 shows the graph for the cosine correlation vs SNR for comparison between HaDLeMO and DFT based DL methods at different learning rates. Clearly, HaDLeMO outperforms DFT-based DL for different learning rates.

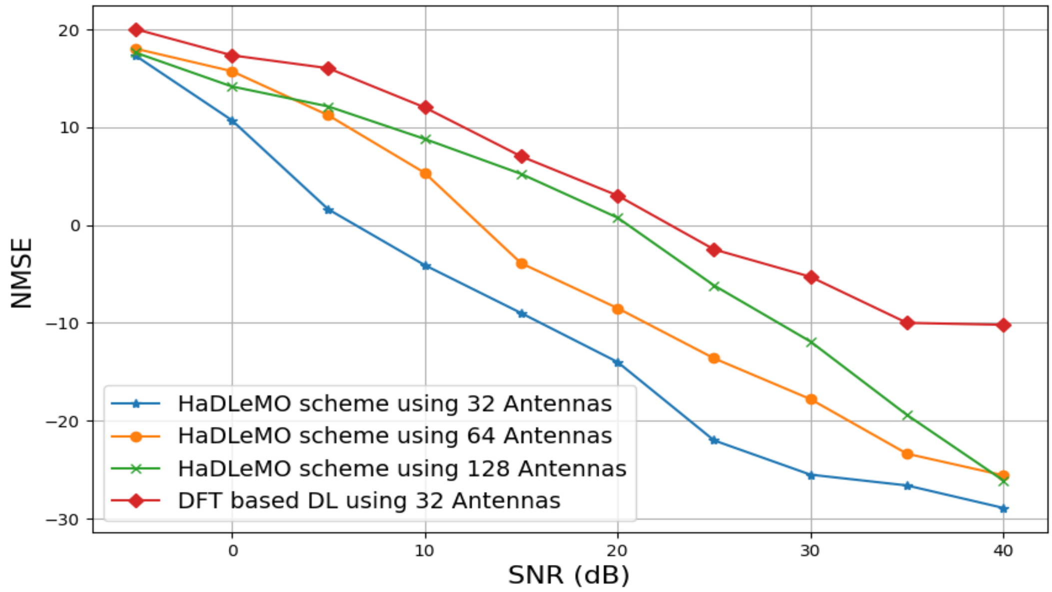

Figure 4.5: NMSE vs SNR (dB) comparison of existing 32 DFT and 32, 64 and 128 HaDLeMO based antennas.

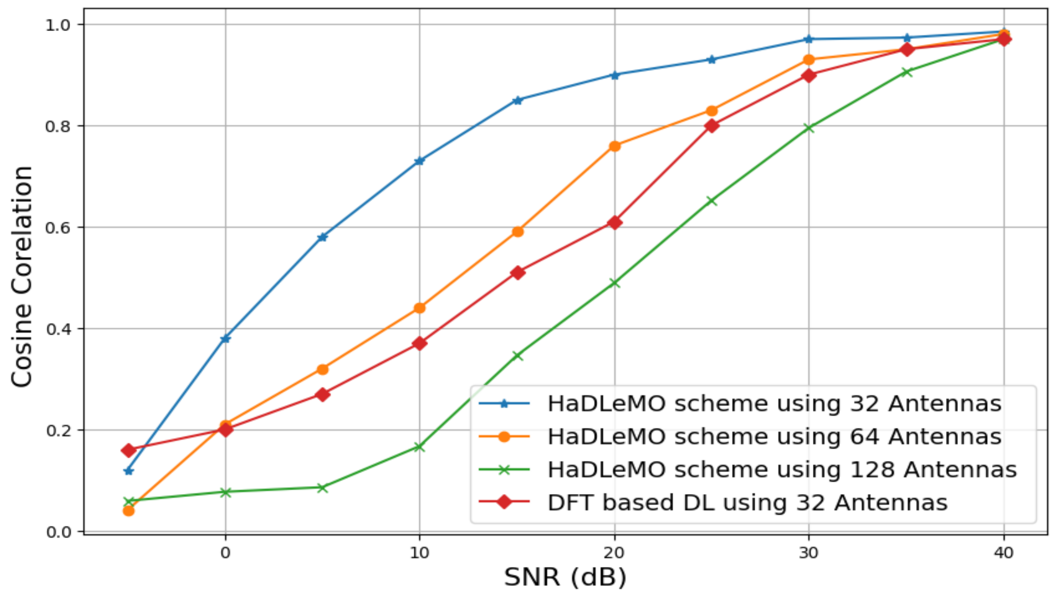

Figure 4.6: Cosine correlation (ρ) vs SNR (dB) comparison of existing 32 DFT and 32, 64 and 128 HaDLeMO based antennas.

4.6 Complexity Analysis of HaDLeMO

The direct computation of DFT requires $O(N^2)$ operations. However, the fast Fourier transform (FFT) an optimized algorithm to compute the DFT reduces this computational complexity to $O(N \log N)$. The complexity of DHT is similar to the FFT, that is $O(N \log N)$. The complexity is expressed in terms of floating point operations per second

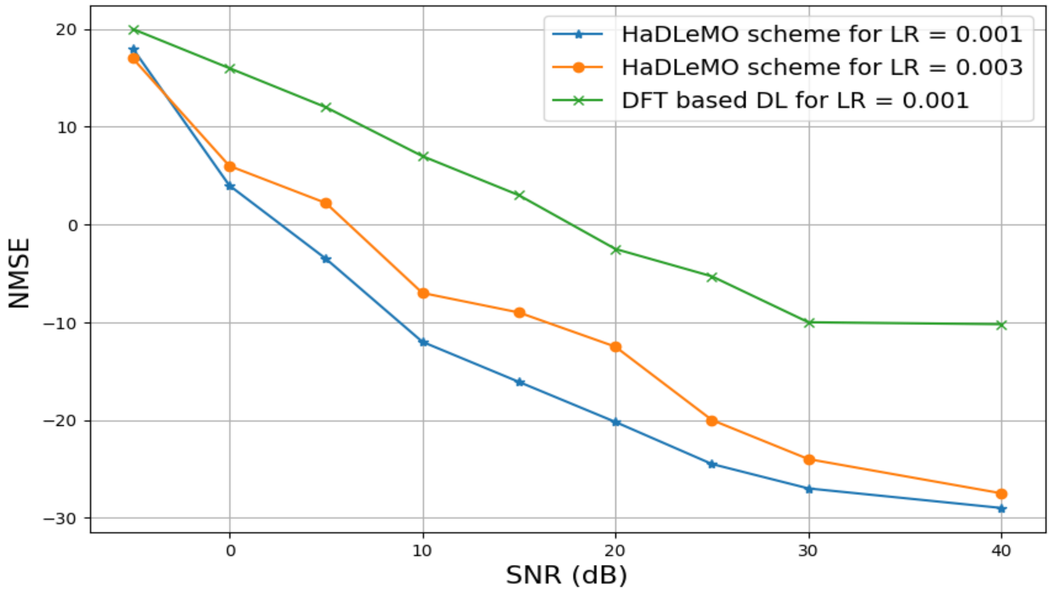

Figure 4.7: NMSE vs SNR (dB) for different learning rates (LR).

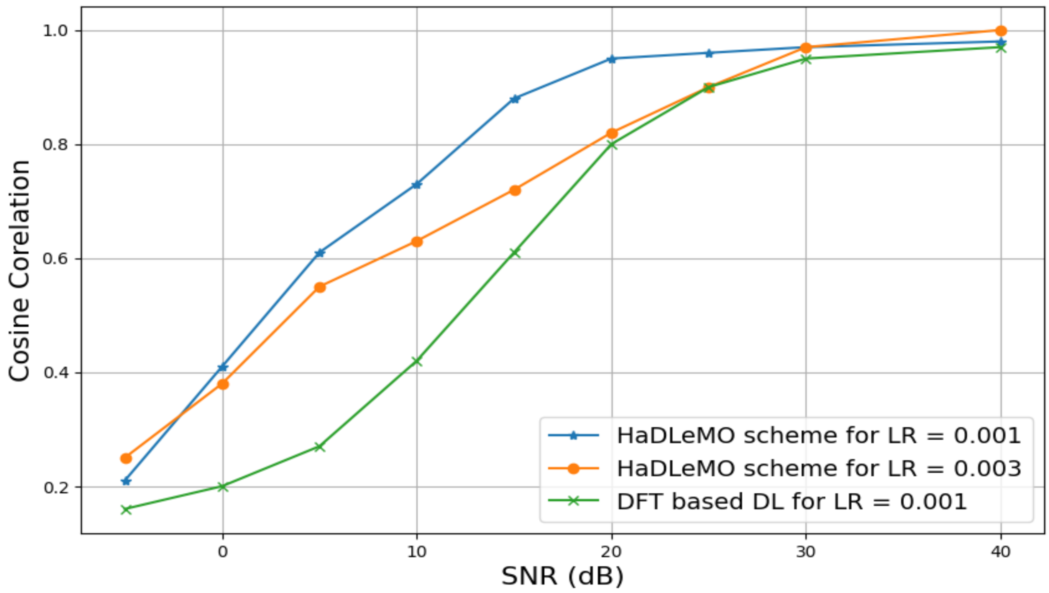

Figure 4.8: Cosine Correlation (ρ) vs SNR (dB) for different learning rates (LR).

(FLOPS).

In neural network architectures, the computational cost is commonly expressed in terms of FLOPS [256] [255]. For a fully connected dense layer, the complexity depends on the number of input features N_{in} and output neurons N_{out}. Each output neuron requires N_{in} multiplications and $(N_{\text{in}} - 1)$ additions, in addition to a bias term. Hence, the overall cost can be written as

$$\text{FLOPS}_{\text{FC}} = 2 \times N_{\text{out}} \times N_{\text{in}} - N_{\text{out}}. \tag{4.21}$$

For large-scale networks, the subtraction term is negligible, and the complexity is approximated by

$$\text{FLOPS}_{\text{FC}} \approx 2 \times N_{\text{out}} \times N_{\text{in}}. \tag{4.22}$$

For a convolutional layer, FLOPS depend on the input feature map size $(H \times W)$, the number of input channels C_{in}, kernel dimensions $(K \times K)$, the number of output channels C_{out}, and the output feature map size $(H_{\text{out}} \times W_{\text{out}})$. Each output value requires K^2 multiplications for each input channel and corresponding additions. Therefore, the computational cost is expressed as

$$\text{FLOPS}_{\text{Conv}} = H_{\text{out}} \times W_{\text{out}} \times C_{\text{out}} \times (C_{\text{in}} \times K^2) \times 2. \tag{4.23}$$

For an entire neural network, the total FLOPS are obtained by summing the contributions of all layers:

$$\text{FLOPS}_{\text{NN}} = \sum_{l=1}^{L} \text{FLOPS}_l, \tag{4.24}$$

where L is the number of layers and FLOPS_l represents the cost of the l^{th} layer.

4.6.1 Discussion of Estimation Accuracy Between HaDLeMO and DRT

It is important to note that HaDLeMO and DRT serve different roles within the proposed framework and therefore cannot be directly compared as equivalent estimation methods. DRT is a signal transform used to enhance the sparsity and representation of CSI prior to compression, whereas HaDLeMO is a complete DL-based CSI compression and reconstruction framework that incorporates the DHT transform together with a CNN-based autoencoder. In terms of estimation accuracy, HaDLeMO consistently achieves superior NMSE and cosine correlation performance because it combines the benefits of transform-domain sparsification with DL-based feature extraction and reconstruction. Therefore, while DRT improves the quality of the CSI representation, HaDLeMO provides a more comprehensive end-to-end solution and delivers higher reconstruction accuracy.

4.7 Conclusion

This chapter introduces a novel HaDLeMO-based approach for improved channel estimation by reducing feedback overhead, in a massive MIMO system. The HaDLeMO scheme independence of input sequence and enhanced noise resistance offers significant advantages over the DFT-based DL algorithm. These findings underscore the potential of HaDLeMO in advancing and improving the quality and efficiency of channel feedback in advanced communication systems.

Chapter 5

DL-Based Denoising in FDD Massive MIMO

In massive MIMO FDD systems, channel state information (CSI) feedback is essential. Traditional CSI methods are highly dependent on the degree of channel sparsity and are based on compressive sensing (CS). In this chapter, we propose a novel DL-based method to transform CSI into a low-dimensionality codeword. We construct DeNoNet, a DL-based denoise network, to enhance channel feedback and mitigate real-world interferences and nonlinear effects. Simulations results show that proposed DeNoNet mechanism performs better than the existing discrete Rajan transform (DRT)-based DL technique, by 113.18 % in normalized mean square error (NMSE) and 72.72 % in cosine correlation (ρ) particularly at varying signal-to-noise ratios.

5.1 Overview

The ability of massive multiple input, multiple output (MIMO) to offer high transmission rates and spectrum efficiency [285] [286] has made it a crucial technology for $5G$ and future-oriented cellular communication networks [287] [288]. Massive MIMO operation is significantly impacted by the accessibility of channel state information (CSI) [216] [289]. In a FDD system, the BS uses feedback channels to gather downlink CSI.

However, when the number of antennas increases, the amount of feedback also increases, resulting in a significant overhead for massive MIMO systems [290].

The use of CS reduces feedback overhead by exploiting the correlation between CSI [291]. However, they fail to perform if there are non-strictly sparse transmission conditions for CS-based techniques. DL has recently been used in communications to enhance performance and solve problems that conventional algorithms fail to solve [292] [293] [294].

Recently, several DL-based techniques [295, 296, 65] have been proposed to reduce the need for stringent sparsity. The expected downlink CSI is initially compacted into a low-dimensionality code-word on the UE and then retrieved from the BS's feedback code-word using an auto-encoder framework called DRT network, which was created in [295] for improved channel capacity and reduced feedback overhead. Compared to CS-based algorithms, DRT can provide superior feedback performance. To lower the overhead associated with CSI feedback, [296] recovers down-link CSI by utilizing the available uplink CSI. Guo et al. [65] shows that a technique based on convolutional neural networks (CNN) is developed to accomplish multirate CSI feedback [297]. The system has the ability to improve the accuracy of rebuilding, but it also reduces the storage space in the UE, Thus improving the system's operational viability.

The primary limitation in the existing work is that they ignore the impact of disruption and nonlinear impacts in real-world feedback channels [298]. As far as the authors are aware [65] and [199] take feedback error into account. To counteract the impact of feedback noise, we propose a distinct DL-based denoise network in this study, termed DeNoNet, to reduce feedback overhead and enhance the efficiency of the channel feedback system. Here is a list of the contributions:

1) Unlike the image denoising mechanism proposed by Zhang et al. in [299], which is not directly applicable to wireless systems, our proposed DeNoNet tailors its architecture specifically for codeword denoising in CSI feedback.

2) The proposed DL-based DeNoNet framework offers enhanced accuracy and implementation simplicity, demonstrating superior performance in terms of cosine simi-

larity (ρ) and robustness across varying signal-to-noise ratio (SNR) conditions.

3) The current DL-based channel feedback system and the suggested DeNoNet systems are trained together using an updated collaborative training process that outperforms instructing them independently.

The remaining part of the chapter is structured as follows. In Section 5.2, system model, problem formulation, and current DL-based CSI feedback techniques have been presented. Section 5.3 shows the framework and training optimization of the suggested DeNoNet to reduce the impact of less than ideal input. Section 5.4 shows the simulation results, and Section 5.5 concludes the chapter.

5.2 System Model and Problem Formulation

Suppose an FDD massive MIMO setup. The BS has N_t transmit antennas, whereas the UE only has single transmit antenna. A frequency-selective fading channel is considered as the transmission medium. It is transformed via orthogonal frequency division multiplexing (OFDM) [300] into several flat fading channels with N_c subcarriers. The CSI at the k^{th} subcarrier is represented as $\boldsymbol{h}_k \in \mathrm{C}^{N_t \times 1}$ and the analogous channel matrix $\tilde{\boldsymbol{H}}$ can be represented as

$$\tilde{\boldsymbol{H}} = \begin{bmatrix} \mathbf{h}_1^H & \mathbf{0} & \cdots & \mathbf{0} \\ \mathbf{0} & \mathbf{h}_2^H & \cdots & \mathbf{0} \\ \vdots & \vdots & \ddots & \vdots \\ \mathbf{0} & \mathbf{0} & \cdots & \mathbf{h}_{N_c}^H \end{bmatrix}_{N_c \times N_c N_t} . \tag{5.1}$$

Let the beamforming matrix at the k^{th} subcarrier be represented by $\boldsymbol{p}_k \in \mathrm{C}^{N_t \times 1}$. The analogous beamforming vector can be expressed as

$$\boldsymbol{P} = \begin{bmatrix} \mathbf{p_1} & 0 & \cdots & 0 \\ 0 & \mathbf{p_2} & \cdots & 0 \\ \vdots & \vdots & \ddots & \vdots \\ 0 & 0 & \cdots & \mathbf{p}_{N_c} \end{bmatrix}_{N_cN_t \times N_c} . \tag{5.2}$$

The beamforming matrix must satisfy the power limitations given by $||\boldsymbol{p}_i||_2^2 = \frac{P_t}{N_c}$, here P_t denotes the total transmission power. The array of signals obtained at UE, in the downlink frequency domain can be expressed as

$$y = \tilde{\boldsymbol{H}}\boldsymbol{P}x + w, \tag{5.3}$$

where $x \in \mathrm{C}^{N_c \times 1}$ denote the transmitted symbol matrix and $w \in \mathrm{C}^{N_c \times 1}$ represent the noise matrix accordingly. For simplicity, we reconfigure the channel matrix as

$$\boldsymbol{H}_{SF} = [\mathbf{h}_1, \mathbf{h}_2.....\mathbf{h}_{Nc}]^H_{N_c \times N_t}, \tag{5.4}$$

where $\boldsymbol{H}_{SF}$ is the CSI in the spatial frequency realm. We use the 2D discrete Fourier transform (DFT) and move $\boldsymbol{H}_{SF}$ into the angle delay domain in order to obtain the CSI characteristics as

$$\boldsymbol{H}_{AD} = \boldsymbol{F}_D \boldsymbol{H}_{SF} \boldsymbol{F}_A^H, \tag{5.5}$$

where the parameters of the DFT vectors $\boldsymbol{F}_D$ and of the order $\boldsymbol{F}_A$ are $N_c \times N_c$ and $N_t \times N_t$, accordingly. Since the time of arrival (TOA) between multipaths is limited, $\boldsymbol{H}_{AD}$ has important parameters mainly in the initial N_P rows in the delay domain, indicating sparsity in CSI [64]. As in [65] and [64], $\boldsymbol{H}_{AD}$'s first N_P rows create a new channel matrix $\boldsymbol{H}$ as $\boldsymbol{H} = [\boldsymbol{H}_{AD}]_{1:N_P}$, where $[\boldsymbol{H}_{AD}]_{1:N_P}$ indicates a sub-matrix composed of $\boldsymbol{H}_{AD}$'s first N_P rows.

5.2.1 DL-based Encoder and Decoder Method

In [65] and [64] DL-based methods are utilized in CSI feedback to reduce the communication overhead. An encoder initially compresses the CSI at the UE to create the codeword s as

$$s = f_{en}(\boldsymbol{H}), \tag{5.6}$$

and then the BS receives the codeword s through a feedback channel. A decoder located at the BS can recreate the CSI as

$$\tilde{\boldsymbol{H}} = f_{de}(s). \tag{5.7}$$

The autoencoder model includes the encoder $f_{en}(\cdot)$ in (5.6) and the decoder $f_{de}(.)$ in (5.7). Assuming that s contains N_{CW} elements, the compression ratio should be

$$\gamma = \frac{N_{CW}}{2 \times N_t \times N_P}. \tag{5.8}$$

The channel feedback process assumed by the DL-based techniques [296], [64] is perfect. However, a variety of real-time disruption and nonlinear impacts affect the CSI feedback [298]. As with [301], we used all imperfection as noise, which is not necessary a Gaussian, and overlay it on the codeword as

$$\tilde{s} = s + n. \tag{5.9}$$

5.3 DeNoNet Architecture

This part comes first outlines the specifics of the proposed DeNoNet. Next, jointly conducted training process for the DL-based CSI feedback technique and DeNoNet has been designed. As shown in Fig. 5.1, we create a codeword denoising architecture for the feedback channel. The fundamental concept of DeNoNet is to use a noise extraction unit (NEU) to remove the noise from the codeword and then subtract that noise from the codeword.

The proposed DeNoNet architecture begins with an encoder that compresses the CSI matrix of size $32 \times 32 \times 2$. The encoder employs two fully connected (FC) layers with 512 and 256 neurons, respectively, both activated using the rectified linear unit function. The encoder output is the codeword N_{CW}, generated by linear activation. The NEU then processes this noisy codeword $\tilde{s}$. The NEU first applies batch normalization, followed by a FC layer of 1024 neurons with sigmoid activation. To avoid overfitting, a sparsity constraint is enforced on the hidden representation. A second FC layer with 1024 neurons and linear activation estimates the noise component $\hat{n}$. Then a skip connection removes this noise from the original codeword, resulting in the denoised codeword $\hat{s} = \tilde{s} - \hat{n}$. The decoder, mirroring the encoder, reconstructs the CSI matrix by passing $\hat{s}$ through two FC layers (256 and 512 neurons), followed by an output layer with linear activation that restores the CSI to its original dimensions $32 \times 32 \times 2$. Training is performed using the Adam optimizer with learning rate $\eta = 0.001$, batch size $= 200$, and for 500 epochs, while the loss function is defined as the normalized mean square error (NMSE).

Table 5.1: Layer-Wise Configuration of the Proposed DeNoNet Architecture

Module	**Layer**	**Details**
Encoder	Input	CSI ($32 \times 32 \times 2$)
	FC Layer 1	512 neurons, RLU
	FC Layer 2	256 neurons, RLU
	Output	Codeword (N_{CW}), Linear
Noise Extraction Unit	BatchNorm	Normalizes input
	FC Layer 1	1024 neurons, Sigmoid
	Sparse Constraint	KL-based sparsity
	FC Layer 2	1024 neurons, Linear ($\hat{n}$)
Skip Connection	Noise Sub.	$\hat{s} = \tilde{s} - \hat{n}$
Decoder	FC Layer 1	256 neurons, RLU
	FC Layer 2	512 neurons, RLU
	Output	CSI ($32 \times 32 \times 2$), Linear
Training	Optimizer	Adam ($\eta = 0.001$)
	Batch Size	200
	Epochs	500
	Loss	NMSE

An entirely interconnected neural system comprising L layers: 1 input layer, 1 output layer, and $L-2$ hidden layers—is used by the NEU. The codeword entered is expressed as

$$\tilde{s} = [\tilde{s_1}, \tilde{s_2}, \tilde{s_3}, ..., \tilde{s}_{N_{CW}}]. \tag{5.10}$$

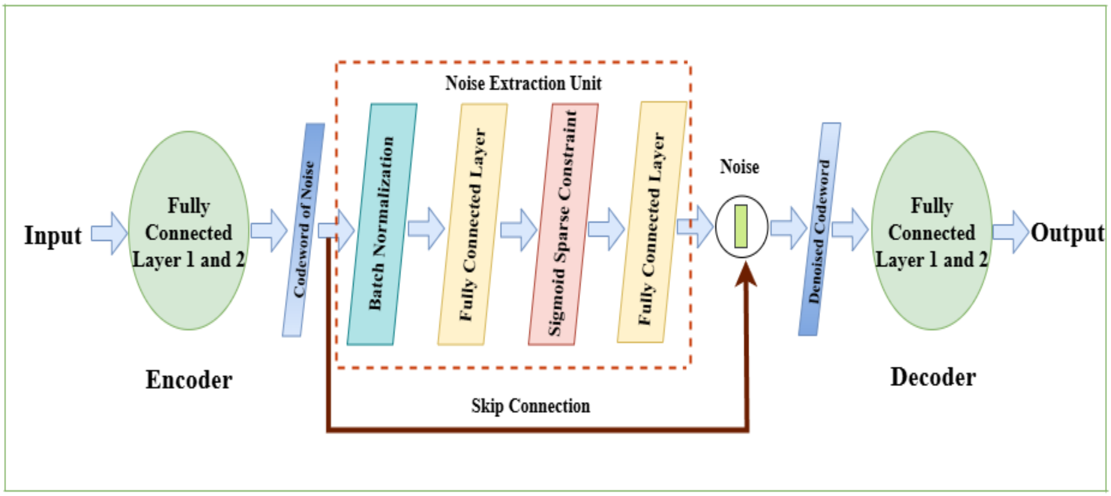

Figure 5.1: Encoder and Decoder Architecture of DeNoNet.

To speed up DNN training and prevent output saturation, we initially execute batch normalization (BN) before inputting the codeword as

$$\tilde{s}' = \frac{\tilde{s} - E[\tilde{s}]}{\sqrt{Var[\tilde{s}]}}. \tag{5.11}$$

The distortion recovered from the codeword corresponds to NEU result [302], i.e.,

$$\hat{n} = G_L(...G_1(\tilde{s}')). \tag{5.12}$$

The l^{th} layer's result is expressed as

$$G_l(z) = \begin{cases} z, & \text{if } l = 1 \\ \zeta(W_l z + b_l), & \text{if } 2 \leq l < L - 1 \\ W_l z + b_l, & \text{if } l = L \end{cases}, \tag{5.13}$$

where z is the input vector to the l^{th} layer, W_l the present weight matrix associated with the l^{th} layer b_l is a bias vector associated with the l_{th} layer, and the sigmoid activation function, which adds a nonlinear modification, is represented by $\zeta(x) = (1+\exp(-x))^{-1}$. In order to readily capture the noise, the buried layer's 1024 neurons are often larger than the codeword dimension. Next, we apply Kullback Leibler (KL) divergent sparsity [303]

Algorithm 3 DeNoNet-Based CSI Feedback Algorithm Implementations

1: **Input:** Noisy codeword $\tilde{s} \in \mathbb{R}^{N_{CW}}$.
2: **Output:** Reconstructed CSI matrix $\hat{\boldsymbol{H}}$.
3: **Batch Normalization:** Normalize codeword to stabilize training.

$$\tilde{s}' = \frac{\tilde{s} - \mathbb{E}[\tilde{s}]}{\sqrt{\mathrm{Var}[\tilde{s}]}}$$

4: **Noise Estimation via NEU Network:**

$$\hat{n} = G_L(\cdots G_2(G_1(\tilde{s}'))), \quad G_l(z) = \begin{cases} z, & l = 1 \\ \zeta(W_l z + b_l), & 2 \leq l < L \\ W_l z + b_l, & l = L \end{cases}$$

Noise extraction unit uses L F layers and $\zeta(x)$ is sigmoid.
5: **Apply KL Divergence Regularization:** Encourages sparsity in hidden units.

$$\mathrm{KL}(\Phi \,\|\, \hat{\Phi}) = \sum_{j=1}^{|\hat{\Phi}|} \Phi \log\left(\frac{\Phi}{\hat{\Phi}_j}\right) + (1 - \Phi) \log\left(\frac{1 - \Phi}{1 - \hat{\Phi}_j}\right)$$

6: **Denoising the Codeword:** Skip connection subtracts predicted noise.

$$\hat{s} = \tilde{s} - \hat{n}$$

7: **Decode Denoised Codeword for CSI Reconstruction:**

$$\hat{\boldsymbol{H}} \leftarrow \text{Decoder}(\hat{s})$$

8: **Loss Function and Training Objective:**

$$L_{\text{loss}} = \frac{1}{N} \sum_{i=1}^{N} \left\| \hat{\boldsymbol{H}}_i - \boldsymbol{H}_i \right\|_2^2$$

9: Optimize L_{loss} using ADAM optimizer.

restrictions to the hidden layer in order to prevent overfitting of the multi-dimensional systems,

$$\mathrm{KL}(\Phi \parallel \hat{\Phi}) = \sum_{j=1}^{|\hat{\Phi}|} \Phi \log\left(\frac{\Phi}{\hat{\Phi}_j}\right) + (1-\Phi)\log\left(\frac{1-\Phi}{1-\hat{\Phi}_j}\right) \tag{5.14}$$

where

$$\hat{\Phi} = \frac{1}{N}\sum_{i=1}^{N} \zeta(Wz_i + b), \tag{5.15}$$

where N represents the batch size, $\hat{\Phi}_j$ is the average activation of the j^{th} hidden unit, Φ is the target sparsity level, $|\hat{\Phi}|$ represents the quantity of neurons, $\zeta(.)$ is the sigmoid activation function, and z_i represents the resulting vector of the FC layer's i^{th} batches.

Additionally, we use a skip link to transfer the codeword to the NEU's output. $\hat{n}$ is subtracted by the codeword to accomplish denoising after noise $\hat{n}$ is extracted using NEU as

$$\hat{s} = \tilde{s} - \hat{n}. \tag{5.16}$$

Subsequently, DeNoNet outputs the denoised codeword, which is then sent to a decoder for CSI reconstruction.

5.3.1 DeNoNet Optimization

To improve the feedback performance, the suggested DeNoNet complements the DL-based channel feedback technique proposed in [65]-[64]. For simplicity, we refer to the DL-based channel feedback as an autoencoder model since all current techniques use this design. We create an entirely novel learning method for DeNoNet and the autoencoder approach. The real and imaginary components of $\boldsymbol{H}$, which has a size of $2 \times N_p \times N_t$, are used as input data to train the autoencoder model. The truncated normal distribution is used as the initialization for the power coefficients of the autoencoder model. The loss function L_{loss} is defined as the NMSE

$$L_{loss} = \frac{1}{N}\sum_{i=1}^{N} \left\| \hat{\boldsymbol{H}}_i - \boldsymbol{H}_i \right\|_2^2, \tag{5.17}$$

and the loss function is optimized using the adaptive moment estimation (ADAM) method. Then, we train DeNoNet by creating a sample set using equations (5.6) and (5.9).

5.4 Simulation Results

We used the COST2100 network method to produce the dataset for performing our simulations [235]. A 5.3 GHz carrier frequency and $N_c = 1024$ subcarriers are used in a picocellular indoor situation. The BS is positioned in the middle of a $20m \times 20m$ square area and has uniform linear array (ULA) antennas with $N_t = 32$. The UE units are randomly located within this square space. The default preferences in [235] are followed by further options.

Next, we take $N_p = 32$ and move it towards the angular delay domain. In addition, training, validation, and testing sets are created from the samples 10^5, 3×10^4, and 2×10^4 accordingly. The number of batches and the learning rate (LR) have been set at 200 and 0.001, respectively. The number of epochs is 500, and the remaining parameters are identical. After the autoencoder model's training, we use (5.6) and (5.9), which add noise n to the codeword, to create the DeNoNet dataset. In order to maintain generality, we presume that σ_n^2 is the noise power and that n is a Gaussian noise vector with $n \sim \mathcal{N}(0, \sigma_n^2\mathbf{I})$. The noise layer in the second step automatically creates the DeNoNet database. Thus, We simply require to construct the dataset for the autoencoder model.

Performance is measured using the NMSE and cosine correlation (ρ) [304], formulated as

$$\text{NMSE} \triangleq \mathbb{E}\left\{\frac{\left\|\boldsymbol{H}_{SF} - \hat{\boldsymbol{H}}_{SF}\right\|_2^2}{\left\|\boldsymbol{H}_{SF}\right\|_2^2}\right\} \tag{5.18}$$

$$\rho \triangleq \mathbb{E}\left\{\frac{1}{N_c}\sum_{n=1}^{N_c}\frac{\left|\hat{\boldsymbol{h}}_n^H \boldsymbol{h}_n\right|}{\left\|\hat{\boldsymbol{h}}_n\right\|_2 \left\|\boldsymbol{h}_n\right\|_2}\right\}. \tag{5.19}$$

In the spatial frequency domain, $\boldsymbol{H}_{SF}$ and $\hat{\boldsymbol{H}}_{SF}$ represent true and reconstructed CSI, whereas $\boldsymbol{h}_n$ and $\hat{\boldsymbol{h}}_n$ represent real and reconstructive CSI for n^{th} subcarrier.

We use the DeNoNet as the DL-based feedback technique in our simulation without sacrificing generality. A normalization level is added to the CSI network after the encoder stage to quantitatively assess the influence of noise as $s = \frac{s}{\|\mathbf{s}\|_2}$. The SNR can thus be described as

$$SNR = \frac{1}{N_{CW}\sigma_n^2}, \tag{5.20}$$

where N_{CW} represents the length of the codeword. We analyze the performance at SNRs ranging from -5 dB to 40 dB.

Fig. 5.2 represents the relationship between NMSE (dB) vs. SNR (dB) of our proposed DeNoNet and existing techniques. The horizontal line at -30 dB is the NMSE of DRT-based DL under noise-free conditions, which we utilize as a reference. When noise n is present, DRT's NMSE significantly degrades compared to the noise-free state. The NMSE of DRT, DeepAE [199], and the proposed DeNoNet generally decreases as the SNR rises because the noise influence is lessened. The suggested DeNoNet approach outperforms the DRT-based technique by 113.18%.

Fig. 5.3 shows the relation between the cosine correlation (ρ) vs. SNR (dB) for the proposed DeNoNet and existing methods. In these results, the algorithm ρ progressively increases with SNR. Furthermore, among the algorithms, DRT-based DL with noise, DeepAE [285], and our suggested DeNoNet approach perform the best at all SNR values. The suggested DeNoNet technique improves by 72.72 % when compared to the existing DRT-based DL with noise technique, according to ρ analysis.

Fig. 5.4 shows the relation between the NMSE (dB) (ρ) vs. SNR (dB) for the proposed DeNoNet and existing methods. In these results, the algorithm ρ progressively increases with SNR. Furthermore, among the algorithms, DRT-based DL with noise and our proposed DeNoNet approach perform the best at all SNR values. The suggested DeNoNet technique improves by 139.84 % when compared to the existing DRT-based DL with noise technique, according to ρ analysis.

Fig. 5.5 shows the relation between the cosine correlation (ρ) vs. SNR (dB) for the proposed DeNoNet and existing methods. In these results, the algorithm ρ progressively in-

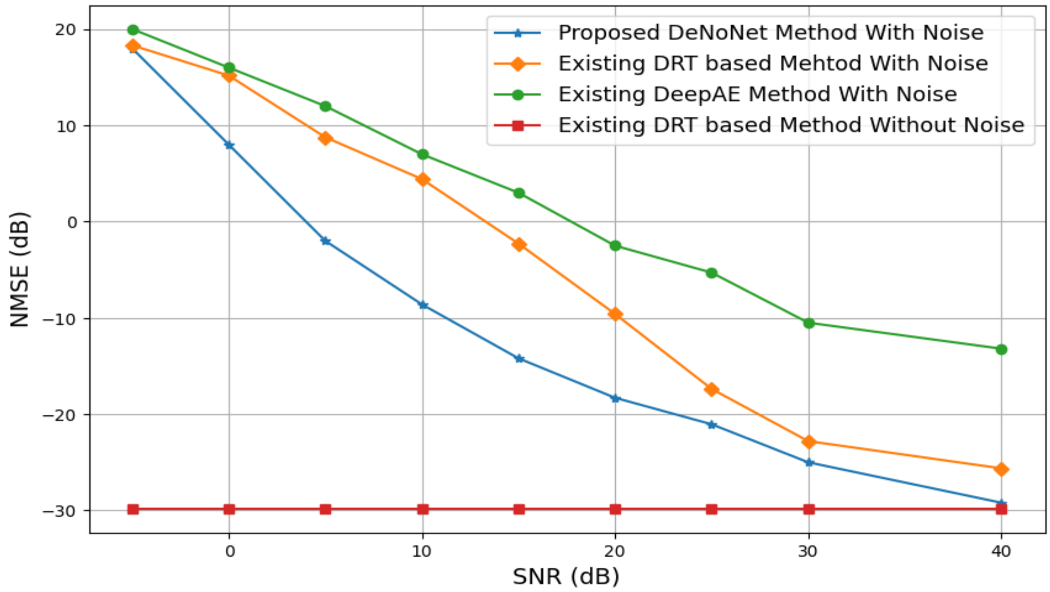

Figure 5.2: NMSE (dB) vs SNR (dB) for DeNoNet and existing methods.

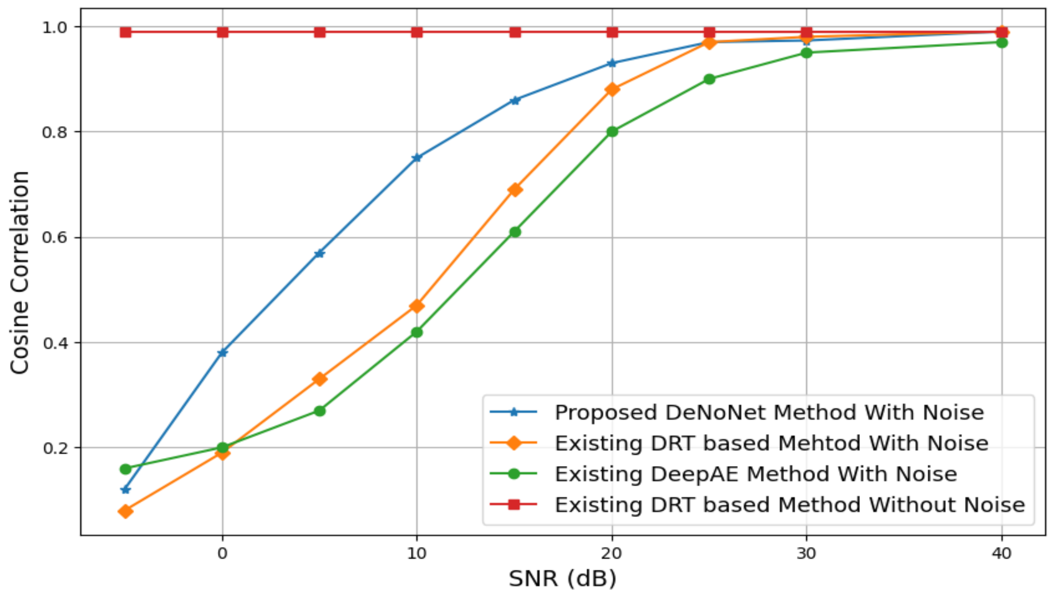

Figure 5.3: Cosine correlation (ρ) vs SNR (dB) for DeNoNet and existing methods.

creases with SNR. Furthermore, among the algorithms, DRT-based DL with noise and our proposed DeNoNet approach perform the best at all SNR values. The proposed DeNoNet technique improves by 46.15 % when compared to the existing DRT-based DL with noise technique, according to ρ analysis.

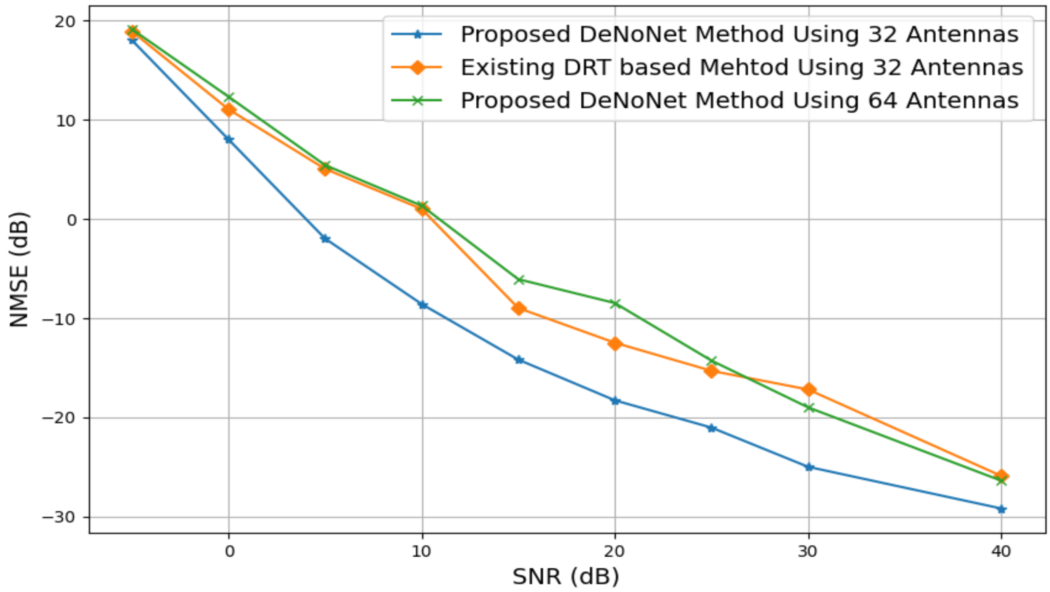

Figure 5.4: NMSE (dB) vs SNR (dB) using 32, 64 antennas for our proposed DeNoNet technique and 32 antennas for existing techniques.

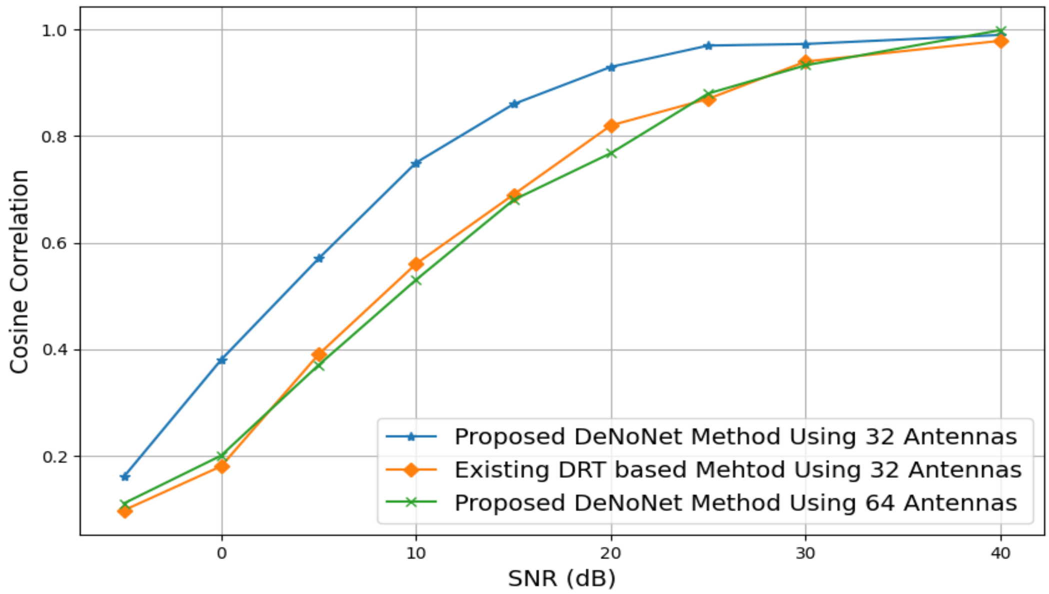

Figure 5.5: Cosine correlation (ρ) vs SNR (dB) using 32, 64 antennas for our proposed DeNoNet technique and 32 antennas for existing techniques.

5.4.1 Performance Degradation of DeNoNet with Increasing Antennas

The performance degradation of DeNoNet with an increasing number of antennas is primarily due to the growth in CSI dimensionality and the corresponding increase in reconstruction complexity. As the number of transmit antennas N_t increases, the size of the

CSI matrix also increases, resulting in a larger amount of channel information that must be compressed, transmitted, and reconstructed. When the compression ratio is kept fixed, the reconstruction task becomes more challenging because the network must recover a higher-dimensional channel representation from a limited latent codeword. Consequently, the inverse reconstruction problem becomes more complex, leading to increased reconstruction error and a reduction in estimation accuracy.

In addition, the DeNoNet architecture used in the experiments maintains a fixed network capacity across all antenna configurations. Although larger antenna arrays provide richer spatial information, they also introduce more complex inter-antenna correlation patterns that must be learned by the network. As the CSI dimension grows, the fixed-capacity model may not be able to fully capture these increasingly complex relationships, resulting in a gradual degradation in NMSE and cosine correlation performance. Similar trends have also been reported in DL-based CSI feedback literature, where reconstruction performance tends to decline with increasing antenna dimensions unless the codeword size or network capacity is scaled accordingly. Therefore, the degradation observed in Fig. 5.4 is an expected consequence of increased CSI dimensionality, higher reconstruction complexity, and fixed model capacity.

I also agree that a fair assessment of the proposed DeNoNet framework requires comparison with the existing DRT-based approach under the same antenna configuration. While Fig. 5.4 currently illustrates the performance trend of DeNoNet as the number of antennas increases, the absence of a corresponding DRT result for the 64-antenna case limits the ability to directly quantify the performance gain achieved by the denoising stage. Including the DRT baseline under identical experimental conditions would provide a clearer benchmark and allow readers to distinguish improvements arising from the denoising network from those obtained through the DRT-based CSI representation itself.

5.4.2 Comparison with Diverse DNN Structures

We further extend our assessment to comparing the proposed DeNoNet-based scheme with diverse state-of-the-art DNN structures. The widely studied DNN structures in resent researches involve vanilla AE (deep learning-based massive MIMO CSI feedback reduction) [64], sparse AE (PRVNet) [68] and Bayesian AE [305].

The vanilla AE autoencoder provides a basic compression reconstruction framework, where the encoder maps the CSI matrix into a low dimensional codeword $s = f_{en}(\mathbf{H})$ and the decoder reconstructs the channel $\hat{\mathbf{H}} = f_{de}(s)$. The optimization objective is minimizing the mean square error,

$$L_{\text{vanilla}} = \|\mathbf{H} - \hat{\mathbf{H}}\|_2^2. \tag{5.21}$$

The sparse AE extends this design by enforcing sparsity in the hidden layer activations, thereby improving feature extraction. A Kullback–Leibler (KL) divergence penalty is added to the loss function given as

$$L_{\text{sparse}} = \|\mathbf{H} - \hat{\mathbf{H}}\|_2^2 + \beta \sum_{j=1}^{m} \mathrm{KL}(\rho \,\|\, \hat{\rho}_j), \tag{5.22}$$

where ρ is the desired sparsity level and $\hat{\rho}_j$ is the average activation of the j^{th} hidden unit.

The Bayesian AE incorporates uncertainty modeling in the latent space by treating the hidden variables as probability distributions. The encoder outputs both mean μ and variance σ^2, and the reparameterization trick is applied: $z = \mu + \sigma \odot \epsilon,\ \epsilon \sim \mathcal{N}(0, I)$. The training objective combines reconstruction loss with a KL regularizer:

$$L_{\text{Bayesian}} = \|\mathbf{H} - \hat{\mathbf{H}}\|_2^2 + D_{\text{KL}}[q(z|\mathbf{H}) \,\|\, p(z)]\,. \tag{5.23}$$

Thus, vanilla AE focuses on direct reconstruction, sparse AE improves feature selection through sparsity, and Bayesian AE enhances robustness by modeling uncertainty in the latent representation.

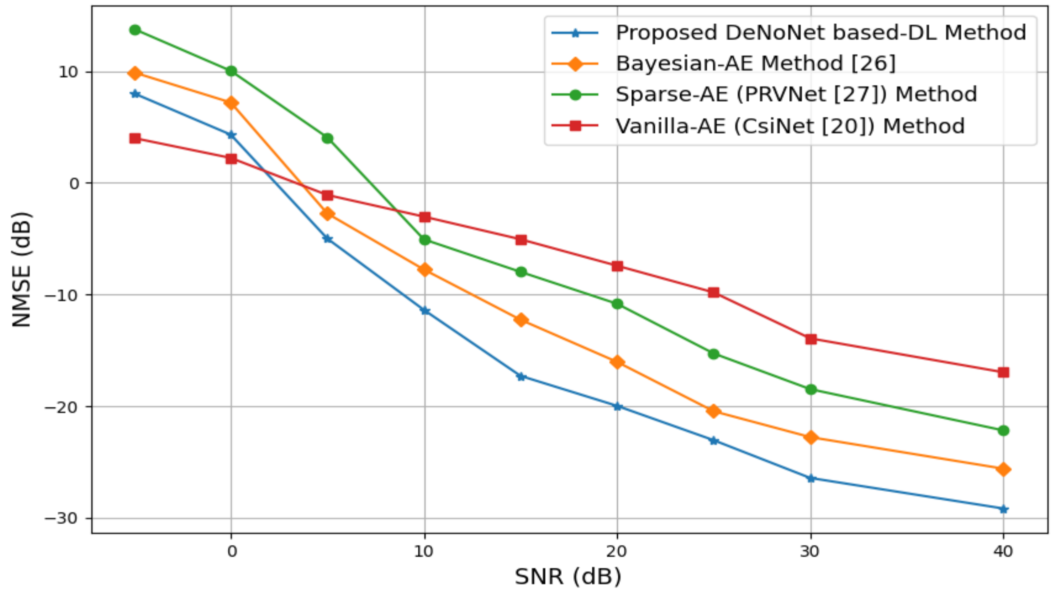

Figure 5.6: NMSE (dB) vs SNR (dB) for DeNoNet and existing Bayesian-AE, sparse AE and vanilla AE methods.

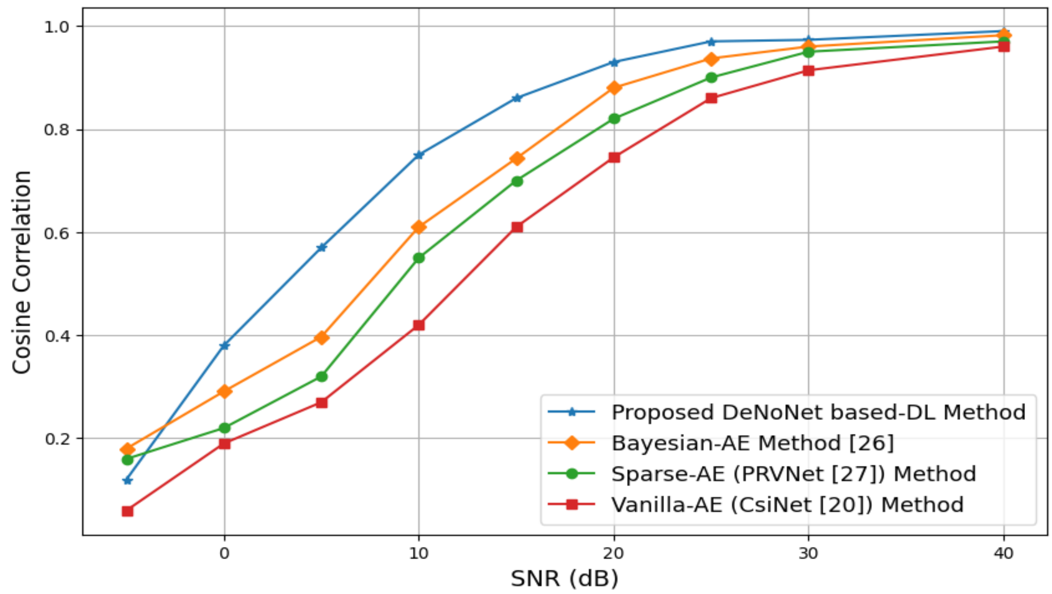

Figure 5.7: Cosine correlation (ρ) vs SNR (dB) for proposed DeNoNet and existing Bayesian-AE, sparse AE and vanilla AE methods.

We simulate all three DNN structures, i.e., Bayesian-AE, sparse-AE, vanilla-AE and our proposed DeNoNet based methods for indoor scenario. Fig. 5.6 shows the comparison of NMSE vs SNR performance of proposed DeNoNet based method with these three schemes. In noisy environments, the NMSE of the DeNoNet based algorithm degrades significantly. As SNR increases, all mechanisms show a gradual NMSE reduction. Now we can clearly see that our DeNoNet-based DL method outperforms the other techniques.

At 10 (dB) SNR, vanilla AE achieves a NMSE of -3.040, sparse AE -5.077, Bayesian AE -7.78, while our proposed mechanism is able to achive NMSE of -11.40. Thus, the proposed DeNoNet scheme outperforms Bayesian AE by 46.52%, sparse AE by 124.54%, and vanilla AE by 275%.

Similarly, Fig. 5.7 illustrates the relation between ρ vs SNR (dB) for proposed DeNoNet as well as all existing methods like Bayesian-AE, sparse AE and vanilla AE. ρ values for all algorithms increase with SNR, we can clearly observe that our proposed DeNoNet-based method consistently outperforms then other existing techniques.

5.5 Conclusion

This chapter proposes DeNoNet, a DL-based system developed to improve the performance of channel feedback and durability in massive MIMO systems. We propose training DeNoNet using the existing DL-based feedback technique. The simulation findings show that the proposed DeNoNet training process outperforms previous methods that include faulty feedback channels. Furthermore, we achieve improvements of 113.18 % in NMSE and 72.72 % in ρ for the estimation of the proposed DeNoNet channel in a range of SNR conditions.

5.6 Limitations and Future Work

The DeNoNet-based CSI feedback scheme delivers notable improvements under noisy conditions but has some limitations. Its performance relies heavily on diverse training data, and its computational complexity may hinder use in resource constrained devices. Moreover, it mainly targets Gaussian noise, whereas real channels involve more complex distortions. Future work could focus on lightweight designs, robustness to diverse impairments, and advanced learning methods such as transfer or federated learning to improve adaptability across varying channel conditions.

5.7 Discussion on Compression Ratio

The choice of SNR on the x-axis reflects our focus on evaluating the robustness of the proposed DeNoNet scheme under varying channel noise conditions, which is critical for practical deployment in wireless environments. By plotting performance against SNR, we demonstrate how effectively the network reconstructs CSI in noisy scenarios. Compression ratio typically tells the level of sparsification performed, as was expressed in (5.8) as $\gamma = \frac{N_{CW}}{2 \times N_t \times N_P}$.

However, it must be noted that SNR and compression ratio are indirectly related to each other. In high SNR regions, a high compression ratio is more likely to give efficient reconstruction. Wheres, in low SNR regions, this behavior is less likely to be observed and a high compression is not possible. Since our proposed DeNoNet scheme performs satisfactorily in all the SNR regions, its application will be efficient for all the ranges of compression ratio.

5.7.1 Adaptive CSI Feedback and Denoising Control Under Dynamic Channel Conditions

I would formulate this problem as a constrained adaptive control policy rather than using a fixed compression ratio or denoising configuration. The controller would continuously monitor the system state, which includes the instantaneous feedback channel SNR, the Doppler spread (or user mobility), the resulting channel coherence time T_c, and the antenna dimension N_t. Based on these inputs, the controller would dynamically select two key parameters, the codeword length or compression ratio and the denoising strength. The primary objective would be to minimize CSI reconstruction error while ensuring that the entire CSI feedback process is completed before the channel becomes outdated. In other words, the controller seeks to achieve the lowest possible NMSE and highest ρ while satisfying a strict latency constraint that includes encoding, feedback transmission, decoding, and denoising delays.

The controller would operate in two stages. During the *offline stage*, a performance database would be constructed using the compression ratio and denoising analyses already performed in Chapters 3-5. For different combinations of compression ratios, feedback channel SNR values, antenna dimensions, and denoising strengths, the corresponding NMSE, ρ, and inference latency would be recorded. This creates a lookup table or predictive model that characterizes the performance complexity trade-off of the framework. During the *online stage*, the controller would estimate the current feedback channel SNR and channel coherence time, where the coherence time can be approximated as

$$T_c \approx \frac{1}{4 f_D}, \tag{5.24}$$

where f_D denotes the Doppler frequency. The controller then selects the operating point that minimizes the expected reconstruction error while satisfying the latency constraint

$$T_{\text{enc}} + T_{\text{fb}} + T_{\text{dec}} + T_{\text{denoise}} \leq T_c, \tag{5.25}$$

where T_{enc}, T_{fb}, T_{dec}, and T_{denoise} denote the encoding, feedback transmission, decoding, and denoising delays, respectively. To prevent frequent switching caused by noisy SNR estimates, a hysteresis mechanism or minimum dwell time can be incorporated before changing operating points.

The adaptive behavior of the controller naturally follows the channel conditions. For high-mobility users, where the coherence time is short, the controller would prioritize CSI freshness by selecting a smaller codeword length and lighter denoising configuration, thereby reducing transmission and processing delays even if a slight increase in NMSE is incurred. However, for low-mobility users with longer coherence times, the controller can afford larger codeword lengths and stronger denoising to maximize reconstruction accuracy. Similarly, when the feedback channel SNR is low, the controller would increase the denoising strength and allocate a larger latent representation to preserve CSI quality, whereas under high-SNR conditions it would employ more aggressive compression and lighter denoising to reduce overhead. Because the proposed framework utilizes a lightweight CNN architecture with only a small number of residual regeneration units, the inference latency remains predictable and relatively small, making transmission delay the dominant factor. Consequently, the controller can reliably satisfy real-time constraints while maximizing reconstruction quality, ensuring that accurate CSI is available before the channel changes and thereby preserving beamforming gain, spectral efficiency, BER performance, and energy efficiency.

Chapter 6

CDN and its Comparison with CNN for CSI Feedback Reduction in Massive MIMO

A crucial prerequisite for the efficiency and adaptability of massive MIMO network structures in 5G and future 6G wireless networks is to minimize the overhead of CSI feedback. CS has been suggested as a solution to this problem. However, CS uses the DFT, which increases processing overhead in the network. The efficiency of the CNN and the channel denoising network (CDN) in addressing the errors brought on by CSI overhead and channel loss in massive MIMO systems is assessed and contrasted in this chapter. Specifically in massive MIMO systems, the study examines CSI precision, resilience to noise, and applicability to different SNR ranges through DL network-driven algorithms. Simulation findings demonstrate that the proposed DL-based approaches make large gains over the present DeepAE-based DL technique. In contrast to the baseline DeepAE system, which only achieved 0.567, it is found that the suggested techniques can obtain a cosine similarity (ρ) of up to 0.770 with the CNN-based DFT model and further improved to 0.890 using CDN model. Similarly, the suggested network techniques significantly reduce the NMSE, going from -5.33 with the DeepAE baseline to -11.42 with the CNN-based DFT framework and then to -16.30 with the CDN model. The efficiency of the suggested designs in channel estimation is demonstrated by these gains, which are constant across SNR levels up to 10 dB. Furthermore, the proposed CDN-based DL network and CNN-based DFT network approach perform exceptionally well under SNR circumstances, indicating that real-world communication networks can be utilized effectively.

6.1 Overview

The fifth and impending sixth generations of wireless communications have introduced improved technology, seeking to increase data throughput, channel capacity, and reduce feedback overhead [306, 307, 201]. Massive MIMO is one such key technology, requiring the integration of multiple antennas at BS and access points to enhance network capacity and reliability [308, 309]. Massive MIMO systems utilize a huge number of antennas ranging from hundreds to thousands at both the transmitter and receiver ends of the wireless channel [216]. These antenna arrays can be deployed either in a centralized configuration [217] or distributed [218] across multiple locations, depending on the system design requirements.

Massive MIMO significantly mitigates multi-user interference and improves overall system performance [219]. However, its deployment requires sophisticated signal processing and high-power hardware, leading to increased operational costs [310]. Therefore, it is essential to investigate low-complexity, energy-efficient implementation strategies that promote environmentally friendly and sustainable communication solutions.

Current MIMO systems collect downlink channel data from users while they are being trained [220]. It is transmitted back to the BS via a feedback link. The difficulty in large-scale MIMO systems is effectively minimizing the feedback overhead of CSI [222], leading to many studies [178, 179, 223, 224, 225, 64]. The use of CS to minimize the feedback load for CSI in massive MIMO systems is suggested by Gao et al. [178] in their research paper. The authors offer adaptive feedback methods that employ sparsity in spatially correlated antenna arrays to adapt dynamically to channel circumstances.

According to Ge et al. [179], correlated CSI may be converted into an uncorrelated sparse vector. This allows for accurate estimation of a sparse vector from an under-determined linear network using CS. Dai et al. [223] suggest LASSO l_1-solver, an estimation approach that executes choice of variables and periodicity to enhance the prediction accuracy and comprehension of the statistical model. The l_1-solver is an optimization technique for solving the LASSO issue.

In [224] AMP was proposed, which solves sparse recovery by iteratively refining signal estimates. BM3D-AMP [225] extends this by combining BM3D with the AMP framework, leveraging block matching and collaborative filtering for denoising. While effective for sparse signal recovery, its reliance on strict sparsity assumptions limits performance in CSI restoration, where the channel matrix is only approximately sparse, leading to degraded reconstruction quality.

Stochastic projections are used to compress data when CS is applied in the aforementioned techniques. It reduces the number of elements of data by multiplying it with a random matrix. Instead of using stochastic projections, Wen et al. [64] suggest a DL-based CNN technique that uses the data in feature maps to generate a truncated codeword. They employ DFT and inverse DFT to sparsify data at the encoder end and retrieve data at the decoder end, accordingly. Using DFT may slow down the algorithm performance for sparse signals [229].

Sparse signals have a large number of zero or near-zero values. DFT converts signals into sums of sinusoidal functions. As a result, it is not fundamentally intended to handle sparsity effectively. DFT-based techniques need more iterations to process sparse signals and reach a solution, leading to higher computing load and inefficient data reduction. Consequently, these technologies may be limited in their ability to meet next generation data rate demands and further communications. Its main emphasis lies in reducing noise distortion and improving feedback accuracy under varying SNR conditions.

In this chapter, we propose CNN-based DFT and a denoising network (CDN) for reducing CSI feedback overhead in massive MIMO systems. CNN effectively captures spatial channel characteristics, while CDN is optimized for noise suppression. The study evaluates performance with different antenna settings (32×32 and 64×64) across varying SNR levels. Comparing both methods to DeepAE [199] reveals significant gains in cosine similarity (ρ) and NMSE. Importantly, the CDN and CNN-based DFT DL achieve better robustness at low SNR levels, making them highly effective for real world applications.

We overcome these limitations and achieve reduction in CSI feedback noise with the application of a CDN based-DL mechanism, which is overhead-oriented, targeting efficient feedback transmission in massive MIMO. The proposed CDN emphasizes reducing feedback overhead with efficient CSI representation, alongside denoising.

We perform the performance evaluation of CNN-based DFT DL [311, 312] as well as a CDN, and show the improvement brought by each of them in DL-based methods for obtaining the CSI in a massive MIMO system. The DFT offers a structured representation of the input sequence, facilitating low-complexity compression, while the CDN enhances reconstruction accuracy by mitigating channel distortions.

The contributions to this chapter are as follows:

1. *Improved Data Sparsification for Effective Feedback*: The proposed DL-based approach improves sparsification of massive MIMO CSI feedback. DL needs feature extraction, while DFT, matched to data properties, gives useful features for DL.

2. *Incorporation of a CDN*: To enhance robustness, a CDN is integrated, effectively mitigating channel noise and improving CSI reconstruction accuracy under practical wireless impairments.

3. *Hybrid Transform Network Framework*: A novel joint framework is proposed that combines the strengths of transform domain representation with neural network–based denoising, outperforming conventional DL-based CSI feedback schemes.

4. *Comprehensive Performance Evaluation*: Thorough tests in a variety of channel conditions validate the effectiveness of the suggested approach, emphasizing improvements in noise resistance, reconstruction accuracy, and environmental adaptability.

This is how the rest of the chapter is organized. The associated works are represented in Section 6.2. The system model of CNN and CDN is shown in Section 6.3. The channel response design is shown in Section 6.4. Algorithms derived from CNN and CDN are presented in Section 6.5. The findings of the tests and simulations are shown in Section 6.6, and the chapter conclusion is shown in Section 6.7.

6.2 Related Works

By using CS to take advantage of the spatial sparsity of massive MIMO networks, the novel MIMO acquisition technique [178] allows for spontaneous control of pilot overhead. In order to improve channel estimation, a closed loop detection technique based on temporal correlation is added to a random sparsity dynamic matching pursuit technique that collectively predicts multiple subcarrier networks. The effectiveness and versatility of this strategy are further supported by performance analysis.

Accordingly, for massive MIMO structures, the compression-driven LMMSE (CLMMSE) approach [179] is suggested to improve channel estimation productivity by utilizing block sparsity by CS. It improves precision as well as resilience by using a single value decomposition instead of computationally costly matrix translation and a block sparsity adaptive matching pursuit (BSAMP) mechanism to dynamically estimate channel sparsity.

Similarly, the LASSO l_1-solver technique [313] uses scaled ℓ_p-regularization $(1 \leq p \leq 2)$ to solve linear inverse problems and encourage sparsity more successfully than conventional quadratic constraints. The regularized outcomes are computed effectively using an iterative technique of the Landweber type with nonlinear thresholding included.

The AMP algorithm for visual image CS is revealed by the AMP-Net structure [225], which builds upon continuous optimization concepts. It incorporates de-blocking phases to minimize distortions and simultaneously learns the sampling vector with network parameters to improve retrieval accuracy and resolution.

Similarly, DL-based CSI measuring techniques like CsiNet [64] use joint encoder decoder instruction to learn compact codeword representations, which maintains robust beamforming ability at minimal compression ratios and achieves better reconstruction efficiency than conventional sensing techniques.

To enhance CSI reduction and quantification efficiency, CsiNet+ [65] presents a dynamic CS neural structure. In order to improve reconstruction accuracy and lower UE storage demands, it integrates adaptive rate variants (SM-CsiNet+ and PM-CsiNet+), sophisticated quantization methodologies, and improved design concepts.

In FDD massive MIMO systems, a deep autoencoder-based CSI feedback structure [199] is developed. The algorithm trains strong feature representations that successfully counteract latency and noise-induced performance deterioration by simulating feedback delay and transmission faults.

Moreover, by using an improved training procedure, the multi resolution feedback system CRNet [66] improves CSI feature extraction and reconstruction, surpassing CsiNet in reconstruction accuracy without needing extra information or raising computational costs.

After that, the transformer-driven structure (TransNet) [67] facilitates further development by enhancing CSI reduction and retrieval for FDD massive MIMO networks, offering better feedback efficiency with communication robustness than conventional techniques.

Finally, the CSI-StripeFormer model [198] extends Transformer-based design principles, employing a high-complexity autoencoder structure that utilizes the CsiNet+ quantization strategy and MSE-based optimization to achieve enhanced reconstruction accuracy and robustness.

6.3 System Model

Consider an FDD-based massive MIMO system where the BS is equipped with N_t transmit antennas, while the UE is equipped with one antenna. The transmission medium is modeled as a frequency-selective fading channel, which is transformed into multiple flat-fading subchannels using OFDMA [300, 314] with N_c subcarriers.

The CSI corresponding to the k^{th} subcarrier is represented as $\boldsymbol{h}_k \in \mathbb{C}^{N_t \times 1}$. The corresponding channel matrix $\tilde{\boldsymbol{H}}$ is written as

$$\tilde{\boldsymbol{H}} = \begin{bmatrix} \mathbf{h}_1^H & \mathbf{0} & \cdots & \mathbf{0} \\ \mathbf{0} & \mathbf{h}_2^H & \cdots & \mathbf{0} \\ \vdots & \vdots & \ddots & \vdots \\ \mathbf{0} & \mathbf{0} & \cdots & \mathbf{h}_{N_c}^H \end{bmatrix}_{N_c \times N_c N_t} . \tag{6.1}$$

Let $\boldsymbol{p}_k \in \mathbb{C}^{N_t \times 1}$ denote the beamforming vector associated with the k^{th} subcarrier. The aggregated beamforming matrix is then written as

$$\boldsymbol{P} = \begin{bmatrix} \mathbf{p_1} & \mathbf{0} & \cdots & \mathbf{0} \\ \mathbf{0} & \mathbf{p_2} & \cdots & \mathbf{0} \\ \vdots & \vdots & \ddots & \vdots \\ \mathbf{0} & \mathbf{0} & \cdots & \mathbf{p}_{N_c} \end{bmatrix}_{N_c N_t \times N_c} . \tag{6.2}$$

The beamforming vectors must satisfy the transmit power constraint, i.e., $||\boldsymbol{p}_i||_2^2 = \frac{P_t}{N_c}$, where P_t denotes the total available transmit power. The received signal vector at the UE in the frequency spectrum can be represented as

$$y = \tilde{\boldsymbol{H}}\boldsymbol{P}x + \omega, \tag{6.3}$$

where $x \in \mathbb{C}^{N_c \times 1}$ is the transmitted symbol vector and $\omega \in \mathbb{C}^{N_c \times 1}$ is the additive noise vector.

For ease of representation, the channel matrix is rearranged as

$$\boldsymbol{H}_{SF} = [\mathbf{h}_1, \mathbf{h}_2, \ldots, \mathbf{h}_{N_c}]^H_{N_c \times N_t}, \tag{6.4}$$

where $\boldsymbol{H}_{SF}$ corresponds to the CSI in the spatial-frequency domain. We use a 2D-DFT to obtain the channel architectural attributes, mapping it onto the angle delay realm in the following manner

$$\boldsymbol{H}_{AD} = \boldsymbol{F}_D \boldsymbol{H}_{SF} \boldsymbol{F}_A^H, \tag{6.5}$$

where the DFT vectors in the lag and angular realms are indicated by $\boldsymbol{F}_D \in \mathbb{C}^{N_c \times N_c}$ and $\boldsymbol{F}_A \in \mathbb{C}^{N_t \times N_t}$, accordingly. Significant values are clustered inside the initial N_P rows [64], indicating sparsity in $\boldsymbol{H}_{AD}$ due to the restricted path delay spread. Following [64, 65], the reduced channel matrix is obtained as

$$\boldsymbol{H} = [\boldsymbol{H}_{AD}]_{1:N_P}, \tag{6.6}$$

where $[\boldsymbol{H}_{AD}]_{1:N_P}$ represents the submatrix containing the first N_P rows of $\boldsymbol{H}_{AD}$.

6.3.1 DL-Driven Encoder and Decoder

DL approach is widely adopted for CSI feedback to minimize the overhead associated with channel reporting [64, 65]. In this framework, the UE employs an encoder to compress the CSI into a compact codeword s, i.e.,

$$s = f_{en}(\boldsymbol{H}), \tag{6.7}$$

which is subsequently transmitted to the BS through the feedback channel. At the BS, a decoder reconstructs the CSI as

$$\tilde{\boldsymbol{H}} = f_{de}(s). \tag{6.8}$$

The autoencoder thus consists of the encoder $f_{en}(\cdot)$ and decoder $f_{de}(\cdot)$. If the codeword s contains N_{CW} elements, the compression ratio is defined as

$$\gamma = \frac{N_{CW}}{2 \times N_t \times N_P}. \tag{6.9}$$

Conventional DL-based feedback approaches [296] assume perfect feedback. However, in practical wireless systems, various impairments and nonlinear effects introduce errors in CSI reporting. Following the approach in [301], we treat all imperfections as additive noise, which may not necessarily follow a Gaussian distribution. The noisy codeword at the BS is therefore modeled as

$$\tilde{s} = s + n, \tag{6.10}$$

where n denotes the impairment term superimposed on the codeword.

6.4 Proposed Structure of Response $\tilde{\boldsymbol{H}}$

6.4.1 Discrete Fourier Transform and Its Inverse

DFT [315] converts a finite sequence of discrete-time samples into its frequency-domain form, representing the signal as a sum of complex sinusoids with distinct frequencies.

Let $x[n]$ be a sequence of length N. the DFT represented as

$$X[k] = \sum_{n=0}^{N-1} x[n] \cdot e^{-j\frac{2\pi}{N}kn}, \quad k = 0, 1, 2, 3 \tag{6.11}$$

where $x[n]$ and $X[k]$ are the input sequence in the time domain and the output sequence in the frequency domain, respectively. N is total number of samples. $w = e^{-j\frac{2\pi}{N}kn}$ represents complex sinusoidal basis functions and k is the frequency index.

The $N \times N$ matrix representation of the DFT is bellow

$$X = \boldsymbol{H}x \tag{6.12}$$

where $\boldsymbol{H}$ shows as symmetric matrix as

$$\boldsymbol{H} = \begin{bmatrix} 1 & 1 & 1 & \cdots & 1 \\ 1 & w & w^2 & \cdots & w^{N-1} \\ 1 & w^2 & w^4 & \cdots & w^{2(N-1)} \\ \vdots & \vdots & \vdots & \ddots & \vdots \\ 1 & w^{N-1} & w^{2(N-1)} & \cdots & w^{(N-1)(N-1)} \end{bmatrix}. \tag{6.13}$$

Similarly, the inverse DFT can represents as

$$x[n] = \sum_{n=0}^{N-1} X[k] \cdot e^{j\frac{2\pi}{N}kn}, \quad k = 0, 1, 2, 3 \tag{6.14}$$

and the IDFT matrix $\tilde{\boldsymbol{H}}$ represented as

$$x = \frac{1}{N}\tilde{\boldsymbol{H}}X \tag{6.15}$$

where $\tilde{\boldsymbol{H}}$ shows bellow:

$$\tilde{\boldsymbol{H}} = \begin{bmatrix} 1 & 1 & 1 & \cdots & 1 \\ 1 & w^{-1} & w^{-2} & \cdots & w^{-(N-1)} \\ 1 & w^{-2} & w^{-4} & \cdots & w^{-2(N-1)} \\ \vdots & \vdots & \vdots & \ddots & \vdots \\ 1 & w^{-(N-1)} & w^{-2(N-1)} & \cdots & w^{-(N-1)(N-1)} \end{bmatrix}. \tag{6.16}$$

Thus, the DFT and its inverse provide a complete framework for efficient CSI compression and reconstruction in the proposed architecture.

6.4.2 CNN-Based Architecture

We design a CNN based encoder-decoder to recover CSI $\boldsymbol{H}$, exploiting its spatial correlations in Fig. 6.1. The sparsified channel $\tilde{\boldsymbol{H}}$, obtained via DFT, is separated into real and imaginary parts $\boldsymbol{H}_r$ and $\boldsymbol{H}_i$, which are processed by the encoder's 3×3 convolutional kernels. A fully connected layer then converts the output into a codeword $s \in \mathbb{R}^M$, enabling efficient compression under CS principles.

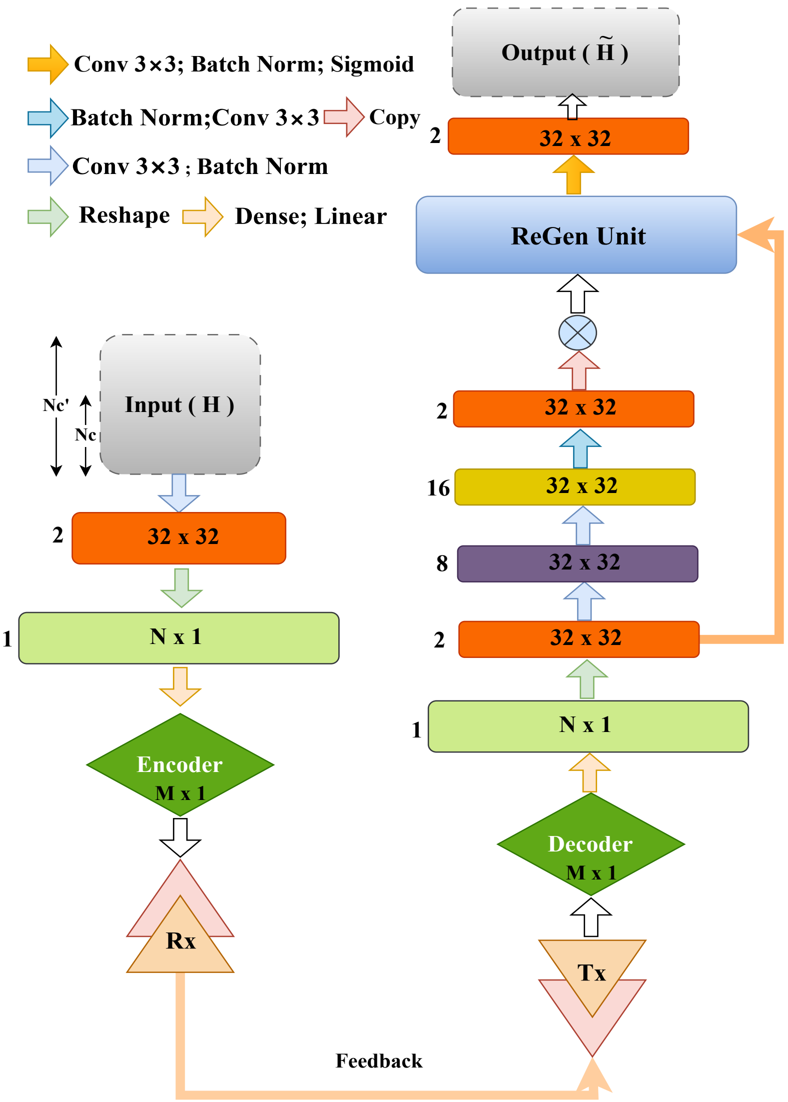

Figure 6.1: A color visualization of the magnitude of $\boldsymbol{H} \in \mathbb{C}^{32\times32}$ illustrates the encoder–decoder architecture of the CNN approach.

The decoder reconstructs $\boldsymbol{H}$ from s. An initial fully connected layer estimates $\boldsymbol{H}_r$ and $\boldsymbol{H}_i$ of size $N_c \times N_t$, followed by ReGen units for refinement. Each ReGen block has four layers with 3×3 kernels, generating 8 and 16 feature maps before producing the final output with zero padding. The rectified linear unit (RecUn) activation, $\text{RecUn}(\zeta) = \max(\zeta, 0)$, with batch normalization ensures stable learning.

Unlike conventional CNNs, ReGen avoids pooling to preserve resolution and employs residual style shortcuts [241] to mitigate vanishing gradients. Two ReGen blocks provide the best performance, and the final convolutional layer with sigmoid activation produces the refined channel estimate.

The encoder-decoder is trained from end to end, with parameters $\nabla = \nabla_{en}, \nabla_{de}$. For the i^{th} input,

$$\boldsymbol{H}i = f(\boldsymbol{H}i; \nabla) = fde(fen(\boldsymbol{H}i; \nabla en); \nabla_{de}). \tag{6.17}$$

Training is unsupervised using ADAM and the purpose is to minimize the square of error:

$$L(\nabla) = \frac{1}{T}\sum_{i=1}^{T} |f(\boldsymbol{s}_i; \nabla) - \boldsymbol{H}_i|_2^2, \tag{6.18}$$

where $|\cdot|_2$ is the Euclidean standard and T is the total number of training sets.

6.4.3 CDN-Based Architecture

This section introduces the proposed CDN, which is designed to enhance CSI feedback by denoising the transmitted codeword. As shown in Fig. 6.2, the architecture integrates a NEU that estimates the distortion in the codeword and subtracts it to recover a cleaner representation.

The NEU is implemented as a fully connected neural network has L layers, including a single input, a single output, and $L-2$ layers that are invisible. The received code-word is given by

$$\tilde{s} = [\tilde{s_1}, \tilde{s_2}, \ldots, \tilde{s}_{N_{CW}}], \tag{6.19}$$

and is normalized using batch normalization [316] to accelerate training and avoid output saturation:

$$\tilde{s}' = \frac{\tilde{s} - E[\tilde{s}]}{\sqrt{Var[\tilde{s}]}}. \tag{6.20}$$

The NEU output corresponds to the estimated noise component,

$$\hat{n} = \mathcal{F}_L(\ldots \mathcal{F}_1(\tilde{s}')), \tag{6.21}$$

where the operation of the l^{th} layer is defined as

$$F_l(z) = \begin{cases} z, & l = 1, \\ \xi(W_l z + b_l), & 2 \leq l < L - 1, \\ W_l z + b_l, & l = L, \end{cases} \tag{6.22}$$

with z denoting the input to the l^{th} layer, W_l and b_l being the weight matrix and bias vector, respectively, and $\xi(x) = (1 + e^{-x})^{-1}$ representing the sigmoid activation. To ensure sufficient noise modeling, the hidden layers are set with 1024 neurons, typically larger than the codeword dimension.

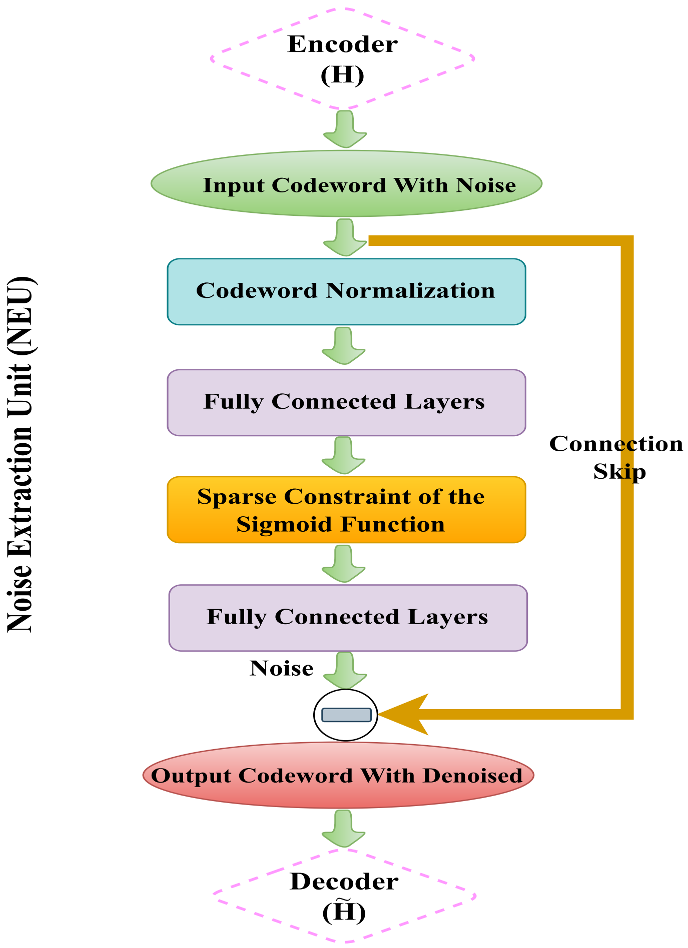

Figure 6.2: CDN schematic architecture of encoder and decoder.

To mitigate overfitting in high-dimensional settings, a Kullback-Leibler (KL) divergence sparsity penalty [303] is applied to the hidden activations:

$$\mathrm{KL}(\Psi \parallel \hat{\Psi}) = \sum_{j=1}^{|\hat{\Psi}|} \Psi \log\left(\frac{\Psi}{\hat{\Psi}_j}\right) + (1-\Psi)\log\left(\frac{1-\Psi}{1-\hat{\Psi}_j}\right), \tag{6.23}$$

where $\hat{\Psi} = \frac{1}{N}\sum_{i=1}^{N} \xi(Wz_i + b)$ with N as the batch size, $\hat{\Psi}_j$ the average activation of the j^{th} hidden unit, Ψ the target sparsity, and z_i the i^{th} batch output.

Finally, a skip connection passes the original codeword to the NEU output. The denoised codeword is obtained by

$$\hat{s} = \tilde{s} - \hat{n}, \tag{6.24}$$

and forwarded to the decoder for CSI reconstruction.

6.5 Implementation of Algorithms

We propose a DL-based framework for enhancing CSI feedback in FDD massive MIMO systems. The methodology consists of two stages: first, preprocessing of complex channel data to obtain a structured representation, and second, training and evaluation of neural network models that learn to efficiently compress and reconstruct the CSI.

The initial preprocessing phase, the complex channel coefficients $\boldsymbol{H}_r$ and $\boldsymbol{H}_i$ are transformed from Cartesian form into their equivalent polar representation through the domain transformations. The phase (ϕ) and magnitude (r) of each coefficient are obtained as

$$\phi = \arctan 2(\boldsymbol{H}_r, \boldsymbol{H}_i), \qquad r = \sqrt{\boldsymbol{H}_r^2 + \boldsymbol{H}_i^2}. \tag{6.25}$$

This transformation enables a more compact separation of amplitude and phase information, thus simplifying the learning process. The inverse transformation is then applied to recover the original complex domain when required, expressed as

$$\boldsymbol{H}_r = r\cos(\phi), \qquad \boldsymbol{H}_i = r\sin(\phi). \tag{6.26}$$

After preprocessing, several DL architectures are designed to model compressed CSI feedback. The initial autoencoder model, which trains compact CSI patterns and regenerates the initial input. The encoder uses dense layers to reduce information into a small latent data and convolutional layers with RecUn activation to extract hierarchical spatial characteristics. From this compressed illustration, the decoder recreates the CSI feedback using convolutional layers and linear activations. For better reconstruction, a deep residual network (ResNet) is incorporated. By using remaining blocks made up of batch normalization stages and Conv2D, the ResNet allows for identity mapping and lessens performance degradation in deeper models. To ensure dependable CSI recovery, a CDN is created concurrently. It has a framework similar to the autoencoder but is specifically tuned to minimize Gaussian noise.

The Adam optimization algorithm with learning rates (LR) of 0.001 and 0.003 is used to train the models. Disparities among the original and regenerated CSI are explicitly penalized by the training outcome parameter, NMSE. A training callback is used to track convergence, enabling ongoing assessment of rebuilding accuracy through the course of the epochs.

To quantitatively measure performance, two evaluation metrics are employed. The NMSE, which can be defined as the distance between the signal reconstruction and the actual real value,

$$\text{NMSE} = E\left\{\frac{\|\boldsymbol{H}_{or} - \boldsymbol{H}_{pr}\|_2^2}{\|\boldsymbol{H}_{or}\|_2^2}\right\}, \tag{6.27}$$

where the real and expected CSI data are indicated by $\boldsymbol{H}_{or}$ and $\boldsymbol{H}_{pr}$, accordingly. Apart from NMSE, ρ is employed to gauge the structural resemblance between the real and regenerated CSI, which is represented as

$$\rho = E\left\{\frac{\sum(\boldsymbol{H}_{or} \cdot \boldsymbol{H}_{pr})}{\|\boldsymbol{H}_{or}\|_2 \cdot \|\boldsymbol{H}_{pr}\|_2}\right\}. \tag{6.28}$$

Finally, the robustness of the proposed models is assessed by simulating noisy channels with varying SNR conditions. Gaussian noise is introduced into the test data, and perfor-

Algorithm 4 CDN-Based Algorithm Using CSI Feedback

1: **Input:** Noisy codeword $\tilde{s} \in \mathbb{R}^{N_{CW}}$ is started.
2: **Output:** Regeneration of the CSI channel vector $\hat{\mathbf{H}}$.
3: **Step 1: Codeword Normalization**

$$\tilde{s}' = \frac{\tilde{s} - \mathbb{E}[\tilde{s}]}{\sqrt{\mathrm{Var}[\tilde{s}] + \epsilon}}$$

where ϵ ensures numerical stability.
4: **Step 2: Implementation of NEU Module for Noise Estimation**

$$\hat{n} = \digamma_L\Big(\digamma_{L-1}(\cdots \digamma_1(\tilde{s}'))\Big),$$
$$\digamma_l(z) = \begin{cases} z, & l = 1, \\ \xi(W_l z + b_l), & 2 \leq l < L, \\ W_l z + b_l, & l = L, \end{cases}$$

where $\xi(\cdot)$ denotes the sigmoid activation.
5: **Step 3: KL Divergence Regularization** Promote sparsity of hidden activations:

$$\mathrm{KL}(\Psi \parallel \hat{\Psi}) = \sum_{j=1}^{|\hat{\Psi}|} \left[\Psi \log \frac{\Psi}{\hat{\Psi}_j} + (1 - \Psi) \log \frac{1 - \Psi}{1 - \hat{\Psi}_j} \right].$$

6: **Step 4: Denoising via Residual Connection**

$$\hat{s} = \tilde{s} - \hat{n}.$$

7: **Step 5: Regeneration of CSI**

$$\hat{\mathbf{H}} = \mathrm{Decoder}(\hat{s}).$$

8: **Step 6: Training Objective** To reduce NMSE.

$$L_{\text{NMSE}} = \frac{1}{N} \sum_{i=1}^{N} \left\| \hat{\mathbf{H}}_i - \mathbf{H}_i \right\|_2^2$$

9: Use Adam's optimization tool for updating network parameters.

mance across SNR levels is evaluated using both NMSE and ρ. This procedure enables analysis of how well the autoencoder, ResNet and CDN generalize under practical noisy environments, where reliable CSI feedback is critical to system performance.

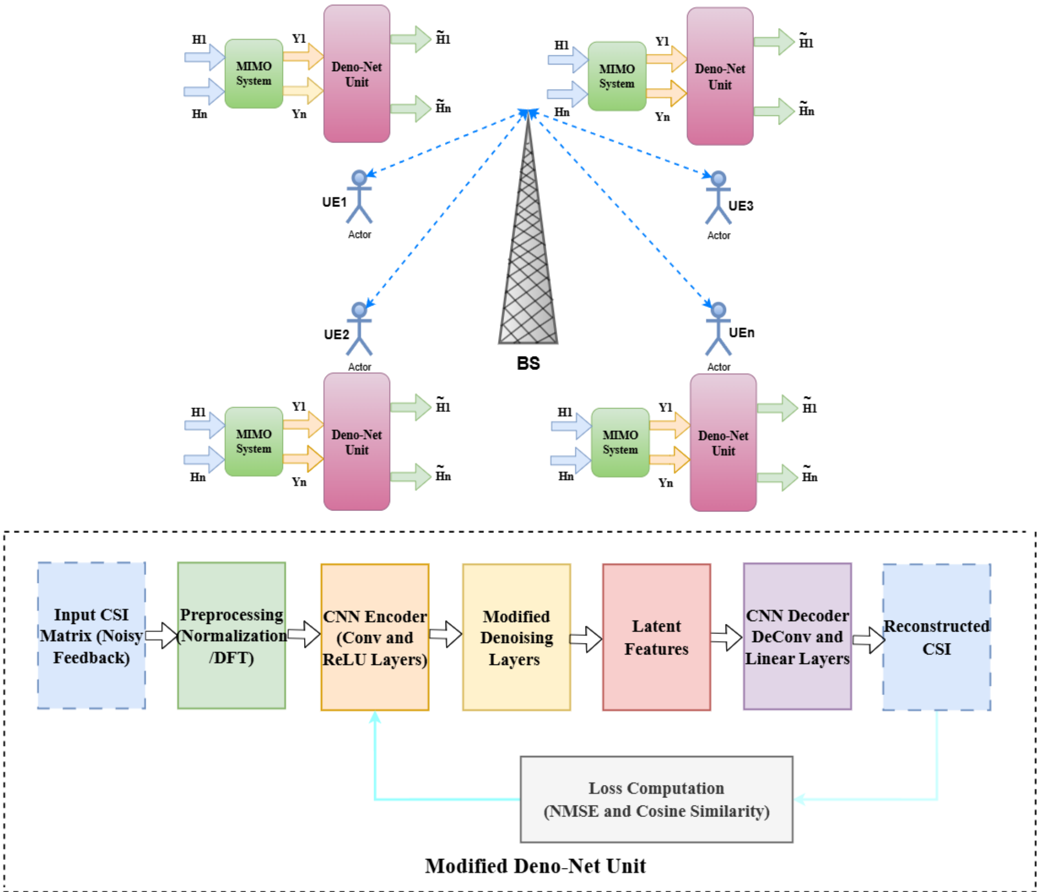

Figure 6.3: Overall structural representation of Deno-Net.

6.6 Experiments and Simulations Results

Simulations were carried out in an indoor pico-cell environment at 5.3 GHz with 1024 subcarriers. The setup employed a 32-antenna BS serving randomly distributed UE within a 20×20 m area. The ResNet-based framework included two residual blocks and a 512-dimensional encoding layer, designed to process a $32 \times 32 \times 2$ CSI input matrix. Model training was performed with $100{,}000$ samples, of which $30{,}000$ were used for validation and $20{,}000$ for testing. The LRs was set to 0.001 and 0.003, with a batch size of 200, and training was conducted over 500 epochs for both the autoencoder and the proposed models.

Performance evaluation was conducted across SNR levels ranging from -5 to 40 dB using NMSE and ρ as metrics on noisy test data. The outcomes show that both the CDN and CNN-based DFT DL method consistently produces better ρ and lesser NMSE when

Algorithm 5 CNN-Driven DL Framework for CSI Feedback in Massive MIMO

Step 1: Pre-processing of Data

Transform complex channel coefficients $\mathbf{H} = \mathbf{H}_r + j\mathbf{H}_i$ into polar representation as

$$r = \sqrt{\mathbf{H}_r^2 + \mathbf{H}_i^2}, \quad \phi = \arctan 2(\mathbf{H}_r, \mathbf{H}_i).$$

Recover real and imaginary components via inverse DFT

$$\mathbf{H}_r = r\cos(\phi), \quad \mathbf{H}_i = r\sin(\phi).$$

Step 2: Neural Network Design

Construct an autoencoder with:

- Convolutional layers (RecUn activation) for hierarchical feature encoding.
- Dense layers to reduce dimension.
- Data regeneration using convolutional layers (linear activation).

Use a ResNet module made up of the following to improve reconstruction:

- Residual batch-normalized Conv2D modules.
- Identification mappings for stabilizing deeper structures.

Step 3: CNN Channel Denoising Improvements

Create a denoising framework that resembles the autoencoder in structure.

Adjust settings to enhance CSI recovery and reduce channel distortion.

Step 4: Training Strategy

Use Adam for optimization with LRs of 0.001 and 0.003.

Reduce the loss due to mean squared error (MSE).

Use customized callbacks (like Loss-History) to monitor convergence.

Step 5: System Assessment

Use the NMSE to assess the correctness of the reconstruction.

$$\text{NMSE} = E\left\{\frac{\|\boldsymbol{H}_{or} - \boldsymbol{H}_{pr}\|_2^2}{\|\boldsymbol{H}_{or}\|_2^2}\right\}.$$

Measure similarity using cosine correlation:

$$\rho = E\left\{\frac{\sum(\boldsymbol{H}_{or} \cdot \boldsymbol{H}_{pr})}{\|\boldsymbol{H}_{or}\|_2 \cdot \|\boldsymbol{H}_{pr}\|_2}\right\}.$$

Step 6: Robustness Testing

Test samples should be subjected to Gaussian noise at various SNR ranges.

Use ρ and NMSE to evaluate resilience in different channel circumstances.

compared to the base models, emphasizing its enhanced reconstruction efficiency as well as greater resilience against interference.

6.6.1 Learning Data Acquisition and Constraints

The training dataset for the DL model was generated using the COST 2100 channel model [317, 318], which provides realistic CSI under different SNR levels, antenna configurations, and propagation environments. For each subcarrier index $n = 1, 2, \ldots, N_c$, the CSI vector was defined as $\boldsymbol{H}_n = [h_{n,1}, h_{n,2}, \ldots, h_{n,N_t}] \in \mathbb{C}^{1\times N_t}$. The dataset consisted of $100{,}000$ training samples, $30{,}000$ validation samples, and $20{,}000$ test samples. Each CSI input was represented as a $32 \times 32 \times 2$ tensor, which separates real and imaginary components, resulting in 2048 values per sample.

Constructing realistic data for massive MIMO is challenging due to the high dimensionality of CSI, sparsity in channel characteristics, and feedback overhead requirements. By providing a compact model of the CSI, the CDN and CNN-based DFT DL efficiently mitigates these problems and reduces computation and storage complexity. In order to increase the system's resistance to channel impairments, artificial noise was added to the database, which was created across a broad range of SNR values because noise affects practical channels.

The sparse representation achieved through CDN and CNN-based DFT DL ensures that these models can process CSI more efficiently while preserving accuracy, making it suitable for real-time deployment. The dataset size and diversity were carefully designed to capture the complexity of massive MIMO propagation and to promote strong generalization performance under varying channel conditions.

6.6.2 Results Evaluation

Fig. 6.4 represents ρ across varying SNR levels, comparing the proposed models with DeepAE-based DL [199]. The noise-free ideal threshold (ρ or NMSE in the absence of noise) is also shown. While ρ improves with SNR for existing method, the proposed CDN and CNN-based DFT consistently outperform the DeepAE baseline (0.567), achieving gains of 0.890 and 0.770, respectively.

Fig. 6.5 illustrates the NMSE performance of DeepAE compared with the proposed CDN and CNN-based DFT frameworks after pre-training. The horizontal line at -30 dB denotes the noise-free benchmark NMSE of DeepAE. Under noisy conditions, DeepAE exhibits a marked performance decline, while both methods show decreasing NMSE with increasing SNR. The proposed approaches consistently outperform DeepAE base value -5.33, achieving improvements of -16.30 for the CDN-driven model and -11.42 for the CNN-based variant.

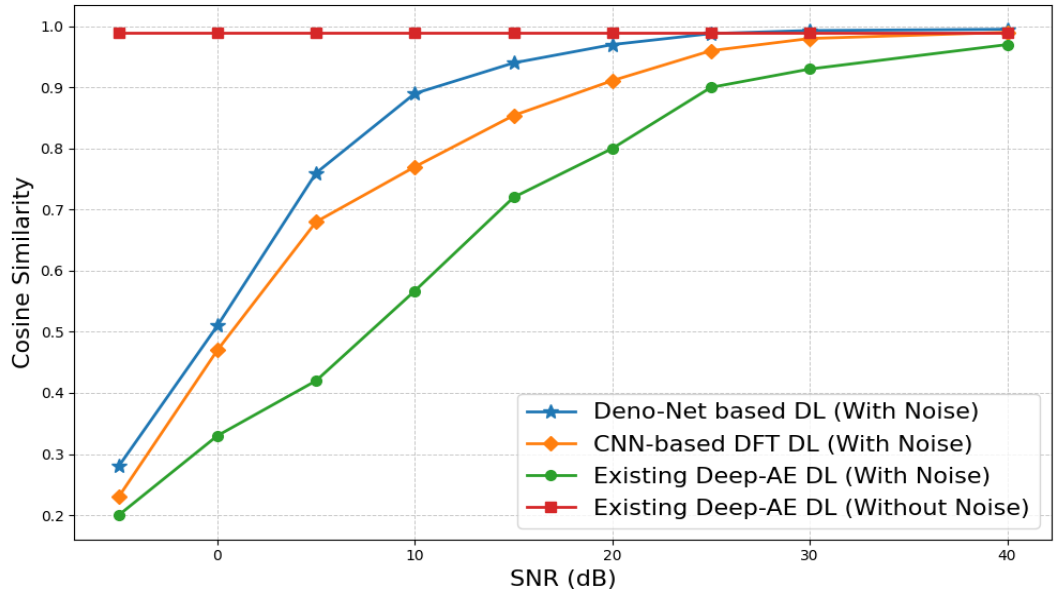

Figure 6.4: ρ vs SNR (dB) with and without noise simulations results for CDN, CNN based DFT DL and existing DeepAE based DL methods.

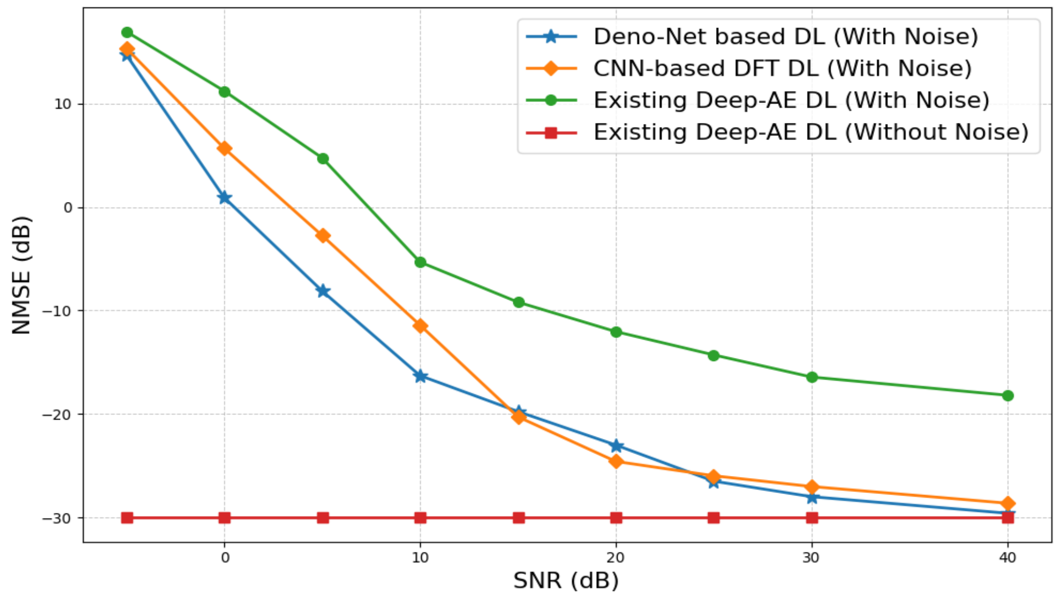

Figure 6.5: NMSE (dB) vs SNR (dB) with and without noise simulations results for CDN, CNN-based DFT DL and existing DeepAE based DL methods.

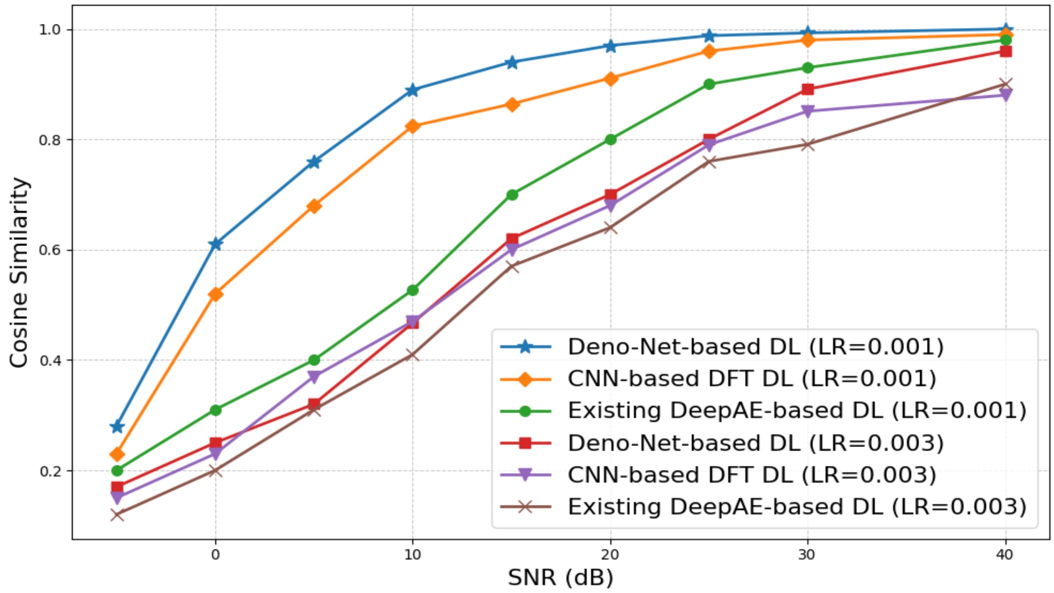

Figure 6.6: ρ vs SNR (dB) of existing DeepAE and CDN and CNN-based DFT DL for different LRs.

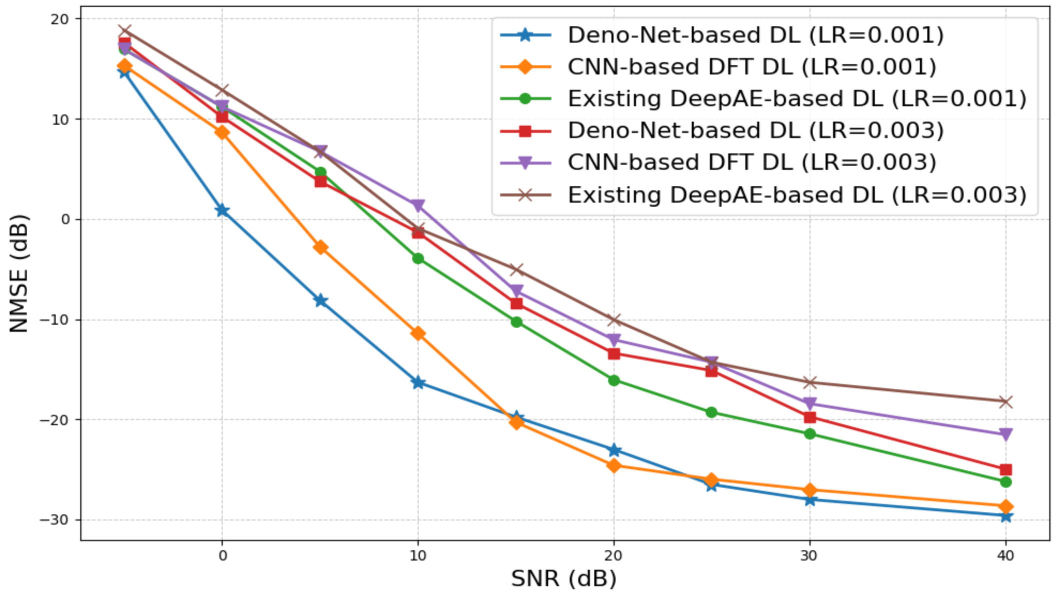

Figure 6.7: NMSE (dB) vs SNR (dB) of existing DeepAE and CDN and CNN-based DFT DL for different LRs.

Figs. 6.6 and 6.7 evaluate the impact of different LRs on the proposed methods. In Fig. 6.6, the ρ vs SNR demonstrates that both CDN and CNN-based DFT models consistently outperform existing DeepAE-based DL across all LRs. Similarly, Fig. 6.7 illustrates NMSE vs SNR, where the proposed frameworks achieve noticeably lower error levels compared to the DeepAE technique under different LRs.

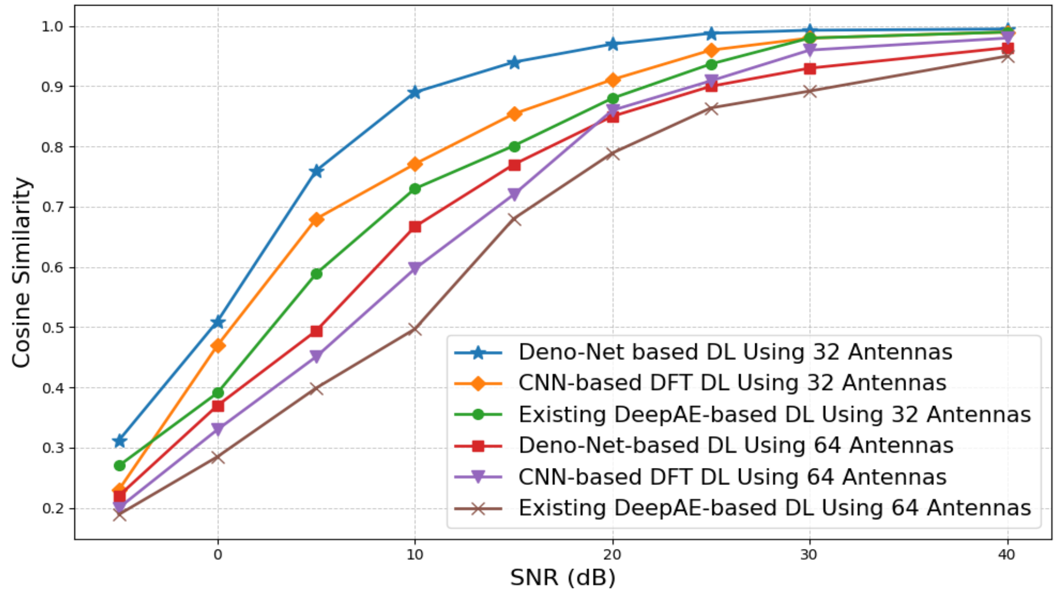

Figure 6.8: ρ vs SNR (dB) comparison of existing DeepAE and CDN and CNN-based DFT DL for 32, 64 antennas.

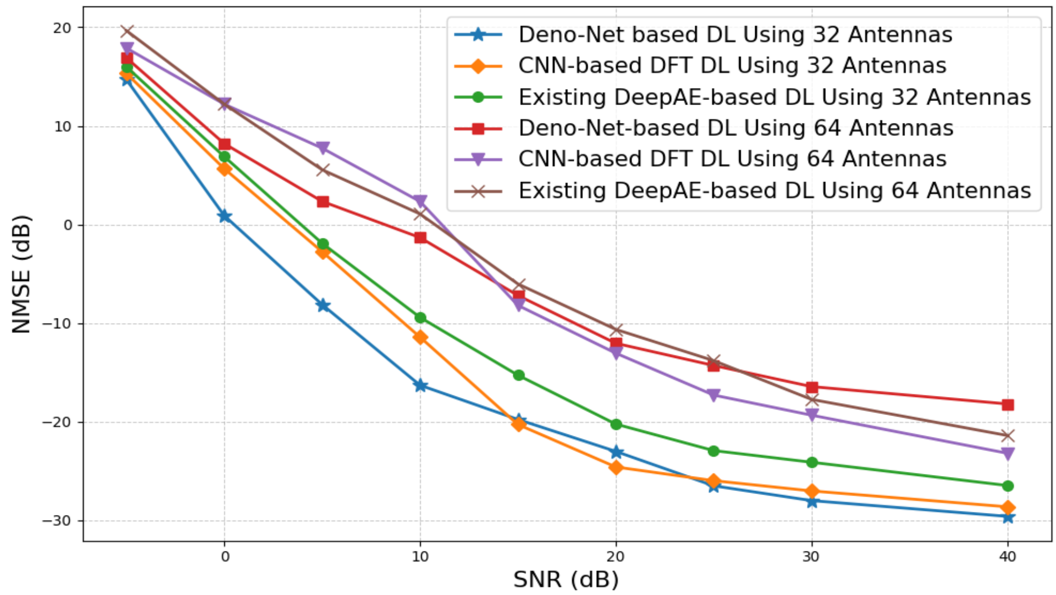

Figure 6.9: NMSE (dB) vs SNR (dB) comparison of existing DeepAE and CDN and CNN-based DFT DL for 32, 64 antennas.

Fig. 6.8 illustrates the ρ vs SNR (dB) for existing DeepAE and the proposed CDN and CNN-based DFT models with antenna configurations of 32 and 64. Across both setups, the proposed methods consistently achieve higher similarity values than existing DeepAE. Likewise, Fig. 6.9 presents the NMSE vs SNR for the same antenna settings, where the CDN and CNN-driven DFT frameworks deliver significantly improved performance compared to DeepAE.

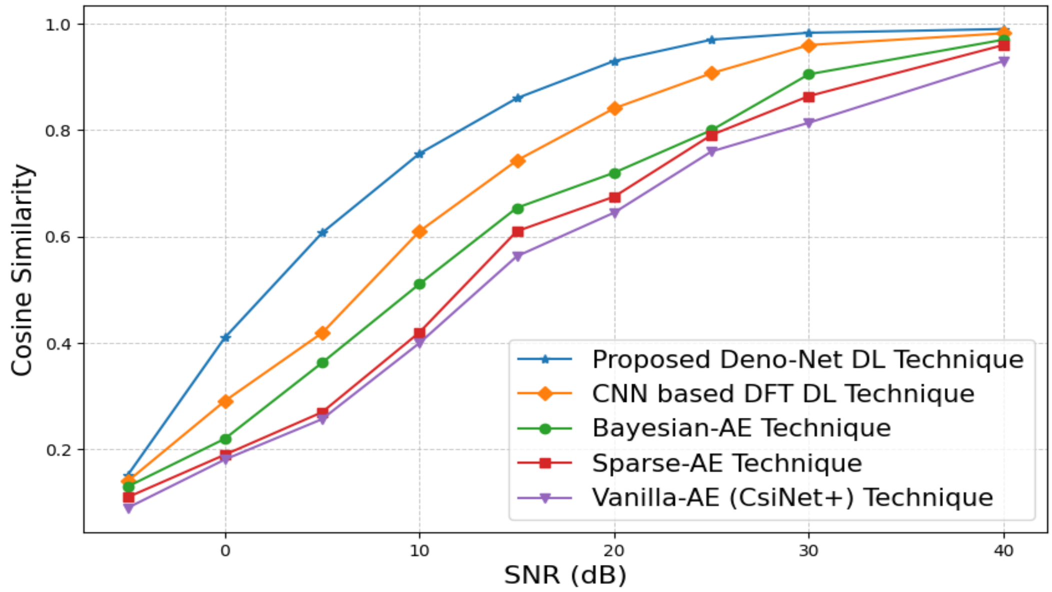

Figure 6.10: ρ vs SNR (dB) for proposed CDN, CNN based DFT DL and existing Bayesian-AE, Sparse-AE and Vanilla-AE techniques.

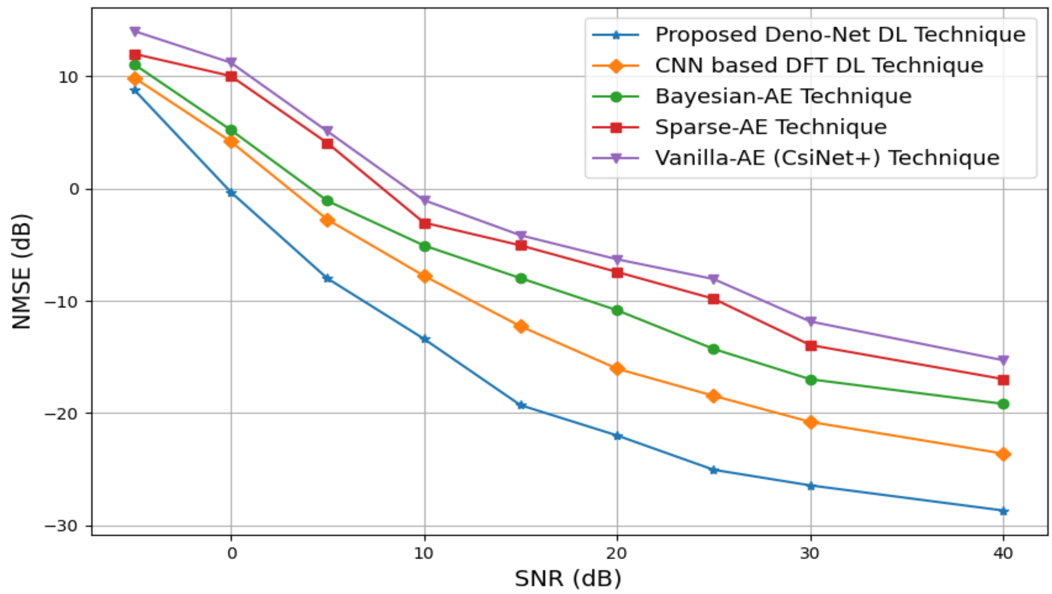

Figure 6.11: NMSE (dB) vs SNR (dB) for proposed CDN, CNN based DFT DL and existing Bayesian-AE, Sparse-AE and Vanilla-AE techniques.

We also assess the performance of three existing DNN architectures Bayesian-AE [305], Sparse-AE [68], and Vanilla-AE [64] alongside the proposed CDN and CNN based DFT DL model in an indoor environment. As shown in Fig. 6.10, the ρ vs SNR analysis indicates that ρ values for all methods increase with rising SNR. However, the proposed frameworks consistently achieves higher correlation coefficients, confirming its superior reconstruction accuracy and robustness compared to other approaches.

Similarly, Fig. 6.11 presents the NMSE vs SNR results, where all models exhibit decreasing NMSE with increasing SNR. Despite the expected NMSE degradation in low SNR conditions, the CDN and CNN based DFT DL methods consistently outperforms the Bayesian-AE, Sparse-AE, and Vanilla-AE networks, demonstrating its effectiveness and resilience across varying noise levels.

6.7 Conclusion

This chapter concludes by presenting a novel DL–based framework that integrates CNN-driven DFT and a CDN to significantly enhance CSI feedback and channel estimation performance in massive MIMO systems. Through a comprehensive comparative evaluation against the conventional DeepAE baseline, the proposed approaches demonstrate substantial gains in both accuracy and robustness. Specifically, the CNN-DFT model improves cosine similarity from 0.567 (DeepAE) to 0.770, while the CDN further elevates it to 0.890. Similarly, NMSE is reduced from −5.33 dB to −11.42 dB and −16.30 dB, respectively. These improvements highlight the effectiveness of spatial feature extraction and integrated denoising in capturing channel structure and mitigating noise. Consistent performance gains across SNR levels up to 10 dB confirm the superior noise resilience and structural efficiency of the proposed methods, particularly in low-SNR regimes. Overall, the results establish CNN-based DFT and CDN frameworks as reliable, high-performance solutions for CSI feedback in practical 5G and future 6G massive MIMO systems.

Chapter 7

Conclusion and Future Scope

This thesis concludes with a comprehensive summary of the research contributions made toward efficient CSI feedback reduction in massive MIMO systems, a crucial factor for 5G and future 6G wireless networks. With more than five billion active internet users today and projections indicating tens of billion connected devices by 2035, wireless networks are expected to support unprecedented data traffic, ultra-reliable connectivity, and massive device density. MIMO technology, particularly massive MIMO, has been historically proven to significantly enhance spectral efficiency and link reliability through spatial multiplexing and diversity gains. However, the practical realization of massive MIMO especially in FDD systems faces a major congestion in the form of excessive CSI feedback overhead. This thesis addresses this fundamental challenge through advanced DL-based and transform-assisted learning frameworks.

Chapter 2, presented a detailed and critical review of existing CSI feedback reduction techniques for massive MIMO systems, with a focus on both CS and DL-based approaches. Conventional CS-based methods exploit channel sparsity but suffer from high computational complexity, noise sensitivity, and dependence on accurate sparsity assumptions. Recent DL-based architectures, such as CsiNet, CsiNet+, CRNet, PRVNet, TransNet, DeepAE, and CSI-StripeFormer, have demonstrated superior performance by learning nonlinear compression and reconstruction mappings. Still, these DL methods introduce new challenges, including large training data requirements, high computational and energy costs, and scalability limitations for real-time systems. This chapter clearly identified the research gap and motivated the development of hybrid transform-assisted DL frameworks that can combine structured signal representations with learning-based efficiency.

In Chapter 3, a novel DRT-assisted DL framework was proposed to overcome the limitations of traditional DFT-based CS and DL approaches. The proposed architecture leverages the DRT to preserve structural sparsity while enabling efficient feature extraction for CSI compression. Extensive simulations using the COST 2100 channel model demonstrated substantial performance gains across a wide SNR range. Specifically, the proposed method achieved improvements of 126.19% in cosine correlation and 81.81% in NMSE compared to DFT-based DL schemes. The results confirmed the robustness, scalability, and reduced feedback overhead of the DRT-based DL framework, particularly under varying SNR and noisy conditions.

Chapter 4, introduced the HaDLeMO framework, a transform-assisted DL approach designed to further enhance CSI feedback efficiency in massive MIMO systems. HaDLeMO exploits permutation invariance, improved sparsification, and strong noise resilience to address the limitations of DFT-based DL models. The independence from input sequence ordering and reduced sensitivity to phase noise make HaDLeMO especially suitable for practical wireless environments. Simulation results validated its superiority in terms of reconstruction accuracy, robustness, and computational efficiency, highlighting its potential for real-time deployment in next-generation wireless systems.

In Chapter 5, proposed DeNoNet, a DL-based denoising framework aimed at improving CSI feedback robustness over imperfect and noisy feedback channels. Unlike conventional approaches that assume ideal feedback links, DeNoNet explicitly learns to mitigate feedback channel impairments. The proposed training strategy significantly outperformed existing DL-based feedback mechanisms, achieving improvements of 113.18% in NMSE and 72.72% in cosine correlation across various SNR conditions. These results demonstrate that incorporating denoising intelligence into CSI feedback frameworks is crucial for realistic massive MIMO deployments.

The final chapter 6, presented a novel DL-based framework combining CDN with CNN-driven DFT processing for enhanced CSI feedback and reconstruction. Compared to conventional DeepAE-based schemes, the proposed approach achieved notable gains in both accuracy and computational efficiency. This chapter reinforced the effectiveness of integrating structured transforms with DL-based models to achieve high performance CSI feedback in large scale antenna systems.

7.1 Future Scope

The findings of this thesis open up several promising directions for future research. First, extending the proposed frameworks to time-varying and high-mobility scenarios using recurrent and attention-based models could further improve CSI prediction and tracking. Second, investigating lightweight and hardware-aware DL architectures will be essential for energy-efficient real-time implementation. Third, applying the proposed CSI feedback techniques to emerging paradigms such as cell-free massive MIMO, THz communications, reconfigurable intelligent surfaces (RIS), and integrated sensing and communication (ISAC) systems represents a valuable extension. Finally, combining federated learning and online adaptation mechanisms could enable robust CSI feedback under dynamic and heterogeneous network conditions.

Overall, this thesis demonstrates that transform-assisted DL-based approach provides a powerful and practical solution to the CSI feedback overhead in massive MIMO systems, contributing to the realization of efficient, scalable, and reliable wireless networks for 5G and future 6G generations.

7.1.1 Extension of the Proposed CSI Compression Framework to Cell-Free Massive MIMO and RIS-Assisted 6G Networks

The proposed CSI compression framework for cell-free massive MIMO and RIS-assisted 6G networks would require substantial redesign of several components because these systems involve distributed access points, distributed users, cascaded propagation channels, and rapidly changing wireless environments. In cell-free massive MIMO, multiple access points (APs) simultaneously observe correlated CSI from the same user, making independent CSI compression inefficient and redundant. Therefore, the encoder should be redesigned as a jointly sparse distributed encoder that exploits spatial correlations among APs and compresses CSI collaboratively rather than independently. Similarly, the transform stage would need to be adapted because RIS-assisted communication introduces a cascaded BS-RIS-UE channel whose structure differs significantly from that of a conventional direct channel. Instead of directly applying DRT or DHT to the effective channel, a hierarchical or two-stage transform could separately process the BS-RIS and RIS-UE links before reconstructing the composite channel. In addition, the feedback protocol would need to evolve from a single point-to-point feedback mechanism to a distributed feedback architecture capable of efficiently aggregating CSI information from multiple APs and users at a central processing unit while satisfying strict latency and bandwidth constraints.

The denoising architecture would also need to become more intelligent and adaptive. Since different APs experience different channel qualities, interference levels, and SNR conditions, a single-stream denoising network would be insufficient. An attention-based fusion mechanism could dynamically assign higher weights to more reliable CSI observations while suppressing noisier inputs, thereby improving overall reconstruction accuracy. To enable continuous adaptation without excessive communication overhead, federated and online learning techniques could be incorporated into the framework. Each AP or UE would locally update its encoder-decoder model using newly observed CSI and periodically share only compressed model updates with a central server instead of transmitting raw CSI data. The overhead could be further reduced through infrequent synchronization, gradient compression, sparse parameter sharing, and a hybrid approach in which a small personalization layer remains local while only a shared backbone network is globally updated. This would allow the framework to adapt rapidly to mobility, channel ageing, and previously unseen propagation environments while preserving user privacy, minimizing signaling overhead, and maintaining scalability for practical deployment in future cell-free massive MIMO and RIS-enabled 6G networks.

References

[1] Harish Rathod and Sanjay Agal. “A study and overview on current trends and technology in mobile applications and its development”. In: *International Conference on ICT for Sustainable Development*. Springer. 2023, pp. 383–395.

[2] Emre Telatar. “Capacity of multi-antenna Gaussian channels”. In: *European transactions on telecommunications* 10.6 (1999), pp. 585–595.

[3] Gerard J Foschini and Michael J Gans. “On limits of wireless communications in a fading environment when using multiple antennas”. In: *Wireless personal communications* 6.3 (1998), pp. 311–335.

[4] Robin Chataut and Robert Akl. “Massive MIMO Systems for 5G and beyond Networksâ€”Overview, Recent Trends, Challenges, and Future Research Direction”. In: *Sensors* 20.10 (2020). ISSN: 1424-8220. DOI: `10.3390/s20102753`. URL: `https://www.mdpi.com/1424-8220/20/10/2753`.

[5] Ajay R Mishra. *Cellular technologies for emerging markets: 2G, 3G and beyond*. John Wiley & Sons, 2010.

[6] AFM Shahen Shah et al. “Survey and performance evaluation of multiple access schemes for next-generation wireless communication systems”. In: *IEEe Access* 9 (2021), pp. 113428–113442.

[7] Andrew J Viterbi, Lindsay A Weaver Jr, and Charles E Whcatley III. “On the capacity of a cellular CDMA system”. In: *IEEE Trans. Veh. Technol* 40.3 (1991), pp. 303–311.

[8] Anders Furuskar et al. “EDGE: Enhanced data rates for GSM and TDMA/136 evolution”. In: *IEEE personal communications* 6.3 (2002), pp. 56–66.

[9] Timo Halonen, Javier Romero, and Juan Melero. *GSM, GPRS and EDGE performance: evolution towards 3G/UMTS*. John Wiley & Sons, 2004.

[10] Vijay K Garg, Samuel Halpern, and Kenneth F Smolik. "Third generation (3G) mobile communications systems". In: *1999 IEEE International Conference on Personal Wireless Communications (Cat. No. 99TH8366)*. IEEE. 1999, pp. 39–43.

[11] Harri Holma and Antti Toskala. *WCDMA for umts: hspa evolution and lte*. john Wiley & sons, 2010.

[12] Erik Dahlman et al. "UMTS/IMT-2000 based on wideband CDMA". In: *IEEE Communications magazine* 36.9 (1998), pp. 70–80.

[13] Johan Bergman et al. "HSPA Evolution–Boosting the performance of mobile broadband access". In: *Ericsson Review* 85.1 (2008), pp. 32–37.

[14] Harri Holma, Antti Toskala, and Pablo Tapia. *HSPA+ Evolution to release 12: performance and optimization*. John Wiley & Sons, 2014.

[15] Erik Dahlman, Stefan Parkvall, and Johan Skold. *4G: LTE/LTE-advanced for mobile broadband*. Academic press, 2013.

[16] ME Augustus. "4th generation (4G) technological infrastructure and enhanced mobile learning: an effective tool for open and distance education". In: *African Journal of Computing & ICT* 8.3 (2015), pp. 111–129.

[17] Mohammed Jaber Alam et al. "An overview of LTE/LTE-A heterogeneous networks for 5G and beyond". In: *Transactions on Emerging Telecommunications Technologies* 34.8 (2023), e4806.

[18] Zahraa Zuhair Abdulhameed and Samir Jasim Mohammed. "Performance LTE Downlink Based on MIMO-OFDM". In: *2024 3rd International Conference on Advances in Engineering Science and Technology (AEST)*. IEEE. 2024, pp. 142–147.

[19] Chaiman Lim et al. "Recent trend of multiuser MIMO in LTE-advanced". In: *IEEE Communications Magazine* 51.3 (2013), pp. 127–135.

[20] Zubair Amjad et al. “Latency reduction in narrowband 4G lte networks”. In: *2018 15th International Symposium on Wireless Communication Systems (ISWCS)*. IEEE. 2018, pp. 1–5.

[21] Young-June Choi, Kwang Bok Lee, and Saewoong Bahk. “All-IP 4G Network architecture for efficient mobility and resource management”. In: *IEEE wireless communications* 14.2 (2007), pp. 42–46.

[22] Lei Wan et al. “4G\/5G spectrum sharing: efficient 5G deployment to serve enhanced mobile broadband and internet of things applications”. In: *ieee vehicular technology magazine* 13.4 (2018), pp. 28–39.

[23] Godlove Suila Kuaban et al. “Performance analysis of packet aggregation mechanisms and their applications in access (eg, IoT, 4G/5G), core, and data centre networks”. In: *Sensors* 21.11 (2021), p. 3898.

[24] Mamta Agiwal, Abhishek Roy, and Navrati Saxena. “Next generation 5G wireless networks: A comprehensive survey”. In: *IEEE communications surveys & tutorials* 18.3 (2016), pp. 1617–1655.

[25] Anabi Hilary Kelechi et al. “The four-C framework for high capacity ultra-low latency in 5G networks: A review”. In: *Energies* 12.18 (2019), p. 3449.

[26] Xiaoming Chen et al. “Massive access for 5G and beyond”. In: *IEEE Journal on Selected Areas in Communications* 39.3 (2020), pp. 615–637.

[27] Prem Chand Jain. “Recent Advances in Next Generation Cellular Mobile Networks-5G, 5G-Adv., and 6G”. In: *2025 International Conference on Innovation in Computing and Engineering (ICE)*. IEEE. 2025, pp. 1–6.

[28] Benish Sharfeen Khan et al. “URLLC and eMBB in 5G industrial IoT: A survey”. In: *IEEE Open Journal of the Communications Society* 3 (2022), pp. 1134–1163.

[29] Petar Popovski et al. “Wireless access in ultra-reliable low-latency communication (URLLC)”. In: *IEEE Transactions on Communications* 67.8 (2019), pp. 5783–5801.

[30] Jihong Park et al. “Extreme ultra-reliable and low-latency communication”. In: *Nature Electronics* 5.3 (2022), pp. 133–141.

[31] Hyoungju Ji et al. “Ultra-Reliable and Low-Latency Communications in 5G Downlink: Physical Layer Aspects”. In: *IEEE Wireless Communications* 25.3 (2018), pp. 124–130. DOI: 10.1109/MWC.2018.1700294.

[32] Carsten Bockelmann et al. “Massive machine-type communications in 5G: Physical and MAC-layer solutions”. In: *IEEE communications magazine* 54.9 (2016), pp. 59–65.

[33] Najib Ahmed Mohammed, Ali Mohammed Mansoor, and Rodina Binti Ahmad. “Mission-critical machine-type communication: An overview and perspectives towards 5G”. In: *IEEE Access* 7 (2019), pp. 127198–127216.

[34] Hasan Ahmed Salman et al. “Difference between 4g and 5g networks”. In: *Babylonian Journal of Networking* 2023 (2023), pp. 41–54.

[35] Jorge Navarro-Ortiz et al. “A survey on 5G usage scenarios and traffic models”. In: *IEEE Communications Surveys & Tutorials* 22.2 (2020), pp. 905–929.

[36] Yong Niu et al. “A survey of millimeter wave communications (mmWave) for 5G: opportunities and challenges”. In: *Wireless networks* 21.8 (2015), pp. 2657–2676.

[37] Mohammed H Alsharif and Rosdiadee Nordin. “Evolution towards fifth generation (5G) wireless networks: Current trends and challenges in the deployment of millimetre wave, massive MIMO, and small cells”. In: *Telecommunication Systems* 64.4 (2017), pp. 617–637.

[38] Robin Chataut and Robert Akl. “Massive MIMO systems for 5G and beyond networks—overview, recent trends, challenges, and future research direction”. In: *Sensors* 20.10 (2020), p. 2753.

[39] Sinan A Khwandah et al. “Massive MIMO systems for 5G communications”. In: *Wireless Personal Communications* 120.3 (2021), pp. 2101–2115.

[40] Mahmoud A Albreem, Markku Juntti, and Shahriar Shahabuddin. “Massive MIMO detection techniques: A survey”. In: *IEEE Communications Surveys & Tutorials* 21.4 (2019), pp. 3109–3132.

[41] Emil Björnson, Jakob Hoydis, Luca Sanguinetti, et al. “Massive MIMO networks: Spectral, energy, and hardware efficiency”. In: *Foundations and Trends® in Signal Processing* 11.3-4 (2017), pp. 154–655.

[42] FCC Staff Technical Paper. “Mobile Broadband: The Benefits of Additional Spectrum”. In: *Federal Communications Commission (FCC)* Washington, DC (October 2010).

[43] Tezcan Cogalan and Harald Haas. “Why would 5G need optical wireless communications?” In: *2017 IEEE 28th Annual International Symposium on Personal, Indoor, and Mobile Radio Communications (PIMRC)*. IEEE. 2017, pp. 1–6.

[44] U Cisco. “Cisco annual internet report (2018–2023) white paper”. In: *Cisco: San Jose, CA, USA* 10.1 (2020), pp. 1–35.

[45] Ericsson. “Ericsson Mobility Report”. In: November (2024), pp. 1–40.

[46] Xiong Wang et al. “Millimeter Wave Communication: A Comprehensive Survey”. In: *IEEE Communications Surveys Tutorials* 20.3 (2018), pp. 1616–1653. DOI: `10.1109/COMST.2018.2844322`.

[47] Selcuk Bassoy et al. “Coordinated Multi-Point Clustering Schemes: A Survey”. In: *IEEE Communications Surveys Tutorials* 19.2 (2017), pp. 743–764. DOI: `10.1109/COMST.2017.2662212`.

[48] Qingqing Wu et al. “Intelligent Reflecting Surface-Aided Wireless Communications: A Tutorial”. In: *IEEE Transactions on Communications* 69.5 (2021), pp. 3313–3351. DOI: `10.1109/TCOMM.2021.3051897`.

[49] Sudeep Bhattarai et al. “An Overview of Dynamic Spectrum Sharing: Ongoing Initiatives, Challenges, and a Roadmap for Future Research”. In: *IEEE Transactions on Cognitive Communications and Networking* 2.2 (2016), pp. 110–128. DOI: `10.1109/TCCN.2016.2592921`.

[50] Mohammad Rowshan et al. “Channel Coding Toward 6G: Technical Overview and Outlook”. In: *IEEE Open Journal of the Communications Society* 5 (2024), pp. 2585–2685. DOI: `10.1109/OJCOMS.2024.3390000`.

[51] Yongjae Kim, Bang Chul Jung, and Youngnam Han. "Coordinated beamforming, interference-aware power control, and scheduling framework for 6G wireless networks". In: *Journal of Communications and Networks* 24.3 (2022), pp. 292–304. DOI: 10.23919/JCN.2022.000013.

[52] Thomas L. Marzetta. "Massive MIMO: An Introduction". In: *Bell Labs Technical Journal* 20 (2015), pp. 11–22. DOI: 10.15325/BLTJ.2015.2407793.

[53] Lu Lu et al. "An overview of massive MIMO: Benefits and challenges". In: *IEEE journal of selected topics in signal processing* 8.5 (2014), pp. 742–758.

[54] Pronaya Bhattacharya et al. "Coalition of 6G and blockchain in AR/VR space: Challenges and future directions". In: *IEEE Access* 9 (2021), pp. 168455–168484.

[55] Changqing Luo et al. "Channel state information prediction for 5G wireless communications: A deep learning approach". In: *IEEE transactions on network science and engineering* 7.1 (2018), pp. 227–236.

[56] Tianqi Wang et al. "Deep learning-based CSI feedback approach for time-varying massive MIMO channels". In: *IEEE Wireless Communications Letters* 8.2 (2018), pp. 416–419.

[57] Lixiang Li et al. "Overview of compressed sensing: Sensing model, reconstruction algorithm, and its applications". In: *Applied sciences* 10.17 (2020), p. 5909.

[58] Jun Won Choi et al. "Compressed sensing for wireless communications: Useful tips and tricks". In: *IEEE Communications Surveys & Tutorials* 19.3 (2017), pp. 1527–1550.

[59] L. Comerford et al. "Compressive sensing with an adaptive wavelet basis for structural system response and reliability analysis under missing data". In: *Computers Structures* 182 (2017), pp. 26–40. ISSN: 0045-7949. DOI: https://doi.org/10.1016/j.compstruc.2016.11.012. URL: https://www.sciencedirect.com/science/article/pii/S0045794916304618.

[60] Mohammad Mustafa Taye. "Understanding of machine learning with deep learning: architectures, workflow, applications and future directions". In: *Computers* 12.5 (2023), p. 91.

[61] Iqbal H Sarker. “Deep learning: a comprehensive overview on techniques, taxonomy, applications and research directions”. In: *SN computer science* 2.6 (2021), pp. 1–20.

[62] Jie Wang et al. “Compressive Sampled CSI Feedback Method Based on Deep Learning for FDD Massive MIMO Systems”. In: *IEEE Transactions on Communications* 69.9 (2021), pp. 5873–5885. DOI: 10.1109/TCOMM.2021.3086525.

[63] Shadman Rahman Doha and Ahmed Abdelhadi. “Deep Learning in Wireless Communication Receivers: A Survey”. In: *IEEE Access* (2025).

[64] Chao-Kai Wen, Wan-Ting Shih, and Shi Jin. “Deep Learning for Massive MIMO CSI Feedback”. In: *IEEE Wireless Communications Letters* 7.5 (2018), pp. 748–751.

[65] Jiajia Guo et al. “Convolutional Neural Network-Based Multiple-Rate Compressive Sensing for Massive MIMO CSI Feedback: Design, Simulation, and Analysis”. In: *IEEE Transactions on Wireless Communications* 19.4 (2020), pp. 2827–2840.

[66] Zhilin Lu, Jintao Wang, and Jian Song. “Multi-Resolution CSI Feedback with Deep Learning in Massive MIMO System”. In: *ICC 2020-2020 IEEE International Conference on Communications (ICC)*. IEEE. 2020, pp. 1–6.

[67] Yaodong Cui, Aihuang Guo, and Chunlin Song. “TransNet: Full Attention Network for CSI Feedback in FDD Massive MIMO System”. In: *IEEE Wireless Communications Letters* 11.5 (2022), pp. 903–907.

[68] Mostafa Hussien, Kim Khoa Nguyen, and Mohamed Cheriet. “PRVNet: A novel partially-regularized variational autoencoders for massive MIMO CSI feedback”. In: *2022 IEEE wireless communications and networking conference (WCNC)*. IEEE. 2022, pp. 2286–2291.

[69] Leonid P Yaroslavsky, Karen O Egiazarian, and Jaakko T Astola. “Transform domain image restoration methods: review, comparison, and interpretation”. In: *Nonlinear Image Processing and Pattern Analysis XII* 4304 (2001), pp. 155–169.

[70] Xiongbin Rao and Vincent KN Lau. "Distributed compressive CSIT estimation and feedback for FDD multi-user massive MIMO systems". In: *IEEE Transactions on Signal Processing* 62.12 (2014), pp. 3261–3271.

[71] Mohammed E Eltayeb, Tareq Y Al-Naffouri, and Hamid Reza Bahrami. "Compressive sensing for feedback reduction in MIMO broadcast channels". In: *IEEE Transactions on communications* 62.9 (2014), pp. 3209–3222.

[72] Mahdi Boloursaz Mashhadi and Deniz Gündüz. "Deep learning for massive MIMO channel state acquisition and feedback". In: *Journal of the Indian Institute of Science* 100.2 (2020), pp. 369–382.

[73] Jiajia Guo et al. "Overview of deep learning-based CSI feedback in massive MIMO systems". In: *IEEE Transactions on Communications* 70.12 (2022), pp. 8017–8045.

[74] In Lee and Kyoochun Lee. "The Internet of Things (IoT): Applications, investments, and challenges for enterprises". In: *Business Horizons* 58.4 (2015), pp. 431–440. ISSN: 0007-6813. DOI: `https://doi.org/10.1016/j.bushor.2015.03.008`. URL: `https://www.sciencedirect.com/science/article/pii/S0007681315000373`.

[75] Pawan Kumar Verma et al. "Machine-to-Machine (M2M) communications: A survey". In: *Journal of Network and Computer Applications* 66 (2016), pp. 83–105. ISSN: 1084-8045. DOI: `https://doi.org/10.1016/j.jnca.2016.02.016`. URL: `https://www.sciencedirect.com/science/article/pii/S1084804516000990`.

[76] Morteza Ghobakhloo. "Industry 4.0, digitization, and opportunities for sustainability". In: *Journal of Cleaner Production* 252 (2020), p. 119869. ISSN: 0959-6526. DOI: `https://doi.org/10.1016/j.jclepro.2019.119869`. URL: `https://www.sciencedirect.com/science/article/pii/S0959652619347390`.

[77] Arthur de M. Del Esposte et al. "Design and evaluation of a scalable smart city software platform with large-scale simulations". In: *Future Generation Computer*

Systems 93 (2019), pp. 427–441. ISSN: 0167-739X. DOI: `https://doi.org/10.1016/j.future.2018.10.026`. URL: `https://www.sciencedirect.com/science/article/pii/S0167739X18307301`.

[78] Hakan Inanoğlu. "Multiple-Input Multiple-Output System Capacity: Antenna and Propagation Aspects". In: *IEEE Antennas and Propagation Magazine* 55.1 (2013), pp. 253–273. DOI: `10.1109/MAP.2013.6474541`.

[79] Muddasar Naeem, Giuseppe De Pietro, and Antonio Coronato. "Application of Reinforcement Learning and Deep Learning in Multiple-Input and Multiple-Output (MIMO) Systems". In: *Sensors* 22.1 (2022). ISSN: 1424-8220. DOI: `10.3390/s22010309`. URL: `https://www.mdpi.com/1424-8220/22/1/309`.

[80] Sherif Adeshina Busari et al. "Millimeter-Wave Massive MIMO Communication for Future Wireless Systems: A Survey". In: *IEEE Communications Surveys Tutorials* 20.2 (2018), pp. 836–869. DOI: `10.1109/COMST.2017.2787460`.

[81] Shuangfeng Han et al. "Large-scale antenna systems with hybrid analog and digital beamforming for millimeter wave 5G". In: *IEEE Communications Magazine* 53.1 (2015), pp. 186–194. DOI: `10.1109/MCOM.2015.7010533`.

[82] Foad Sohrabi and Wei Yu. "Hybrid Analog and Digital Beamforming for mmWave OFDM Large-Scale Antenna Arrays". In: *IEEE Journal on Selected Areas in Communications* 35.7 (2017), pp. 1432–1443. DOI: `10.1109/JSAC.2017.2698958`.

[83] Mohamed A. ElMossallamy et al. "Reconfigurable Intelligent Surfaces for Wireless Communications: Principles, Challenges, and Opportunities". In: *IEEE Transactions on Cognitive Communications and Networking* 6.3 (2020), pp. 990–1002. DOI: `10.1109/TCCN.2020.2992604`.

[84] Yuanwei Liu et al. "Reconfigurable Intelligent Surfaces: Principles and Opportunities". In: *IEEE Communications Surveys Tutorials* 23.3 (2021), pp. 1546–1577. DOI: `10.1109/COMST.2021.3077737`.

[85] Yusuf Usman et al. "AI-Enhanced Deep Neural Network Architecture for Accurate Channel Estimation in 6G Networks". In: *2025 IEEE World AI IoT Congress (AIIoT)*. 2025, pp. 0732–0736. DOI: `10.1109/AIIoT65859.2025.11105312`.

[86] Mi Yang et al. "AI-Enabled Data-Driven Channel Modeling for Future Communications". In: *IEEE Communications Magazine* 62.4 (2024), pp. 112–118. DOI: 10.1109/MCOM.019.2300072.

[87] Anthony Ngozichukwuka Uwaechia and Nor Muzlifah Mahyuddin. "A Comprehensive Survey on Millimeter Wave Communications for Fifth-Generation Wireless Networks: Feasibility and Challenges". In: *IEEE Access* 8 (2020), pp. 62367–62414. DOI: 10.1109/ACCESS.2020.2984204.

[88] Alessandro E. C. Redondi et al. "A Survey on Future Millimeter-Wave Communication Applications". In: *IEEE Access* 12 (2024), pp. 133165–133182. DOI: 10.1109/ACCESS.2024.3438625.

[89] Ibrahim A. Hemadeh et al. "Millimeter-Wave Communications: Physical Channel Models, Design Considerations, Antenna Constructions, and Link-Budget". In: *IEEE Communications Surveys Tutorials* 20.2 (2018), pp. 870–913. DOI: 10.1109/COMST.2017.2783541.

[90] Sundeep Rangan, Theodore S. Rappaport, and Elza Erkip. "Millimeter-Wave Cellular Wireless Networks: Potentials and Challenges". In: *Proceedings of the IEEE* 102.3 (2014), pp. 366–385. DOI: 10.1109/JPROC.2014.2299397.

[91] Ming Xiao et al. "Millimeter Wave Communications for Future Mobile Networks (Guest Editorial), Part I". In: *IEEE Journal on Selected Areas in Communications* 35.7 (2017), pp. 1425–1431. DOI: 10.1109/JSAC.2017.2698698.

[92] Ian F. Akyildiz, Josep Miquel Jornet, and Chong Han. "Terahertz band: Next frontier for wireless communications". In: *Physical Communication* 12 (2014), pp. 16–32. ISSN: 1874-4907. DOI: https://doi.org/10.1016/j.phycom.2014.01.006. URL: https://www.sciencedirect.com/science/article/pii/S1874490714000238.

[93] Hadeel Elayan et al. "Terahertz communication: The opportunities of wireless technology beyond 5G". In: *2018 International Conference on Advanced Communication Technologies and Networking (CommNet)*. 2018, pp. 1–5. DOI: 10.1109/COMMNET.2018.8360286.

[94] Kazi Mohammed Saidul Huq et al. "Terahertz-Enabled Wireless System for Beyond-5G Ultra-Fast Networks: A Brief Survey". In: *IEEE Network* 33.4 (2019), pp. 89–95. DOI: 10.1109/MNET.2019.1800430.

[95] Josep Miquel Jornet and Ian F. Akyildiz. "Graphene-based Plasmonic Nano-Antenna for Terahertz Band Communication in Nanonetworks". In: *IEEE Journal on Selected Areas in Communications* 31.12 (2013), pp. 685–694. DOI: 10.1109/JSAC.2013.SUP2.1213001.

[96] Alice Faisal et al. "Ultramassive MIMO Systems at Terahertz Bands: Prospects and Challenges". In: *IEEE Vehicular Technology Magazine* 15.4 (2020), pp. 33–42. DOI: 10.1109/MVT.2020.3022998.

[97] Zhongshan Zhang et al. "Full-Duplex Wireless Communications: Challenges, Solutions, and Future Research Directions". In: *Proceedings of the IEEE* 104.7 (2016), pp. 1369–1409. DOI: 10.1109/JPROC.2015.2497203.

[98] Mohammadali Mohammadi et al. "A Comprehensive Survey on Full-Duplex Communication: Current Solutions, Future Trends, and Open Issues". In: *IEEE Communications Surveys Tutorials* 25.4 (2023), pp. 2190–2244. DOI: 10.1109/COMST.2023.3318198.

[99] Rongpeng Li et al. "Full-Duplex Cellular Networks". In: *IEEE Communications Magazine* 55.4 (2017), pp. 184–191. DOI: 10.1109/MCOM.2017.1600361CM.

[100] Nurul H. Mahmood et al. "Full duplex communications in 5G small cells". In: *2017 13th International Wireless Communications and Mobile Computing Conference (IWCMC)*. 2017, pp. 1665–1670. DOI: 10.1109/IWCMC.2017.7986534.

[101] P. H. Pathak et al. "Visible Light Communication, Networking, and Sensing: A Survey, Potential and Challenges". In: *IEEE Communications Surveys Tutorials* 17.4 (2015), pp. 2047–2077.

[102] Sridhar Rajagopal, Richard D Roberts, and Sang-Kyu Lim. "IEEE 802.15. 7 visible light communication: modulation schemes and dimming support". In: *IEEE Communications Magazine* 50.3 (2012), pp. 72–82.

[103] Sridhar Rajagopal, Richard D Roberts, and Sang-Kyu Lim. "IEEE 802.15. 7 visible light communication: modulation schemes and dimming support". In: *IEEE Communications Magazine* 50.3 (2012), pp. 72–82.

[104] Samuel M Berman et al. "Human electroretinogram responses to video displays, fluorescent lighting, and other high frequency sources". In: *Optometry and vision science* 68.8 (1991), pp. 645–662.

[105] Ram Sharma et al. "Optimal LED deployment for mobile indoor visible light communication system: Performance analysis". In: *AEU-International Journal of Electronics and Communications* 83 (2018), pp. 427–432.

[106] Zhiyong Du et al. "Context-aware indoor VLC/RF heterogeneous network selection: Reinforcement learning with knowledge transfer". In: *IEEE Access* 6 (2018), pp. 33275–33284.

[107] Jia Wang et al. "A general channel model for visible light communications in underground mines". In: *China Communications* 15.9 (2018), pp. 95–105.

[108] Bugra Turan et al. "Vehicular VLC frequency domain channel sounding and characterization". In: *2018 IEEE Vehicular Networking Conference (VNC)*. IEEE. 2018, pp. 1–8.

[109] Andreas F. Molisch et al. "Hybrid Beamforming for Massive MIMO: A Survey". In: *IEEE Communications Magazine* 55.9 (2017), pp. 134–141. DOI: 10.1109/MCOM.2017.1600400.

[110] Binqi Yang et al. "Digital Beamforming-Based Massive MIMO Transceiver for 5G Millimeter-Wave Communications". In: *IEEE Transactions on Microwave Theory and Techniques* 66.7 (2018), pp. 3403–3418. DOI: 10.1109/TMTT.2018.2829702.

[111] Song Noh, Michael D. Zoltowski, and David J. Love. "Training Sequence Design for Feedback Assisted Hybrid Beamforming in Massive MIMO Systems". In: *IEEE Transactions on Communications* 64.1 (2016), pp. 187–200. DOI: 10.1109/TCOMM.2015.2498184.

[112] Sameer Ahmad Bhat et al. "Sensing direction of human motion using single-input-single-output (SISO) channel model and neural networks". In: *IEEE Access* 10 (2022), pp. 56823–56844.

[113] Arogyaswami J Paulraj and Thomas Kailath. *Increasing capacity in wireless broadcast systems using distributed transmission/directional reception (DTDR)*. US Patent 5,345,599. Sept. 1994.

[114] Quentin H Spencer et al. "An introduction to the multi-user MIMO downlink". In: *IEEE communications Magazine* 42.10 (2004), pp. 60–67.

[115] Aditya Kurve. "Multi-user MIMO systems: The future in the making". In: *IEEE Potentials* 28.6 (2009), pp. 37–42.

[116] Daisuke Nojima et al. "Performance evaluation for multi-user MIMO IEEE 802.11 ac wireless LAN system". In: *2012 14th International Conference on Advanced Communication Technology (ICACT)*. IEEE. 2012, pp. 804–808.

[117] Ming Jiang and Lajos Hanzo. "Multiuser MIMO-OFDM for next-generation wireless systems". In: *Proceedings of the IEEE* 95.7 (2007), pp. 1430–1469.

[118] Lin Hui and Wang Wen Bo. "Performance analysis of network MIMO technology". In: *2009 15th Asia-Pacific Conference on Communications*. IEEE. 2009, pp. 234–236.

[119] Giuseppe Caire, Sean A Ramprashad, and Haralabos C Papadopoulos. "Rethinking network MIMO: Cost of CSIT, performance analysis, and architecture comparisons". In: *2010 Information Theory and Applications Workshop (ITA)*. IEEE. 2010, pp. 1–10.

[120] Hironori Kusumoto et al. "Performance comparison between single-user MIMO and multi-user MIMO in wireless mesh networks". In: *The 15th International Symposium on Wireless Personal Multimedia Communications*. IEEE. 2012, pp. 202–206.

[121] Stefan Pratschner, Stefan Schwarz, and Markus Rupp. "Single-user and multi-user MIMO channel estimation for LTE-Advanced uplink". In: *2017 IEEE International Conference on Communications (ICC)*. IEEE. 2017, pp. 1–6.

[122] Daewon Lee et al. “Coordinated multipoint transmission and reception in LTE-advanced: deployment scenarios and operational challenges”. In: *IEEE Communications Magazine* 50.2 (2012), pp. 148–155.

[123] Erik G Larsson et al. “Massive MIMO for next generation wireless systems”. In: *IEEE communications magazine* 52.2 (2014), pp. 186–195.

[124] Noor Hidayah Muhamad Adnan, Islam Md Rafiqul, and AHM Zahirul Alam. “Massive MIMO for fifth generation (5G): Opportunities and challenges”. In: *2016 International Conference on Computer and Communication Engineering (ICCCE)*. IEEE. 2016, pp. 47–52.

[125] Emil Björnson, Erik G Larsson, and Thomas L Marzetta. “Massive MIMO: Ten myths and one critical question”. In: *IEEE Communications Magazine* 54.2 (2016), pp. 114–123.

[126] Trinh Van Chien and Emil Björnson. “Massive MIMO communications”. In: *5G mobile communications*. Springer, 2016, pp. 77–116.

[127] Areeb T Tariq and Pavan Koteshwar Srinath. “Uplink Multi-user MIMO Scheduling in Next-gen Communication Systems”. In: (2022).

[128] Thomas L Marzetta. “Massive MIMO: an introduction”. In: *Bell labs technical journal* 20 (2015), pp. 11–22.

[129] Qiang Hu, Meixiang Zhang, and Renzheng Gao. “Key technologies in massive MIMO”. In: *ITM Web of Conferences*. Vol. 17. EDP Sciences. 2018, p. 01017.

[130] Deli Qiao, Ye Wu, and Yan Chen. “Massive MIMO architecture for 5G networks: Co-located, or distributed?” In: *2014 11th International Symposium on Wireless Communications Systems (ISWCS)*. IEEE. 2014, pp. 192–197.

[131] Stefano Fortunati et al. “Massive MIMO radar for target detection”. In: *IEEE Transactions on Signal Processing* 68 (2020), pp. 859–871.

[132] Fuyuan Liu et al. “Power Allocation for Sum Rate Maximization of Uplink Massive MIMO System with Maximum Ratio Combining”. In: *International Conference on Machine Learning and Intelligent Communications*. Springer. 2021, pp. 28–37.

[133] Amr A Alammari, Mohd Sharique, and Athar Ali Moinuddin. “User-Centric Cell-Free and Co-Located Cellular Large Scale MU-MIMO Systems: A Comparative Performance Study With Spatial Channel Correlation in Dense Urban Scenario”. In: *IEEE Access* 10 (2022), pp. 48792–48809.

[134] Mohammadali Mohammadi et al. “Next-generation multiple access with cell-free massive MIMO”. In: *Proceedings of the IEEE* (2024).

[135] Lifeng Wang et al. “Massive MIMO in spectrum sharing networks: Achievable rate and power efficiency”. In: *IEEE Systems Journal* 11.1 (2015), pp. 20–31.

[136] Hussein A Ammar et al. “User-centric cell-free massive MIMO networks: A survey of opportunities, challenges and solutions”. In: *IEEE Communications Surveys & Tutorials* 24.1 (2021), pp. 611–652.

[137] Wei Jiang et al. “Terahertz communications and sensing for 6G and beyond: A comprehensive review”. In: *IEEE Communications Surveys & Tutorials* 26.4 (2024), pp. 2326–2381.

[138] Shuchi Tripathi et al. “Millimeter-wave and terahertz spectrum for 6G wireless”. In: *6G Mobile Wireless Networks*. Springer, 2021, pp. 83–121.

[139] Ian F Akyildiz et al. “Terahertz band communication: An old problem revisited and research directions for the next decade”. In: *IEEE Transactions on Communications* 70.6 (2022), pp. 4250–4285.

[140] M Qurratulain Khan et al. “Machine learning for millimeter wave and terahertz beam management: A survey and open challenges”. In: *IEEE Access* 11 (2023), pp. 11880–11902.

[141] Stefan Schwarz, Robert W Heath Jr, and Markus Rupp. “Single-user MIMO versus multi-user MIMO in distributed antenna systems with limited feedback”. In: *EURASIP Journal on Advances in Signal Processing* 2013.1 (2013), p. 54.

[142] Zahra Mokhtari, Maryam Sabbaghian, and Rui Dinis. “A survey on massive MIMO systems in presence of channel and hardware impairments”. In: *Sensors* 19.1 (2019), p. 164.

[143] Annu Singh and Sunil Joshi. "A survey on hybrid beamforming in MmWave massive MIMO system". In: *J Sci Res* 65.1 (2021), pp. 201–213.

[144] Sandeep Narayanan et al. "Multi-user spatial modulation MIMO". In: *2014 IEEE Wireless Communications and Networking Conference (WCNC)*. IEEE. 2014, pp. 671–676.

[145] Veljko Stankovic. "Multi-user MIMO wireless communications". In: *PhD, Technischen Uni-versitat Ilmenau, Ilmenau* (2006).

[146] Elahe Gholami, Hamid Meghdadi, and Ali Shahzadi. "Optimizing Spectral Efficiency in Downlink Millimeter Wave Distributed Massive Multi-User MIMO: A Fully Connected Two-Stage Iterative Hybrid Precoding Approach". In: *Wireless Personal Communications* (2025), pp. 1–32.

[147] Rajesh Kumar, Deepak Sinwar, and Vijander Singh. "Experimental evaluation of MU-MIMO in TDD environment for 5G NR using exploiting channel reciprocity". In: *International Journal of Information Technology* 16.7 (2024), pp. 4651–4666.

[148] Mujtaba Ghous et al. "Cooperative power-domain NOMA systems: An overview". In: *Sensors* 22.24 (2022), p. 9652.

[149] Yuanwei Liu et al. "Evolution of NOMA toward next generation multiple access (NGMA) for 6G". In: *IEEE Journal on Selected Areas in Communications* 40.4 (2022), pp. 1037–1071.

[150] Ogenyi Fabian Chukwudi, Ugwu Chinyere Nneoma, and Ugwu Okechukwu Paul-Chima. "A narrative review of power allocation strategies and successive interference cancellation enhancement in NOMA based 5G and future wireless networks". In: *Discover Internet of Things* 5.1 (2025), p. 109.

[151] Yongming Huang et al. "Signal processing for MIMO-NOMA: Present and future challenges". In: *IEEE Wireless Communications* 25.2 (2018), pp. 32–38.

[152] Syed Agha Hassnain Mohsan et al. "A survey of deep learning based NOMA: State of the art, key aspects, open challenges and future trends". In: *Sensors* 23.6 (2023), p. 2946.

[153] Satyanarayana Murthy Nimmagadda, Shaik Fayaz Ahamed, and Vijaya Kumar Padarti. “A Comprehensive Review on Massive MIMO Systems for 6G and Beyond Networks Using ML and DL Techniques”. In: *Wireless Personal Communications* (2025), pp. 1–38.

[154] P Ashok et al. “Developed a Machine Learning and Deep Learning Model for 5G MIMO Data Based Beam Selection and Intelligent Network Analytics”. In: *SN Computer Science* 6.3 (2025), pp. 1–21.

[155] F Fazel Mojtahedi et al. “Deep learning for time series forecasting: Review and applications in geotechnics and geosciences”. In: *Archives of Computational Methods in Engineering* (2025), pp. 1–31.

[156] Burak Ozpoyraz et al. “Deep learning-aided 6G wireless networks: A comprehensive survey of revolutionary PHY architectures”. In: *IEEE Open Journal of the Communications Society* 3 (2022), pp. 1749–1809.

[157] Panagiotis K Gkonis. “A survey on machine learning techniques for massive MIMO configurations: Application areas, performance limitations and future challenges”. In: *IEEE Access* 11 (2022), pp. 67–88.

[158] Steffen Malkowsky et al. “The world’s first real-time testbed for massive MIMO: Design, implementation, and validation”. In: *IEEE Access* 5 (2017), pp. 9073–9088.

[159] Paul Harris et al. “An overview of massive MIMO research at the University of Bristol”. In: *Radio Propagation and Technologies for 5G (2016)* (2016).

[160] Zhaoqi Deng and Youyang Hou. “Massive MIMO System For 5G Networks”. In: *2023 3rd International Conference on Computer Science, Electronic Information Engineering and Intelligent Control Technology (CEI)*. IEEE. 2023, pp. 56–60.

[161] Roshan Raju and Gita Madhuri. “Vodafone and Idea Merger: A shareholder’s dilemma”. In: *Global Business Review* 25.1 (2024), pp. 216–231.

[162] TL Marzetta. “Non-cooperative multiantenna base stations with unlimited number of antennas”. In: *IEEE Trans. on Wireless Commun* 9 (2010), pp. 3590–3600.

[163] M Nguyen. “Massive MIMO: A survey of benefits and challenges”. In: *ICSES Trans. Comput. Hardw. Electr. Eng* 4.4 (2018), pp. 1–4.

[164] Jakob Hoydis et al. “Making smart use of excess antennas: Massive MIMO, small cells, and TDD”. In: *Bell Labs Technical Journal* 18.2 (2013), pp. 5–21.

[165] Volker Jungnickel et al. “The role of small cells, coordinated multipoint, and massive MIMO in 5G”. In: *IEEE communications magazine* 52.5 (2014), pp. 44–51.

[166] Xiang Gao et al. “Linear pre-coding performance in measured very-large MIMO channels”. In: *2011 IEEE vehicular technology conference (VTC Fall)*. IEEE. 2011, pp. 1–5.

[167] Jubin Jose et al. “Pilot contamination and precoding in multi-cell TDD systems”. In: *IEEE Transactions on Wireless Communications* 10.8 (2011), pp. 2640–2651.

[168] Mohammed Ali Mohammed Moqbel, Wangdong Wangdong, and Al-marhabi Zaid Ali. “MIMO channel estimation using the LS and MMSE algorithm”. In: *IOSR J. Electron. Commun. Eng* 12.1 (2017), pp. 13–22.

[169] Christoph Studer, Markus Wenk, and Andreas Burg. “MIMO transmission with residual transmit-RF impairments”. In: *2010 international ITG workshop on smart antennas (WSA)*. IEEE. 2010, pp. 189–196.

[170] Nusrat Fatema et al. “Massive MIMO linear precoding: A survey”. In: *IEEE systems journal* 12.4 (2017), pp. 3920–3931.

[171] Yo-Seb Jeon et al. “One-bit sphere decoding for uplink massive MIMO systems with one-bit ADCs”. In: *IEEE Transactions on Wireless Communications* 17.7 (2018), pp. 4509–4521.

[172] Ali Elghariani and Michael Zoltowski. “Successive interference cancellation for large-scale MIMO OFDM”. In: *2015 IEEE international conference on electro/information technology (EIT)*. IEEE. 2015, pp. 657–661.

[173] Hong Yang. “User scheduling in massive MIMO”. In: *2018 IEEE 19th International Workshop on Signal Processing Advances in Wireless Communications (SPAWC)*. IEEE. 2018, pp. 1–5.

[174] T Al-Naffouri, Masoud Sharif, and Babak Hassibi. "How much does transmit correlation affect the sum-rate scaling of MIMO Gaussian broadcast channels?" In: *IEEE Transactions on Communications* 57.2 (2009), pp. 562–572.

[175] Sungho Choi and Eui-Rim Jeong. "Digital predistortion based on combined feedback in MIMO transmitters". In: *IEEE Communications Letters* 16.10 (2012), pp. 1572–1575.

[176] Meenu Rani, Sanjay B Dhok, and Raghavendra B Deshmukh. "A systematic review of compressive sensing: Concepts, implementations and applications". In: *IEEE access* 6 (2018), pp. 4875–4894.

[177] Yu Han et al. "Efficient Downlink Channel Reconstruction for FDD Multi-Antenna Systems". In: *IEEE Transactions on Wireless Communications* 18.6 (2019), pp. 3161–3176.

[178] Zhen Gao, Yikun Mei, and Li Qiao. "Compressive Sensing CSI Acquisition and Feedback in FDD Massive MIMO Systems". In: *Sparse Signal Processing for Massive MIMO Communications*. Springer, 2023, pp. 51–81.

[179] Lijun Ge et al. "Compression-Based LMMSE Channel Estimation With Adaptive Sparsity for Massive MIMO in 5G Systems". In: *IEEE Systems Journal* 13.4 (2019), pp. 3847–3857.

[180] David L Donoho. "Compressed sensing". In: *IEEE Transactions on information theory* 52.4 (2006), pp. 1289–1306.

[181] Mudassir Masood, Laila H Afify, and Tareq Y Al-Naffouri. "Efficient coordinated recovery of sparse channels in massive MIMO". In: *IEEE Transactions on Signal Processing* 63.1 (2014), pp. 104–118.

[182] Zhen Gao et al. "Super-resolution sparse MIMO-OFDM channel estimation based on spatial and temporal correlations". In: *IEEE communications letters* 18.7 (2014), pp. 1266–1269.

[183] Zhen Gao et al. "Structured compressive sensing-based spatio-temporal joint channel estimation for FDD massive MIMO". In: *IEEE Transactions on Communications* 64.2 (2015), pp. 601–617.

[184] Juei-Chin Shen et al. "High-Dimensional CSI Acquisition in Massive MIMO: Sparsity-Inspired Approaches". In: *IEEE Systems Journal* 11.1 (2016), pp. 32–40.

[185] Jinming Wen, Rui Zhang, and Wei Yu. "Signal-dependent performance analysis of orthogonal matching pursuit for exact sparse recovery". In: *IEEE Transactions on Signal Processing* 68 (2020), pp. 5031–5046.

[186] Jingjing Liu, Chao Zhang, and Changyong Pan. "Priori-information hold subspace pursuit: A compressive sensing-based channel estimation for layer modulated TDS-OFDM". In: *IEEE Transactions on Broadcasting* 64.1 (2017), pp. 119–127.

[187] Hao Hu et al. "An improved SAMP algorithm for sparse channel estimation in OFDM system". In: *Sensors* 23.15 (2023), p. 6668.

[188] Min Soo Sim et al. "Compressed channel feedback for correlated massive MIMO systems". In: *Journal of Communications and Networks* 18.1 (2016), pp. 95–104.

[189] Pengbiao Wang et al. "A wavelet compression based channel feedback protocol for spatially correlated massive MIMO systems". In: *2015 22nd International Conference on Telecommunications (ICT)*. IEEE. 2015, pp. 303–307.

[190] Wenqian Shen et al. "Compressive sensing-based differential channel feedback for massive MIMO". In: *Electronics Letters* 51.22 (2015), pp. 1824–1826.

[191] Wang Kai et al. "Two-dimensional compressed sensing of channel state information in massive MIMO system". In: *2017 7th IEEE International Conference on Electronics Information and Emergency Communication (ICEIEC)*. IEEE. 2017, pp. 434–437.

[192] Alessio Zappone, Luca Sanguinetti, and Merouane Debbah. "User association and load balancing for massive MIMO through deep learning". In: *2018 52nd Asilomar Conference on Signals, Systems, and Computers*. IEEE. 2018, pp. 1262–1266.

[193] Yuwen Yang et al. "Deep learning-based channel estimation for doubly selective fading channels". In: *IEEE Access* 7 (2019), pp. 36579–36589.

[194] Yong Liao et al. "CSI feedback based on deep learning for massive MIMO systems". In: *IEEE Access* 7 (2019), pp. 86810–86820.

[195] Xudong Zhang et al. "Quantization Adaptor for Bit-Level Deep Learning-Based Massive MIMO CSI Feedback". In: *IEEE Transactions on Vehicular Technology* (2023).

[196] Chengyong Jiang et al. "Deep learning-based implicit CSI feedback for time-varying massive MIMO channels". In: *ICC 2023-IEEE International Conference on Communications*. IEEE. 2023, pp. 4955–4960.

[197] Klaus Greff et al. "LSTM: A search space odyssey". In: *IEEE transactions on neural networks and learning systems* 28.10 (2016), pp. 2222–2232.

[198] Qingyong Hu et al. "CSI-StripeFormer: Exploiting Stripe Features for CSI Compression in Massive MIMO System". In: *IEEE INFOCOM 2023-IEEE Conference on Computer Communications*. IEEE. 2023, pp. 1–10.

[199] Youngrok Jang et al. "Deep Autoencoder Based CSI Feedback With Feedback Errors and Feedback Delay in FDD Massive MIMO Systems". In: *IEEE Wireless Communications Letters* 8.3 (2019), pp. 833–836.

[200] Xin Wang et al. "Blockchain-Enabled Decentralized Edge Intelligence for Trustworthy 6G Consumer Electronics". In: *IEEE Transactions on Consumer Electronics* 70.1 (2024), pp. 1214–1225.

[201] Lijun Ge et al. "Deep Neural Network Based Channel Estimation For Massive MIMO-OFDM Mystems With Imperfect Channel State Enformation". In: *IEEE Systems Journal* 16.3 (2021), pp. 4675–4685.

[202] Kan Zheng et al. "Survey of large-scale MIMO systems". In: *IEEE Communications Surveys & Tutorials* 17.3 (2015), pp. 1738–1760.

[203] Ananthanarayanan Chockalingam and B Sundar Rajan. *Large MIMO systems*. Cambridge University Press, 2014.

[204] Kai Yu et al. "Modeling of wide-band MIMO radio channels based on NLoS indoor measurements". In: *IEEE Transactions on Vehicular Technology* 53.3 (2004), pp. 655–665.

[205] Hao He, Petre Stoica, and Jian Li. "Wideband MIMO systems: Signal design for transmit beampattern synthesis". In: *IEEE transactions on Signal Processing* 59.2 (2010), pp. 618–628.

[206] Lovish Matta, Bhanu Sharma, and Manish Sharma. "A review on bandwidth enhancement techniques and band-notched characteristics of MIMO-ultra wide band antennas". In: *Wireless Networks* 30.3 (2024), pp. 1339–1382.

[207] Qinghua Li et al. "MIMO techniques in WiMAX and LTE: a feature overview". In: *IEEE Communications magazine* 48.5 (2010), pp. 86–92.

[208] Christopher Cox. *An introduction to LTE: LTE, LTE-Advanced, SAE, VoLTE and 4G mobile communications*. John Wiley & Sons, 2014.

[209] Lingjia Liu et al. "Downlink mimo in lte-advanced: Su-mimo vs. mu-mimo". In: *IEEE Communications Magazine* 50.2 (2012), pp. 140–147.

[210] Andreas F Molisch. *Wireless communications*. Vol. 34. John Wiley & Sons, 2012.

[211] Hien Quoc Ngo et al. "Cell-free massive MIMO versus small cells". In: *IEEE transactions on wireless communications* 16.3 (2017), pp. 1834–1850.

[212] Emil Björnson and Luca Sanguinetti. "Scalable cell-free massive MIMO systems". In: *IEEE Transactions on Communications* 68.7 (2020), pp. 4247–4261.

[213] Zhe Wang et al. "Extremely large-scale MIMO: Fundamentals, challenges, solutions, and future directions". In: *IEEE Wireless Communications* 31.3 (2023), pp. 117–124.

[214] Zhe Wang et al. "A tutorial on extremely large-scale MIMO for 6G: Fundamentals, signal processing, and applications". In: *IEEE Communications Surveys & Tutorials* 26.3 (2024), pp. 1560–1605.

[215] Makan Zamanipour. "A survey on deep-learning based techniques for modeling and estimation of massivemimo channels". In: *arXiv preprint arXiv:1910.03390* (2019).

[216] Felipe Augusto Pereira de Figueiredo. "An Overview of Massive MIMO for 5G and 6G". In: *IEEE Latin America Transactions* 20.6 (2022), pp. 931–940.

[217] Pradip Kumar Barik et al. "A Resource Sharing Scheme for Intercell D2D Communication in Cellular Networks: A Repeated Game Theoretic Approach". In: *IEEE Transactions on Vehicular Technology* 69.7 (2020), pp. 7806–7820.

[218] Yoshio Karasawa. "Channel Capacity of Massive MIMO With Selected Multi-Stream Transmission in Spatially Correlated Fading Environments". In: *IEEE Transactions on Vehicular Technology* 69.5 (2020), pp. 5320–5330.

[219] Hidetomo Ochiai et al. "An Enhanced Channel Estimation for IEEE 802.15. 4 OFDM Receiver in High-Speed Mobile IoT Communication Systems". In: *IEEE Internet of Things Journal* 10.13 (2023), pp. 11910–11921.

[220] Wei Chen et al. "CSI-PPPNet: A One-Sided One-for-All Deep Learning Framework for Massive MIMO CSI Feedback". In: *IEEE Transactions on Wireless Communications* (2023).

[221] Xiaofu Ma et al. "Dynamic Sounding for Multi-User MIMO in Wireless LANs". In: *IEEE Transactions on Consumer Electronics* 63.2 (2017), pp. 135–144.

[222] Mahdi Boloursaz Mashhadi, Qianqian Yang, and Deniz Gündüz. "Distributed Deep Convolutional Compression for Massive MIMO CSI Feedback". In: *IEEE Transactions on Wireless Communications* 20.4 (2020), pp. 2621–2633.

[223] Ronghuo Dai, Cheng Yin, and Da Peng. "A Hybrid Iterative Thresholding Method for Solving Sparsity-Regularized Linear Inverse Problems and Its Application in Seismic Sparse-Spike Deconvolution". In: *IEEE Geoscience and Remote Sensing Letters* 20 (2023), pp. 1–5.

[224] Huake Wang, Ziang Li, and Xingsong Hou. "Versatile Denoising-Based Approximate Message Passing for Compressive Sensing". In: *IEEE Transactions on Image Processing* 32 (2023), pp. 2761–2775.

[225] Zhonghao Zhang et al. "AMP-Net: Denoising-Based Deep Unfolding for Compressive Image Sensing". In: *IEEE Transactions on Image Processing* 30 (2020), pp. 1487–1500.

[226] Yifan Ma et al. "Low-Complexity CSI Feedback for FDD Massive MIMO Systems via Learning to Optimize". In: *arXiv preprint arXiv:2406.16323* (2024).

[227] Santosh S Vempala. *The random projection method*. Vol. 65. American Mathematical Soc., 2005.

[228] Tiziano Bianchi, Valerio Bioglio, and Enrico Magli. "Analysis of one-time random projections for privacy preserving compressed sensing". In: *IEEE Transactions on Information Forensics and Security* 11.2 (2015), pp. 313–327.

[229] G Prashanthi et al. "Sparsification of Voice Data Using Discrete Rajan Transform and Its Applications in Speaker Recognition". In: *2014 IEEE International Conference on Systems, Man, and Cybernetics (SMC)*. IEEE. 2014, pp. 429–434.

[230] EG Rajan. "On The Notion of Generalized Rapid Transformation". In: *World multi conference on Systemics, Cybernetics and Informatics, Caracas, Venezuela*. 1997.

[231] E.G. Rajan. *Symbolic Computing and Signal and Image Procesing*. Bsp Books Pvt. Limited, 2019. ISBN: 9789352300341. URL: `https://books.google.co.in/books?id=CfqFzQEACAAJ`.

[232] Ekambaram Naidu Mandalapu and EG Rajan. "Rajan transform and its uses in pattern recognition". In: *Informatica* 33.2 (2009).

[233] Mandalapu Ekambaram Naidu and EG Rajan. "Two Dimensional Object Recognition Using Rajan Transform." In: *Engineering Letters* 13.4 (2006).

[234] Jiajia Guo, Chao-Kai Wen, and Shi Jin. "CAnet: Uplink-Aided Downlink Channel Acquisition in FDD Massive MIMO Using Deep Learning". In: *IEEE Transactions on Communications* 70.1 (2021), pp. 199–214.

[235] Lingfeng Liu et al. "The COST 2100 MIMO Channel Model". In: *IEEE Wireless Communications* 19.6 (2012), pp. 92–99.

[236] S Venugopal. "Pattern Recognition for Intelligent Manufacturing Systems Using Rajan Transform". PhD thesis. MS Thesis, Jawaharlal Nehru Technological University, Hyderabad, 1999.

[237] Ekambaram Naidu Mandalapu and EG Rajan. "Rajan Transform and Its Uses in Pattern Recognition". In: *Informatica* 33.2 (2009).

[238] Sonali Bagchi and Sanjit K Mitra. *The nonuniform discrete Fourier transform and its applications in signal processing*. Vol. 463. Springer Science & Business Media, 2012.

[239] Suhas Lohit et al. “Convolutional Neural Networks for Noniterative Reconstruction of Compressively Sensed Images”. In: *IEEE Transactions on Computational Imaging* 4.3 (2018), pp. 326–340.

[240] Ali Mousavi, Gautam Dasarathy, and Richard G Baraniuk. “Deepcodec: Adaptive Sensing and Recovery Via Deep Convolutional Neural Networks”. In: *ArXiv Preprint ArXiv:1707.03386* (2017).

[241] Hantao Yao et al. “Dr2-Net: Deep Residual Reconstruction Network for Image Compressive Sensing”. In: *Neurocomputing* 359 (2019), pp. 483–493.

[242] Xuelei Li et al. “FPGA Accelerates Deep Residual Learning for Image Recognition”. In: *2017 IEEE 2nd Information Technology, Networking, Electronic and Automation Control Conference (ITNEC)*. IEEE. 2017, pp. 837–840.

[243] Ahmed Alzahmi. “One Indoor Channel Model Per Cluster for MIMO Systems Polarized”. In: *International Journal of Research in Engineering, Science and Management* 4.11 (2021), pp. 45–50.

[244] Haider AH Alobaidy et al. “Wireless Transmissions, Propagation and Channel Modelling for IoT Technologies: Applications and Challenges”. In: *IEEE Access* 10 (2022), pp. 24095–24131.

[245] L Liu. “A Public COST 2100 Channel Model Matlab Source Code”. In: *WG2. 3_Model* (2010).

[246] Chong Tian and Yegang Chen. “Image Segmentation and Denoising Algorithm Based on Partial Differential Equations”. In: *IEEE Sensors Journal* 20.20 (2019), pp. 11935–11942.

[247] Paul White, Oliver Baumann, and Antonio De Stefano. “On Improving the Noise Reduction Algorithms Using Image Segmentation”. In: *2004 12th European Signal Processing Conference*. IEEE. 2004, pp. 501–504.

[248] Hongyuan Ye et al. “Deep Learning-Based Denoise Network For CSI Feedback in FDD Massive MIMO Systems”. In: *IEEE Communications Letters* 24.8 (2020), pp. 1742–1746.

[249] Mengyuan Ma et al. “Digital and Hybrid Precoding Designs in Massive MIMO with Low-Resolution ADCs”. In: *arXiv preprint arXiv:2409.17638* (2024).

[250] Hao Gao, Danpu Liu, and Zhilong Zhang. “Energy Efficiency Maximization for Partially-Connected Hybrid Beamforming Architecture with Low-Resolution DACs”. In: *IEEE Transactions on Communications* (2024).

[251] Wence Zhang et al. “Hybrid and Full-Digital Beamforming in mmWave Massive MIMO systems: A Comparison Considering Low-Resolution ADCs”. In: *China Communications* 16.6 (2019), pp. 91–102.

[252] Kilian Roth et al. “A Comparison of Hybrid Beamforming and Digital Beamforming with Low-Resolution ADCs for Multiple Users and Imperfect CSI”. In: *IEEE Journal of Selected Topics in Signal Processing* 12.3 (2018), pp. 484–498.

[253] Mohamed Reyad, Amany M Sarhan, and Mohammad Arafa. “A Modified Adam Algorithm for Deep Neural Network Optimization”. In: *Neural Computing and Applications* 35.23 (2023), pp. 17095–17112.

[254] Anders Øland. “Efficient Deep Learning”. PhD thesis. Google, 2024.

[255] Pengyu Cong and Chenyang Yang. “Number of FLOPs of Training DNNs for Learning Precoding”. In: *2023 IEEE 97th Vehicular Technology Conference (VTC2023-Spring)*. IEEE. 2023, pp. 1–6.

[256] Pedro Freire et al. “Computational Complexity Evaluation of Neural Network Applications in Signal Processing”. In: *arXiv preprint arXiv:2206.12191* (2022).

[257] Muhammad Zawish, Steven Davy, and Lizy Abraham. “Complexity-Driven Model Compression for Resource-Constrained Deep Learning on Edge”. In: *IEEE Transactions on Artificial Intelligence* (2024).

[258] Muhan Chen et al. “Deep Learning-Based Implicit CSI Feedback in Massive MIMO”. In: *IEEE Transactions on Communications* 70.2 (2022), pp. 935–950. DOI: 10.1109/TCOMM.2021.3138097.

[259] Apoorva Chawla et al. “Distributed Detection for Centralized and Decentralized Millimeter Wave Massive MIMO Sensor Networks”. In: *IEEE Transactions on Vehicular Technology* 70.8 (2021), pp. 7665–7680.

[260] Xiaotong Zhao et al. “Communication-Efficient Decentralized Linear Precoding for Massive MU-MIMO Systems”. In: *IEEE Transactions on Signal Processing* 71 (2023), pp. 4045–4059.

[261] Deepak Puthal et al. “The Blockchain as A Decentralized Security Framework [Future Directions]”. In: *IEEE Consumer Electronics Magazine* 7.2 (2018), pp. 18–21.

[262] Silvio Mandelli et al. “Power Optimization for Low Interference and Throughput Enhancement for 5G and 6G Systems”. In: *2021 IEEE Wireless Communications and Networking Conference Workshops (WCNCW)*. IEEE. 2021, pp. 1–7.

[263] Bassant Tolba et al. “A Meta Learner Autoencoder for Channel State Information Feedback in Massive MIMO Systems”. In: *2021 28th International Conference on Telecommunications (ICT)*. IEEE. 2021, pp. 1–5.

[264] Yacong Ding and Bhaskar D Rao. “Dictionary Learning-Based Sparse Channel Representation and Estimation for FDD Massive MIMO Systems”. In: *IEEE Transactions on Wireless Communications* 17.8 (2018), pp. 5437–5451.

[265] Chenwei Wang, Ozgun Bursalioglu Yilmaz, and Haralabos Papadopoulos. *Method and Apparatus for Extracting Large-Scale Features in Propagation Channels via Non-Orthogonal Pilot Signal Designs*. US Patent 10,594,459. Mar. 2020.

[266] Peizhe Liang et al. “Deep Learning and Compressive Sensing-Based CSI Feedback in FDD Massive MIMO Systems”. In: *IEEE Transactions on Vehicular Technology* 69.8 (2020), pp. 9217–9222.

[267] Gal Shalom, Eran Treister, and Irad Yavneh. “pISTA: Preconditioned Iterative Soft Thresholding Algorithm for Graphical Lasso”. In: *SIAM Journal on Scientific Computing* 46.2 (2024), S445–S466.

[268] Christopher A Metzler, Arian Maleki, and Richard G Baraniuk. “From Denoising to Compressed Sensing”. In: *IEEE Transactions on Information Theory* 62.9 (2016), pp. 5117–5144.

[269] William K Pratt, Julius Kane, and Harry C Andrews. “Hadamard Transform Image Coding”. In: *Proceedings of the IEEE* 57.1 (1969), pp. 58–68.

[270] A Hedayat and Walter Dennis Wallis. “Hadamard Matrices and Their Applications”. In: *The annals of statistics* (1978), pp. 1184–1238.

[271] Saeid Haghighatshoar and Emmanuel Abbe. “Polarization of The Rényi Information Dimension for Single and Multi Terminal Analog Compression”. In: *2013 IEEE International Symposium on Information Theory*. IEEE. 2013, pp. 779–783.

[272] Hongyi Pan, Diaa Badawi, and Ahmet Enis Cetin. “Fast Walsh-Hadamard Transform and Smooth-Thresholding Based Binary Layers in Deep Neural Networks”. In: *Proceedings of the IEEE/CVF Conference on Computer Vision and Pattern Recognition*. 2021, pp. 4650–4659.

[273] Jaeyoon Park and Sunggu Lee. “Energy-Efficient Image Processing Using Binary Neural Networks With Hadamard Transforms”. In: *Proceedings of the Asian Conference on Computer Vision*. 2022, pp. 4711–4725.

[274] Hongyi Pan et al. “A Hybrid Quantum-Classical Approach Based On The Hadamard Transform for The Convolutional Layer”. In: *International Conference on Machine Learning*. PMLR. 2023, pp. 26891–26903.

[275] Xiongbin Rao, Kin Nang Lau, and Xiangming Kong. *Channel Measurement Method, Channel Measurement Apparatus, User Equipment, and System*. US Patent 10,057,799. Aug. 2018.

[276] Xiangyi Li and Huaming Wu. “Spatio-Temporal Representation With Deep Neural Recurrent Network in MIMO CSI Feedback”. In: *IEEE Wireless Communications Letters* 9.5 (2020), pp. 653–657.

[277] Chao Lu et al. “MIMO Channel Information Feedback Using Deep Recurrent Network”. In: *IEEE Communications Letters* 23.1 (2018), pp. 188–191.

[278] Kaiming He et al. "Deep Residual Learning for Image Recognition". In: *Proceedings of The IEEE Conference on Computer Vision and Pattern Recognition*. 2016, pp. 770–778.

[279] Qiao Cheng et al. "Compressive Sensing Radar Imaging with Convolutional Neural Networks". In: *IEEE Access* 8 (2020), pp. 212917–212926.

[280] Hongyi Pan et al. "Deep Neural Network With Walsh-Hadamard Transform Layer for Ember Detection During a Wildfire". In: *Proceedings of the IEEE/CVF Conference on Computer Vision and Pattern Recognition*. 2022, pp. 257–266.

[281] Hongyi Pan, Diaa Badawi, and Ahmet Enis Cetin. "Block Walsh–Hadamard Transform based Binary Layers in Deep Neural Networks". In: *ACM Transactions on Embedded Computing Systems* 21.6 (2022), pp. 1–25.

[282] Andrew Thompson. "The Cascading Haar Wavelet Algorithm for Computing the Walsh–Hadamard Transform". In: *IEEE Signal Processing Letters* 24.7 (2017), pp. 1020–1023.

[283] François Quitin et al. "A Polarized Clustered Channel Model for Indoor Multiantenna Systems at 3.6 GHz". In: *IEEE Transactions on Vehicular Technology* 59.8 (2010), pp. 3685–3693.

[284] Roberto Verdone and Alberto Zanella. *Pervasive Mobile and Ambient Wireless Communications: COST Action 2100*. Springer Science & Business Media, 2012.

[285] Jiajia Guo et al. "Deep learning for joint channel estimation and feedback in massive MIMO systems". In: *Digital Communications and Networks* 10.1 (2024), pp. 83–93.

[286] Yang Liu et al. "Low-complexity neural network based DOA estimation for wideband signals in massive MIMO systems". In: *AEU-International Journal of Electronics and Communications* 138 (2021), p. 153853.

[287] Yiming Huo et al. "Technology trends for massive MIMO towards 6G". In: *Sensors* 23.13 (2023), p. 6062.

[288] Rizwan Khan et al. "An effective algorithm in uplink massive MIMO systems for pilot decontamination". In: *Results in Engineering* 21 (2024), p. 101873.

[289] Tulsi Pawan Fowdur and Bhuvaneshwar Doorgakant. "A review of machine learning techniques for enhanced energy efficient 5G and 6G communications". In: *Engineering Applications of Artificial Intelligence* 122 (2023), p. 106032.

[290] Hoang-Yang Lu, S Pourmohammad Azizi, and Shyi-Chyi Cheng. "Deep-SOR detection for massive MIMO systems". In: *AEU-International Journal of Electronics and Communications* (2025), p. 155815.

[291] Xin-Lin Huang et al. "Rate-adaptive feedback with Bayesian compressive sensing in multiuser MIMO beamforming systems". In: *IEEE Transactions on Wireless Communications* 15.7 (2016), pp. 4839–4851.

[292] Chengchen Mao et al. "Deep learning in physical layer communications: Evolution and prospects in 5G and 6G networks". In: *IET Communications* 17.16 (2023), pp. 1863–1876.

[293] Giuseppe Aceto et al. "MIMETIC: Mobile encrypted traffic classification using multimodal deep learning". In: *Computer networks* 165 (2019), p. 106944.

[294] Yuwen Yang et al. "Deep transfer learning-based downlink channel prediction for FDD massive MIMO systems". In: *IEEE Transactions on Communications* 68.12 (2020), pp. 7485–7497.

[295] Amit Kumar et al. "A Novel DRT-Assisted Deep Learning-Based Channel Feedback Mechanism for Massive MIMO". In: *IEEE Transactions on Consumer Electronics (Early Access)* (2024).

[296] Zhenyu Liu, Lin Zhang, and Zhi Ding. "Exploiting bi-directional channel reciprocity in deep learning for low rate massive MIMO CSI feedback". In: *IEEE Wireless Communications Letters* 8.3 (2019), pp. 889–892.

[297] Satish Kumar, Anurag Singh, and Rajarshi Mahapatra. "DLNet: Deep learning-aided massive MIMO decoder". In: *AEU-International Journal of Electronics and Communications* 155 (2022), p. 154350.

[298] Moritz Wiese et al. "Identification over additive noise channels in the presence of feedback". In: *IEEE Transactions on Information Theory* 69.11 (2022), pp. 6811–6821.

[299] Kai Zhang et al. "Beyond a gaussian denoiser: Residual learning of deep CNN for image denoising". In: *IEEE transactions on image processing* 26.7 (2017), pp. 3142–3155.

[300] M Meenalakshmi, Saurabh Chaturvedi, and Vivek K Dwivedi. "Enhancing channel estimation accuracy in polar-coded MIMO–OFDM systems via CNN with 5G channel models". In: *AEU-International Journal of Electronics and Communications* 173 (2024), p. 155016.

[301] Liangyuan Xu et al. "On the uplink achievable rate of massive MIMO system with low-resolution ADC and RF impairments". In: *IEEE Communications Letters* 23.3 (2019), pp. 502–505.

[302] Sergey Ioffe and Christian Szegedy. "Batch Normalization: Accelerating Deep Network Training by Reducing Internal Covariate Shift". In: *Proceedings of the 32nd International Conference on Machine Learning*. Ed. by Francis Bach and David Blei. Vol. 37. Proceedings of Machine Learning Research. Lille, France: PMLR, July 2015, pp. 448–456.

[303] Zhiyuan Shen and Yitao Wei. "A high-precision feature extraction network of fatigue speech from air traffic controller radiotelephony based on improved deep learning". In: *ICT Express* 7.4 (2021), pp. 403–413. ISSN: 2405-9595.

[304] Ruohan Zhao et al. "Hybrid CNN-transformer network for efficient CSI feedback". In: *Physical Communication* 66 (2024), p. 102477.

[305] Huayan Guo and Vincent KN Lau. "Bayesian hierarchical sparse autoencoder for massive MIMO CSI feedback". In: *IEEE Transactions on Signal Processing* 72 (2024), pp. 3213–3227.

[306] Praveen Gorla et al. "A Novel Framework of Federated and Distributed Machine Learning for Resource Provisioning in 5G and Beyond Using Mobile-edge SCBS". In: *IEEE Transactions on Network and Service Management* 20.2 (2022), pp. 985–994.

[307] Liangliang Li et al. “Compressed PARAFAC-Based Parameter Estimation for mmWave Polarized Massive MIMO Systems”. In: *IEEE Sensors Journal* 25.9 (2025), pp. 16170–16181.

[308] Muhammad Asghar Khan et al. “Swarm of UAVs for Network Management in 6G: A Technical Review”. In: *IEEE Transactions on Network and Service Management* 20.1 (2022), pp. 741–761.

[309] Amit Kumar et al. “A Novel DRT-Assisted Deep Learning-Based Channel Feedback Mechanism for Massive MIMO”. In: *IEEE Transactions on Consumer Electronics* 71.2 (2025), pp. 6734–6743. DOI: `10.1109/TCE.2024.3520220`.

[310] Rajesh Gupta and Sudeep Tanwar. “A Zero-Sum Game-Based Secure and Interference Mitigation Scheme for Socially Aware D2D Communication with Imperfect CSI”. In: *IEEE Transactions on Network and Service Management* 19.3 (2022), pp. 3478–3486.

[311] Shin-Chi Lai et al. “Low Computational Complexity, Low Power, and Low Area Design for The Implementation of Recursive DFT and IDFT Algorithms”. In: *IEEE Transactions on Circuits and Systems II: Express Briefs* 56.12 (2009), pp. 921–925.

[312] Duraisamy Sundararajan. *The Discrete Fourier Transform: Theory, Algorithms and Applications*. World Scientific, 2001.

[313] Ingrid Daubechies, Michel Defrise, and Christine De Mol. “An Iterative Thresholding Algorithm for Linear Inverse Problems With a Sparsity Constraint”. In: *Communications on Pure and Applied Mathematics: A Journal Issued by the Courant Institute of Mathematical Sciences* 57.11 (2004), pp. 1413–1457.

[314] Fulai Liu et al. “Deep Learning Based Hybrid Precoder and Combiner Approach for MIMO-OFDM Systems”. In: *IEEE Sensors Journal* 25.5 (2025), pp. 8942–8949.

[315] Tianjian Lu et al. “Large-Scale Discrete Fourier Transform on TPUs”. In: *IEEE Access* 9 (2021), pp. 93422–93432.

[316] Sergey Ioffe and Christian Szegedy. “Batch Normalization: Accelerating Deep Network Training by Reducing Internal Covariate Shift”. In: *International conference on machine learning*. pmlr. 2015, pp. 448–456.

[317] Lingfeng Liu, Jiabin Jin, and Sian Xiong. “Performance Optimization of Polarized MIMO Relay Channels Based on The Cost 2100 Channel Model”. In: *IEEE Antennas and Wireless Propagation Letters* 21.6 (2022), pp. 1188–1192.

[318] Lingfeng Liu et al. “The COST 2100 MIMO Channel Model”. In: *IEEE Wireless Communications* 19.6 (2012), pp. 92–99.